Deciphering the molecular and cellular mechanisms underlying the radiosensitizing activity of metal complexes : Towards the development of drug candidates for improving chemoradiotherapy for cancer treatment.

Deepanjan Ghosh

PSL UNIVERSITÉ PARIS

THÈSE DE DOCTORAT
DE L'UNIVERSITÉ PSL

Préparée à l'Institut Curie

Deciphering the Molecular and Cellular Mechanisms Underlying the Radiosensitizing Activity of Metal Complexes: Towards The Development of Drug Candidates for Improving Chemoradiotherapy for Cancer Treatment

Décrypter les mécanismes moléculaires et cellulaires qui sous-tendent l'activité de radiosensibilisation de complexes métalliques : vers le développement de candidats médicaments pour améliorer la radiochimiothérapie pour le traitement du cancer

Soutenue par

Deepanjan Ghosh

Le 22 September 2020

Ecole doctorale n° 474
FIRE (Frontières de l'Innovation en Recherche et Éducation)

Spécialité
Frontières du vivant

Confidentielle jusqu'au 30/09/2023

institutCurie

Composition du jury :

Gilles, GASSER Professeur, Chimie ParisTech PSL Université	***Président***
François, BOUSSIN DR, CEA – Institut de Biologie François Jacob	***Rapporteur***
Marie-Joseph, GIRAUD-PANIS DR, IRCAN - CNRS Université de Nice	***Rapporteur***
Marie, DUTREIX DR, Institut Curie Université Paris Saclay	***Examinateur***
Anna, CAMPALANS Chercheur, CEA - Institut de Biologie François Jacob	***Examinateur***
Sophie, BOMBARD DR, Institut Curie - CNRS	***Directeur de thèse***

Acknowledgements

I would like to give a huge thanks to my thesis supervisor, **Dr. Sophie Bombard** for guiding me through all of the four years of my PhD. I am grateful and extremely appreciative of the discussions and the level of attention to detail you provided during my time in the lab.

I would like to thank **Dr. François Boussin** and **Dr. Marie-Joseph Giraud-Panis** for agreeing to be the rapporteurs of my thesis. It truly means a lot. A special shout out to Dr. Marie-Joseph Giraud-Panis for agreeing to it during the truly last-minute jury crisis.

I would like to thank **Dr. Marie Dutreix**, **Dr. Gilles Gasser** and **Dr. Anna Campalans** for being the examiners of my thesis. I feel very lucky to have you all as part of my thesis jury.

Thank you, **Laetitia Besse** and **Marie-Noelle Soler**, for all the help with the microscopy platform and the macro you helped create for the immunofluorescence experiments. **Charlene Lasgi**, I would like to thank you for being a great manager of the Cytometry platform and being ever so patient with all the questions I have had.

Dr. Tao Jia, thank you for being in the lab for my final year of the thesis. I appreciate our friendship a lot and would like to give a special thanks for all the advices and help you have provided me during our time together.

I would like to thank **Carine Mota Jesus**, **Adam Dehgane** and **Ytabelle Siasia** for being amazing students that I had the good fortune to supervise. Your help in my thesis cannot be understated. I wish you all a lot of happiness and a great career in the future.

To my labmates and friends **Linda Silina, Fatlinda Maksut** and **Jaime Franco Pinto**, I would like to thank you for all the fun times together, be it in the lab or the Orsay special 'Happy Friday'.

Ralfs Buks and **Ana Loncar**, thank you for bringing your idiosyncrasies in my life. You guys have been a much needed breath of fresh air. I truly cherish our friendship.

Sandra Curras Alonso, thank you for being my friend, neighbor and office partner for the last 3 years. I think it's time for your obsession with me to stop. **Tommaso Galgani**, thank you for being the only Italian who likes pineapples on pizza. **Silvia Benito Martinez**, thank you for being one of

the most empathetic person I know and also to teach me how to live as a minimalist. **Samyukhta Suresh**, thank you for being a great friend and our special dinners together. **Anne Celine Derrien**, you have been one of my surprisingly few French friends. Thank you for being there for me when I needed you and also your pool house. Thank you **Raquel Vivet-Nouger** for giving me fitness goals that I could never live up to. Viva Catalonia!!

Sofia Ferreira, thank you for being the absolute best person I know south of the Boulevard Périphérique. Our special talks during the lunch hour or after a couple of beverages are going to be cherished forever. Thank you for being the person I didn't even realize I needed in my life.

Sebastian Hoffman, you have been one of the closest friends I have made during my time in Paris. Thank you for all the jokes, talks about life and other topics not quite suitable to be mentioned in a PhD thesis. Please know that I have loved doing it all with you.

To one of the most important person I have met in the last decade, **Darine Samander Eweis**, thank you for everything. I will not be reductive by stating only a few memories of ours. You know who you are to me and how much you mean in my life. Thank you for everything. Everything.

I would like to thank my parents **Dipten Ghosh** and **Sahana Ghosh** for supporting me throughout my life. Ma, everything I have done in my life can be traced back to you. You mean more to me than I could ever put into words. I would also like to thank my brother **Gaurav Narayan,** you were not the brother I was born to but you helped prove the saying that 'The blood of the covenant is thicker than the water of the womb'.

Finally, Thank you Paris for all the memories, for all the people and one excellent degree.

List of abbreviations

G4 G- quadruplex

RS Radiosensitization

ATM Ataxia-Telangiectasia Mutated

ATR ATM Rad3 Related

ALT Alternative Lengthening of Telomeres

BRCA1 Breast Cancer 1

BRCA2 Breast Cancer 2

CtIP CtBP interaction protein

GSC Glioma Stem Cells

HR Homologue Recombinition

hTERT human Telomerase Reverse Transcriptase

hTR human Telomerase RNA

MMR mismatch repair

MRN (MRE11/Rad3/Nbs1)

NER Nucleotide Excision Repair

NHEJ Non-Homologous End Joining

POT1 Protection Of Telomere 1

TIN2 TRF1-Interacting Nuclear Protein 2

TPP1 TIN2 and POT1 Interacting Protein

TRF1 Telomere Repeat-Binding Factor 1

TRF2 Telomere Repeat-Binding Factor 2

PARP poly (ADP-ribos) polymerase

RAP1 Repressor Activator Protein 1

DSB Double stranded Break

SSB Single stranded Break

ICL Interstrand crosslinks

SSBR Single stranded break repair

DDR DNA Damage Response

Contents

INTRODUCTION

1. G-quadruplex

1.A. Structure

A 100 years ago, it was noticed that guanylic acid derivatives have a capacity to self-aggregate, however, it took 50 years to propose that the structure formed by the guanylic acids are stabilized via hoogsteen hydrogen bonded guanines that form planar G-quartets [1, 2]. Biophysical studies of G-rich sequences like the telomeric sequence consisting of tandem repeats of –(TTAGGG)- then led to the formation of G-quadruplex (G4s) structures *in vitro* at near physiological conditions helping us to understand its morphology and stability. Eventually the sequence motif created to identify potential G4s in the genome was $G_{\geq}3N_x\ G_{\geq}3N_x\ G_{\geq}3N_x\ G_{\geq}3$ [3, 4] since 4 runs of 3 or more successive guanines were required to make the G4. It is a four stranded DNA or RNA structure that can be monomolecular, bimolecular or tetramolecular. G4s can be intramolecular, where all the guanines involved are present in the same strand of DNA and RNA, or intermolecular where multiple DNA/RNA strands come together to form the G4 structure.

Four guanines make a G-quartet, these quartets are then stacked leading to the formation of a G4 (Figure 1). The G-quartet is a planar structure that is stabilized to an extent by the hydrogen bonding network between N_7:N_2H and O_6:N_1H. The thermodynamic stability of the quartet requires the presence of a monovalent cation of a correct size to counter the geometrical arrangement of lone pair of electrons from the four Guanine O_6 formed in the central core of the quartet. Na^+ and K^+ ions generally perform the role with the smaller Na^+ able to sit in the plane of the G-quartet. The larger size of K^+ ions however lead it to lie in between two quartets in a stack[5]. The metal ion stabilizing influence is linked to the increasing radii from $Li^+ < Na^+ < K^+$ with potassium being optimal, and dramatically increasing G4 stability [6].

In monomolecular G4s, they can be classified based on the strand polarities and the location of the loops joining the guanine strands of the G4 (Figure 1). In the sequence motif of $G_{\geq}3N_x\ G_{\geq}3N_x\ G_{\geq}3N_x\ G_{\geq}3$, the Nx nucleotides would constitute the loops of the G4 structure. A parallel G4 is one where the direction of all the strands are in the same direction, leading to the formation of a propeller loop to join the bottom of the G-tetrad to the top. G4s are designated as anti-parallel when at least one of the four strands is anti-parallel to the others. Three different types of loops,

namely, lateral, diagonal and reverse loops are seen with this topology. In total, there exists around 26 different topologies of G4s *in vitro*[7, 8]. For example, the telomeric sequence was seen to form a parallel stranded structure in the presence of K^+ [9], however, further work has shown that major G4s formed by this sequence is hybrid type intramolecular structures. 2 distinct hybrid structures are found that are both three parallel G-strands and one antiparallel, but they differ in loop arrangements, strand orientations and G-tetrad arrangements [10].

Figure 1. (a) Structure of guanine tetrads formed by the coplanar arrangement of four guanines

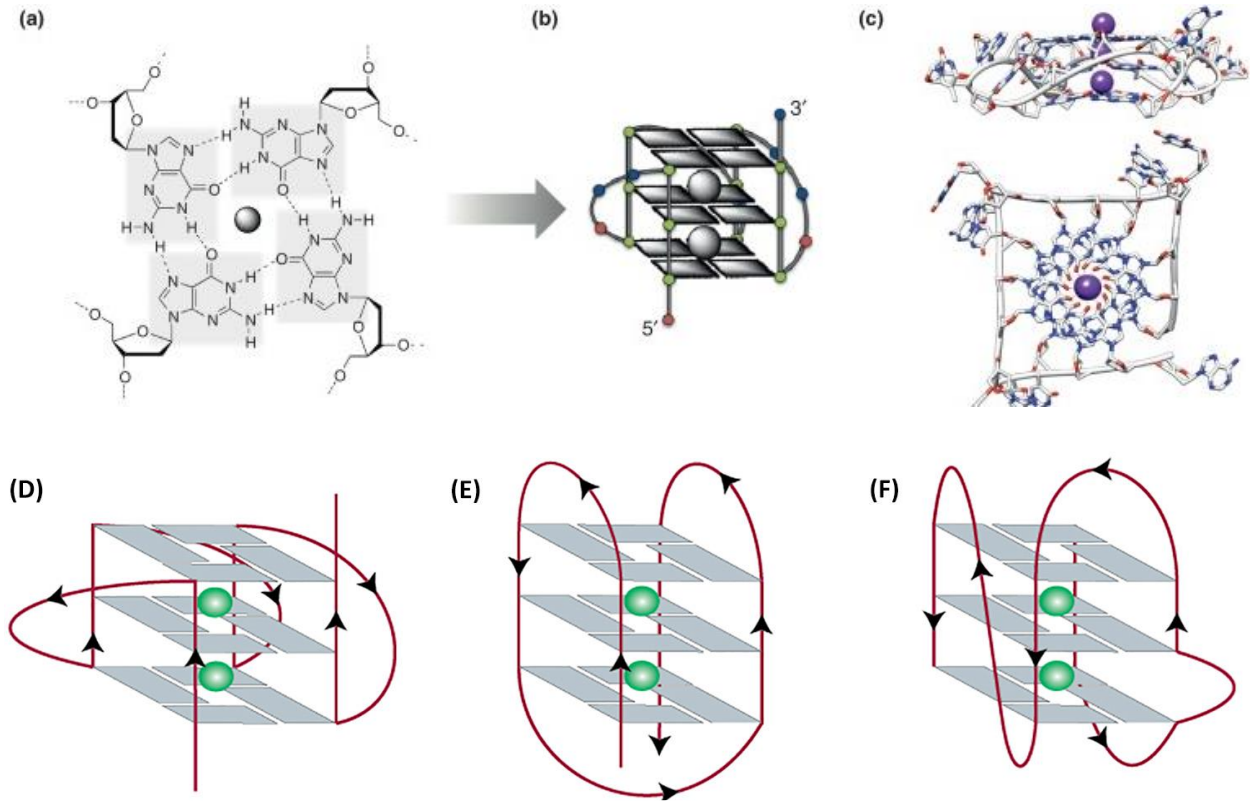

held by Hoogsteen bonds and stabilised by monovalent cations (usually K^+). (b) Schematic representation of a G4 motif formed by guanine rich DNA sequences and stabilized by the stacking of guanine tetrads. (c) Side and top view of the crystal structure of the human telomeric quadruplex [11]. The schematic representation of intrastrand G4s based on its strand direction is shown as (D) Parallel, (E) anti-parallel and (F) hybrid with a bulge[12].

1.A.2. Identification of G4s using biophysical and biochemical methods[8]

G4 formation and investigation of its structural properties can be done using different biophysical techniques. For example, by monitoring the positive or negative circular dichroism (CD) signals at specific wavelengths, the topology of the G4 structure can be determined [13]. In general, G4s with parallel topology have negative and positive CD signals at 240 and 262 nm, respectively, whereas antiparallel topology places these signals at 262 and 295 nm, respectively as seen in figure 2. To verify G4 formation, one should also perform the CD experiments under non-G4 stabilizing (Li+) and G4 stabilizing conditions (such as K+ or with G4 ligands), and scan toward the far-UV region (180–230 nm). Similarly, the thermostability of the G4 structure can be investigated by observing the UV signal at 295 nm [14]. It is seen that upon G4 melting, the UV absorbance at 295 nm decreases, leading to a hypochromic shift that is a distinctive feature of G4 structure.

Figure 2: The CD spectra is shown for the different topologies of G4s (A) anti-parallel lateral loop,

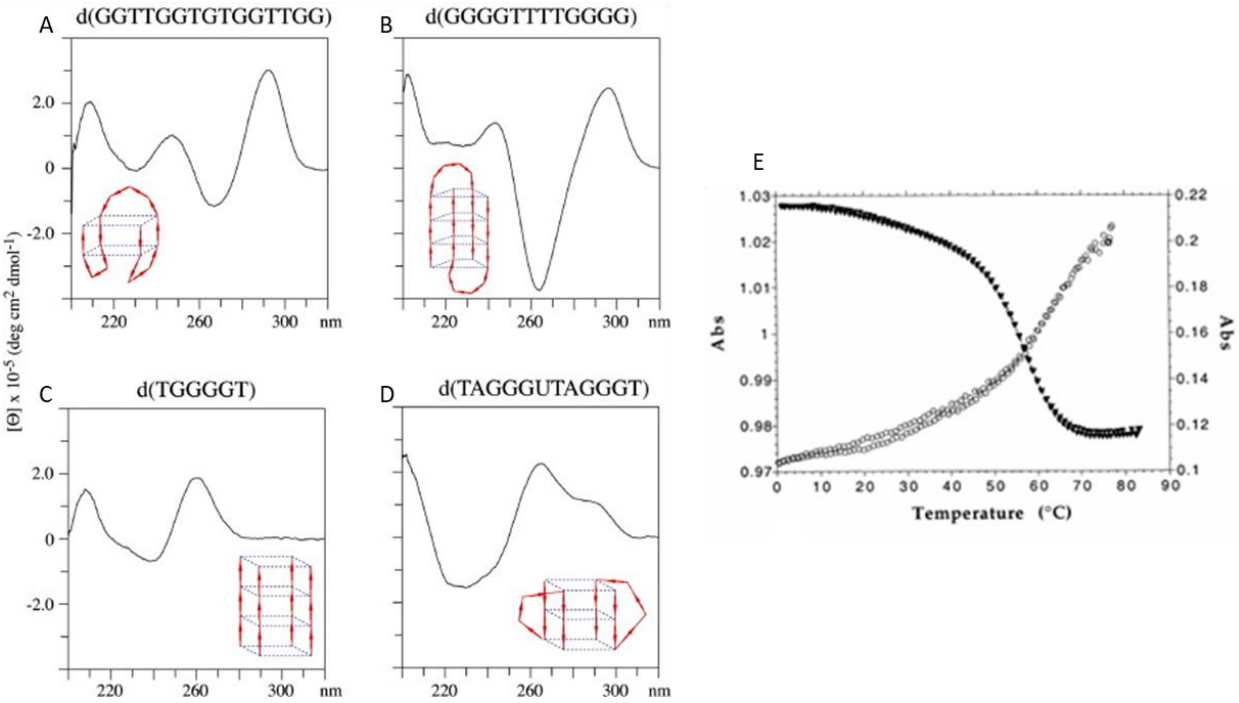

(B) anti-parallel diagonal loop, (C) four stranded parallel and (D) parallel propeller loops [13]. The 295nm UV absorbance is shown to be reduced with the melting of the G4 as seen in the black triangles. The open circles represent the 260nm absorbance. The left axis is for 260nm and the right axis is for the 295nm absorbance [14].

Biochemical techniques were used to understand G-4 formation in a longer sequence. An example is that of the DNA polymerase stop assay, it can be used to identify G4s since the formation of a G4 in a DNA template can act as a roadblock and cause polymerase stalling which halts the primer extension, the scheme of which is shown later in the chapter. Salazar and colleagues [15] previously applied this method to study the DNA G4 structure formed by telomeric DNA sequences, d(T2G4)4 or d(T2AG4)4, in the template strand. Cech and colleagues [16] tried another assay on telomeric sequence. They observed that dimethyl sulfate (DMS) induced N7 guanine methylation will not be formed on G4 structures leading to a protection pattern observed at the DNA G4 region after piperidine cleavage.

Several new biochemical methods were developed to study RNA G4s as well, such as reverse transcriptase can be stalled by RNA G4 structures during reverse transcription. Kwok and Balasubramanian [17] developed a reverse transcriptase stalling (RTS) assay and coupled this with ligation-mediated PCR to identify the *in vitro* G4 formation in low-abundance RNA.

1.B. G4s in cells

1.B.1. Computational analysis of G4s

G4s are primarily found in the telomeres, that are located at the ends of the chromosomes, due to the G-rich presence of –TTAGGG- repeat double stranded sequence followed by a 3 single stranded overhang. However, the number of possible G4s in genome has been demonstrated by bioinformatics to be between 350,000- 600,000 in number and are present in the first introns of oncogenes or genes amplified in cancers and 3' and 5' UTRs of some mRNAs [3, 18]. However, there are limitations to the identification of PQS (Potential Quadruplex forming Sequences) by algorithms due to the presence of G4s having larger loops or a non-guanine bulge which are not taken into account. This leads to individual algorithms having different parameters and having to balance the false positives and false negatives[8].

For intramolecular G4s, many algorithms have been published over the past decade to predict the potential formation of G4s directly from DNA sequence, including QuadParser [3], QGRS Mapper [19], G4P Calculator [20], QuadBase [21] and most recently, G4 Hunter [18].

1.B.2. Visualization of G4s by specific antibodies imaging

Visualization of G4s in the cells can be done through the use of immunofluorescence. Development of antibodies against G4 was focused on cumulating in the production of the first quadruplex-specific antibody, Sty49, which was used in the year 2001 to visualize Gquadruplexes in ciliate macronuclei [22], that had a large amount of telomeric DNA that offered an abundance of G4s. There was a significant delay between this and successful visualization in mammalian fixed cells that have comparatively much less telomeres. Since whole cell immunofluorescence can be challenging due to chromatin packaging that can obscure G4s as well as the fact that G4s are dynamic in nature and adopt the quadruplex structure only transiently *in vivo*, several different protein probes were developed. This included a zinc-finger protein GQ1 [23], a range of designed ankyrin repeat binding proteins or 'DARPins' [24], and a single-chain antibody hf2 [25]. However, it was noticed that these could all detect G4s *in vitro* but proved unsuitable for whole-cell immunofluorescence[24].

Two new antibodies, BG4 [26] and 1H6[27] were discovered recently and have proved suitable for whole-cell immunofluorescence on fixed mammalian cells. However, the lab that discovered IH6 later showed that the antibody is no specific of G4s but rather has a strong affinity for single stranded poly(T) DNA [28]. The number of BG4 foci detected in fixed human cells is orders of magnitude lower than the number of G4-forming sequences predicted by computational analysis present in the genome (see 1B3). By G4 ChIP-seq, It was seen that ~10,000 G4s were present in precancerous HaCaT cells, while only ~1000 were detected in the normal NHEK cells [29], representing only 1% of the sites that have the potential to form G4s [30]. One good reason could be that the dynamic and transient folding of G4s could limit detection *in vivo*, moreover most antibodies will not detect every possible structural variant of G4. Both the antibodies were generated via different practices, 1H6 by immunizing mice with stable G4 structures and BG4 by phage display and *in vitro* selection on such structures. IH6 is not capable of detecting RNA quadruplexes, whereas BG4 can successfully do so [31].

1.B.3. Mapping of G4s in genome by sequencing

Mapping of G4s in the genome needed to be done with the help of Next Generation sequencing (NGS) to give a more comprehensive understanding of the number of G4s formed in *in vivo* conditions and the ability to map it in the genome. There are multiple approaches in using the NGS tool for G4 detection and mapping, such as ChIP seq of G4 binding proteins, ChIP seq of DNA damage markers, G4 ChIP seq using G4 binding antibodies, G4 seq using polymerase stalling and permanganate footprinting (Figure 3).

The computational predictions for G4 formation do not take into account the effects of chromatin and all its associated proteins, hence, studies have been done to explore the native G4 landscape in cells. It can be done by using proteins that bind to G4 and are then pulled down with antibodies against those proteins through ChIP followed by high throughput sequencing (figure 3A). Enrichment of genomic regions that have computationally predicted G4 structures have been seen with ATR-X, XPB and XPD helicases, yeast telomere binding protein Rif, and yeast PIF1 helicase [32-35].

Another approach to gain information of the number and location of G4s in the genome. This process can be termed 'indirect ChIP' approach[36], as it evaluates the sites of DNA damage marked by the histone variant H2AX when pulled down after treating cells with the quadruplex-stabilizing drug pyridostatin, on the hypothesis that persistent quadruplexes would induce transcription- and/or replication dependent DNA damage. This yielded large sequence domains because the histone mark spreads broadly at sites of damage, but the domains were indeed enriched in putative quadruplex-forming sequences [36].

For the antibody-mediated pull-down approach, successful chromatin immunoprecipitation of G-quadruplexes (G4 ChIP-seq) was reported only very recently – possibly because suitable antibodies proved elusive, because the native chromatin context tends to mask the majority of G4 epitopes, and/or because the PQSs are folded into G4s only in specific cellular conditions. Circumventing some of these issues, an antibody pull-down was conducted from naked genomic DNA using the hf2 antibody, but this detected only around 700 G4s [37]; subsequently, the BG4 antibody (which was also used in a chromatin context for whole-cell immunofluorescence assays) was used to isolate G4-containing fragments from human chromatin, yielding around 10,000 or 1000 motifs from two different human cell lines[29]. The isolated regions tended to be noncoding regulatory regions of highly transcribed genes, suggesting that nucleosome depletion and active transcription probably favour the folding of G4s[29].

Polymerase stalling approaches such as G4-seq offer, by contrast, the comprehensive experimental identification of sequences that 'can' form G4s [30], yielding an *in vitro* genome-wide G4 map. Here, sheared DNA is subjected to NGS in the presence or absence of conditions that favour quadruplex folding (potassium ions and/or the G4-stabilizing ligand pyridostatin). Under stabilizing conditions, G4s impede the polymerase, causing a characteristic increased mutation rate in sequence data at the G4 folded region. The G4-seq technique identified around 700,000 G4es in the human genome: orders of magnitude more than G4 ChIP-seq and two times the number predicted in silico by standard algorithms. This could be because many of the sequenced motifs were bulged or long looped which are not counted by the algorithms [38]. Interestingly, the majority of G4s found by G4 ChIP-seq (79%) were not of the canonical G3 N1–7-type either, however, those that were of this type tended to represent the strongest ChIP

peaks, and there was also a reassuring degree of agreement between the G4 ChIP-seq and G4-seq experiments: 87% of the DNA fragments from G4 ChIP-seq contained sequences identified in G4-seq [30].

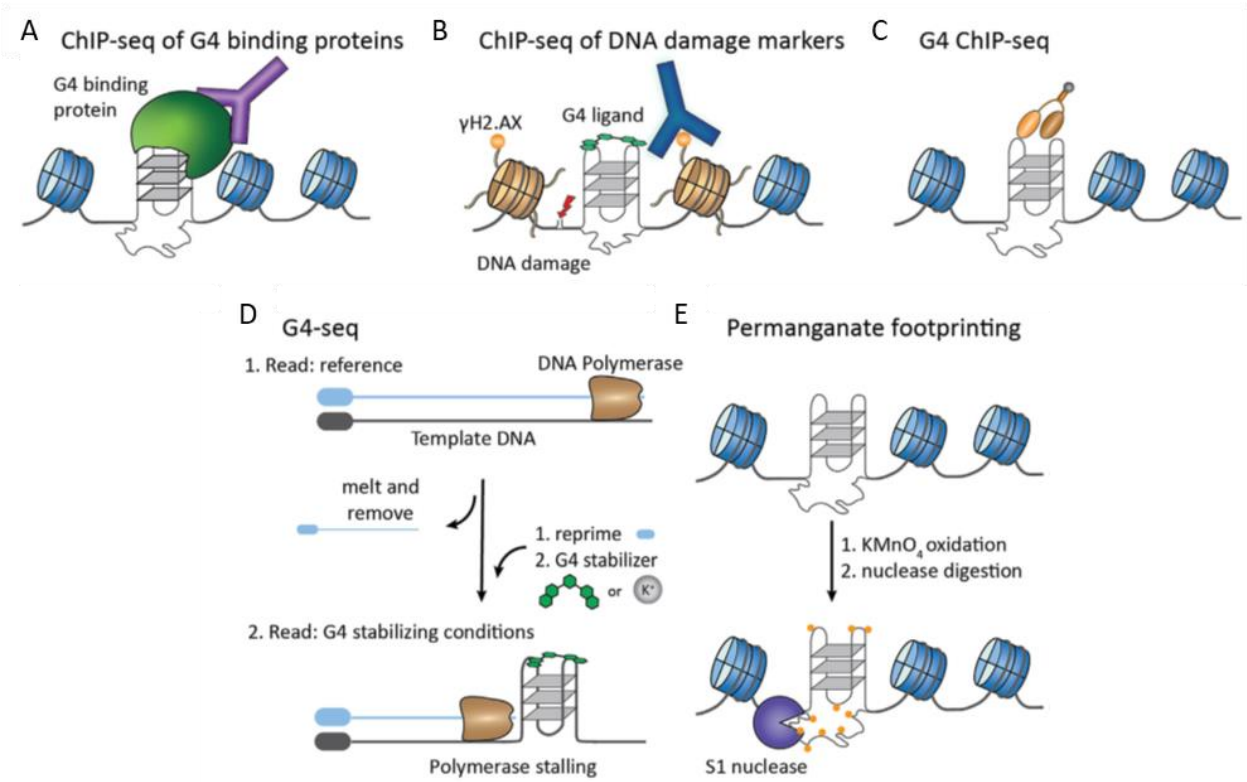

Figure 3: Various schemes for detection and mapping of G4s. (A) ChIP assay done using antibodies against G4 binding proteins and next gen sequencing done with the pulled down DNA seq. (B) ChIP assay done with antibodies against DNA damage markers (like gH2AX) post G4 binding drug treatment, followed by sequencing. (C) ChIP done with antibodies against G4s such as BG4 followed by sequencing. (D) High throughput sequencing of G4s (G4 seq) done with the polymerase stalling experiment. (E) Permanganate oxidation of nucleotides in transiently unwound regions traps the unpaired state, resulting in sensitivity to a single-strand specific nuclease, post which computational analysis helps deciphering the non- B-DNA structure. [12]

A genome wide potassium permanganate dependent nuclease footprinting was done on mouse B cells to identify single stranded non B-DNA. This was then combined alongside computational analysis to identify the type of non B-DNA and the enrichment of these structures. The study revealed 20,000 hypersensitivity sites featuring G4 motifs. It also suggested a transcription dependent formation of non-canonical DNA structures as was discovered comparing resting B cells and liposaccaride interleukin 4 activated B cells [39].

The difference in the number of G4s reported from data sets obtained *in vitro* and *in vivo* (i.e., G4-seq vs. G4-ChIP) suggests that the cellular environment may play a central role in affecting the dynamics of G4 formation in cells. Specifically, many cellular factors, such as G4 binding proteins and helicase, can likely remodel the DNA G4 landscape *in vivo*. Nevertheless, more technical explanations for the difference in G4 detection rates *in vivo* versus *in vitro* cannot be excluded, such as limited sensitivity of ChIP and condition dependence for G4 formation in native chromatin. Results are also likely to be influenced by sensitivity/specificity of the antibody used, choice of cell line, and variation in experimental protocols and bioinformatics pipelines[8].

1.C. Importance of G4s in cell physiology

1.C.1. Telomere Protection

Telomeres are nucleoprotein structures that protect the end of linear chromosomes. The telomeric DNA consists of tandem repeats of G rich sequence with (TTAGGG)n repeats found in humans that can form G4s. These sequences of about 4–10 kbp protrude at the 3' extremity by a single strand of the G-rich sequence of about 50 to 200 bases. The telomeres first protect the stability and structural integrity of chromosomes, since telomeric dysfunction leads to chromosomal instability and abnormalities, senescence, apoptosis, etc. Secondly, telomeres maintain the genomic integrity by protecting chromosomes from the progressive erosion of 5' extremity of each chromosome that happens at each replication. In normal cells, the telomeres erode with each replication leading to shortening of the telomeres until a critical length (Hayflick limit) is reached, after which the cell induces signals to enter senescence. In most cancer cells however, the enzyme telomerase is active which is a telomere specific reverse transcriptase. It adds the telomeric repeats at the end of the 3' overhang of telomeres using its RNA component TERRA that is complementary to the telomeric sequence. This mechanism helps prevent replicative senescence in most cancer cells [40].

In order to protect the end of chromosomes being recognized as a Double Stranded Break (DSBs) and prevent chromosome fusions, telomeres protect their ends with a complex of proteins called Shelterin complex [41]. It is a conglomerate of 6 proteins TRF1, TRF2, RAP1, POT1, TIN2 and TPP1, as shown in figure 4. In these proteins, TRF1 and TRF2 are capable of binding to duplex DNA and POT1 binds to the 3' overhang single stranded DNA [42]. TRF2 and POT1 are shown to be directly involved in the maintenance of the telomeric structure [43, 44]. TRF2 is thought to promote the formation of the T-loop, where the single stranded overhang invades the double stranded telomeric DNA [45]. Displacement of TRF2 from the shelterin complex leads to recognition of telomeres as DSBs, ATM kinase signaling DNA damage response pathway, end to end chromosome fusions and accelerated senescence entry [46-49] and TRF1 plays a special role in S phase by facilitating the replication of telomeres and preventing ATR activation [50]. POT1 has

been shown to act, by interacting with TRF1 and TPP1, as either an activator or a repressor the telomerase enzyme [51-53].

Chromatin homeostasis at the telomeric and sub-telomeric regions is dependent on the recruitment of histone methyltransferase due to its importance in telomeric heterochromatin maintenance. This recruitment can be achieved by the co-binding of TERRA (telomeric repeat RNA) G4 and telomere G4 which is done with the help of FUS (Fused Sarcoma) protein [54]. TRF2 and EWS proteins have also shown ability to co-bind TERRA G4 with the telomere G4[55, 56].

The formation of G4s in the telomeres persistently is a problem. Several proteins that interact with the telomeric sequence such as CTC1–STN1–TEN1 (CST) complex [57] and RTEL1 helicase [58], upon depletion would result in telomere shortening, altered telomere replication rate and/or formation of fragile telomeres due to stalled replication forks at telomeres[50]. Similarly, in the presence of G4 stabilizing ligands, these problems are worsened. When CST complex depletion is combined with the G4 ligand Pyridostatin (PDS) treatment, there is seen to be a sudden telomere loss [57].

Telomere dysfunction can be created either by inhibiting the telomerase activity or by the displacement of shelterin proteins. The G4 binding drug telomestatin was found to induce delayed growth arrest in cells by inhibiting the function of telomerase and blocking the telomere elongation step [59]. The telomeric G4 formation can restrict the access of telomerase. Formation of anti- parallel intramolecular telomere DNA G4s, prevents telomere extension by limiting access to the 3’ end of the telomere to telomerase [60], however, conversely the formation of parallel intermolecular telomere DNA G4s can be extended due to partial G4 resolution by telomerase *in vitro* [61]. This is corroborated in Saccharomyces cerevisiae, parallel telomeric G4 stabilization by the telomere elongation protein Est1 is essential for telomerase recruitment [62]. Furthermore, in S phase, when G4s can co-localize with human telomerase, intermolecular G4s between sister chromatids have been hypothesized to form[61].

BRACO-19 could trigger DNA damage response at the telomeric end by uncapping the telomeric structure. This was done by displacement of TRF2 and POT1 proteins leading to cell cycle arrest, apoptosis and sensescence [63]. Many other G4 drugs have shown the capability to displace the

shelterin complex proteins from the telomere ends leading to ATM kinase activation, chromosome fusions and cell apoptosis which are detailed in the next chapter.

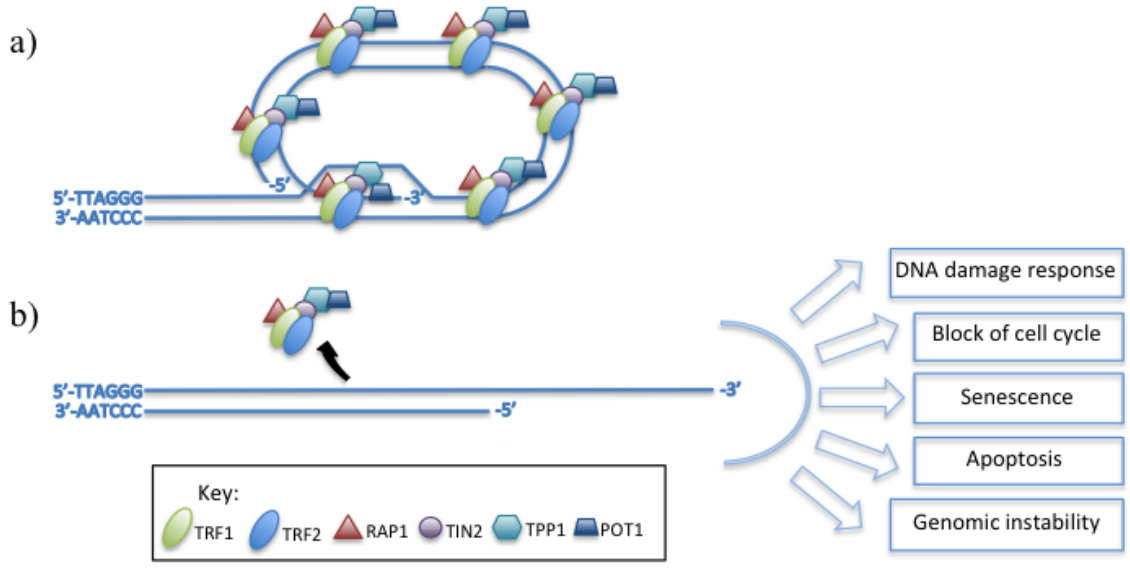

Figure 4: Schematic representation of the (A) telomere at its closed state in the presense of the shelterin proteins TRF1, TRF2, POT1, RAP1, TIN2, TPP1. When the shelterin proteins are delocalized from the telomeres (B) telomere dysfunction occurs leading to DNA damage response, blockage of cell cycle and cell death [64]

1.C.2. Gene Regulation

It has been found that more than 40% of human genes contain pG4s (potential G4s) near their promoter regions which suggests their role in regulating gene expression [3]. The regulatory potential of G4s towards cancer cell growth is strongly substantiated by their possible formation in the promoter regions of several human genes (such as the retinoblastoma susceptibility, insulin, muscle-specific, vascular endothelial growth factor, hypoxia inducible factor 1α, fragile X mental retardation genes5b) and oncogenes (such as c-myc, k-ras, bcl-2, c-kit, or RET oncogenes) [65]. Several instances of using small molecules or synthetic oligonucleotides targeting G4s for modulation of genes are known. For example, in a zebrafish model, Putative G-quadruplex sequences (PQS)s were identified in certain developmental genes and were targeted by G4 binding ligand TMPyP4 and G4 sequence specific oligonucleotides. This led to lower transcription of the targeted genes and the formation of a zebrafish phenotype consistent with the targeted gene morphants [66]. It is considered the first work to show the importance of G4s *in vivo* in embryonic development.

It is seen that G4s structures form in transcriptionally active chromatin in human cells through data from (i) G4 chip seq data[29], (II) genomic binding sites of the transcriptional helicases XPB and XPD[33] and transcription factor Sp1, and (III) colocalization data of G4 antibodies BG4 or IH6 with transcriptionally active regions [29]. Apart from the roles of G4s in the transcription regulation of oncogenes, they also play a role in the translation regulation. G4s are known to form in mRNAs and are present in the 3’ or 5’UTR regions which can help regulate their ability to form proteins (Figure 5) [67].

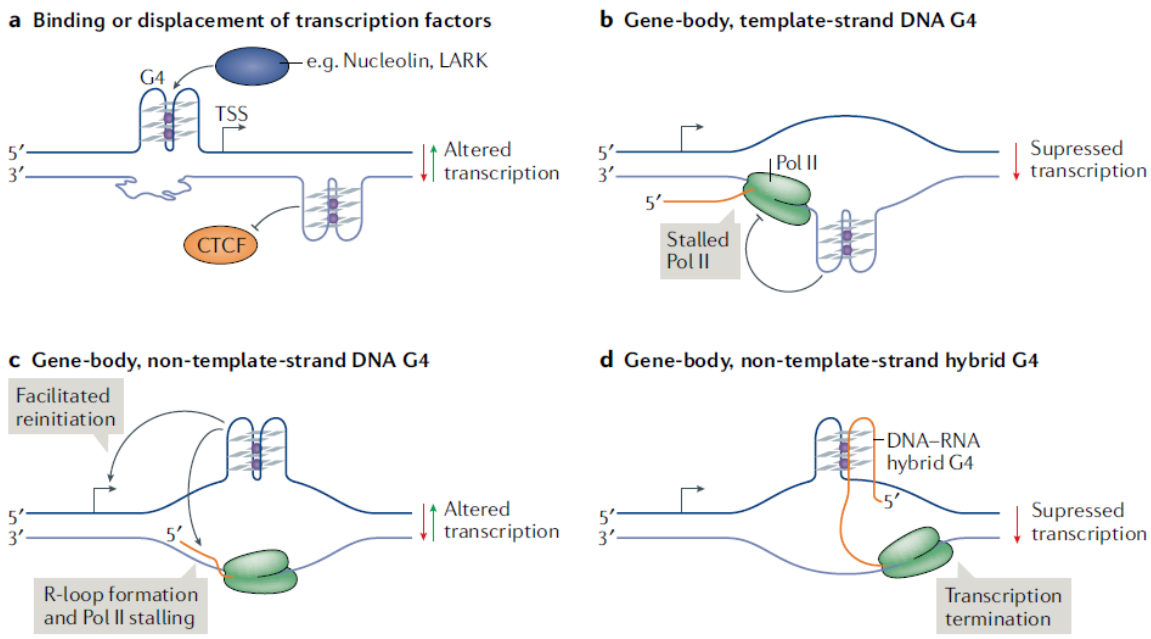

Figure 5: These are the different models of G4s influencing transcription. (A) G4 being present upstream of TSS leads to recruitment of transcription factor. (B) G4 being present in the template strand can lead to transcription stalling. (C) G4 being present in the non-template strand can help transcription re-initiation and (D) formation of DNA-RNA hybrid G4s formed between non-template DNA strand and nascent RNA can lead to premature transcription termination [68]

1.C.3. Genetic Instability

G4s are formed when DNA single strands are exposed during replication or transcription, which can cause replication-stalling leading to the use of G4 helicase. G4 DNA can be resolved using the RecQ family of helicases such as WRN and BLM, moreover ChIP seq analysis of human helicases XPB and XPD of the regular transcription factor complex shows that they bind to G4 motifs (40% of their total binding sites) [33]. Deficiencies in WRN and BLM helicases can cause diseases such as Werner and Bloom syndromes[33]. The first suggestion of G4s causing genetic instability was studied on *Caenorhabditis elegans* where they showed that DOG-1 helicase suppressed the genetic deletions that occurred in G-rich sequences. DOG-1 was shown to be a worm ortholog of human FANCJ. FANCJ was shown to be a structure specific DNA helicase that had the capability to unwind G4 DNA with 5'-to-3'direction. Patients lacking FANCJ helicase are shown to have large genomic deletions that contain pG4s [69].

The involvement of G4 DNA in genomic instability and site-specific DNA damage, has led to a suggestion that a combination of G4 ligands either with inhibitors of DNA repair or associated pathways could be an efficacious strategy for consideration in the future treatment of tumors. RHPS4 has a synergistic effect with camptothecin in solid tumors [70], WRN helicase inhibitor, NSC 19630, sensitizes cancer cells to the G4 ligand telomestatin [71], G4 ligand PDS acts synergistically with NU7441, an inhibitor of the DNA-PK kinase crucial for non-homologous end joining repair of DNA double strand breaks [36].

1.C.4. Replication Origin

DNA replication is a carefully regulated cellular process and is initiated at thousands of loosely defined genomic sites called DNA replication origins. In recent times, human replication origins were mapped by deep sequencing of short nascent strands and were predicted to contain G4 motifs [72].

Since a high number of G4s are considered to be replication origins, which could mean that components of origin recognition complex can identify G4s. During G1, the chromatin is filled with pre-replication complexes (pre-RCs) that cannot function due to the lack of certain kinases during that phase. At S phase, on activation of CDKs (Cyclin Dependent Kinases) and other kinases, the pre-RCs are activated and then released from the chromatin to avoid re-replication.

Potential G4s (pG4s) may be involved in these events. There are a number of reasons to support the statement [73]. Pre-RCs formation is favored in nucleosome depleted regions; pG4s tend to exclude nucleosomes. Formation of G4s can help in DNA unwinding that can initiate replication. Moreover, it is also found that origin replication complex (ORC) binds to G4s formed on RNA or ssDNA [74].

1.C.5. Mitochondria

Mitochondria are of interest in the study of G4s as it has been seen that the mitochondrial DNA has potential G4 forming sites. Mitochondria are cell organelles having a double membrane structure and play numerous crucial roles in cell biology. These organelles are involved in bioenergetics signaling, apoptosis, calcium signaling, and immune innate signaling. It is known as the powerhouse of the cell and due to it being the hub of cellular metabolism. Mitochondria is also involved in a host of other functions such as heme biosynthesis, iron-sulfur cluster biosynthesis, branched chain amino acid biosynthesis, fatty acid biosynthesis and catabolism, the Kreb's cycle, and high efficiency ATP production through oxidative phosphorylation (OXPHOS). During OXPHOS, electron transport coupled proton (H+) translocation across the inner membrane into the intermembrane space generates an electrochemical gradient that is harnessed by Complex V to catalyze the ATP synthesis (Figure 6A) [75].

The human mitochondrial genome is a double stranded circular DNA of 16,569 nucleotides that encodes 13 proteins essential for OXPHOS function, as well as the 22 tRNAs and two rRNAs required for their translation (Figure 6B) [76]. The other proteins involved in OXPHOS are encoded in the nucleus, translated in the cytoplasm and imported into the mitochondria. Mitochondria contain multiple copies of their genome ranging from ~100 to ~100000 copies in somatic cells[77].

The mtDNA is more vulnerable to damage compared to the nuclear DNA as only Base Excision Repair has been noted to work in mitochondria [78]. The mammalian mitochondrial genome shows significant asymmetry in strand composition with a two-fold enrichment of guanines on one strand. This enrichment of guanines contributes to the higher PQS density in the

mitochondrial DNA compared to the nuclear genome. In a recent in silico study, PQS per kb in the human mtDNA is estimated to be 2.4 to 3.6-fold higher than in the nuclear DNA [18]. During replication and transcription, the DNA strand rich in PQS sequences is temporarily single stranded, which suggests an increased opportunity to form G4 structures. Moreover, due to the high potassium concentration in the matrix which is estimated to be 150 mM, the mitochondrial environment would be permissive to G4 formation[79].

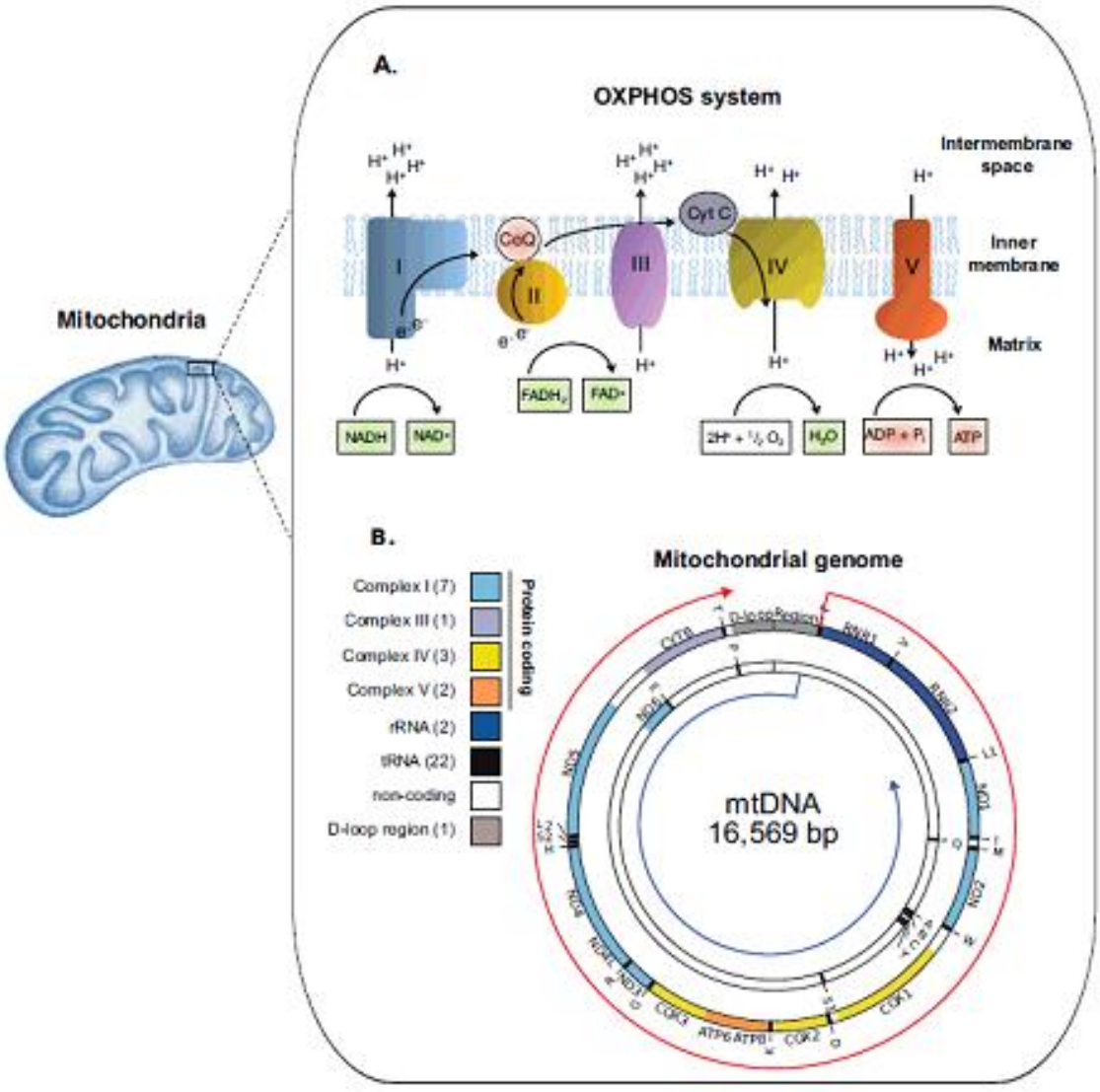

Figure 6: Schematic representation of the (A) mitochondrial oxidative phosphorylation system and the (B) mitochondrial genome [75]

Among the various sequences that form secondary structures, PQS had the strongest correlations with the deletions observed in the mitochondrial genome. Moreover, the enrichment of PQS in the displaced strand during mitochondrial replication, which forms the template for the synthesis of the second strand, shows that G4 stabilization inhibit replication and can play a regulatory role in mtDNA depletion [80, 81]. Since, QFP are found in both RNA sequences and transcription templates, the formation of G4 structures may also regulate mitochondrial transcription elongation[75].

The importance of targeting mitochondria in cancer cells is based on the ability of mitochondrial dysfunction inducing increased Reactive oxygene species (ROS) and apoptosis. The mitochondria of cancer cells have a higher mitochondrial membrane potential than the mitochondria of normal cells rendering them more susceptible to anti-mitochondrial agents and offers an opportunity for selectivity. Certain G4 drugs have shown mitochondrial targeting capability such as RHPS4 [82]. Metal complexes have also been shown to target mitochondria like cisplatin and a host of other metal complexes [83]. Platinum metal drugs in particular suffer from several cons such as side-effects, toxicity and an acquired resistance, however, mitochondrial targeting agents overcome this resistance are selective for tumor cells, hence, there is considerable interest in the search of discovering metal complexes that can target mitochondria.

2. G-quadruplex binding drugs

2.A. Definition

Since G4 structures are featured throughout the genome and have potential roles in all aspects of the central dogma (replication, transcription & translation), investigation of ligands binding to these structures and influencing their role has been studied ever since Neidle reported that the telomeric G4 can be targeted by aromatic compounds from the anthraquinone family [84]. G-quadruplex binding drugs are able to induce anti-proliferative properties by either blocking cell replication, transcription, translation or impairing telomere stability [12, 59, 85-87]. The main interactions of the ligands and G4s are through π-π stacking and electrostatic interaction between the ligand and the external G-quartet face of the G4. Due to the relatively large size of the G-quartet, the ligand needs to be an aromatic compound with a large surface area to provide better aromatic-aromatic overlap and specificity. The central cation of the metal complex G4 ligands are known to provide the positive charge that would help to stabilize the G4 structure but more research needs to be done to understand its role in ligand binding. The specificity of the ligands to bind to G4 sequences are evaluated biophysical methods such as FRET and FID assays with different G4 sequences, as mentioned in the previous chapter.

2.B. Classes of G-quadruplex binding drugs

The various series of G4 binding ligands can be classified into different categories based on several factors, in this thesis the classification would be done based on their chemical scaffold. The four categories are:

1. Condensed Heteroaromatics
2. Macrocycles
3. Unfused bisquinoliniums
4. Metal complexes

We will discuss each category with some examples of prominent G4 ligand members and give their most important biological effect.

2.B.1. Condensed Heteroaromatics

While most ligands from this group was developed by addition of two or three cationic chains with the aim of targeting the grooves of G4s in order to enhance selectivity for G4s over duplex DNA, it was essentially revealed that the main binding mode of G4 ligands is the π-π interaction between the ligand and the external quartet of the G4.

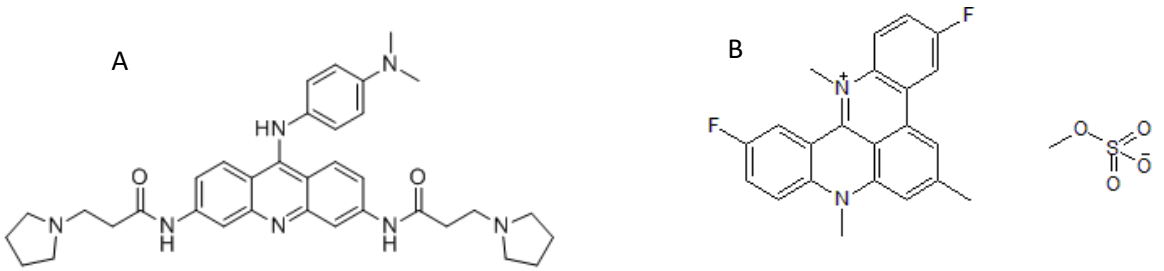

Figure 7: Chemical structure of (A) BRACO-19 and (B) RHPS4

BRACO-19 -

One popular examples of this category are the trisubsituted acridine BRACO-19 (Figure 7A). In a structure activity relationship (SAR) study showed that an anilino substitution in position 9 inferred a greater G4 selectivity[88, 89]. BRACO-19 is shown to target the human telomeric sequence *in vitro* at a 60x higher binding affinity compared to the control hairpin DNA sequence[90]. BRACO-19 is also shown to be preferentially bound at the interface between two parallel G4s from telomeric sequence, sandwiched between a G-tetrad surface and a TATA tetrad, as shown in figure 8 [88]. The TATA tetrad is constructed from the 5'-TA ends of two strands of one quadruplex.

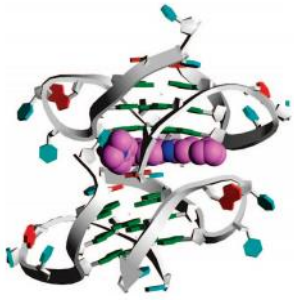

Figure 8: The BRACO-19 molecule is shown, in mauve color, at the interface of two quadruplexes, a G4 on top and a TATA tetrad at the bottom [88].

BRACO-19 has shown an anti-proliferative effect on glioblastoma cells and can target telomeres inducing DNA damage response leading to p53 and p21 mediated cell arrest, apoptosis and senescence [63].

RHPS4 –

Another important member of the category is the ligand RHPS4 (Figure 7B) which is part of a pentacyclic acridinium salt series developed as an analogue of a natural ligand Necatarone [91]. The biological effect of RHPS4 was discovered in 2001 when it was shown to be a telomerase inhibitor in *in vitro* conditions and could inhibit cell growth in breast cancer and vulval carcinoma cell lines at non-acute cytotoxic concentrations. It was also shown to inhibit cell growth in a cell line using the ALT pathway instead of telomerase to maintain telomere length [92]. Several other studies have commented on RHPS4's ability to bind to telomeres, induce telomeric damage and inhibit cell survival [93].

RHPS4 is capable of inducing radiosensitization in a glioblastoma cell line using X-rays[94] and carbon ion beams [95] and the mechanism of action is hypothesized to be due to the drug induced telomeric damage before irradiation along with delayed DSBs repair, increased chromosomal aberrations and a G2/M cell cycle block in cells. RHPS4 along with irradiation is also able to inhibit growth of a heterotropic GBM xenografted tumor in mice for a period of 65 days[96]. However, RHPS4's radiosensitization potential was not observed in Glioblastoma stem like cells (GSCs) that are hypothesized to be the reason of recurrence in GBM tumors. In spite of that, RHPS4 is still able to induce a strong reduction of GSC proliferation by impairing its replication stress response and DNA repair[96].

RHPS4 is also able to target mitochondria as is shown by the work by Falabella et al [82] through its G4 binding properties. RHPS4 is seen to be localized to the mitochondria at low sub-toxic concentrations and can inhibit mtDNA transcript elongation. It is also able to inhibit mtDNA levels and synthesis both in cells and in isolated mitochondria. It is also shown that in a mtDNA sequence variant that has an increased G4 formation and stability characteristic, due to the presence of an extra G in the G-rich stretch, RHPS4 can create higher respiratory defects signifying its mitochondrial targeting is via G4s.

2.B.2. Macrocycles

Macrocycle compounds are a relatively small category but within it rests one of the most important G4 ligand, namely Telomestatin (Figure 9).

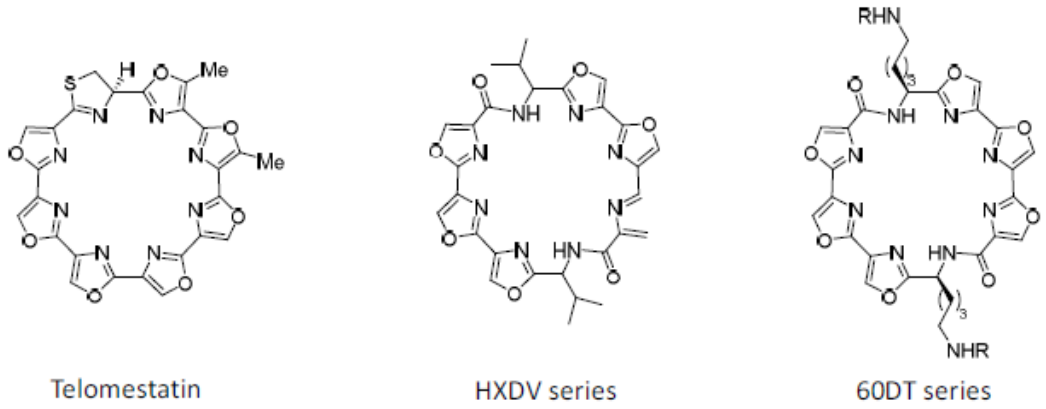

Figure 9: Chemical structures of different macrocyclic compounds

Telomestatin –

It has a polyheteroaromatic ring structure with 24 member ring and was first discovered by Shin-ya [97] in a screening test for telomerase inhibitors, however it was seen that *in vitro* it was more potent than every other known telomerase inhibitor. It was also capable of binding to telomeric G4 with high selectivity than some of the known G4 ligands such as TMPyP4 [98, 99]. The binding strength of Telomestatin to telomeric DNA is strong even though the binding parameters have not been studied. It is seen that the interaction of the ligand to telomeric DNA is based solely on hydrophobic and Van Der Waal's forces, however, some studies have commented that telomestatin could form a coordinate bond with the K+ cation explaining its uncanny high affinity [100, 101]. An interesting characteristic of this ligand is its complete lack of affinity for duplex DNA, presumably due to its neutral charge and steric hindrance due to its structure. In cancer cells, telomestatin not only inhibits telomere elongation but also induces TRF2 loss from telomeres and is shown to cause anaphase bridge formation [102].

Telomestatin was one of the first ligands to be studied intensively *in cellulo*. It induces replication stress in Glial stem cells by uncoupling the protein TRF2 from the telomeric ends [103]. The hypothesis regarding the dissociation of TRF2 proteins is that, since TRF2 binds to double

stranded DNA, stabilization of the telomeric G4 using telomestatin can block the binding of TRF2 to the DNA. Telomestatin can also inhibit telomerase activity inducing cell cycle arrest but this process takes time, as it would need to involve multiple mitosis [104]. Uncoupling of TRF2, however, is much faster and provides a quicker response.

Some other members of this category are the **HXDV** [105] and the **6ODT** [106] series. They were developed since telomestatin is reportedly hard to obtain [107] and its proposed synthesis pathway doesn't seem compatible with large scale production [108]. HXDV Is seen to greatly stabilize G-quadruplex structure, without any significant action on duplex- or triplex-DNA, and to have a high cytotoxicity against cancer cell lines [109]. 6ODT is also a high affinity binder of G4 telomeric sequence and shows a high selectivity of G4s over duplex DNA.

2.B.3. Unfused bisquinoliniums

The bisquinoliniums series contains some very popular G4 ligands such as 360A (also known as PDC), PhenDC3 and PDS (Figure 10).

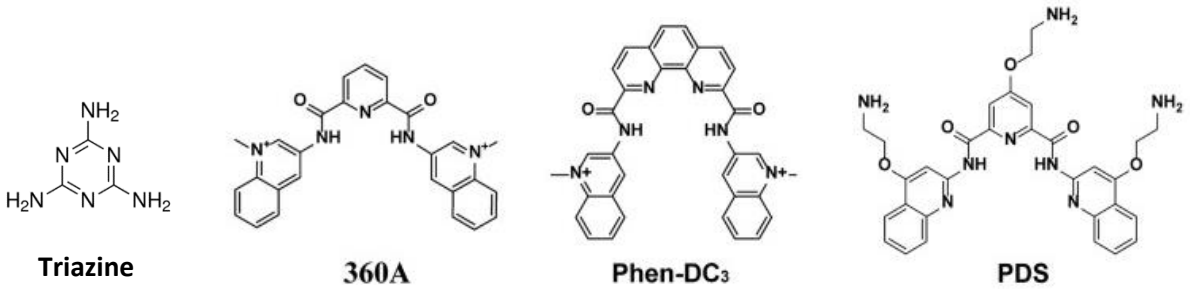

Figure 10: Chemical structures of the popular members of the unfused bisquinoliniums category [110]

360A, which is also known as PDC (Pyridine Dicarboxamide core) is created from the triazine series by making some modifications. The triazine series was the first series that has shown a direct evidence of telomere shortening with cells following telomerase inhibition [59]. In order to improve the G4 affinity, the N-C bonds was replaced by an amide bonds and the central triazine by a pyridine unit. 360A is seen to be selective for G4 sequences over duplex DNA with a potent selectivity for the telomeric 3' overhangs. Metaphase spread from cells treated with 360A has shown the drug to be present at the metaphase terminal regions showing its high selectivity for

telomeric G4s [111]. 360A induces the degradation of telomeric 3' overhangs and activates a DNA damage signaling in an ATM-dependent manner in cancer cells suggesting that 360A destabilizes telomere structure and induced specific telomere instability[112, 113]. Both DSB repair pathways Homologous Repair (HR) and Non-Homologous End Joining (NHEJ) are involved in the telomeric aberrations induced by 360A [114].

Phen-DC3 was created by replacement of a the PDC core by a more rigid extended core like phenanthroline dicarboxamide that show a perfect geometrical match with a G-quartet. The selectivity of the Phen-DC series for G4 [115] and its affinity for the telomeric G4 sequence [116] is seen to be higher than that of telomestatin and 360A respectively. Phen-DC3 is capable of inhibiting the unwinding of the human minisatellite DNA CEB1 which can form a G4 by inhibiting the PIF1 G4 helicase in yeast [117]. *In vivo* it is also capable of forming recombination dependent rearrangements in CEB1 DNA in yeast. Phen-DC3 also inhibits the protein nucleolin from binding to G4s [116] which can lead to physiological changes such as in the case of the Epstein Barr virus where Phen DC3 and a one of its derivative could increase the expression of a protein that helps in the recognition of the virus by the immune system [118, 119]. Both Phen-DC3 and Phen-DC6 are potent molecular tools for probing the formation of G-quadruplexes *in vivo*, interfere with their processing and elucidate their biological roles.

PDS (Pyridostatin) combines the PDC core with three cationic amino terminated side-chains distributed on the central pyridine and two quinoline units [120]. It shows a high selectivity of G4s over duplex DNA and its binding affinity to Telomeric G4 is between Phen-DC3 and 360A [121]. In cells it is shown to target telomeres by inducing telomeric dysfunction and long term growth inhibition [122] and also by uncapping the shelterin protein POT1 resulting in a DNA damage response [120]. Moreover, a γH2AX ChIP sequencing post PDS treatment showed that its targets on the genomic DNA have clusters of sequences with G4 potential. One example is that of the proto-oncogene SRC that is identified as a target for PDS as the drug treatment reduces the protein in the cells and inhibits SRC mediated cell motility[36].

2.C. Metallo-Organic ligands

Metal complexes as small molecule G4 ligands are studied as they can bind strongly and selectively to G4 structures [123-125]. The ease of synthesis and controlled variation (changing the ligand/ metal atom) makes it more advantageous than its organic counterparts (Figure 11).

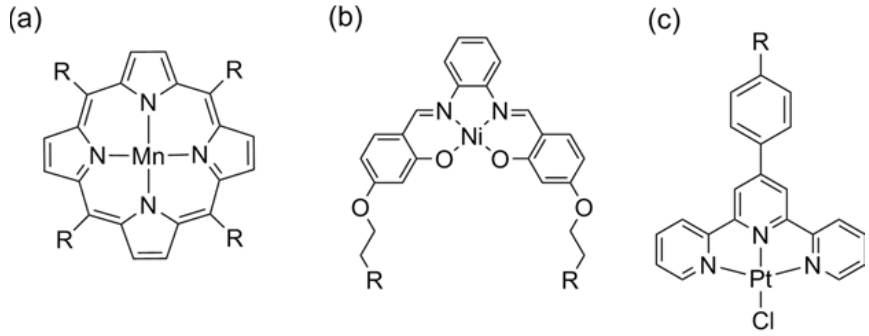

Figure 11: Chemical structures of the first classes of metal G4 binding complex series. (A) metal-porphyrins, (B) metal- salphens and (C) metal- terpyridines [124]

In metal-complex ligands, the metal atom is the central locus that helps to organize ligands into a specific geometry such as octahedral, square based pyramidal, square planar, etc; and orientation for effective G4 binding. It is also able to reduce the electron density in the ligand around the metal allowing it to make stronger interaction with the external G-quartet. The metal in the ligand can also substitute the alkali metal (K+/Na+) that is stabilizes the G4 leading to a stronger association[123]. Apart from the advantages of the metallic cation and the π-π interaction of the ligand with the G4, platinum complexes (Pt(II)) are also able to coordiante directly to purines thereby causing a stable adduct and irreversibly trapping the G4 [126-128]. There are various kinds of metal-complex ligands belonging to different ligand series however, only a select few would be discussed in this thesis belonging to the metal- porphyrins, metal-salphens and metal- terpyridines.

2.C.1. Metal-porphyrin series

The earliest G4 metal complexe was the metal-porphyrin series which was derived from its flagship ligand TMPyP4 (tetra mesomethylpyridinium porphyrin) (Figure 12). It is one of the most studied G4 metal complex even though it has a poor selectivity of G4 over duplex DNA. The complex had first shown G4-htelo sequence stabilization by end stacking and inhibiting telomerase activity [129].

Several modifications were done on the complex to improve its G4 binding affinity and selectivity (Figure 12). It was seen that the Mn^{III} porphyrin complex showed a 10,000-fold increase in its selectivity for G4s [130]. Another complex from the series Ni^{II} porphyrin with four phenyl guanidinium substituents, has high *in vitro* affinity for telomeric G4 DNA, is able to displace hPOT1 from telomeres, and has a moderate antiproliferative effect on A549 (Adenocarcinoma) cells [131]. Se2SAP, an analogue with a modified core showed that it can bind to the G4 in c-MYC promoter in order to silence its transcriptional activity. This complex showed greater selectivity and a 40-fold increase in stabilization of the G4 than its counterpart TMPyP4 [132].

Figure 12: Chemical structures of complexes from the porphyrin series – TMPyP4, Ni^{II} porphyrin and Mn^{II} porphyrin

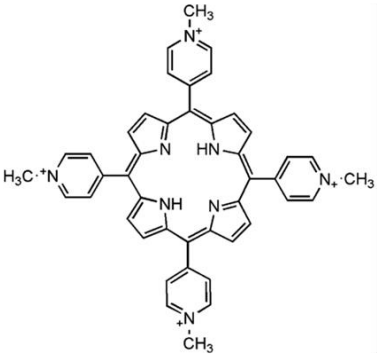

TMPyP4

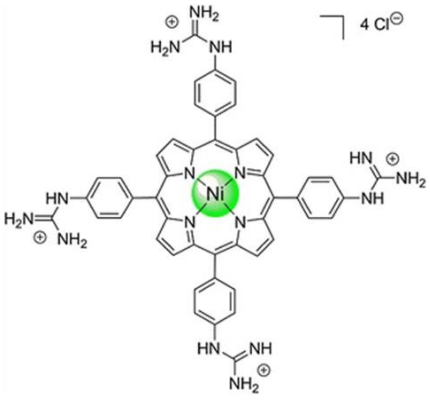

Ni^{II} porphyrin

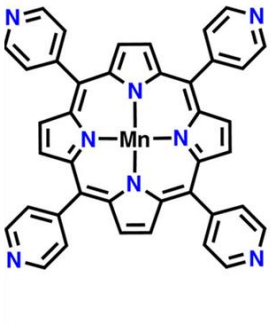

Mn^{III} porphyrin

2.C.2. Metal-Salphen series

Salphen series complexes as G4 binders were first reported by R. Vilar[133] (Figure 13). They are planar structures (due to coordination of the metal center) and their appropriate spacing makes these metal complexes very efficient G4 stabilizers, such that they are able to inhibit telomerase at low micromolar concentrations. The relative ease of their synthesis and structural stability makes it easy to generate libraries of these complexes. The size, geometry and electronic properties can be modified by changing the metal center. Some of the metals used are Ni^{II}, Cu^{II}, Pt^{II} and Zn^{II} [133, 134]. X-ray crystal structures of metal-salphens bound to a parallel bimolecular quadruplex show that the corresponding metal center (either Ni^{II} or Cu^{II}) is positioned almost in line with the channel formed by the K+ ions bound to the G4 structure. This confirmed the initial design principle that a metal complex would be better suited to interact with G4s than purely organic species[135].

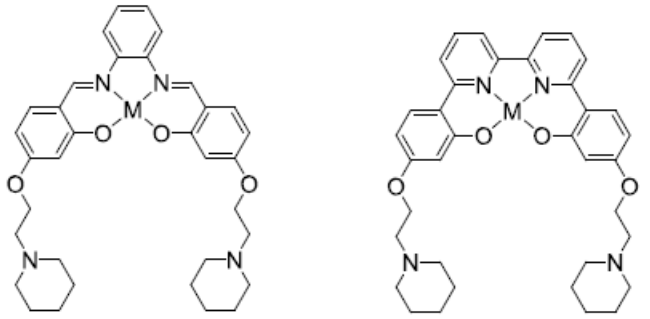

Figure 13: Chemical structure of ligands of metal-salphen and derivatives series. The numbers associated with the ligands are corresponding to the metal inside the structure [135]

A large number of members of this metal-salphen series have shown high affinity towards G4 DNA such as telomeric and c-myc sequences[124]. In one study by Ramon VIlar's lab [136], 5 different metal-salphen complexes were studied and it showed that one Ni^{II} salphen complex (4) had higher G4 affinity over others.

2.C.3. Metal-Terpyridine series

Terpyridine metal complex ligands are G4 stabilizers that can have different metal atoms such as Cu, Pt, Pd, Zn and Ru [137-140]. The metal terpyridine series is designed based on the coordination of a transition metal cation to a terpyridine (tpy derivatives) or an extended tolyl-terpyridine (ttpy-derivatives). The central metal ion, the number of aromatic rings, as well as the number and position of the substituents on the terpyridine scaffold play critical roles for G4 recognition and stabilization[123]. A series of comparative studies of metal–terpyridine complexes demonstrated that the binding affinity and selectivity for G4 DNA depend mainly dependent on the geometry of the complex and must exhibit at least one planar aromatic surface accessible for π–π stacking interactions with G-quartets with a square planar geometry (Figure 14) . For example, the non-planar structure with Zn show poor binding compared to the planar structures of the Cu(II) and Pt(II) complexes[139, 140].

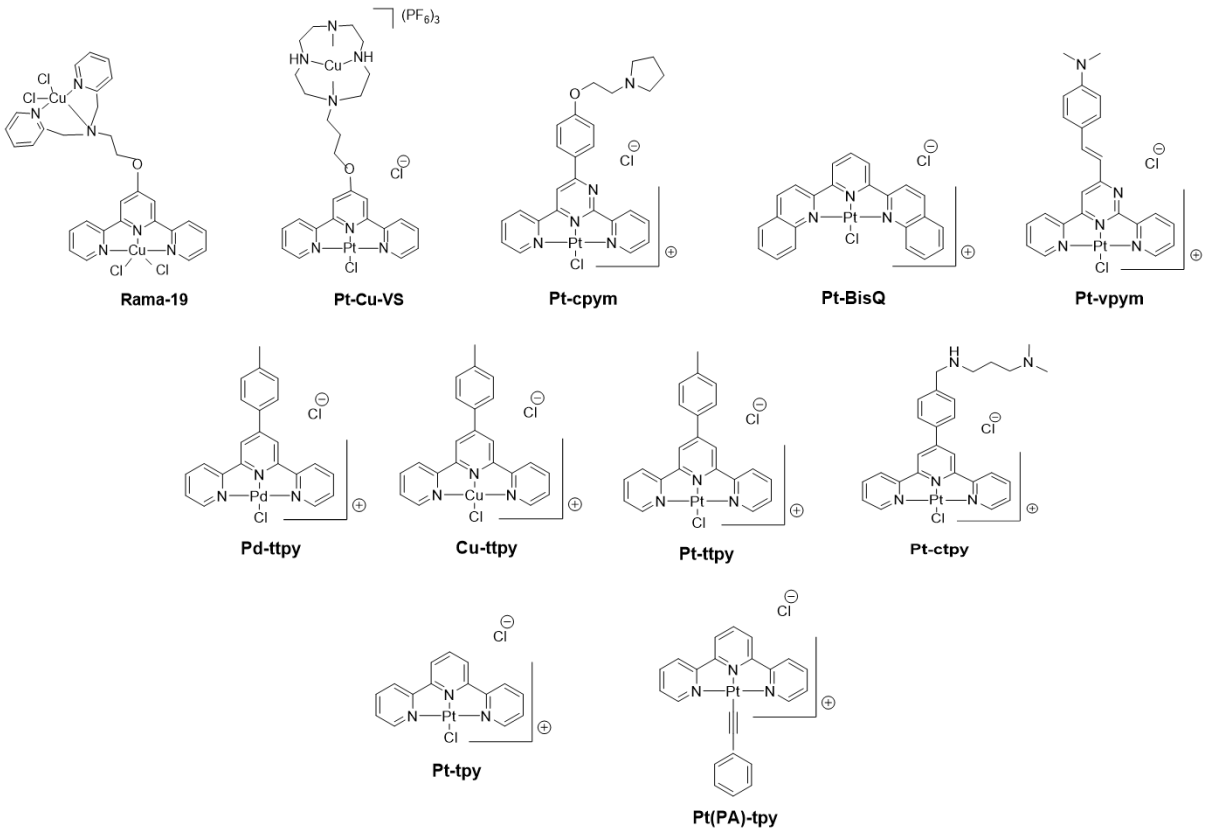

Figure 14: Chemical structures of the various members of metal-Terpyridine series.

The presence of Pt atom leads to a direct coordination of the compound to G4 DNA providing additional anchorage. Pt-ttpy (figure 15A) is capable of making a covalent bond to the adenine residues located in the loops of telomeric G4 [126]. The adenine of the 5‘end as well as one guanine of the external G-tetrad of the c-myc G4 (CMA) [141]. It is seen to bind the G4 at both tetrads by NMR. Cu-ttpy, on the other hand does not bind covalently to the G4, the metal atom probably is placed directly over the quadruplex ion channel and its shape impedes the intercalation of the compound with duplex DNA [140].

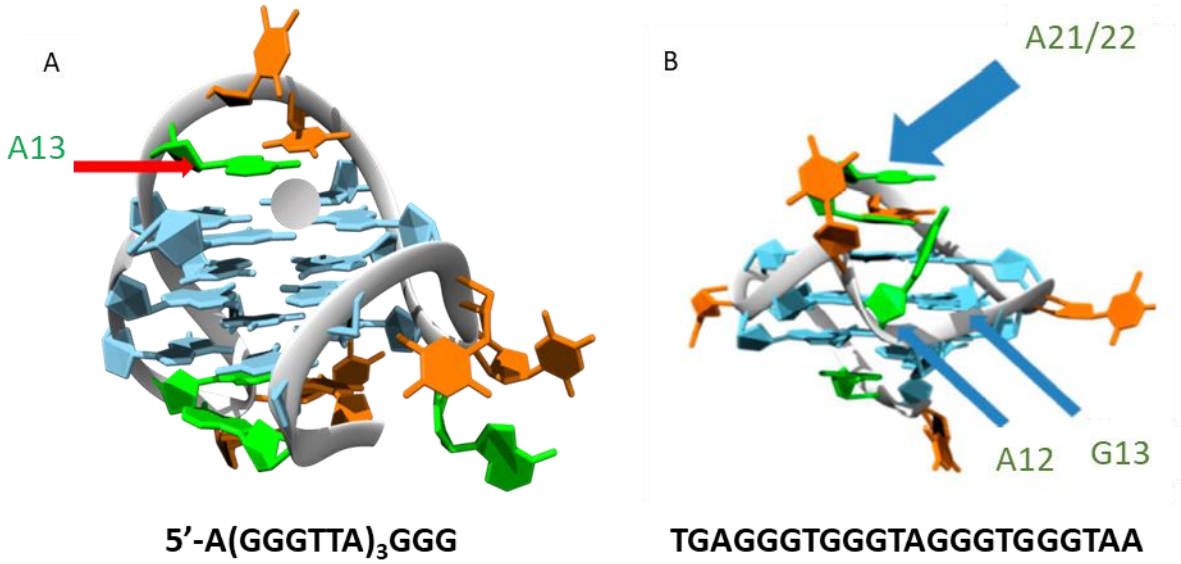

Figure 15: The platination sites of Pt-ttpy on (A) the loop of telomeric G4 sequence and (B) the c-MYC G4 sequence [142] (Annex 1).

The biological effect of metal terpyridine ligands such as Pt-ttpy and Pt-ctpy have been studied and show that they are capable of targeting telomeres [127, 143]. Pt-ttpy has been shown to be covalently bound to telomeric DNA, through quantification by ICP-MS (Inductively Coupled Plasma Mass Spectrometry), in an amount similar to genomic DNA in a G4 independent manner [127]. However, Pt-ttpy is able to induce telomere dysfunction and deprotection by uncoupling TRF2 from the telomeres, suggesting that the non-covalent binding of Pt-ttpy by G4 recognition is involved in this action. Moreover, in the lab it has also been shown that Pt-ttpy induced γH2AX foci elsewhere in the genome and the identification of the damaged sequences has been performed using ChiP-sequencing method. The results show that, in contrast to the PDS ligand

that induce damages mainly in oncogene promoters, Pt-ttpy induced damages mainly in G- and A rich tandemly repeated sequences found in satellite DNA, rDNA and pseudogenes regions but they are not specifically located on potential G4 forming sequences (publication pending submission in Annexe 2). In addition, Pt-ttpy has been shown to induce chromosome loss which is co-related to telomere associated DNA damage [144].

Pt-ctpy was shown to be a radiosensitizing agent in glioblastoma and non-small cell lung carcinoma cell lines. It is hypothesized that this ability is due to the telomeric damage induced by the complex in presence of irradiation[143]. In this thesis, we will show that Pt-ttpy has also a high radiosensitization potential and will decipher its mechanism of action.

2.C.4. Hybrid Pt-G4 complexes

It is seen that addition of a metal, like Platinum, to already established G4 ligands could help in the biological efficacy of the ligand. The strategy is to combine a classical G4 ligand to afford specific π-stacking and a platinum moiety for coordination to nucleobases so that the new complex can then bind irreversibly to their G4 target. This would allow interaction of the hybrid complex with G4 through a double noncovalent/covalent binding.

For example, combining acridine [145, 146] or quinacridine [128] (MPQ) with a Pt metal complex using suitable linkers showed the proof of concept *in vitro*. In addition, *in cellulo*, Pt-MPQ shows telomeric dysfunction by displacement of two telomeric proteins (TRF2 and TRF1) from telomeres, and by the formation of telomere damage and telomere sister losses [147] whereas the G4 binding MPQ does not.

Then a stronger G4 ligand, PDC (Pyridodicarboxamide) was combined with Pt-NHC (Pt-containing N-Heterocyclic Carbenes) with linker chains of various lengths to form the Pt-NHC-PDC complexes (work from the laboratory in collaboration) (Figure 16). PDC are known to bind to telomeres and cause telomere dysfunction [111]. Pt-NHC are trans- square planar Pt series that has shown anti-proliferative properties on both cisplatin sensitive and resistant cell lines [148]. This trans geometry was chosen in order to induce different DNA lesion (intrastrand GNG or interstrand DNA crosslinks) than cisplatin that induce mainly platinum adducts between two adjacent

guanines (GG adduct) and consequently could counteract some cell resistance with cisplatin [149] and be less recognized by DNA repair machinery [148].

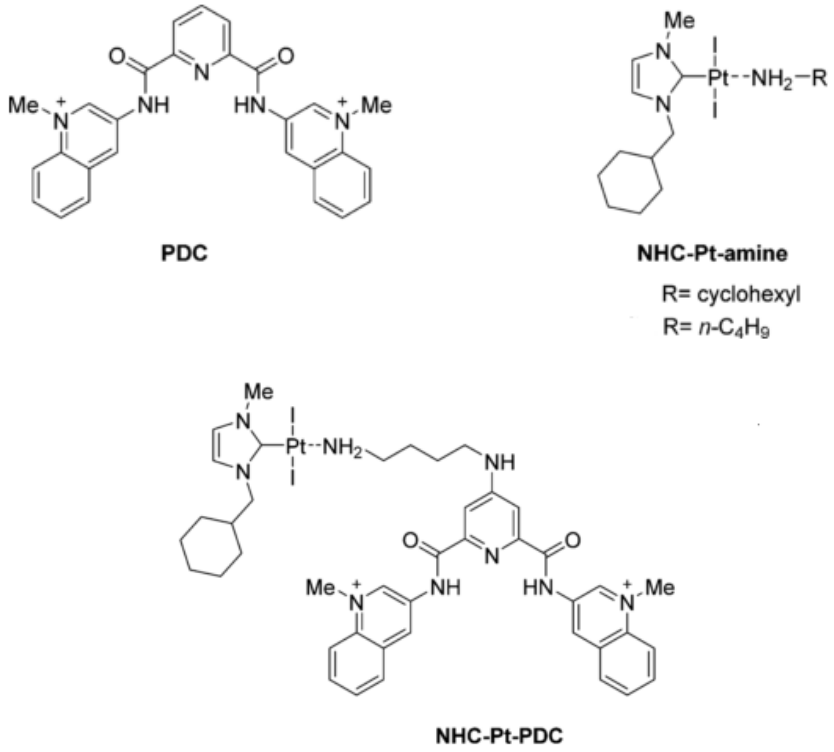

Figure 16: The chemical structure of PDC (360A) and Pt-NHC and the hybrid ligand Pt-NHC-PDC [150]

This Pt-NHC family has been developed such as the mononuclear and dinuclear complexes possibly in order to favor interstrand crosslinks. This property has been shown *in vitro*. In addition, even if they induce cytotoxicity at a higher concentration than cisplatin in different cancer cell lines, they do not cross react with cisplatin, making them potential drugs for anticancer therapy. In ovarian cancer cells, the mono (3) and bimetallic complex (5a) compounds (as shown in the figure 17) accumulate more easily than cisplatin in A2780 cells, but the amount of DNA binding is lower than expected, with regard to their cell accumulation. The high level of accumulation might suggest that the two NHC complexes do not suffer to the same extent from the increased efflux mechanisms which operate in the case of cisplatin. Interestingly, the mono

or bimetallic Pt-NHC complexes do not show any cell cycle arrest whereas cisplatin shows a S/G2M accumulation. Moreover, they are seen to induce apoptosis in a caspase independent manner, predominantly through the translocation of AIF and caspase 12 to the nucleus [151].

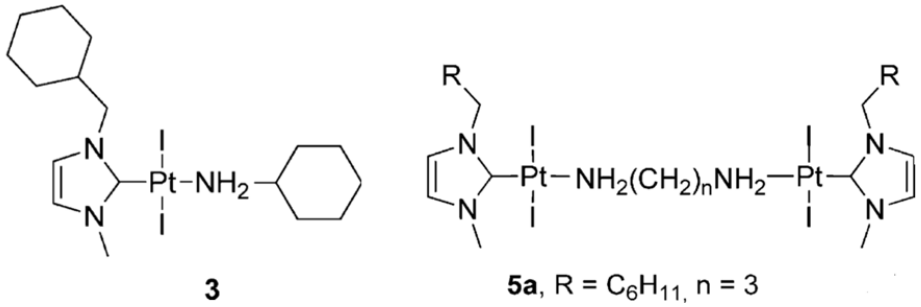

Figure 17: Structure of the Pt-NHC complex (A) mononuclear 3 and (B) dinuclear 5a [151]

Therefore, due to its efficient cytotoxicity Pt-NHC has been chosen to be combined with the efficient G4 ligand PDC [111]. They form a new class of metal complex ligands that can bind efficiently to G4s of telomeric sequences *in vitro* with metal coordination [150]. While the binding affinity for certain G4 sequences may be a little reduced compared to PDC, the hybrid complex retains the high selectivity of G4s over duplex DNA as PDC. Pt-NHC-PDC has different platination sites, but always in the loops of the structure (A7, A19, same side of the G4) than Pt-NHC (A7, A13 both sides of the G4) in the telomeric G4 *in vitro* suggesting that the ligand has got a preferential binding site on the G4 structure. The complex enjoys a higher accumulation in the cells and being bound to DNA compared to Pt-NHC. Bombard et al, have shown that the Pt-NHC-PDC complex has good cellular permeability and IC_{50} values of 8 and 15 µM on A2780 (Ovarian carcinoma cell line) and A2780cis (Ovarian carcinoma resistant to cisplatin), respectively. Interestingly, Pt-NHC-PDC complex is able to reduce 50% of the TRF2 foci in ovarian cancer cells compared to none from PDC and 30% in case of Pt-NHC. The displacement of TRF2 by this complex was significantly higher than its individual components suggesting an important synergistic effect between the coordinating Pt^{II} moiety and the G4-DNA binding group of the conjugate [150].

2.D. Biological effect of G4 drugs

Various G4 complexes have been known and extensively studied for their effect on telomeres as mentioned before. Some of them where shown to inhibit telomerase inducing reversible telomere shortening. They are also able to displace shelterin proteins TRF2 and or POT1 from the telomeric ends such as telomestatin, PDC, PDS and Pt-MPQ, Pt-NHC-PDC [36, 102, 111, 147, 150], leading to telomere damages, and/or telomeres shortening that can contribute to the cellular cytoxicity of these ligands. However, it has been shown that complexes being able to bind to telomeric ends do not necessarily dislocate TRF2 protein [127], However, even if TRF2 is removed from telomeric DNA, it does not necessarily lead to telomeric dysfunction, as has been shown with different Pt-complexes [147]. The mechanism of removal of shelterin proteins from telomeres following treatment by G4 ligand is not yet elucidated. It could arise from physical hindrance, such that the binding of the drug at telomeres could physically not allow the shelterin proteins to be bound. But, cisplatin is seen to induce TRF2 loss from telomeres without having the sufficient amount bound to telomeres to create a physical hindrance indicating that there could be alternate mechanisms as a form of biological regulation to DNA damage response [127].

Apart from targeting telomeres, G4 drugs also have other targets such as downregulation of oncogenes, inhibition of rRNA biogenesis, R-loop formation, inducing autophagy, etc [152]. I will mention a couple of drugs with these effects.

c-MYC transcription: QN-1, IZCZ-3 and TH3 are some of the G4 ligands that have shown the ability to downregulate c-MYC transcription. QN-1 can target the G4 structure within the c-MYC promoter and can selectively downregulate c-MYC alone, sparing other G4 driven oncogenes such as BCL2, c-KIT, VEGF and HRAS [153]. Another compound IZCZ-3, binds and stabilizes the c-MYC G4 and reduces its expression. This leads to a significant growth inhibitory effect by induction of cell cycle arrest at G0/G1 and apoptosis. It also did not have any effect on the other G4 driven oncogenes [154]. TH3 is a thiazole peptide that also binds and stabilizes the c-MYC G4 and shows a clear preference of this structure over other G4s such as c-KIT or BLC2 [155].

KRAS expression: Another important target of the G4 ligands is the KRAS oncogene. Two porphyrin derivates, Tetrakis and Octaacetyl were shown to strongly bind and stabilize the KRAS

32R G4 and inhibit its expression in two different pancreatic cell lines. It also hindered metastasis by arresting EMT (Epithelial to Mesenchymal Transition) which is a hallmark of pancreatic cancer [156]. The ligand C8 which is an acridine orange derivative also induced downregulation of the KRAS expression by targeting its G4 [157]. Another compound which is a anthrafurandione derivative is shown to target the KRAS mRNA G4 and downregulate the translation of the KRAS gene [158]. It induces apoptosis in KRAS addicted cells.

rRNA expression: Certain G4 drugs also target ribosomal DNA leading to an inhibition of rRNA biogenesis leading to apoptosis. CX-3543 [159] and CX-5461 [160] are two such drugs. They also show DNA damage and an *in vivo* tumor growth inhibition. The drug CX-3543 is currently in clinical trial phase II as a therapeutic candidate against several tumors. The drug CX-5461 is also currently in a clinical trial at an advanced Phase I stage for patients with BRCA1/2 deficient tumors [152].

DNA damage: G4 drugs such as pyridostatin and RHPS4 have shown to induce DNA damages and activate DNA repair pathways [36, 161]. Hence the use of repair pathway inhibitors in combination with the G4 drugs is an efficient therapeutic approach. Pyridostatin has been shown to synergize with NU7441, a DNA-PK inhibitor affecting the NHEJ pathway [162], It is also shown to be toxic to HR deficient cells that are resistant to the PARP inhibitor, Olaparib [163]. RHPS4 has also shown that combination with PARP inhibitor GPI 15427, there was a high reduction of growth in HT29 colon tumor mice xenografts compared to RHPS4 and GPI 15427 treatments alone [161]. Cancer cell that are deficient in BRCA2, important for the homologous repair pathway, are also seen to be sensitive to RHPS4 [163].

All these recent findings suggest that G4 ligands could be considered for cancer therapy due to their roles in telomere stability, gene regulation and genome instability particularly in cells with deficiencies in DNA repair. Even though great advances have been made in the knowledge of endogenous function of G4s and development of new interacting G4 drugs, we still need to pursue producing treatments using these drugs that would be useful in the clinic.

3. Radiotherapy

Radiotherapy (RT) is the use of irradiation to kill cancer cells. It is often accompanied by another form of treatment, either chemotherapy or surgery. Radiotherapy is used in more than half of cancer treatment regimens in the western countries and is an important treatment strategy for non-complicated locoregional tumors [164, 165]. In inoperable tumors, radiotherapy is often the most common and most effective treatment strategy. Apart from being an indispensable tool for curative intent, radiotherapy is also used in palliative treatments [165].

This form of therapy, however, is not without its limitations. The effects of tumor control versus normal tissue damage has been a point of concern since the beginning of radiotherapy studies which led to different treatment modalities. One such example is the introduction of fractionated irradiation for treatment. Moreover, with recent substantial technological advancement in 3D conformal radiation treatments, such as stereotactic (body) radiotherapy (SBRT), intensity-modulated radiation therapy (IMRT) and improved imaging systems (i.e., image-guided radiation therapy, IGRT), it is now possible to have precise delivery of radiation doses to the exact dimensions of tumor while minimizing radiation exposure of surrounding normal tissue [166]

3.A. Radiation

Radiation using in medical sciences for cancer therapeutics belongs to the category of ionizing radiation. Ionizing radiation is a type of energy released by atoms that travels in the form of electromagnetic waves (gamma or X-rays) or particles (neutrons, beta or alpha). They have sufficient energy to detach electrons from atoms or molecules, hence, ionizing them. Ionizing radiation injects energy into a material as it passes through it, like a microscopic bullet, until the radiation is stopped by the material due to absorption [167]. This can induce damages to DNA, irreversible or difficult to repair leading to cell death of reduction of the tumor. The radiation units have their own representation in the international system. The absorbed dose is the energy absorbed per unit mass of tissue as a result of an exposure to ionizing radiation. The international system of radiation absorbed dose is the Gray (Gy): 1 Gy = 100 rads = 1 joule/kg – joules are units of energy [168].

The type of radiation used conventionally is the photon radiation (for example gamma rays and X-rays). These are termed as Low LET irradiation. LET (Linear Energy Transfer) is used to indicate the average amount of energy that is lost per unit path-length as a charged particle travels through a given material. Low LET irradiation typically deposits 1000 tracks of electrons in the nucleus at the dose of 1Gy. This is completely different for high LET irradiation where there are 3-4 dense tracks of ionizations across the nucleus leading to a higher efficacy of direct action of damage compared to the indirect action [169].

Though photon radiation is the most common form used for radiotherapy, other methods of radiotherapy are getting prevalent as well. A lot of research has gone into developing proton based radiation in recent years [170]. Proton beam radiation aside, other heavy ion radiation techniques involve the use of helium ion, carbon ion and fast neutron radiation[171, 172]. The use of heavy ion radiotherapies is developed since they exhibit a distinct Bragg peak on interaction with human tissues (Figure 18). The Bragg peak is a pronounced peak on the Bragg curve that plots the energy deposition of a radiation particle on its travel through matter, for photons the Bragg peak is observed soon after its interaction with the solid matter, however for high ion particles it is noticed at a certain depth in the tissue. This phenomenon is exploited to target tumors located at a certain depth in the body and of varying sizes as well [168].

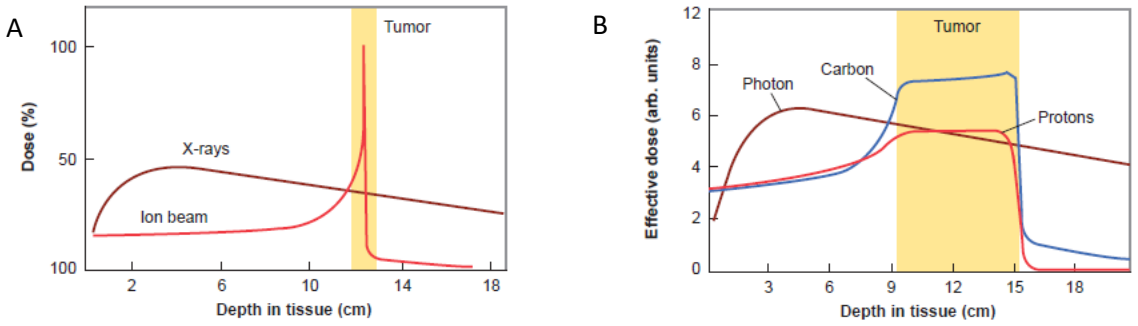

Figure 18: Illustration of the Bragg peak by different radiation profiles. (A) Graph showing the sharp Bragg peak at the end of the ion beam particle's depth compared to the X-ray showing a higher energy deposition at the start. (B) Proton beams and Carbon ion beams are capable of enlarging the Bragg peak to suit the tumor size by varying the energy of the beam (carbon-ion) or using a range shifter (passing the beam through a rotating wheel with sectors of varying thickness – Proton beam)[171]

3.B. Effect of radiation on DNA

Ionizing radiation is when the photon has sufficient energy to strip an electron from the outer shell of an atom, effectively ionizing them. Ionizing radiation injects energy into the material it is passing through and can break long molecular chains, which could be different proteins or DNA in cells. Ionizing radiation forms DNA damage bases and DNA breaks. A human cell is capable of repairing damage DNA sequences, but the repair ability is limited. The DNA damage when exceeds this limit, starts to accumulate and eventually would have an effect on the survival of the cell [168, 173].

3.B. 1. Direct effect of radiation

Radiation is able to affect DNA molecules in the target tissue by directly interacting with them. The direct ionization of the atoms of DNA during its interaction with radiation is due to two physical effects- Photoelectric effect and Compton interactions. This causes breakage of one DNA strand or both. A single broken strand can usually be repaired by the cell, while two broken strands commonly result in cell death. This direct effect of radiation, however, is significantly less with low LET radiation such as X-rays and gamma rays. It is seen that only about one-third of the molecular damage by radiation is due to the direct effect, the major effector of damage is the indirect effect of radiation[168, 173] (Figure 19).

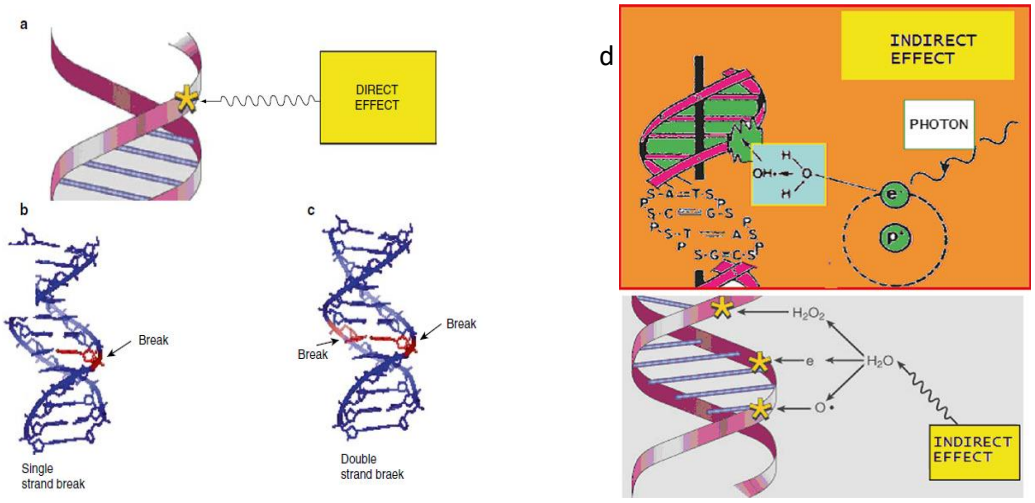

Figure 19: (a) Illustration of direct effect of radiation causing (b) SSBs and (c) DSBs [167], as well as (d) Illustration of the indirect effect of irradiation [174]

3.B.2. Indirect effect of radiation

The indirect effect of radiation is due to the formation of free radicals by the energy transfer from radiation. These free radicals then interact with DNA causing molecular damage. The indirect effect is mostly from the free radicals formed from the interaction of radiation and water, the free radicals have unbound electrons and are highly nucleophilic and reactive. The simple free radicals ($H^{\bullet}$ and $OH^{\bullet}$) are very transient in nature but in some cases $H^{\bullet}$ combines with O2 and creates a longer lasting, DNA damaging molecule called hydrogen peroxide (H_2O_2). The indirect effect of radiation causes three times more damage than the direct action of radiation [173, 175].

3.C. Radiation and DNA damage

It has been stated that DNA is the principal target for the biological effects of radiation. Most of the functional changes occurring in the cell post its exposure to radiation stems from DNA damage, be it cell killing, carcinogenesis or mutations [168, 169].

There are two ways it can cause damage to DNA, the first being the Direct action where the charged particle (electron or an ion) is able to ionize the DNA molecule in its path. The second way to induce DNA damage is the Indirect action where the charged particle is able to ionize the water molecules around the DNA leading to the formation of free radicals such as $OH^{\bullet}$ which then reacts with the DNA. (See 3B) The most prevalent form of DNA damage by low LET irradiation is through the indirect action as it outnumbers the damage by direct action by a ratio of 3:1.

Radiation induces a host of DNA damages, most of which are single stranded breaks and base damages. It is however the limited induction of double stranded breaks that is lethal for the cell [176]. Radiation is capable of creating DSBs by itself, however, SSBs induced by radiation can be converted to DSBs in the cell by its attempt to repair or other cellular processes such as transcription and replication. The cytotoxicity associated with irradiation is mainly from DSBs and clustered DNA damage. Clustered DNA damage is defined as two or more DNA lesions formed within one or two helical turns of DNA [177]. Such a collection of DNA lesions inhibits regular DNA processing and repair. DSBs are the most deleterious type of DNA lesion and are also one of

the most difficult to repair [178], thus making irradiation one of the most effective forms of cancer therapy.

1Gy dose of X-ray radiation is able to induce approximately 3000 damaged bases, 1000 SSBs and 40DSBs in a cells [171]. Hence, in order to maintain its genetic stability, it needs to recognize and repair the damages via different repair pathways. In general, a cell's DNA damage response (DDR) involves DNA lesion recognition, followed by initiation of a cellular signaling cascade to promote DNA repair, which can be helped by a pause in cell-cycle progression (checkpoint activation).

3.D. DNA damage and repair

There are different ways to induce DNA damage in cells. They can be both intrinsic (a cell can have around 200,000 DNA lesions per day) [179] as well as extrinsic (UV light, ionizing radiation and genotoxic agents) [180]. Hence, it is extremely important that there exists a robust repair mechanism in cells to counter these DNA damages. A functioning DDR (DNA Damage Response) is important to counter the genetic damage incurred by the cells. Since damage suffered by the DNA is of a varied nature, so are the cellular responses for its repair. While there are some functional redundancies to DNA repair pathways in order to continue survival in the presence of a dysfunctional repair pathway, inhibition/dysfunction of certain DNA damage signalling or DNA damage repair pathways is a hallmark of cancer[181].

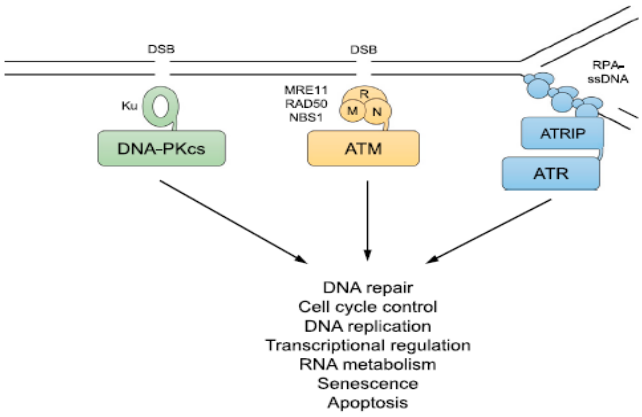

Figure 20: Scheme of the three DDR pathways and the sensor proteins recruiting them. DNA-Pk is recruited and activated by Ku bound to DSBs, ATM by the MRN complex and ATR by RPA-coated ssDNA with ATRIP [182]

Post DNA damage, several steps occur in the cells that are highly orchestrated and regulated. First, the detection of DNA damage is done by specific sensors which then reports to transducer proteins (Figure 20). These proteins would then help initiate a signalling cascade promoting post translational modifications on effector proteins activating them and coordinating them to start damage repair if possible [183]. The proteins involved differ depending on the DDR signalling activated which is in turn dependent on the type of DNA damage but the general pathway of sensor proteins followed by transducers and effectors remain the same.

Before entering into the DSB and SSB repair, there is a need to introduce one of the most important DNA damage sensors, PARP1. PARP1 is one of the most abundant proteins from the PARP family and is involved in regulation of transcriptional control, maintenance of genomic integrity, DNA repair and regulation of apoptotic and survival balance in cells [184, 185]. PARP1 is abundantly localized in nucleus and 80% of its enzymatic activity includes PARylation of nuclear proteins, recruitment of DNA repair factors and stabilization of chromatin for transcriptional regulation[186]. Upon induction of various kinds DNA damage, PARP1 is recruited onto the damage sites (Figure 21) [184, 187] which induces its catalytic activity leading to formation of PAR (Poly-ADP ribose) chains on itself, histone and non-histone proteins [188-190]. Proteins

involved in DDR and DNA metabolism can then bind non-covalently to the damaged sites by interacting with these PAR chains [191].

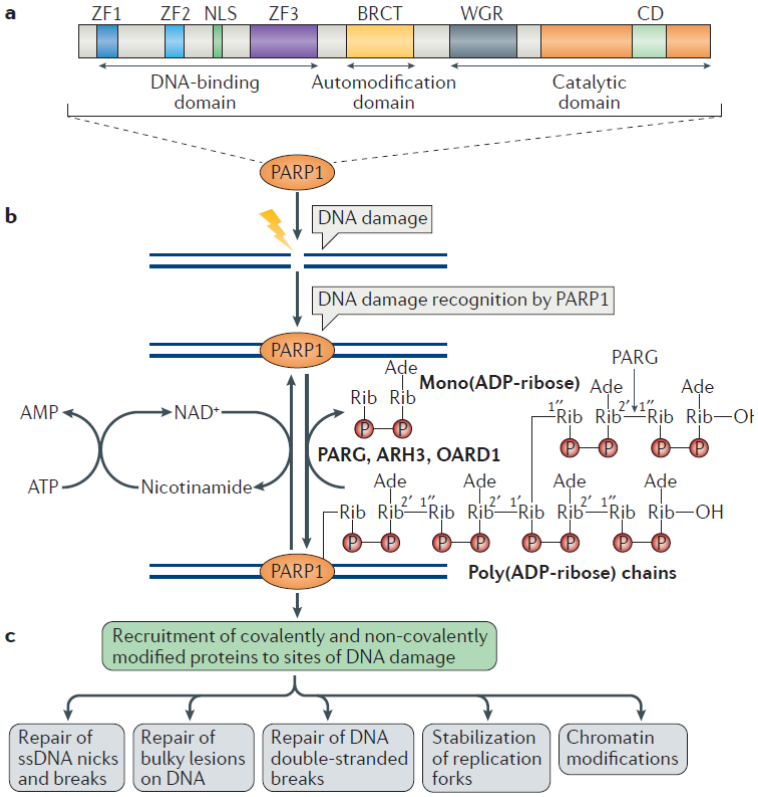

Figure 21: (a) The various domains of PARP1 is represented including the 3 zinc finger motifs in the DNA binding domain, the automodification domain and the catalytic domain. (b) Schematic representation of PARP1 recognizing DNA damage and its activation by inducing PAR chains onto itself and its target proteins. NAD+ is the substrate for PAR formation. (c) PARylation of PARP1 and target proteins at the site of damage leads to the recruitment of multiple proteins that are involved in the repair process [192]

3.D.1. Double Stranded Break signaling and repair

Double stand–breaks (DSB) are recognised by two signalling pathways (ATM and DNA PKs) that are then processed by three repair mechanisms classical and alternative Non-Homologous End-Joining, (c-NHEJ and alt-EJ) and Homologous recombination (HR).

1) <u>DSB Signalling</u>

ATM (ataxia telangiectasia mutated) signaling pathway is one of the three most important DDR signaling pathways. It is activated when it is recruited to the chromatin in response to DSBs. The MRE11-RAD50-NBS1 (MRN) complex can bind to DSBs and initiate the processing of its repair (Figure 22) [193]. It does so by recruiting and then stimulating ATM activity at the DSBs [194, 195]. ATM is not only activated by blunt dsDNA ends, but also by dsDNA ends with short ssDNA overhangs [196]. In the presence of short ssDNA overhangs, the junctions of ssDNA and dsDNA are critical for ATM activation suggesting that MRN recognizes dsDNA ends or dsDNA/ssDNA junctions and may move into flanking dsDNA regions to activate ATM. After its activation, ATM induces a wide spectrum of signal transduction pathways that connect processes involved in DNA repair, cell metabolism, bioenergetics, as well as protein translation and transcription. The best-characterized effector of ATM signaling is Chk2 , which is phosphorylated by ATM following DSB formation[197].

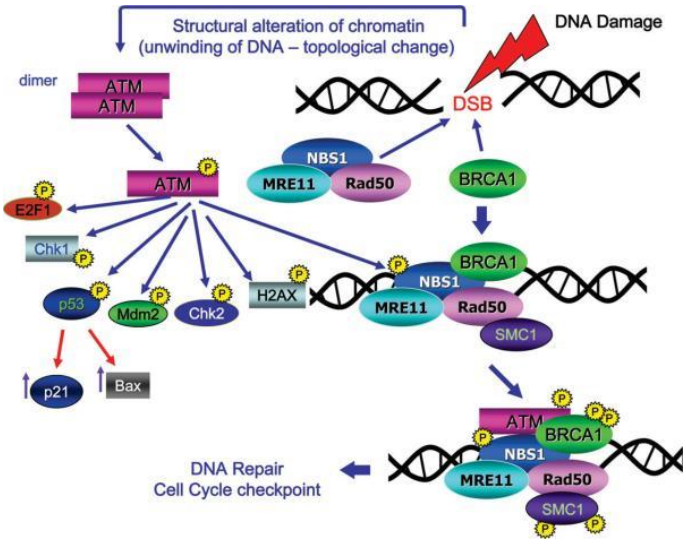

Figure 22: Schematic representation of ATM activated DDR response to DSBs created by radiation[198]

One of the key results of ATM activation is the phosphorylation of the histone variant H2AX by ATM. γH2AX, a DSB marker in cells, is formed by the phosphorylation of H2AX at the Ser139 position by ATM, ATR or DNA-PKs. The DSB-induced phosphorylation of H2AX occurs within minutes after DNA damage, and it rapidly spreads over large chromatin domains (>500 kb) flanking the DNA breaks [199, 200]. The initial activation of ATM by DNA ends may result in phosphorylation of the H2AX immediately adjacent to DSBs. However, it is the protein Mdc1, that can bind both γH2AX [201-203] and ATM [204], which enables ATM to bind the nucleosomes containing γH2AX, providing a mechanism for ATM to recognize the chromatin flanking DSBs and to propagate H2AX phosphorylation along the chromatin in a feedback loop. The phosphorylated H2AX is required for the accumulation of numerous DNA repair proteins and chromatin-remodeling complexes around DSBs. Then ATM promotes HR or NHEJ (see DBS repair).

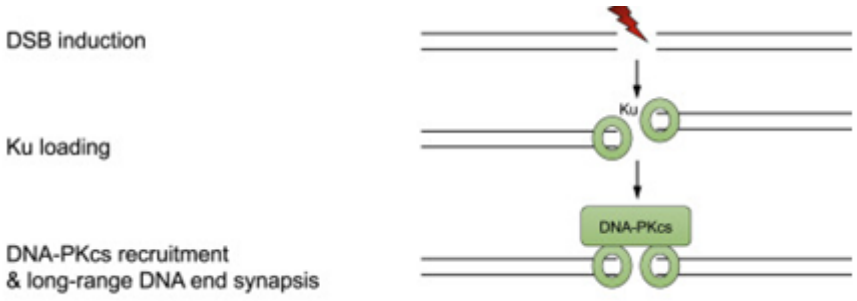

Figure 23: Schematic representation of DNA-PK activated DDR response on DSB formation [182]

DNA-PK is another DDR signaling protein recruited at DSBs. It is recruited by Ku proteins that bind to DSBs [205, 206] that is then process by c-NHEJ (Figure 23).

Since DNA-PK is not known to phosphorylate any other proteins apart from itself and does not block the recruitment of downstream proteins [207], it is thought that DNA-PK is a physical block to itself and auto-phosphorylation relieves this to complete the repair process.

2) Double Stranded Break Repair pathways-

DSBs are repaired either through Homologous Recombination (HR) or through classical Non-Homologous End Joining (NHEJ) or alternative Non-Homologous End Joining (alt-EJ). It depends on the cell cycle phase and the chromatin context [208, 209] (Figure 24)

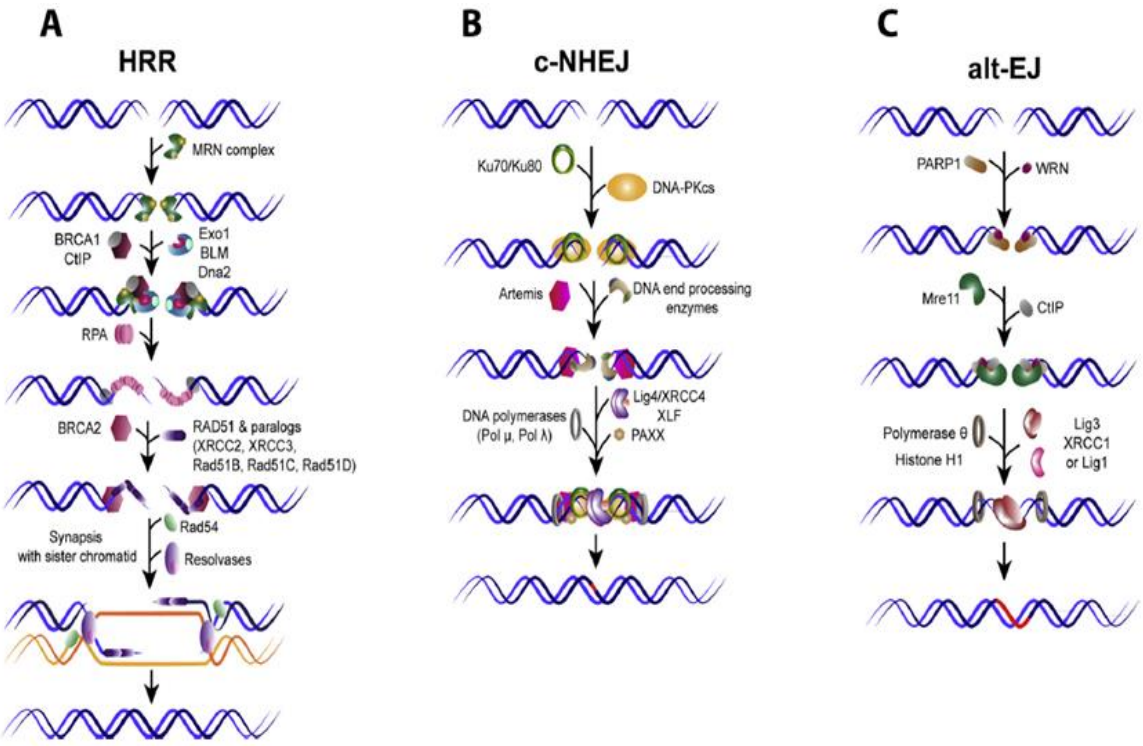

Figure 24: Schematic representation of the different DSB repair pathways (A) Homologous Recombination repair, (B) classical- Non Homologous End Joining and (C) Alternative-NHEJ [210]

Although classical NHEJ is often described as error prone and mutagenic [211], in reality it is remarkably efficient and mostly accurate [212]. Only when classical NHEJ fails, cells use an alternative end-joining pathway such as that mediated by DNA polymerase θ (POLQ), which can introduce extensive mutations [213].

Homologous Repair process is promoted by ATM by the recruitment of BRCA1. Interestingly, the induction of γH2AX by ATM near DSBs result in elaborate ubiquitylation and SUMOylation cascades to recruit the tumor suppressor BRCA1 and the DNA damage response mediator 53BP1, both of them regulating the balance between HR and NHEJ[214].

ATM also promotes NHEJ by phosphorylating 53BP1 since 53BP1 protects DNA broken ends from resection by recruiting two downstream factors, RIF1 and PTIP [215]. 53BP1 is not an enzymatic protein but contains multiple interaction surfaces that help recruit multiple DSB responsive proteins[216]. There exists a balance between the two proteins BRCA1 and 53BP1 in regulating the HR/NHEJ pathway [217]. BRCA1 is able to antagonize the 53BP1 mediated NHEJ pathway in S/G2 phase of the cell cycle by preventing the translocation of PIF1 to the DSBs, hence maintaining the dominance of HR pathway in S/G2 phase [215]. (Figure 25)

ATM is also able to induce NHEJ repair by phosphorylating DNA-PK and the recruitment of Artemis[182], but similar to the phenomenon observed with BRCA1-53BP1 interaction, the expression of Ku heterodimers is implied to be reduced in S/G2 cell cycle phases[218]. This showing the cellular preference to choose HR over NHEJ for repair at S/G2 phase of the cell cycle.

Figure 25: Scheme showing the balance of ATM directed NHEJ/HR repair pathway depending on

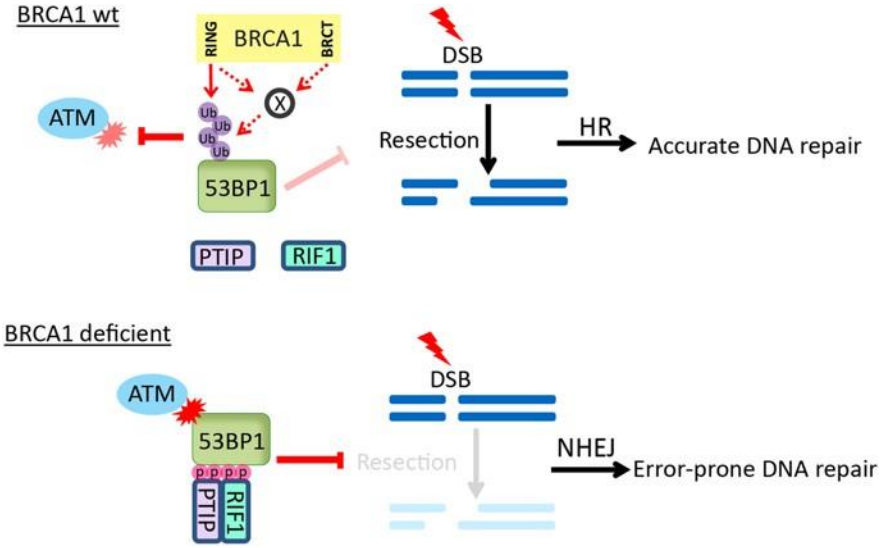

the inhibitory role of BRCA1 for 53BP1 mediated NHEJ repair [215].

Homologous Recombination Repair-

In HR repair, the DSB processing is done by the rapid recruitment of the proteins RAD50, MRE11 and NBS1 to the DSB site. This constitutes the MRN complex. This then leads to the recruitment and activation of ATM. The DNA end resection of the 5' DNA occurs next by the recruitment of phosphorylated CtIP and the endonuclease activity of MRE11. It is followed by RPA binding to 5' single-strand DNA to prevent formation of secondary structures or uninhibited annealing [219] and is later replaced by Rad51 monomers [220]. The Rad51 nucleoprotein filament formation is achieved with the help of Rad51 paralogs Rad51B, Rad51C, Rad51D, Xrcc2 and Xrcc3, as well as BRCA2 [221]. The homology search is RAD-51 mediated [222] and the subsequent D-loop strand formation is done with the help of Rad54 [223]. The synthesis of the DNA is done preferentially by DNA polymerase δ [224] and the final resolution with or without the Holliday junctions by DNA ligase I [225].

PARP1 is implicated in the control and recruitment of various important HR proteins. One of the most important proteins is BRCA1 which not only drives the initial steps of HR but also helps attach RAD51 to the DNA which is essential for the DNA strand exchange in HR. PARP1 is shown to be important for early and rapid recruitment of BRCA1 to DSBs[226], however, there exists PARylation independent mechanisms for recruiting BRCA1 to DSBs[227]. PARP1 inhibition or loss results in hyper-recombinogenic phenotypes that shows a much higher number of Sister Chromatid Exchanges (SCEs). There is also a higher number of RAD51 foci on sites of DNA damage[192]. The studies seem to suggest that PARP1 is used to control and fine tune the HR process [228]. Since, synthetic lethality is observed with PARP1 inhibition to the loss of BRCA1 or BRCA2, the proposed mechanism for the observed genotoxicity is that inhibition of PARP1 increases the number of SSBs due to its involvement in SSBR. These SSBs then turn to DSBs during DNA replication and they are particularly cytotoxic because of the reduced DSB repair capabilities in these BRCA1 and BRCA2 deficient cells [229, 230]. However, alternate models have also been proposed to explain the synthetic lethality.

Non Homologous End Joining Repair-

NHEJ repair the majority of DSBs in mammalian cells except the one that occur in replication forks which is usually repaired by HR, since HR is the dominant DSB repair pathway in S phase of the cell cycle [231].

Classical-NHEJ is initiated by recognition of the DSBs which is done by the Ku heterodimer that assembles at the break sites within seconds in order to protect it from degradation and recruits DNA-PKcs which would in turn be activated [232, 233]. The activated DNA-PKcs then phosphorylates itself and recruits the endonuclease Artemis[234] which favors the repair pathway of NHEJ over HR [235] and is important for the DNA end-processing[207, 236]. Further c-NHEJ core proteins are then recruited such as XRCC4 [237], XLF [238] and DNA Ligase IV [239]. The entire c-NHEJ machinery is stabilized on damaged chromatin by PAXX [240] which is a protein paralog of XRCC4 and XLF. The compatible DNA ends are finally ligated by the DNA ligase IV/XRCC4 complex. XLF and PAXX which is an analog of XCC4 are also shown to be involved [210].

In NHEJ, PARP1 has been shown to PARylate the catalytic subunit of DNA-PK called DNA-PKcs *in vitro*, which is an important NHEJ factor. PARylation of DNA-PKcs induces its kinase activity without the requirement of Ku70-Ku80 complex [241]. Furthermore, it is seen *in vivo* that PARP1 and DNA-PKcs form a complex, suggesting that they act in the same pathway[242]. However, combined deficiency of PARP1 and DNA-PKcs has increased genomic instability and hypersensitivity to irradiation when compared to its individual knockouts, suggesting their involvement in parallel paths to repair DSBs as well [243]. It has been seen recently that PARP1 is able to influence the recruitment of the chromatin modifier CHD2 via the recruitment of XRCC4, hence, increasing the efficiency of classical NHEJ (c-NHEJ) [244].

PARP1 may promote alternate NHEJ (atlEJ) by competing with the Ku complex for access to DSB sites since in the absence of Ku complex, PARP1 binding to DSB sites induces alt-EJ [245, 246]. Alt-EJ is inherently mutagenic and generates insertions or deletions at sites of repair. Since, inhibition of PARP1 induces fewer translocations post treatment with DNA damaging agents, it is further proof of PARP1 involvement in alt-EJ[247]. In the absence of c-NHEJ, PARP1 helps alt-EJ create telomere end-joining and fusions when shelterin complex proteins are absent [248].

PARP1 is helpful in the binding of MRN complex to the DSB sites in the absence of Ku70/Ku80, moving the repair pathway towards the alt-EJ [245, 249]. Since BRCA1 deficient tumors are heavily dependent on Pol Θ-mediated, error prone alt-EJ repair for survival[250], it is possible that the synthetic lethality between PARP1 inhibition and BRCA1 deficiency is due to the loss of alt-EJ as those cells already lacked the function of HR[251].

3.D.2. Single Stranded DNA damage repair

1. **ATR Signaling**

While ATM is largely involved in DSBs, Ataxia telangiectasia and Rad3-related protein (ATR) is activated by a wide range of damages [214]. The ATR-Chk1 pathway protects the genome against DNA damage and replication stress by regulating and coordinating multiple cellular processes, which include but are not limited to cell-cycle arrest, inhibition of replication origin firing, protection of stressed replication forks, and DNA repair [252] (Figure 26).

It is recruited by a protein called ATRIP to ssDNA coated by RPA protein[253] due to the ability of ATRIP to recognize and bind RPA[254]. The coating occurs due to various forms of DNA damage or by helicase/polymerase uncoupling at stalled replication forks. Several other regulators of ATR, including the Rad17 complex, the Rad9–Rad1–Hus1 (9-1-1) complex, and RIHNO, are recruited to junctions of RPA-ssDNA which helps the important protein TopBP1 in activating the ATR kinase pathway. ATR is used to phosphorylate and activate CHK1 which is used in a number of cellular functions. CHK1 helps in the degradation of CDC25. This helps slow or arrest the cell cycle allowing more time to repair[255]. ATR also plays other roles such as restraining replication origin firing, limiting replication fork collapse and by regulating deoxyribonucleotide availability in response to DNA damage[182].

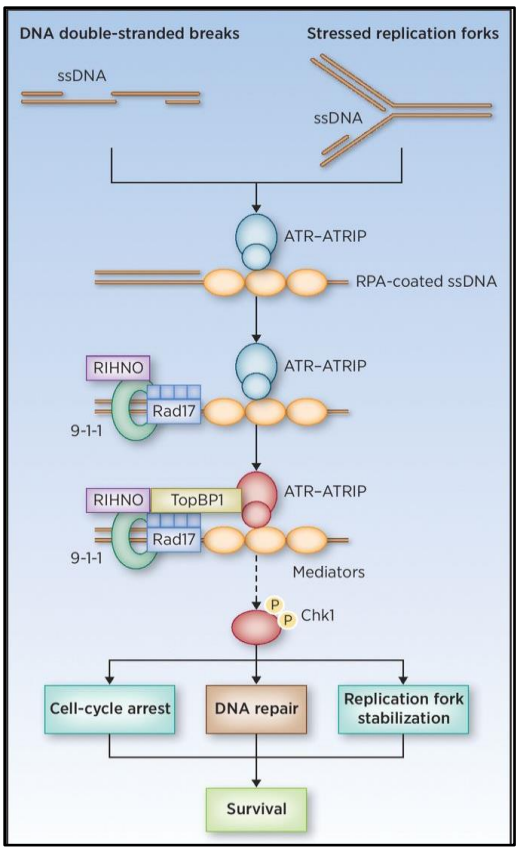

Figure 26: Schematic representation of ATR activated DDR response on ssDNA breaks and stalled replication forks [252]

2. Single Stranded Break Repair

In SSB repair, PARP1 is important because it helps in the accumulation and recruitment of SSBR components to the damaged sites. PARP1 and PARP2 help in the recruitment of the protein XRCC1, which acts as a scaffold for other proteins involved in the repair process such as Lig3, PNKP and DNA polymerase β [256, 257]. This helps initiate the repair process. PARP1 may also be involved in the promotion of the gap-filling step of the repair process and in the final DNA ligation step by regulating the supply of ATP [258, 259] (Figure 27).

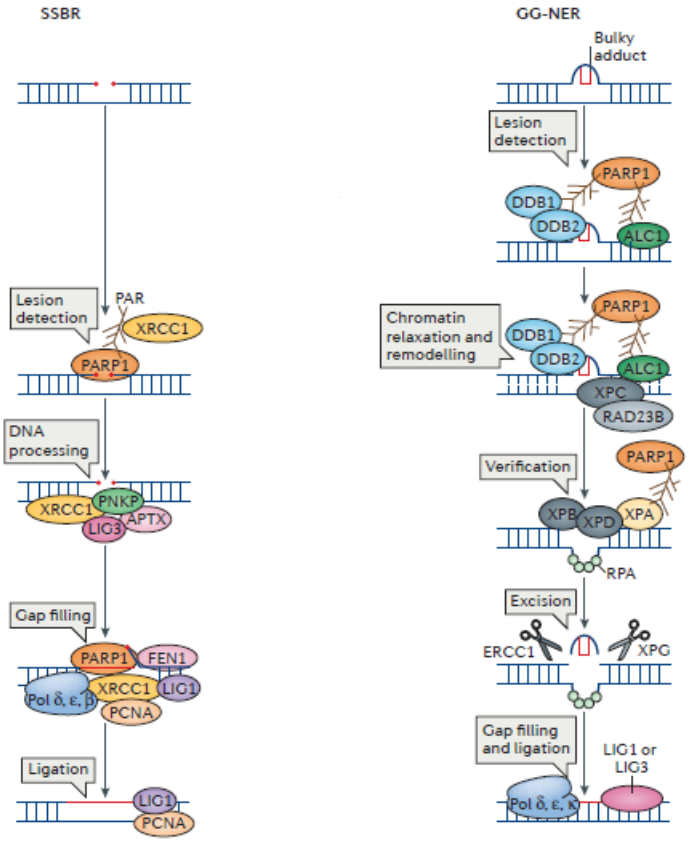

Figure 27: Schematic representation of the role and involvement of PARP1 in the different SSBR. As described in the text, PARP1 is involved in the recruitment of different repair proteins in lesion detection in SSBR, later stages of BER and in the recruitment of multiple repair proteins in NER [192]

3.D.3. Base DNA damage repair

1. Base Excision Repair

BER (Base Excision Repair) is a major pathway for the repair of oxidative base damage, induced by irradiation for example, alkylation damage and abasic sites on the DNA. In this repair pathway the damaged bases are removed by glycosylases, that cleaves the N-glycolsidic bond to release the base, leaving an abasic (apurinic/apyrimidinic) sites (AP sites) detected by AP endonucleases that cleave it and create SSBs. It is after that the short and long patch repair begins, as shown in figure 28A [258]. Multiple studies have suggested that PARP1 is involved in BER [260], however, certain studies have showed that inhibition of PARP1 doesn't necessarily render the cells hypersensitive to Base damage causing agents[261, 262]. It shows that the presence of catalytically inactive PARP1 might slow the kinetics of BER, unlike the SSBR process[258]. Nevertheless, the importance of PARP1 in downstream processing of the SSBs that arise due to the initial steps of BER, cannot be discounted. Recently, it has been suggested that a subset of DNA lesions, the purine base damage when repaired by BER pathway could require PARP1 [263]. Pyrimidine base damage could be PARP1 independent.

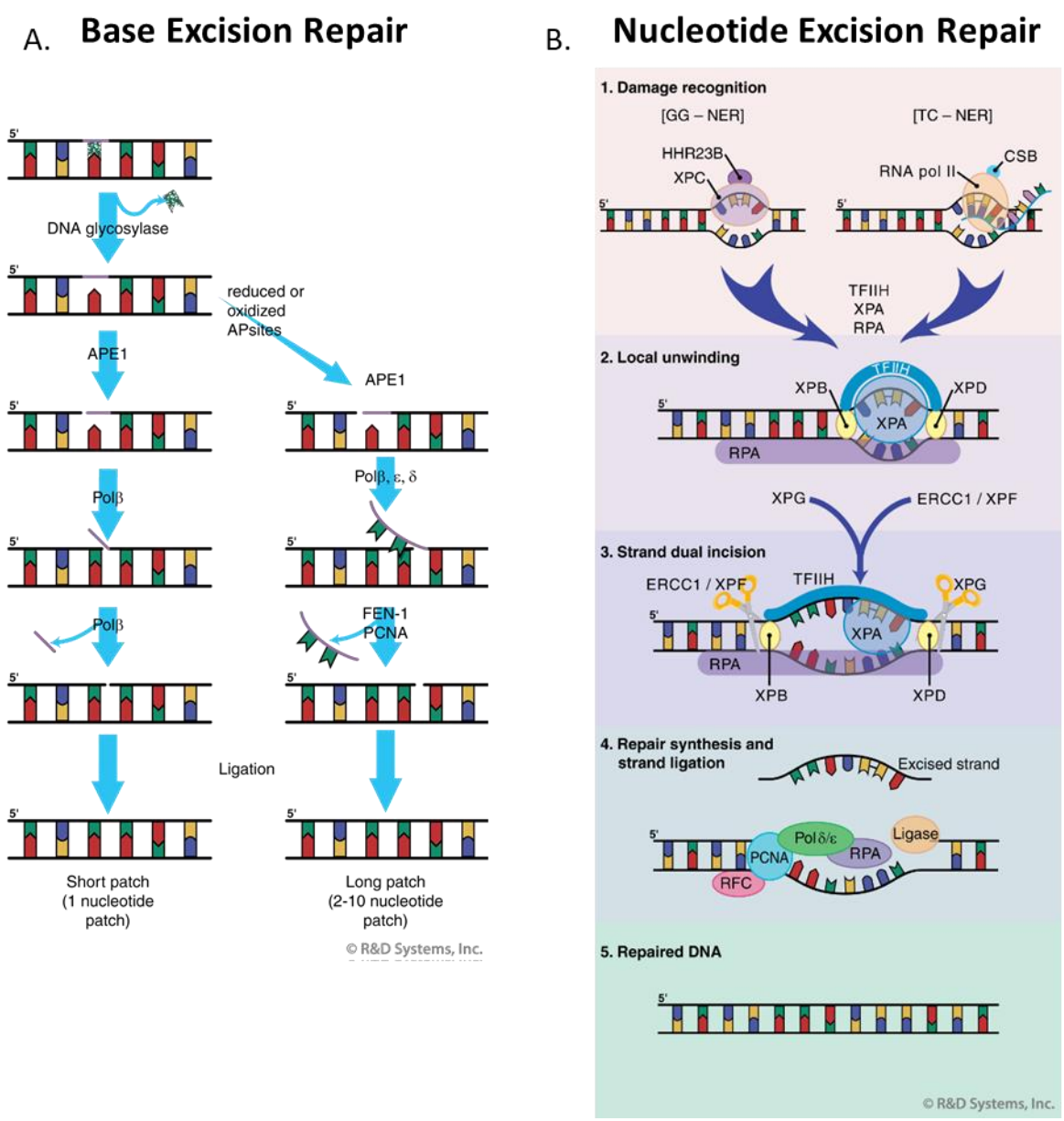

Figure 28: Schematic representation of (A) Base Excision Repair with short and long path repair and (B) Nucleotide Excision Repair with both GG-NER and TC-NER *(Image from R&D Systems-DNA Damage Response)*

2. Nucleotide Excision Repair

The NER pathway is the primary repair pathway used in the repair of bulky intrastrand DNA adducts, as the ones induced by UV radiation, mutagen or chemicals such as cisplatin [264]. NER can be divided in two pathways, the global genomic (GG-NER) and transcription-coupled NER (TC-NER) that differ by the initial site of DNA damage recognition but follow the same process for the repair mechanism (Figure 28B). In GG-NER, the DNA damage is recognized by XPC proteins and RAD23B which then associate with DDB1-DDB2 complex [265]. A short single-stranded DNA segment that contains the lesion is removed and then the undamaged single-stranded DNA that remains is used as template to synthetize a short complementary sequence. DNA ligase proceeds to the final ligation. This process helps ubiquitylate core histones, leading to nucleosome displacement and stimulation of repair [266, 267]. The role of PARP1 in this is to create PAR which binds to XPC and helps in its recruitment to the DNA lesions. This is done by its interaction with DDB2 at the damaged chromatin which initiates the PARP1 catalytic activity [268, 269]. The PARylation helps recruit ALC1 protein which has a PAR binding domain. ALC1 then helps in chromatin remodeling and recruitment of XPC, XPA, and other proteins for lesion verification and repair [270]. The role of PARP1 in NER seems to be significant as its inhibition leads to greater sensitivity to UV lesions that require the NER pathway [268].

4. Radiosensitization

4.A. Definition and requirement

Ionizing Radiation, being a common tool in cancer therapy, is not without its limitations. The dose administered to the patient can induce negative side effects particularly by affecting the normal cells around the tumor. There are two broad directions in which radiation therapeutic index can be broadened.

1) increasing the radiosensitivity of the tumor cells and/or

2) increasing the radioprotection of the normal tissue around it.

In order to do either, it is essential to understand the cellular pathways involved when cells are irradiated in order to find clear targets or decipher the mechanism of action for certain radiosensitizing drugs [169].

Radiosensitization can defined as the ability of a drug to decrease the amount of radiation required for irreversible inhibition of proliferation. Radiosensitization ability of a compound is usually investigated *in vitro* by clonogenic assays or cell proliferation assays. In this assay, the cells are treated with the drugs from their sub toxic to higher concentrations prior to irradiation exposure. The cells are then incubated with or without the drug for a minimum of 5 mitotic cycles, or in the case of clonogenic assay till 50 cell colonies are formed. The effect of radiosensitivity is estimated based on the comparison of cell survival between drug treated and non-drug treated cells [271].

The model designed by Steel and Peckham[272], was used to make a isobologram that could help predict the effect of the drug with respect to radiation, as seen in figure 29. In this isobologram, the X axis shows the isoeffective levels of the drug while the Y axis shows the same for the radiation dose. The thick black line represents the line of additive effect. If the increase of the drug dose is proportional to the decrease of the radiation dose for maintaining the isoeffect of cell lethality, then the combined effect is additive. If the increase of the drug dose leads to a very low decrease of the radiation dose for the same isoeffect, then it is considered sub-

additive/protective/antagonistic. On the other hand, if the increase of drug dose requires a huge decrease of radiation dose required to have the same effect, then it is considered supra-additive or synergistic. These synergistic drugs are considered capable of radiosensitization. The envelope of additivity shown in the graph is determined by the combined standard errors of the line of additivity[273].

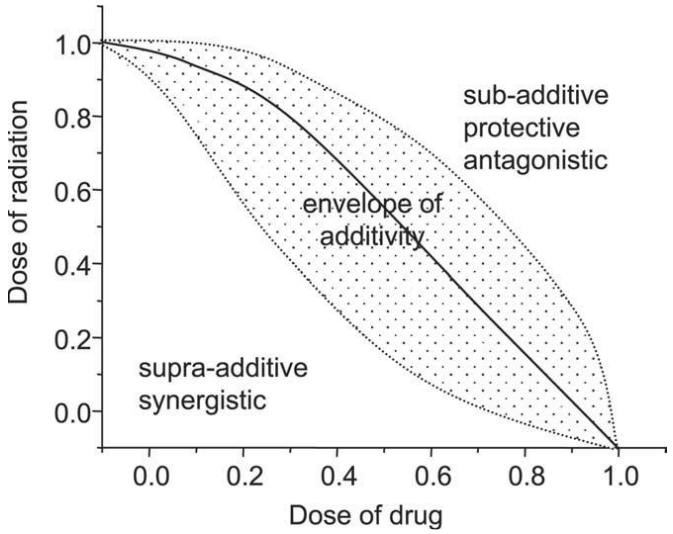

Figure 29: Schematic isobologram to determine the effect for the combination of a drug and radiation[274].

4.B. Classification of different forms of radiosensitization

Radiosensitization can be achieved through different, non-singular mechanisms of action on cancer cells. Some different forms of radiosensitization are represented below

1. Inhibition of IR-induced DNA damage repair

Since DNA damage is the primary effect of IR, drugs that are able to induce an inhibition of the various DNA damage repair pathways will help increase the total number of unrepaired IR induced DNA damage. This will lead to increased radiotoxicity and radiosensitization.

Popular examples from this category of radiosensitizing agents are Olaparib [275] (Figure 30A), a PARP inhibitor that is able to induce radiosensitization at low concentrations and is now involved in phase I clinical trials in combination with IR [276]. Another example is VX-970 [277] (Figure 30B), an ATR inhibitor that is being considered a positive lead for radiosensitization against triple negative breast cancer and glioblastoma multiforme (GBM). Dbait/AsiDNA™ is a double stranded oligonucleotide molecule that mimicks DSBs leading the cell to hyperactivate DDR systems and overlook actual damage by genotoxic elements [278, 279] (Figure 30C). It is currently in a phase I/II clinical trial with radiotherapy and has shown promising results on its effectiveness [280]. Interestingly, no dose limiting toxicity is achieved with AsiDNA™.

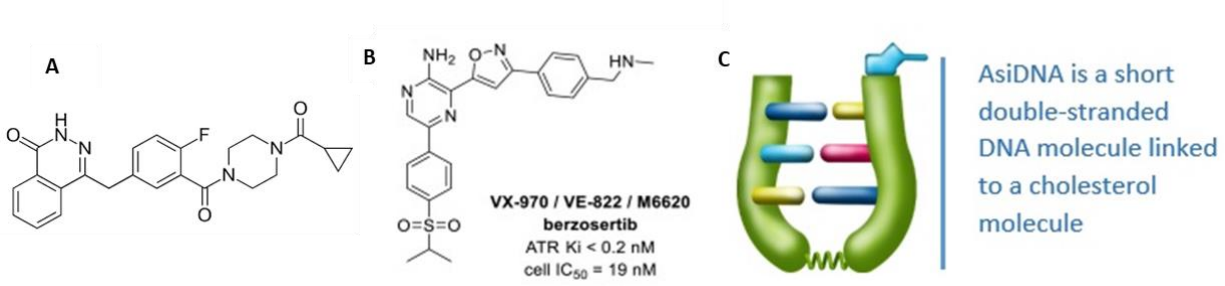

Figure 30: Chemical structure of the (A) PARP inhibitor Olaparib, (B) ATR inhibitor VX-960 and the (C) schematic visualization of AsiDNA™ since its structure is protected by patents (*Image from the Onxeo – products – AsiDNA webpage*).

2. Cell-cycle dysregulation

Cells are sensitive to radiation induced damages in certain phases of the cell cycle. It is noticed that S phase of the cell cycle is the most resistant to irradiation whereas the late G2 and M phases of the cell cycle are the most sensitive[281]. This knowledge can be used for targeted therapies, specifically by using drugs that can arrest the cell cycle at the G2 or M phase. This combined with irradiation would lead to increased damage and cell death.

Paclitaxel is a drug that stabilizes microtubules and can cause an arrest at the G2/M phase of the cell cycle[282] and is a target drug for radiosensitization**.** Genexol-PM is a nanoparticle chemotherapeutic that has a controlled Paclitaxel drug release profile. This nanoparticle is now in pre-clinical trials for its use as a radiosensitizer[283] (Figure 31).

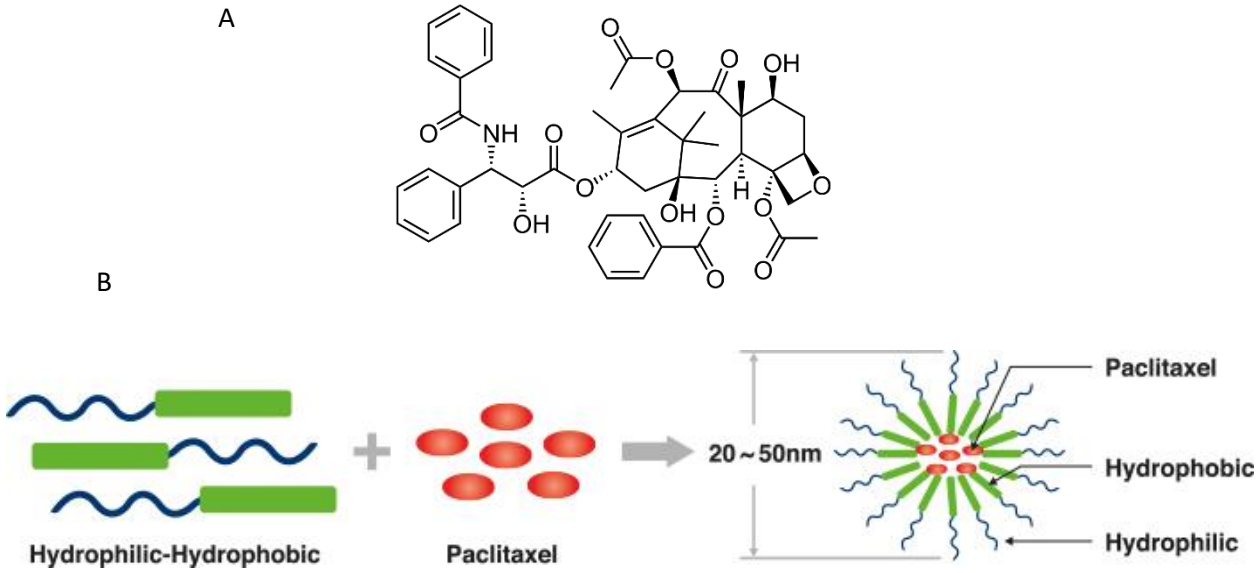

Figure 31: (A) Chemical structure of the Paclitaxel drug. (B) Schematic representation of the formation of Genexol-PM is shown (*Image from the Samyang Biopharm – products – Genexol-PM webpage*)

3. Activity enhancement in hypoxic cells

Hypoxic cancers are usually radioresistant due to the lack of oxygen availability, hence they present an attractive target for radiosensitizer design [164, 284]. Since irradiation induced ROS is one of the major causes of DNA damage, a drug that can artificially increase ROS production in the cancer cells will be able to augment the ROS produced by IR thereby increasing the cancers sensitivity to irradiation.

Hypoxic radiosensitization by inducing Nitric Oxide (NO) in the cancer cells have shown to increase ROS induced DNA damage [285]. Inhibition of anti-oxidant enzymes is another pathway to radiosensitize hypoxic cancers, for example Buthionine sulphoximine (BSO) (Figure 32A) is a drug that inhibits the formation of antioxidant glutathione synthesis. Glucocorticoids are used to reduce the consumption of oxygen in tumors and hence increase the presence of oxygen and radiosensitivity. Targeting mitochondria to perturb ROS homeostasis is also shown to induce radiosensitization, Arsenic trioxide is able to target and inhibit mitochondrial complex IV and induce ROS production and radiosensitivity of hypoxic tumors[286] (Figure 32B).

Moreover, due to the vast differences in the chemical environment between a hypoxic biological system and one with normal oxygen levels, it can provide an opportunity for targeted compound delivery to hypoxic regions by using bio reductive prodrugs as well [287].

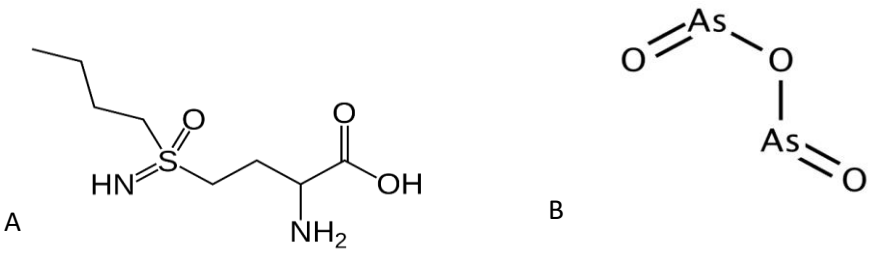

Figure 32: Chemical structures of radiosensitizers (A) Buthionine sulphoximine and (B) Arsenic trioxide

4. Inhibition of prosurvival/radioresistance pathways and abrogation of rapid tumour cell repopulation

Certain drugs are observed to have radiosensitization potential due to their ability to manipulate gene expression levels in certain cancer cells compared to the normal tissue. This has led to the investigation of inhibitors of signal transduction pathways for their radiosensitivity.

One example is that of Cetuximab, which is an epidermal growth factor receptor (EGFR) antibody that is able to induce radiosensitization in head and neck cancer[288] (Figure 33). Moreover, it was noticed that since the EGFr signaling pathway involves multiple downstream phosphorylation reactions and crosstalk with other signaling pathways, it is possible that the anti-tumor effects of EGFr inhibition can be enhanced by inhibiting other downstream effectors of EGFr signaling. It was seen that the dual inhibition of EGFr (cetuximab) and JAK-STAT-3 (JAK1i) leads to greater radiosensitization than with either cetuximab or JAK1i alone[289].

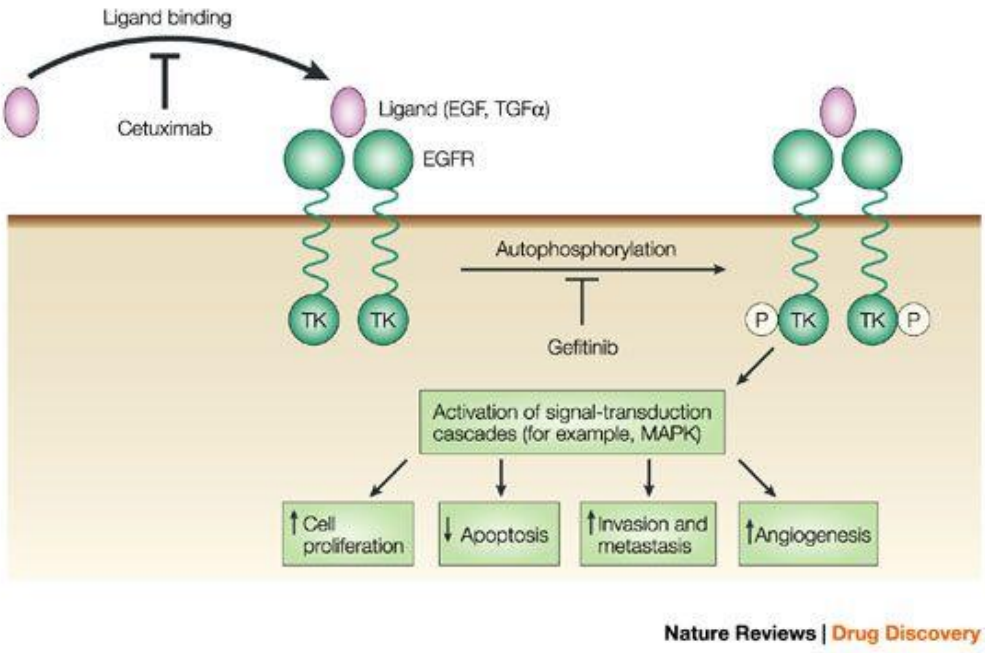

Figure 33: Cartoon depiction of how Cetuximab is able to stop EGFR activation leading to lower cell proliferation, increased apoptosis and radiosensitization [290]

5. Modulating the tumor microenvironment and amelioration of IR damage to healthy tissues

Another approach is to modulate changes in the tumor vasculature which can be achieved by inhibiting tumor cell signaling, resulting in enhanced tumor oxygenation. This in turn can affect chemo or radiosensitization[291].

6. Increasing the local effect of irradiation on cells by the presence of high atomic number materials

High atomic number metals can cause what is known as the Auger effect, in which an inner orbital electron is ejected due to a high energy applied to the atom. This resulting vacancy is filled by an electron from the outer orbital, and the energy difference between the two shells leads to a fluorescence photon or an outer orbital electron being ejected. Hence, the loss of one inner shell electron translates to 2 outer shell electron loss. With more outer orbitals present, more electrons are ejected leading to an auger cascade. This resultant Auger cascade may generate cytotoxic DNA damage if it occurs in close proximity to DNA [292] as shown in the figure 34. Other effects occurring due to the interaction of radiation and the atom include the Compton scattering (change in the angle of scattering of the radiation upon interaction with an atom) and the Photoelectric effect (ejection of electron upon gaining energy from the incoming photon).

Metal-Nanomaterials with high atomic number such as gold, silver and bimetallic nanoparticles are studied for radiosensitization [293]. These high Z nanomaterials have strong capabilities for absorbing irradiation and emitting secondary electrons, leading to local dose enhancement, mainly via Compton scattering, photoelectric effect and the auger effect. These physical effects help increase the irradiation dose in the tumors and can potentiate radiosensitization.

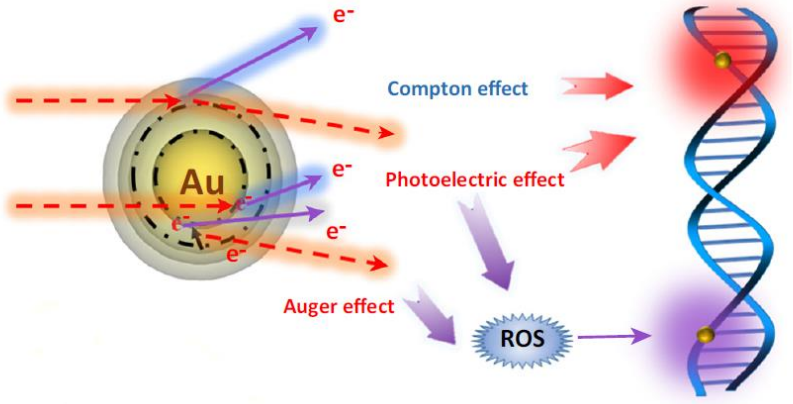

Figure 34: Schematic diagram of the different effects of radiation on the atom leading to Compton effect, Photoelectric effect and Auger effect. These effects can cause either direct or indirect DNA damage[293]

4.C. Ongoing Clinical trials of Radiosensitization

There are several radiosensitizing drugs being tested in the clinical trials for their effect with radiation and other chemotherapeutic agents. Here is a non-exhaustive list of radiosensitizers, where the drugs are in active clinical trials. Several other important drugs in each category are not mentioned if their clinical trial has been completed and proved unsuccessful. However, there are some exceptions in the table 1.

Cisplatin is mentioned in the table even though the phase III clinical trial results showed that the overall survival level between hyper-fractionated radiation with and without cisplatin is not significantly different. However, cisplatin with radiation did maintain improved rates of locoregional control, distant metastasis-free survival, and cancer-specific survival compared to that of hyperfractionated radiotherapy alone. Several DNA repair targeting drugs also tend to affect the cell cycle, however, CHK1/2 inhibitor is a promising cell cycle inhibitor radiosensitizer that would be entering the clinical trials in the coming years.

Drug Category	Drug class	Drug name	Phase	Cancer type
DNA repair & genome instability[294]	PARP inhibitor	Olaparib	I	Oesophageal
	ATR inhibitor	AZD6738	I	Solid tumors
	Topoisomerase I inhibitor	CRXL101	Ib/II	Rectal cancer
	DNA-PK inhibitor	M3814	Ia/Ib	Solid tumors
	MEK1/2 inhibitor	Trametinib	I	Rectal tumors
	DNA damage mimick	AsiDNA[295]	I	Advanced solid tumor
	Chemotherapeutic drug	Cisplatin [296]	III	Head & Neck
Cell cycle	CHK1/2 inhibitor	AZD7762	preclinical	Pancreatic
	Wee1 inhibitor	AZD1775[294]	I	Head & Neck
Hypoxia[297]	Oxygen mimetic	Nimorazole	III	Head & Neck
	Mitochondrial inhibitor	atovaquone	I	NSCLC
Growth signaling pathways[294]	Monoclonal Ab - EGFR	Cetuximab	I/II	Rectal cancer
	Monoclonal Ab - EGFR	Panitumumab	II	Rectal cancer
Tumor microenvironment[298]	VEGF inhibitor	Bevacizumab	II	GBM
	Tyrosine kinase inhibitor	Sorafenib	I	Hepatocellular carcinoma
Nanoparticles[299]	Gadolinium based	AGulX	I	Multiple brain metastasis

Table 1: List of radiosensitizers involved in clinical trials

4.D. Metal complexes

Metal complex ligands, especially transition metal complex ligands, have been investigated as potential anti-cancer drugs for a long time. They possess certain attractive features for the study of drug interaction in a cell. One can study the cellular uptake and localization of some of the metal complex drugs by their luminescent quality [300]. Moreover, biophysical assays such as mass spectrometry can be used to accurately and quantitatively analyze the drug localization and bio-distribution.

Some of the popular metals used in transition metal complexes to induce radiosensitization are Platinum, Ruthenium, Iron, Copper, Cobalt and Rhodium to name a few. While, each metal can be studied in great detail, we will focus on Platinum complexes for this thesis. But before that, I would like to briefly mention the interests of metals in non-ionizing radiation as well.

4.D.1. Metal complexes and non-ionizing radiation: photodynamic therapy

Metal complexes have been used with nonionizing radiation, such as light in the 600-800 nm spectrum of wavelengths, to treat cancer as a modality known as photodynamic therapy (PDT). The three components required for PDT are – 1. Photosensitizer (A light-absorbing compound that initiates a photochemical or photophysical reaction), 2. Light and 3. Oxygen. Though benign separately, when put together these 'photosensitizers' (PS) absorb photons of a certain wavelength and enter an excited state that can interact with O2 to produce singlet oxygen, leading to free radical cascade and oxidative cytotoxicity [301, 302].

An ideal PS agent should be a single pure compound to allow quality control analysis. It should have a high absorption peak between 600 and 800 nanometers (nm), because absorption of photons with wavelengths longer than 800 nm does not provide enough energy to excite oxygen to its singlet state and to form a substantial yield of reactive oxygen species. Because the penetration of light into tissue increases with its wavelength, agents with strong absorbance in the deep red such as chlorins, bacteriochlorins, and phthalocyanines offer improvement in tumor control. It should have no dark toxicity and relatively rapid clearance from normal tissues, thereby minimizing phototoxic side effects [301]. Ru (II) complexes have been recently developed for efficient Photodynamic therapy [303]. The first PS used clinically was a water soluble mix of

porphyrins called hematoporphyrin derivative (HPD), and later a purified version, porfimer sodium, came to be called as Photofrin. Due to certain disadvantages regarding low absorbance at the optical window of biological tissues and long lasting skin photosensitivity, a second generation of PS were to be discovered.

Metal porphyrin derivatives were developed that are able to target tumor sites by targeting their surface receptors and can be induced by the near infrared or infrared wavelengths using two photon absorption Some examples are shown in Figure 35 [304, 305]. With the ability to get induced by a higher wavelength, deep tissue tumors can be targeted and with the two photon absorption method, enough energy can be contributed to induce singlet oxygen.

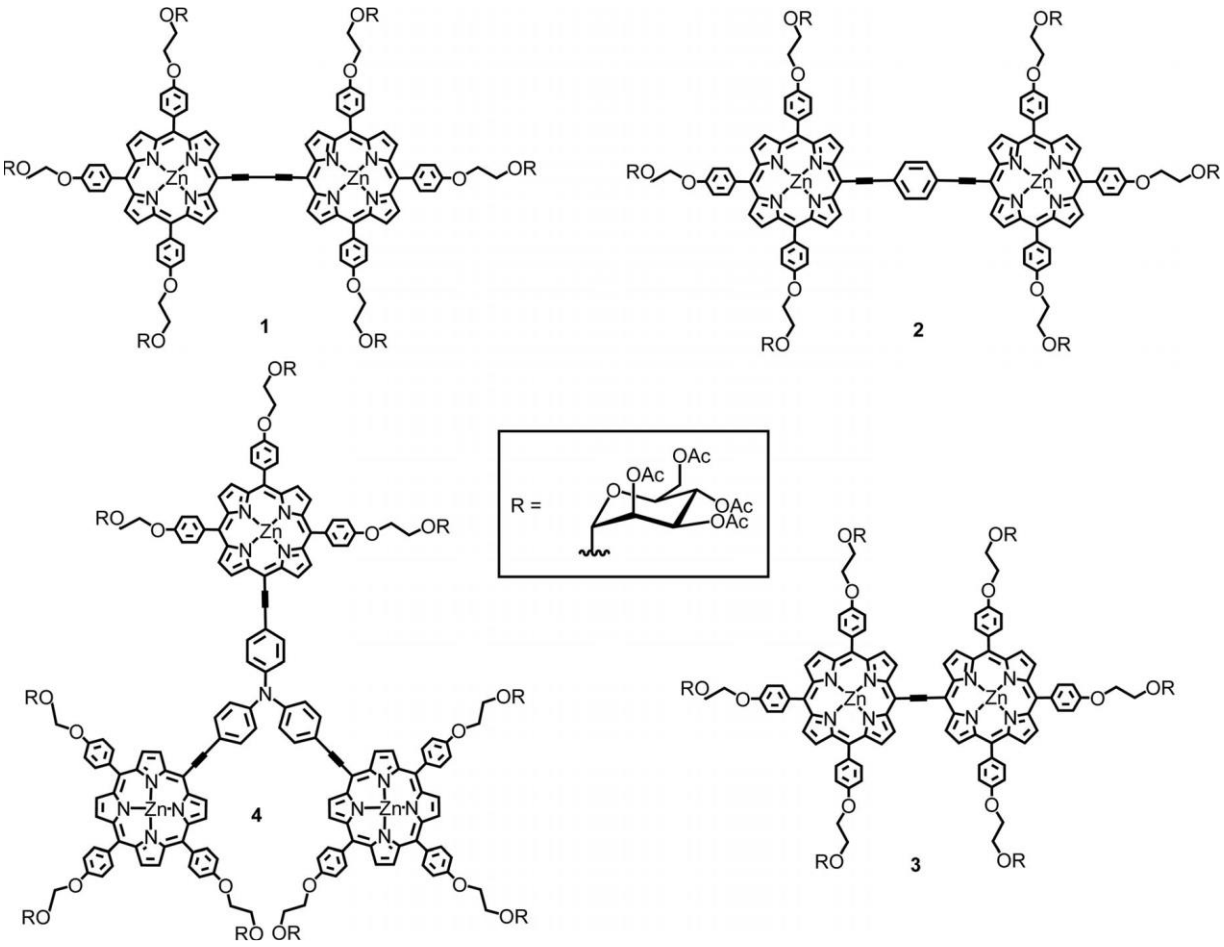

Figure 35: Structures of conjugated zinc- porphyrin oligomers [305].

4.D.2. Metal complexes and ionizing radiation: Platinum complexes

Platinum metal has been used to make complexes for anti-cancer therapy for more than 40 years. The ability of platinum metal to bind covalently to DNA is of particular interest as it can be used to induce direct DNA damage. I would like to discuss about two of the most significant examples of platinum based metal complex, related to my project, that are cisplatin which is the one used in almost 50% of cancer treatment and is associated with radiation in some therapeutic protocols [306-308], and the terpyridin-platinum series that has been shown to induce radiosensitization.

4.D.2.1. Cisplatin

Cisplatin (cis-diamminedichloro-platinum(II), CDDP) is a square planar Pt(II) complex that has been approved for cancer therapeutics in 1978. Though initially approved for testicular cancer, it is now used in a broad spectrum of cancers such as ovarian, lung, bladder and eosophageal cancers apart from the testicular cancer [149, 309, 310]. Certain derivatives of cisplatin such as carboplatin and oxaloplatin (Figure 36) are also developed that have lower toxicity and are being studied for their potential to induce radiosensitization[311-314], but their radiosensitizing properties are not extensively studied so far.

The mechanism of action of cisplatin is that it can create DNA adducts by forming coordination bonds with the N_7 site of purine bases leading to the formation of intrastrand or interstrand DNA crosslinks. The intrastrand crosslinks are the major forms of DNA adducts and account for 85–90% of DNA lesions by cisplatin with 1,2-intrastrand GpG and ApG crosslinks comprising of 65% and 25% of the total lesions respectively. Interstrand crosslinks play a role in the cytotoxicity of cisplatin, however, despite some controversy intrastrand lesions are seen to be the more important form of lesion produced by the drug leading to its cytotoxicity [309]. The genotoxicity of the drug is also based on other factors such as ‘repair shielding’ from NER pathways and ‘hijacking’ of nuclear factors leading to certain impaired cellular functions [309]. Cisplatin was one of the first drugs to exhibit a direct correlation between the amount of Pt bound to DNA and the cytotoxicity of the drug , however it is to be noted that only less than 1% of cellular cisplatin are bound to DNA, in fact majority of the drug is bound to proteins, RNA and small thiol compounds but the relative contribution of these interactions have not been yet elucidated [315, 316]. The Pt-DNA adduct creates a distortion in the DNA structure and the presence of the

adducts inhibit DNA replication and transcription. The cells treated with cisplatin show a G2/M cell cycle arrest while triggering apoptosis in proliferating cells. It is hypothesized that agents inducing arrest at the G2/M phase of the cell cycle would show synergistic relationship with cisplatin[317, 318]. The Pt-adducts formed by cisplatin are shown to be repaired by the Nucleotide Excision Repair Process (NER) [264, 319].

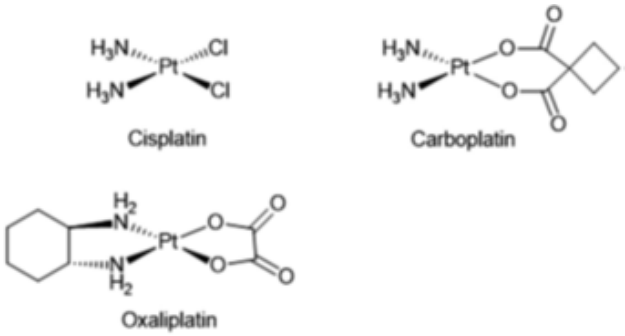

Figure 36: Chemical structures of Cisplatin and its derivatives Carboplatin and Oxaliplatin.

Since cisplatin is able to induce DNA damage and cause cell cycle arrest at a radiosensitive phase, it is naturally a prime target for investigation of its radiosensitizing prowess. There are multiple proposed mechanisms of action mentioned for cisplatin induced radiosensitization, however, they have not been fully demonstrated. Moreover, the radiosensitization seems to be dependent on the cell line, drug treatment time and the chronology of drug-irradiation treatment. There also seems to be contradictory results regarding some of the studies [274, 320].

1) **Direct and indirect effect of ionizing radiation on cisplatin proposed from *in vitro* experiments and its criticisms**

Many contributions of direct and indirect effect of ionizing radiation on cisplatin have been proposed to elucidate the radiosensitizing effect of cisplatin based on biochemical and physical studies. Sanche et al, show via *in vitro* cell free studies, that when cisplatin is bound to plasmid DNA, the formation of SSBs and DSBs by LEE (low energy electrons) is increased, figure 37.

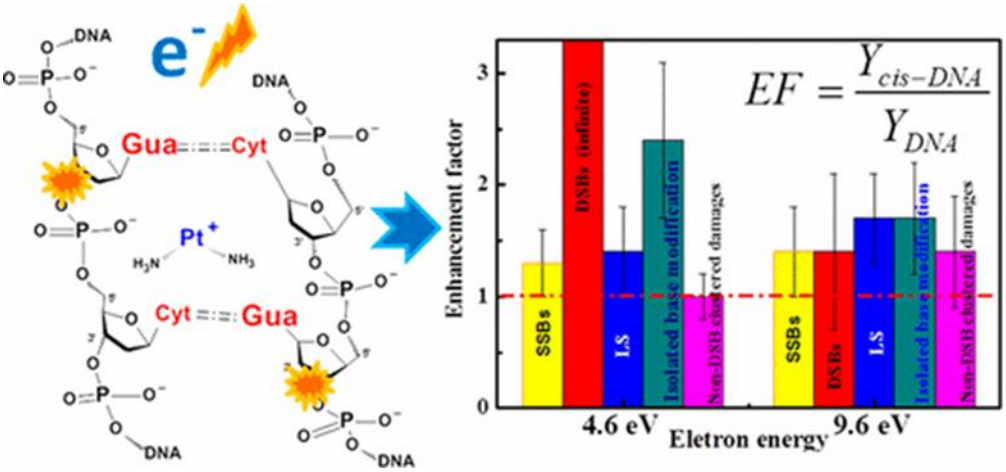

Figure 37: The depiction of enhanced LEE induced damages post cisplatin binding to plasmid DNA [321].

They propose that the DNA damage is induced by secondary electrons and transient anions formation in cisplatin-DNA adducts that trigger phosphodiester bond cleavage located next to the adduct. Low energy electrons are a major secondary product after high energy irradiation. This increase of DNA damage caused by LEE has been postulated to be one of the reasons for cisplatin induced radiosensitization [321, 322]. However, this effect is supposedly quite minor in respect to the biological effects of the drug. In addition, Rousseau et al. found that the additive effect is independent of the X-ray beam energy and concluded that the hypothesized production of auger electrons is not at the origin of the radiosensitization potential of cisplatin [323]. Moreover, it has been shown that under gas-phase LEE favors the loss of two Cl atoms of cisplatin, generating the reactive aqua intermediate which would then form the cisplatin-DNA adducts[324]. Therefore, the ionizing radiation may increase the Pt-Cl cleavage of cisplatin, *in*

cellulo, allowing an increased binding to DNA. And finally, another study also showed that the presence of cisplatin bound to a plasmid DNA enhances the yield of DNA strand breaks under ionizing radiation in a way that depends on the radiolysis species of water that are hydroxyl radical and hydrated electrons. They proposed that the structural modifications in cisplatin containing DNA adduct increases the accessibility of the radiolysis species to DNA [325]. In conclusion, the clear contribution of all these pathways has not been evidenced *in cellulo*.

2) **Effect of ionizing radiation on cisplatin *in cellulo*: use of different cell lines and drug incubation protocols - and its inconsistencies**

Both Myint et al [326], as well as Gorodestsky et al [327], showed that radiosensitization potential of cisplatin is only observed at lower doses of both drug and irradiation. Myint shows radioresistance with MEFs (Murine Embryonic Fibroblasts) with increasing concentration of cisplatin and Gorodestsky shows almost no radiosensitization in OV-1063 and EMT-6 cell lines with increased irradiation levels. Gorodestsky further showed that cisplatin is radiosensitizing only when added post irradiation in both cell lines, providing only an additive effect with pre-irradiation treatment[327]. This, however, is refuted by Turchi and his colleagues as they show that pre-irradiation of cisplatin induces radiosensitization in H460 and A549 (NSCLC cell lines) and post irradiation treatment does not [328].

Moreover, while Turchi showed a radiosensitizing effect of cisplatin in A549 cell line, Toulany et al does not detect any radiosensitizing effect in this cell line[329]. The radiosensitizing protocol is quite different from each other. While Turchi showed radiosensitization with 2h cisplatin treatment pre-irradiation and removal of the drug before irradiation, the concentration used was 4µM (LD50), Toulany's protocol (being successful in H460 cell line) used a much lower concentration, 1µM for 20h treatment pre-irradiation. The duration of drug treatment and the concentration used could play a factor in the difference of result seen in either case. One additional fact to take into consideration is that while Toulany showed radiosensitization (or lack thereof) over multiple radiation doses ranging from 0-4Gy, Turchi used one a single dose of 1Gy. Hence, radiosensitization potential of a drug can be manipulated based on a number of factors depending on drug dose, length of drug incubation, and radiation dose.

3) **Involvement of DDR in radiosensitizing effect of cisplatin**

Inhibition of ATM activity has shown a markedly increase of cisplatin radiosensitization [329]. In this paper, they concluded that activation of ATM activity by cisplatin can abrogate its radiosensitizing effect while ATM deficient cells (with an ATM inhibitor) were significantly sensitized to irradiation by cisplatin. This is in contrast with the results shown before where cisplatin is seen to radiosensitize only HR proficient yeast cells, not yeast lacking Rad52-dependent HR repair, thus implying a role of HR [330].

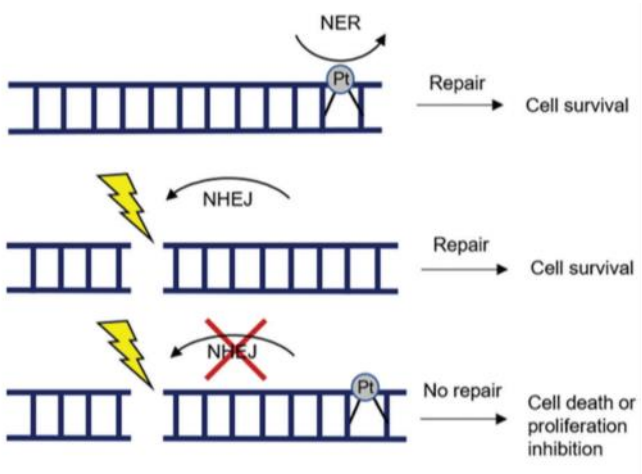

Figure 38: Schematic diagram of the proposed mechanism of radiosensitization by Cisplatin, showing that NHEJ is unable to repair irradiation damage near a Pt-DNA adduct [271].

In addition, Turchi et al, proposed that cisplatin is able to induce radiosensitization in non-small cell lung cancer by interfering in the ability of NHEJ based repair [328]. This is supported by a significant amount of research highlighting the importance of NHEJ in cisplatin radiosensitivity (Figure 38). It has been shown that deficiencies in cisplatin lesion repair causes radiosensitization and that NHEJ deficient cells show additive and not synergistic effect with cisplatin and irradiation, highlighting the importance of NHEJ [326, 331]. Moreover, cisplatin DNA adduct is capable of inhibiting the translocation of Ku to the DNA damage site and DNA-PK activation *in vitro* [332, 333]. Lastly, the presence of cisplatin adducts are seen to impair the ability of NHEJ to repair adjacent DNA termini in *in vitro* assays, which suggests that the inability of NHEJ to repair irradiation induced damages next to a cisplatin adduct could be a potential radiosensitization mechanism [334].

The cisplatin-irradiation induced inhibition of DSB repair leads to a presence of persistent γH2AX foci 24h post irradiation, ensuring the presence of unrepaired breaks leading to enhanced cell death [328]. It is also noted that the cisplatin induced G2/M block is abrogated when combined with irradiation. Progression through the cell cycle without repair of the cisplatin-DNA lesions could result in the development of complex DSBs at the site of stalled replication forks or non-DSB cluster lesions (comprised of two or more DNA SSBs on opposing DNA strands) in close proximity to cisplatin lesions. These complex DSBs which are found close to cisplatin adducts are not supposed to be easily repaired as the NHEJ catalyzed DSB repair is shown to be impaired at these sites [335]. Thus shedding more light into the mechanism of action of cisplatin induced radiosensitization.

4.D.1.2. Pt-ctpy

Pt-ctpy (Figure 39A) is a part of the terpyridine series of complexes and is shown to be a G4 binding ligand since it stabilizes G4s but not duplex DNA *in vitro* [336]. *In cellulo* [143], Pt-ctpy could induce a cell cycle accumulation in the S-phase while reducing cells present in G0/G1 phase. Additionally, in SF763 cells it also induced a G2/M block. Pt-ctpy treatment also showed to target indirectly telomeres: an upregulation in the levels of hTERT, could extend the telomeric overhang and therefore counteract the potential damaging effect of Pt-ctpy on telomeres as seen for the triazine 12459 G4 ligand [337] and a downregulation in the level of TRF1, known for limiting the access of telomerase to telomeres [338]. These compensatory effects are in agreement with the action of the TAC G4 ligand [339].

Pt-ctpy is then shown to induce radiosensitization in multiple glioblastoma (SF763 and SF767) and NSCLC (H1299 and A549) cell lines, as shown in the figure 39B. Moreover, when tested on GBM xenografts on nude mice, Pt-ctpy combined with irradiation was able to show an inhibition in tumor growth over 90 days compared to the 30 day inhibition with irradiation alone (Figure 39C and 39D) [143].

One possible mechanism of action for radiosensitization by Pt-ctpy is hypothesized to be telomeric dysfunction post irradiation. There is a significant increase of TIFs (telomere dysfunction induced foci) observed 24 hours post irradiation when treated with the drug, as is the number of total telomere loss in a metaphase chromosome spread. Moreover, they show that the number of 53BP1 foci 0.5h post–irradiation was significantly higher following the combined treatment than each individual treatment. The higher amount of 53BP1 foci persists 24h post-irradiation in the combined treatment: however, the number of foci varies from 3 to 5 only.

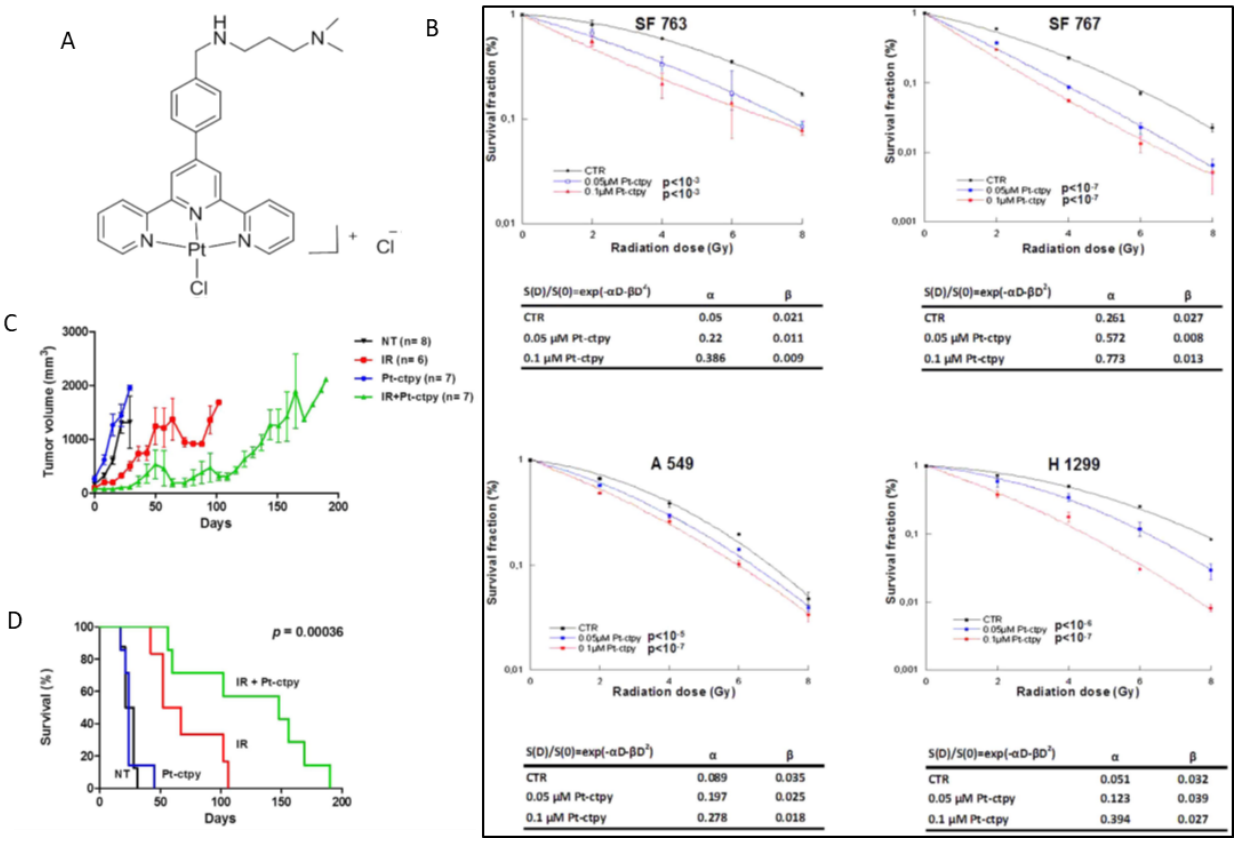

Figure 39: Radiosensitizing effect of Pt-ctpy. Chemical structure of (A) Pt-ctpy. Radiosensitization potential of Pt-ctpy in (B) 4 different cell lines. Pt-ctpy with irradiation is capable of (C) decreasing tumor volume in xenografted mice and (D) increasing the survival of the xenografted mice post treatment [143].

In addition, the authors never detect radiosensitisation with cisplatin in these cell lines. They conclude consequently that the mechanism of radiosensitisation of Pt-ctpy should not depend on its platination properties.

The mechanism of action of this radiosensitizing effect has not been resolved. Since there exist other members of the terpyridine family that are or not G4 ligands, and that none have been exclusively studied for their radiosensitization properties, it is important to investigate further the mechanism of action of this family that could help to 1) decipher the radiosensitazing effet and 2) discover novel radiosensitizing drugs. Since G4 binding drugs could potentially induce telomeric dysfunction, and telomeres have been proposed to be a radiosensitization target [340, 341], we decided to perform a screening of terpyridine family ligands for their radiosensitization potential.

4.E. G- quadruplex binding drug induced radiosensitization

4.E.1. TAC

TAC is a G-quadruplex binding drug that can induce DSBs in Glioblastoma cell lines by itself as is shown by an increase of 53BP1 foci formation with increasing dose of the drug [339]. It is also indicated that TAC could affect telomeres since it causes chromosomal fusions, a sign of telomeric instability, as well as hTERT and TRF2 overexpression which could be attributed to compensatory mechanism of the cell in response to G4 drug treatment. While these are indications, it is to be noted that no direct evidence is provided to show telomeric DNA damage or dysfunction caused by TAC.

It is also able to show radiosensitization in two GBM cell lines SF763 and SF767 as shown in figure 40. The mechanism of action is hypothesized to be due to reduced DSB repair as they show an increased γH2AX at 24hrs with the co-treatment of drug and radiation compared to radiation alone. The amount of phosphorylated γH2AX was counted by Flow cytometry and not by the more accepted and accurate method of immunofluorescence. The co-treated cells were shown to have a cell cycle block at G2-M indicating high DNA damage that needed repair and the authors also suggest that the excess DNA damage could explain the radiosensitization at a cellular level, but not necessary due to its G4 binding properties. No apoptosis is shown 72 hours post co-treatment and has been hypothesized to be due to the blockage of cells at the G2-M stage of the cell cycle.

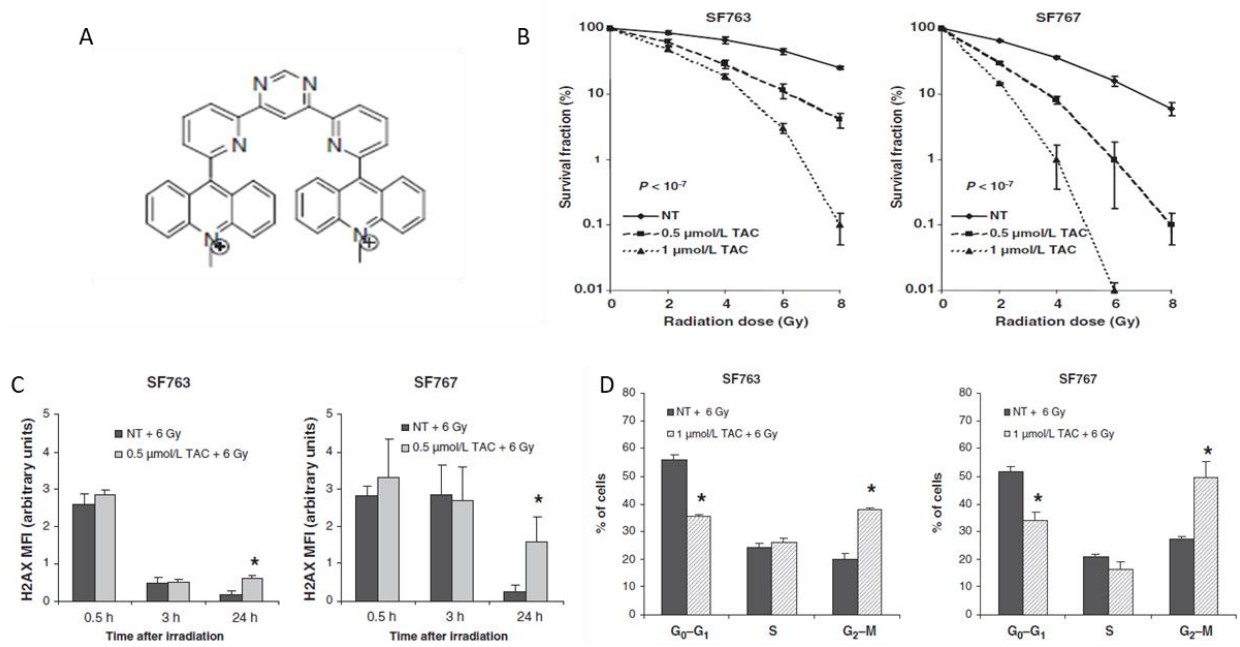

Figure 40: Chemical Structure of (A) TAC and its (B) radiosensitization potential on two GBM cell lines are shown. The (C) increase of gH2AX formation at 24hrs and the (D) G2-M block achieved by co-treatment of TAC with irradiation is shown [339].

4.E.2.RHPS4

Apart from Pt-ctpy and TAC, another G-quadruplex binding drug that is capable of inducing radiosensitization in cancer cells. RHPS4 is a pentacyclic acridine compound (3,11-difluoro-6,8,13-trimethyl-8H-quino[4,3,2-kl] acridinium methosulfate), as shown in the figure 41A. It is considered as one of the most effective G4 stabilizing molecules. In absence of irradiation, it can cause telomere deprotection leading to telomeric fusions, anaphase bridges and cell proliferation blockage. In long-term exposure, it was found to induce telomerase inhibition and the down-regulation of the human telomerase catalytic subunit (hTERT) gene, telomere erosion, arrest at the G2/M transition and suppression of cell proliferation in cancer cells [92, 342, 343].

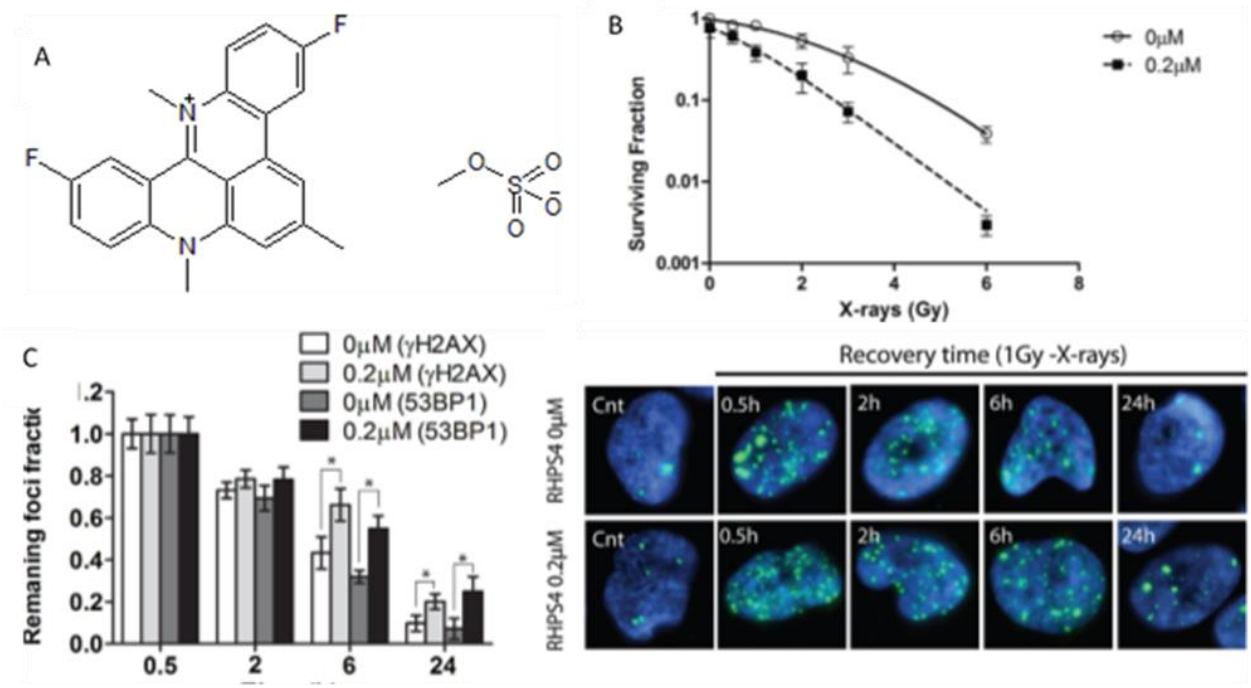

Figure 41: Chemical structure of (A) RHPS4 and its (B) radiosensitization potential. RHPS4 is able to (C) induce a delay in DSB foci repair which is attributed to its mechanism of radiosensitization [344].

RHPS4 is able to induce radiosensitization in Glioblastoma Multiforme (GBM) cells (Figure 41B) that has been linked to telomere dysfunction. It has been shown that increasing duration of RHPS4 exposure to cells before irradiation leads to a decrease in survival of GBM cells. This has been correlated to the levels of TIFs (Telomere dysfunction induced foci) generated before

irradiation. Moreover, in addition to the role of telomeres dysfunction in the radiosensitivity of cells to RHPS4, RHPS4 induces a delay in DNA repair kinetics when co-treated with irradiation in comparison of irradiation alone (Figure 41C) [344]. These results clearly show the role of uncapped telomeres in the radiosensitization effect and highlight the role of telomere dysfunction inducing compounds that could play in radiotherapy. However, it is not clear if the delayed DSB repair kinetics observed is due to the presence of dysfunctional telomeres or another reason such as increased chromatin compaction.

The radiosensitization ability of RHPS4 is confirmed in a heterotopic GMB-xenografted mouse model derived from U251MG cells that are Glioblastoma Stem-like cells (GSCs), where the combined treated led to a very potent and durable inhibition of tumor growth till the 65th day post treatment. This led to the hypothesis that RHPS4 could target the GSCs present in the tumor that are primarily responsible for the reoccurrence of the tumor. However, the ability of RHPS4 to target telomeres is seen to be non-effective in GSCs but it is able to reduce cell proliferation of GSCs by depleting levels of CHK1 and RAD51 with consequent replicative stress and cell cycle blockage. Moreover it does not show any increased effectivity when co-treated with irradiation [345]. It is now suggested that combined inhibition of cell-cycle checkpoints and DNA repair proteins can provide the most effective means to overcome resistance of GSC to genotoxic insults.

RHPS4 is therefore a powerful radiosensitizer in GBM *in vivo* although GBM cells and GSCs respond differently to this ligand.

Hence, RHPS4 is a shown to be a potent radiosensitizer of glioblastoma cancer cells *in cellulo* as well as in a xenograft mouse model, potentially due to its ability to induce telomeric dysfunction and perturb the rate of DSB repair. However, it is not universal in its radiosensitization potential owing to its inability to synergize with irradiation for the GSCs.

4.E.3. Other G-quadruplex interactions and radiosensitization

Finally, G4 ligands have been shown to radiosensitize ATRX (α-thalassemia mental retardation X-linked) deficient normal human astrocytes (NHA) and glioma stem cell (GSC) models [346]. Among the many functionalities of ATRX, one hypothesis is that it serves to resolve G4s present in the genome and diminish their deleterious effects [32]. Hence, deletion of ATRX using shRNA has shown an increase of stabilized G4s present in the genome. It is also shown that an increased lethality is observed when G4 drugs such as CX-3543 and others are treated to the ATRX deficient cells.

Regarding radiosensitization, the authors observe an interesting result where CX-3543 is capable of inducing radiosensitization on the NHA cells, however, the synergy is greatly increased when in ATRX deficient NHA cells. This synergistic increase can be rescued to an extent when the shATRX2 is inactivated via its dox-inducible promoter. This clearly shows that G4 stabilization can dramatically increase the radiosensitization of ATRX deficient NHA cells. The mechanism of action for radiosensitization is not clear, however, it is hypothesized that ATRX deficiency leads to greater genomic instability and a loss of NHEJ functionality [347]. This would sensitize the cells to DNA damage inducing agents such as irradiation.

However, with all the studies on how stabilization of G4s could lead to radiosensitization, interestingly, there exists a paper which is on the other side of the argument. It states that the formation of G4s in the genome could actually lead to radioprotection [348]. The paper shows that genomic regions abundant in G4 are protected from radiation induced breaks; moreover, the G4 structures at the telomeric ends safeguard the chromosome ends against irradiation induced damages. This study also shows that G4 forming regions in the genome are undamaged post irradiation and that resolving these structures can lead to their sensitivity. While the paper acknowledges that the G4 resolving helicases could induce sensitization based on other cellular phenomenon, they provide us with a hypothesis for the radioprotective effect of the G4 structures. The G4 planar quartet shows a low oxidation potential and exhibits hole trapping properties against the hydroxyl radicals induced by the radiolysis of water. Since, guanines in the ssDNA show high oxidation potential, the G4 structures seem to be protected against the DNA

damage effects of irradiation. Hence, the radioprotective effect of G4s is attributed to the hoogsteen hydrogen bonding in the G4 quartets.

This paper does not necessarily go against all we have learnt from G4 binding radiosensitizers. One could argue that even if the G4 drugs are stabilizing the G4 structures leading to protection from irradiation damage at those specific sequences, the mechanism of action proposed for most G4 radiosensitizers are telomeric dysfunction and an impairment of DSB repair. The drugs could very well protect the G4 structure from IR damage and cause a delay in repair concurrently. Hence, the paper should help us understand the global mechanism at a greater detail.

OBJECTIVES

Objective

Chemoradiotherapy is a standard treatment for many different cancers such as ovarian, NSCLC, glioblastoma, bladder, rectal, colon cancer etc. Hence, the requirement of potent radiosensitizers is paramount that can help ameliorate the two big limitations of radiotherapy, 1. Radioresistance in tumor cells and 2. Effect on the normal cells around the tumor [169]. Various radiosensitizers are studied with some already in clinical trials, however, not much is known about radiosensitizers that have specific DNA targets, such as G4s, and can cause DNA damage. Two G4 binding drugs (Pt-ctpy and RHPS4) were identified with radiosensitization (RS) potential in glioblastoma and NSCLC cell lines[143, 344]. Pt-ctpy is a metal complex from the tolyl-terpyridine family and has a platinum metal bound to it. The other important platinum metal drug shown to induce RS is cisplatin [326-329]. The mechanism of action for RS by both of these metal complexes are either not specified or dependent on specific conditions such as cell line, concentration of drug and the time of treatment. Hence, we wanted to find if there are other metal complex ligands that can induce RS and to understand their mechanism of action.

The first objective was to identify other metal complex ligands that can cause RS in several cancer cell lines and study their structure activity relationship. We want to decipher if the ligand structure (terpyridine G4 series, salphen G4 series and Pt-NHC series) played a role in radiosensitization. Secondly, if the metal atom (Pt, Ni, Cu, V, Zn) was able to provide an advantage for radiosensitization and lastly, if G4 targeting was essential for radiosensitization. Hence, we performed a screening of different metal complexes from different families (G4 targeting or not) with different metals bound to them.

The second objective was to decipher the mechanism of action of the drug selected from the screening performed, the platinum tolyl-terpyridine, Pt-ttpy. First, we wanted to see the effects of the drug alone and identify its DNA damage sites, followed by its mechanism of action for RS. There are multiple reasons for drugs to be able to induce RS [271]. Pt-ctpy was shown to induce radiosensitization by creating telomere dysfunction post irradiation. The radiosensitization of RHPS4 on the other hand was correlated to telomeric dysfunction pre-irradiation and also to delay in the DNA repair post irradiation. Due to the various mechanisms within G4 binding drugs, we wanted to determine if the RS of Pt-ttpy was due to the increased efficiency of its binding to

DNA post irradiation, a DNA damage repair delay, cell cycle progression modification, ROS production and/or telomere dysfunction pre- or post-irradiation. Deciphering the mechanism of action of the metal complex ligand would help us identify and develop future potential drugs that would lead in ameliorating the limitations of radiotherapy.

RESULTS

1: Radiosensitization Screening

1.1. Cellular activity of metal complex G4 ligands

We wanted to first evaluate the cellular cytotoxicity of the G4-binding metal complex on the ovarian carcinoma cell line A2780. This cell line was isolated from an untreated patient's tumor. It was selected for our studies as cisplatin has been widely used to treat ovarian carcinoma and multiple studies have been done on the A2780 cell line [349, 350]. The cell line is also a good candidate to evaluate the cytotoxicity of Pt-complex drugs [142, 150] (Annex 1).

Another cell line A2780cis, a cisplatin resistant cell line from the lineage of A2780, is used to determine if the complexes are able to overcome the cisplatin resistance by inducing cellular cytotoxicity. This cell line had been created by chronic exposure of A2780 cell line to the drug cisplatin and maintained by a monthly treatment of 1µM cisplatin for 4 days.

Finally, a normal lung fibroblast cell line CCD19Lu was used to determine if the metal terpyridine complexes are selective in inducing toxicity to cancer cells. This cell line is not immortalized and can be cultured for 8/9 PDL (Population Doubling Level) before it enters senescence. The doubling time of CCD19Lu is almost twice that of A2780 cell line.

The proliferation assay was performed after 96 hours drug treatments. The survival curves are drawn based on the count of adherent cells and the IC50 is determined. There are multiple ways to perform a cell cytotoxicity assay such as MTT, Cell Titer Glow, etc, however, the survival curves from each assay do not necessarily correlate to each other [351]. We used Cell Titer Glow as well as the counting method for determining the IC_{50} for the metal complexes but we realized that the counting method provided a more realistic survival curve due to the correlation between the inhibition observed by microscope and cell counter device. Hence we proceeded to use it for all the required experiments.

Metal-Terpyridine complexes

Metal terpyridines have been shown to have good affinity towards G4 structures, due to their square planar and square-based pyramidal geometries [140]. They have been synthetized by the chemists of our laboratory. Pt-ttpy has also been shown to stack to the G-quartets at both ends of the c-myc promoter G4 (by NMR) and to platinate the c-myc promoter G4 as well as the telomeric G4 (via gel electrophoresis) [126, 141] as well as modify the structure of telomeres in cells by direct platination [127]. Hence a study was done to better understand the properties of the metal terpyridine series (Pt-ttpy, Pt-tpy, Pt(PA)-tpy, Pt-vpym, Pt-cpym, Pt-BisQ and Pt-ctpy) (figure 1) for their G4 affinity and selectivity with *in vitro* experiments using FRET melting assay and Fluorescence Intercalator Displacement (FID) (figure 2) [142] (Annex 1).

The *in vitro* results from FRET melting assay show that Pt-BisQ, Pt-ctpy and Pt-ttpy exhibit higher G4 stabilization independently from the G4 topology. The same trend was obtained on the different G4 used: 22AG from human telomeric sequence (polymorphic), 21CTA from human telomeric sequence variant (antiparallel), CEB25-WT from minisatellite sequence (parallel with a central long propeller loop), and from c-myc proto-oncogene sequence (parallel with short propeller loops). A selectivity for G4s over duplex DNA is seen in experiments using duplex DNA in competition. This same trend is seen with the FID assays, with the three more stabilizing complexes being efficient in displacing Thiazole Orange (TO) from the G4s as compared to the duplex DNA.

Regarding the complexes ability to induce cytotoxicity in ovarian carcinoma cell lines, we added two more complexes that are not with a Pt-metal- Cu-ttpy and Pd-ttpy; along with the positive control of a known chemotherapeutic drug cisplatin. The cells were treated with an increasing concentration of the drugs for a period of 96h to determine their IC_{50} (concentration at which 50% of the cell population can survive).

Platinum complexes of the terpyridine family show inhibition of the cell growth proliferation in the µM range (IC_{50} from 0.08 to 6 µM) as a function of their structure and can be classified as follows: Pt(PA)-tpy > Pt-vpym > cisplatin > Pt-ttpy > Pt-tpy > Pt-ctpy > Pt-cpym > Pt-BisQ (as shown in the Table 1). Moreover, none of the platinum complexes show a significant cross-resistance to

cisplatin since no significant differences between cisplatin-sensitive and resistant cell lines could be highlighted. This is noted by calculating the Resistance Factor which is a ratio of the IC_{50} value of A2780 cis and A2780 cell line and it was seen that the ratio remained under the factor of 1.6, whereas the one for cisplatin was 9.1. All of them show no specificity for cancer cell lines, similar to the clinical anticancer drug cisplatin. Pt-ttpy, Pt-ctpy and Cu-ttpy were additionally also tested for their cell growth proliferation in T98G and H1299 cell lines (Table 2) and their IC_{50} is comparable to that of A2780 cell line.

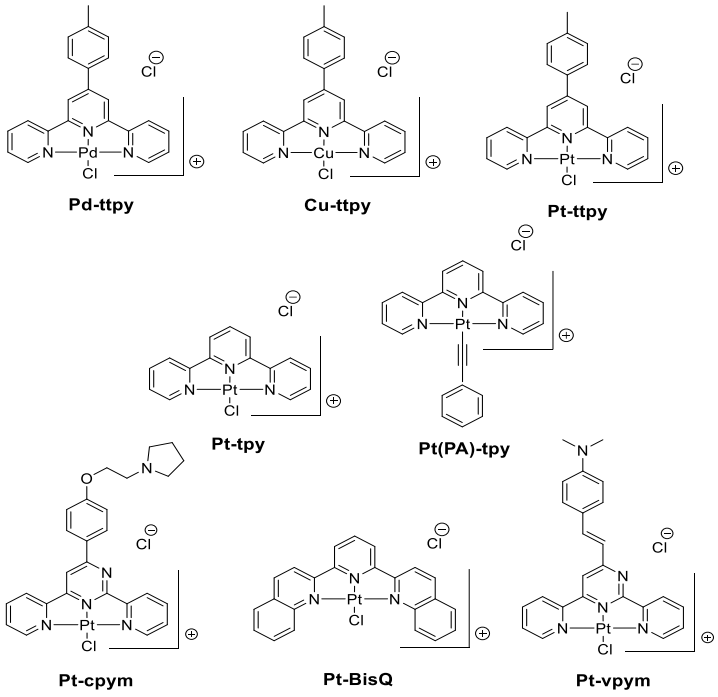

Figure 1: Structure of the different members of the terpyridine series selected for the radiosensitization screening

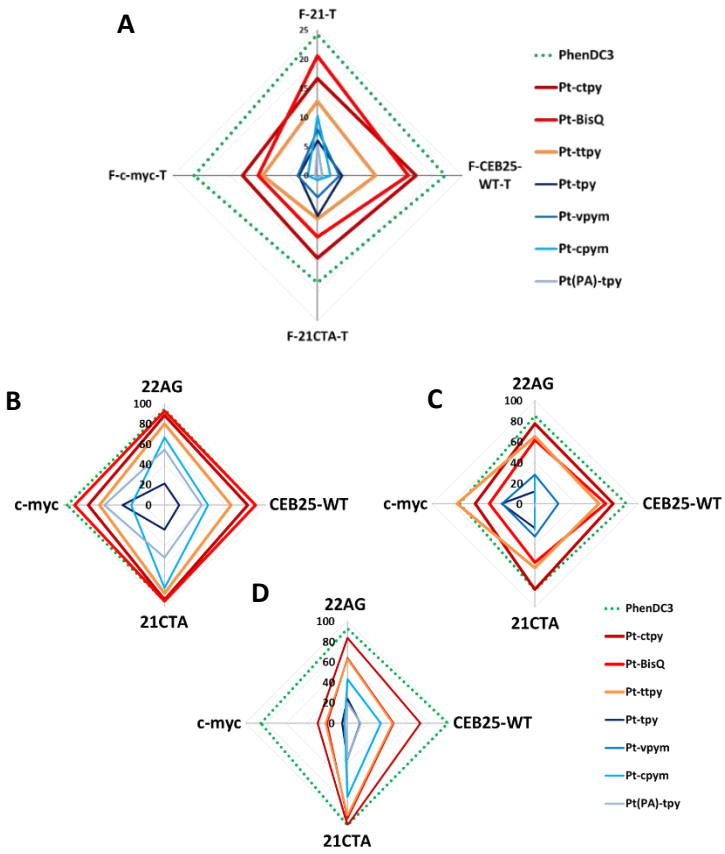

Figure 2: (A) A radar plot representing ΔTm values obtained from FRET-melting experiments in the presence of various terpyridine-Pt complexes: Pt-ctpy, Pt-BisQ, Pt-ttpy, Pt-tpy, Pt-vpym, Pt-cpym and Pt(PA)-tpy and PhenDC3, used as a control. The radar plot representing the percent of the probe displacement at 1 µM of the Pt(II) complexes and PhenDC3 used as control for the G4-FID assay, performed in the presence of 22AG, c-myc, 21CTA, and CEB25-WT with (B) Thiazole Orange (TO), (C) TO-PRO-3, or (D) Phen DV in K+100 buffer.

Drugs	A2780 (µM)	A2780cis (µM)	Resistance factor	CCD19Lu (µM)
Pt-ttpy	2.5	2.5	1	1.75
Pt-tpy	3	5	1.6	3
Pt(PA)-tpy	0.08	0.05	0.6	0.12
Pt-vpym	0.7	0.4	0.6	0.7
Pt-cpym	3.8	5	1.3	1.8
Pt-BisQ	4	6	1.5	4.10
Cu-ttpy	0.06	N/A	N/A	N/A
Pd-ttpy	0.06	N/A	N/A	N/A
Cisplatin	0.33	3	9.1	0.2

Table 1: The IC_{50} (µM) of the various platinum complexes calculated from the proliferation of A2780, A2780cis, and CCD19Lu cell lines after 96h treatments and their resistance factor (IC_{50} ratio A2780cis/A2780).

Drugs	T98G (µM)	H1299 (µM)
Pt-ttpy	2	2.5
Pt-ctpy	N/A	3
Cu-ttpy	0.2	0.07

Table 2: The IC_{50} values (µM) of certain metal-terpyridine complexes calculated from the proliferation of two different cell lines T98G and H1299 after 96h treatments.

Conclusion

The structure activity relationship in the terpyridine series shows that modifications to the ligand structure can have a change on the affinity of the drug to G4s. Pt-tpy and Pt-(A)tpy do not show G4 affinity; addition of a tolyl group (Pt-ttpy), or tolyl with a protonable side chain (Pt-ctpy) or replacing the terpyridine core by a bisquinoline (Pt-BisQ) increases the G4 affinity; and modifying the terpyridine core (Pt-vpym and Pt-cpym) reduces the G4 affinity.

Regarding the cytotoxicity of the complexes, all show an IC_{50} in the µM range except for Pt-(A)tpy which is in the nM range for the A2780 cell lines. More importantly they are able to overcome the cisplatin resistance in A2780cis cell line. This could be due to an independent pathway used by the drugs to enter cells, different from the copper carrier proteins used by cisplatin [352]. Moreover, due to Pt-(A)tpy being the most cytotoxic complexes, we observe that the drug efficiency is probably not based on their affinity for G4s and their capability to platinate DNA in vitro. This work leads to a publication in the journal, Molecules [142] (Annex 1).

The knowledge of the metal-terpyridine series cytotoxicity helps us move further in testing their radiosensitization potential since we need to use the drug's subtoxic concentration to screen for their capability to induce radiosensitization.

Pt-NHC complex

The Pt-NHC complexes have synthetized by our chemist collaborators at 'Institut de Chimie des Substances Naturelles' in Gif sur Yvette (JF Betzer and A. Marinetti). FNI-324 and its conjugate to the G4 ligand pyridodicarboxamid (PDC) creating Pt-NHC-PDC via a linker chain containing 4 or 8 carbons (C4 or C8) have been studied for their anti-proliferative ability and telomere targeting [150]. FNI-324 shows a much higher cytotoxicity with its IC_{50} 18-fold lower than that of C4-PDC. Moreover, they do not show any cross-resistance with cisplatin as there is no significant difference between the IC_{50} in A2780 and A2780cis cell lines. Both Pt-NHC and Pt-NHC-PDC complex are able to target telomeres by inducing TRF2 displacement, with the Pt-NHC-C4-PDC complex being more efficient than FNI-324 probably due to its PDC moiety that can recognize the telomeric G4 thereby directing the molecule to the target.

In addition, other Pt-NHC were also synthetized in order to induce DNA cross-links different from cisplatin and induce other biological answers. Among them the dinuclear Pt-NHC complex, MC1-121D is also able to induce a proliferation loss better than cisplatin in multiple cell lines, including A2780 and A2780cis [151]. Like the other Pt-NHC complexes, this dinuclear Pt-NHC also does not show any cross-resistance to cisplatin. It has been shown to accumulate in A2780 cells more easily than cisplatin but its binding to DNA is lower than expected with respect to its cellular accumulation. It seems to induce apoptosis in a caspase independent pathway and may also induce necrosis.

FNI-324 and MC1-121D complexes showed to induce radiosensitization in preliminary results. However, due to its existing publication record, these complexes could not be patented. Hence, new complexes were designed by the lab of J.F. Betzer and Angela Marinetti at 'Institut de Chimie des Substances Naturelles' and screened for their radiosensitization potential.

The new complexes are represented under their general formulae in figure 3 due the confidentiality necessary for patent. We focused our work on two mononuclear-Pt-NHC named MS113 and MS140; four Dinuclear-Pt-NHC complexes named C4, C6, C6cy and C8; Pt-NHC complex conjugated to the PDC molecule Pt-NHC-C4-PDC and Pt-NHC-C8-PDC were tested also for their cytotoxicity in A2780, H1299 (non-small cell lung carcinoma) and T98G (Glioblastoma

multiforme) cell lines. The complexes were used in increasing concentrations for a period of 96h in order to determine their IC_{50} for survival.

The results show that the IC_{50} of Pt-NHC complexes are in the range of 1-5µM, except for the Pt-NHC complexes conjugated with PDC whose IC_{50} value is above 25µM showing low cytotoxicity. Their IC_{50} values of the different complexes in each cell line is noted in the Table 3.

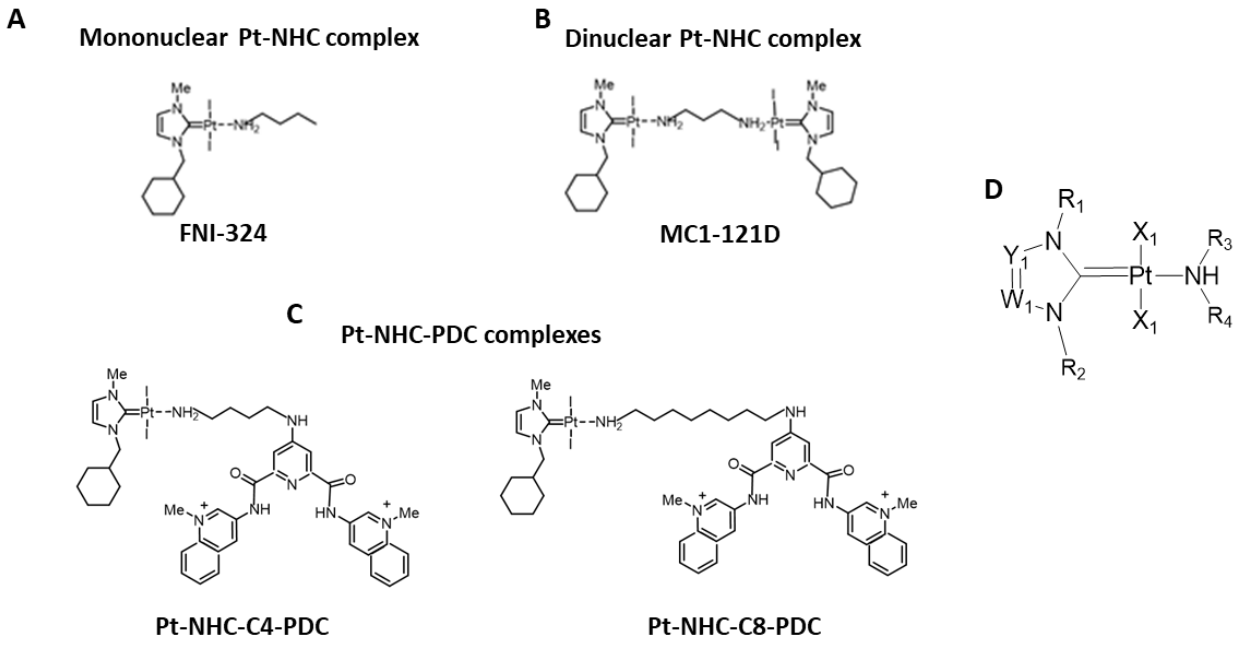

Figure 3: Structure of the different members of the Pt-NHC complex published in literature belonging to (A) mononuclear Pt-NHC, (B) dinuclear Pt-NHC complex and (C) Pt-NHC-PDC complexes [150, 151]. The new Pt-NHC complexes are hidden due to the filing of a patent. (D) A generalized structure is shown here.

Drugs	A2780	T98G	H1299
MS113	2.86 ±1.09	N/A	N/A
MS140	4.2 ± 0.2	N/A	N/A
FNI-324	1.35	1.5	N/A
C4	0.4 ± 0.2		2.1
C6	1.60 ± 0.15	5.1	3.2
C6cy	1.77 ± 0.09		
C8	1.86 ± 0.8		
Pt-NHC-C4-PDC	10	N/A	N/A
Pt-NHC-C8-PDC	>25	N/A	N/A

Table 3: The IC_{50} (µM) values of the Pt-NHC series calculated from the proliferation of three different cell lines A2780, T98G and H1299 after 96h treatments.

Conclusion

The Pt-NHC complexes studied in literature have shown cell growth at 50% inhibition in µM range and an ability to overcome the cisplatin resistance in A2780cis cell line [150, 151]. The new Pt-NHC complexes, mononuclear and dinuclear have shown high cytotoxicity compared to the PDC conjugated complexes. This trend has been seen previously [150].

The new Pt-NHC complexes are submitted for a patent as they are efficient drugs that can bind to DNA via coordination and can also overcome cisplatin resistance. They are screened in this study for their radiosensitization potential at subtoxic concentrations, hence, studying their cytotoxicity profile was important.

Metal-Salphen complexes

The metal salphen complexes were designed and synthetized in the lab of Ramon Vilar, Imperial College London. The metal-Salphen complexes (S-NI, S-Cu) and the metal-bipyridine complex (C-Ni) show higher G4 affinity over duplex DNA. These complexes are studied for their selectivity against six different G4 DNA structures of different topology via FRET melting assays and all of them show a preference towards antiparallel and hybrid conformations over parallel ones. Moreover, these complexes have the ability to stop the Taq polymerase from elongating a primer when a G4 structure forms in the template strand [136].

In order to screen for potential radiosensitizing properties in the metal-Salphen series, we first needed to find the cytotoxicity of the Salphen complexes S-Ni, S-Cu, S-V, S-Zn and C-Ni. They were tested on the three cell lines, A2780, T98G and H1299. The complexes were used in increasing concentrations for a period of 96h in order to determine their IC_{50} for survival.

C-Ni shows the highest cytotoxicity with an IC_{50} of 0.8µM and S-Zn is the least cytotoxic with 5.8µM. The cytotoxicity is decreased in T98G cell line; however, the complexes retain their cytotoxic trend. The IC_{50} values of the drugs for each cell line is noted in the Table 4.

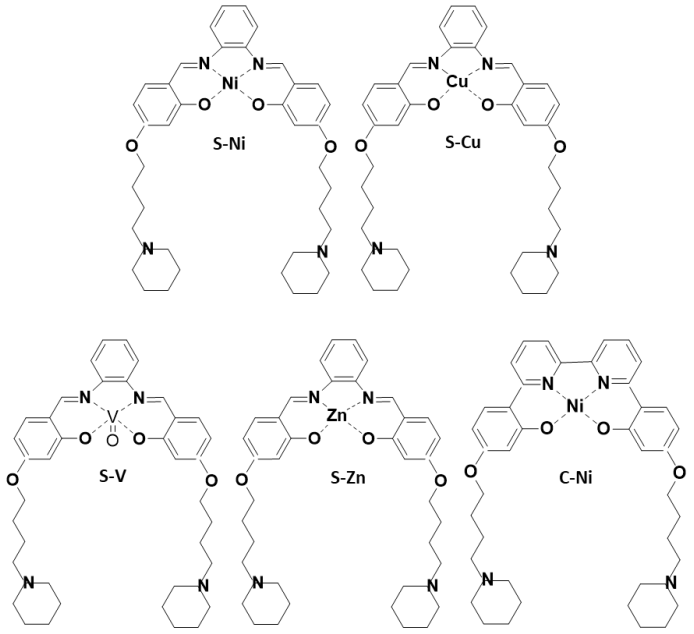

Figure 4: Structure of the different members of the Salphen series

Drugs	A2780	T98G	H1299
C-Ni	0.8	3	1.5
S-Ni	2.2	3.5	2
S-Cu	2	4	N/A
S-V	3.5	6	N/A
S-Zn	5.8	>15	N/A

Table 4: The IC_{50} values of the salphen series calculated from the proliferation of three different cell lines A2780, T98G and H1299 after 96h treatments.

Conclusions-

The metal-salphen series are G4 binding complexes that can be cytotoxic to cancer cells. The IC_{50} was determined on 5 different metal salphen complexes in 3 different cell lines and was seen to be in the μM range. The cytotoxicity profile helps determine the subtoxic concentrations to be used in order to screen them for their radiosensitization potential.

1.2. Screening of metal complexes from different series for RS shows no preference for metal or G-quadruplex binding capability

The screening of the metal complexes for radiosensitization was done on three cell lines (A2780, T98G and H1299) that are telomerase positive but have different p53 status- A2780 is TP53 WT, T98G is TP53 mutated and H1299 is TP53 null. It followed a strict protocol that we established personally. The cells were seeded at a low concentration of 8000 cells per condition in order to avoid a confluent state after a minimum of 5 population doublings. The cells were then incubated overnight with their IC_{30} concentration (determined after 4 days incubation), and irradiated at increasing dose from 1-4Gys for A2780 cell line and 2-8Gys for T98G and H1299 cell lines, the following day. The cells, in the presence of the drug, were then incubated for further 6 days and the cell count taken. Interestingly, the inhibition of cell proliferation after 6days treatment is always less than the one observed after 4 days incubation (no more than 30% cell growth inhibition).

The decision to count the cells at the end of 6 days post irradiation instead of a clonogenic assay was taken since not all cell lines, example T98G, were able to form colonies. The clonogenic assay post irradiation was performed with the drug Pt-ttpy on A2780 cell line and compared with the cell count method, both yielding similar results. Hence, we decided to perform the radiosensitization assay using the cell count method.

The survival curve obtained at the end of the experiment is used to determine the D10 value of the drug-irradiation combined treatment. The survival curve is fitted with the linear-quadratic model: $S(D)/S(0) = \exp(-\alpha D - \beta D^2)$. The α and β parameters were used to calculate the D10 value. D10 is the dose of irradiation administered at which the cell survival is at 10% of the un-irradiated. If a drug is radiosensitizing, its combined treatment would show a lower D10 value than that of the control condition, but not for an additive drug as the D10 takes into account the cell survival at 0Gys. The D10 values can then be used to compare multiple drugs for their radiosensitization potential in the same cell line.

Metal- Terpyridine complexes

Pt-ctpy is the first terpyridine metal complex used to show radiosensitization[143]. In order to understand if the radiosensitization is dependent on the metal platinum, the ligand structure and/or its ability to bind to G4s, we performed a screening of different complexes from the metal terpyridine family. These complexes involve several different metals, variations to the terpyridine structure and an ability/disability to bind to the G4s covalently (Figure 1 before).

First, these complexes were tested for their cytotoxicity profile by proliferation assay in ovarian carcinoma cell line (A2780), non-small cell lung carcinoma cell line (H1299) and glioblastoma cell line (T98G). The IC_{30} values were defined from the previous assays used for the determination of their IC_{50} after 96h treatment (Table 1 and 2) and this concentration was used for the radiosensitization assay in A2780 cell line. Cisplatin was used a positive control for the radiosensitization assay, as it is the Pt- complex of reference used in clinic and has been shown to be a radiosensitizer but depending on the cellular context and cell treatment [326-329]. The cells were incubated overnight with the drugs pre-irradiation, and post irradiation the drug incubation was continued for 6 days. The results of the screening for radiosensitization showed only one G4-ligand complex, Pt-ttpy, and the non G4-ligand Pt-(A)tpy were able to induce radiosensitization in A2780 cell line. Some of the complexes were also tested for radiosensitization on the two other cell lines, however, only Pt-ttpy were successful in radiosensitizing all three cell lines.

The screening showed that the presence of platinum metal alone does not guarantee radiosensitization. Moreover, Pt-ttpy, Cu-ttpy and Pd-ttpy all possess the same tolyl-terpyridine structure and only Pt-ttpy was successful in inducing radiosensitization, indicating that radiosensitization does not depend on a single particular ligand structure (figure 5B). The ability to bind to G4s covalently (exclusive for platinum metal complexes bearing a labile ligand) also does not influence the capability of a drug to be radiosensitive in nature, since Pt-(A)tpy is radiosensitizer without the possibility to bind covalently to DNA. Cisplatin, that is not always observed to be radiosensitizing in cell lines due to various experimental conditions [326-329], is seen to be a radiosensitizer in our conditions on the A2780 cell line. Interestingly, in the normal

cell line, Pt-ttpy shows radioprotection (figure 5F). However, it needs to be considered that the doubling time is increased with the drug and irradiation combined treatment and a true survival curve is not possible, unlike the other cancer cell lines.

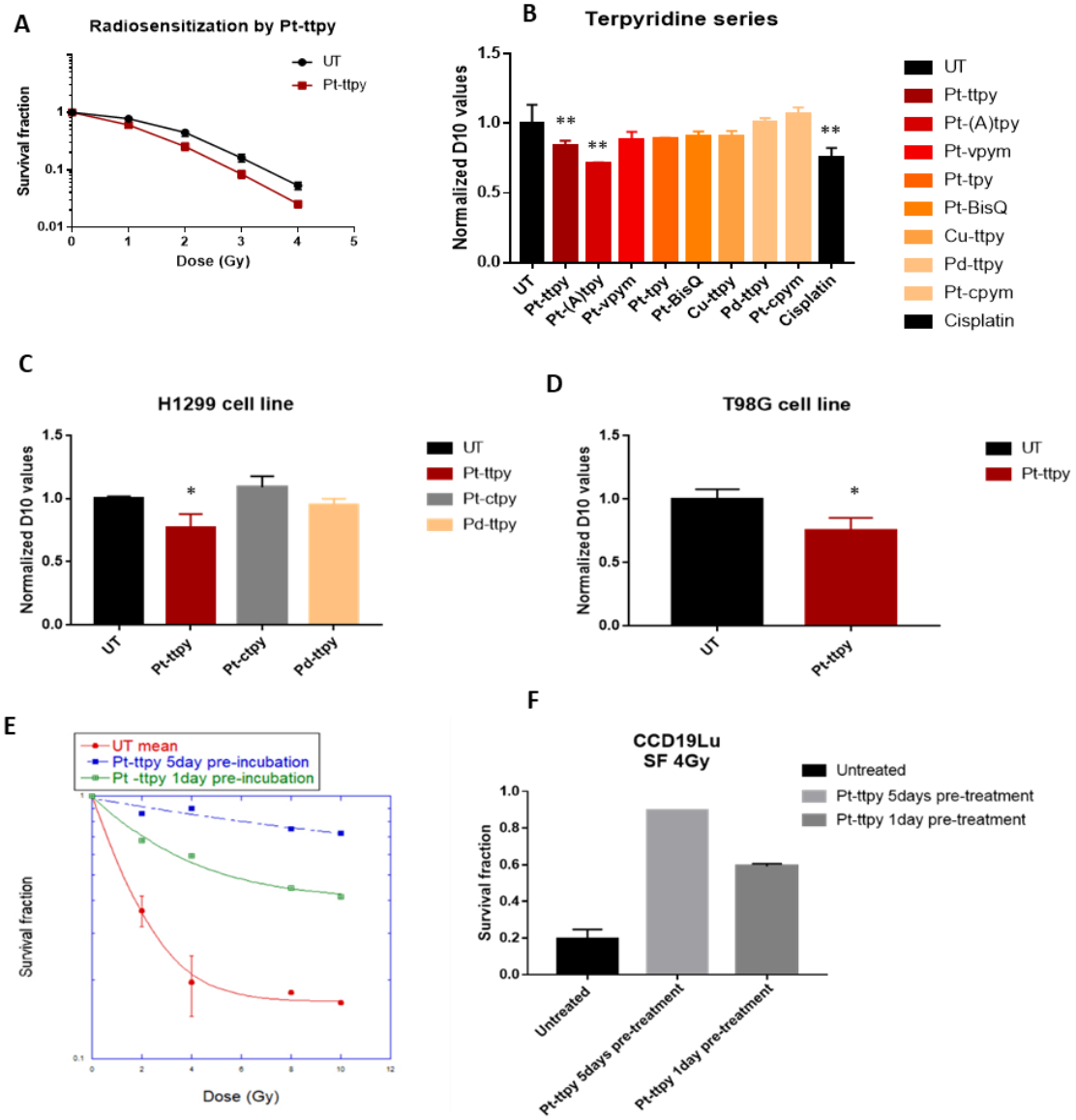

Figure 5: **Differential radiosensitization is induced by Terpyridine series drugs.** (A) Survival curve showing radiosensitization of A2780 cells with 1day pretreatment by Pt-ttpy at its IC_{30} concentration (1.5µM). Screening of Terpyridine complexes are shown with their D10 values normalized to UT (irradiation only) in (B) A2780 cell line and certain specific terpyridine complexes in (C) H1299 and (D) T98G cell line. (E) Normal lung fibroblast cells CCD19Lu shows no radiosensitization and (F) the survival fraction at 4Gy is compared. Concentrations of drugs used

(IC_{30}): Pt-ttpy- 1.5µM, Pt-(A)tpy – 0.08µM, Pt-cpym – 2µM, Pt-vpym – 0.4µM, Pt-tpy – 3µM, Pt-BisQ – 1.5µM, Pd-ttpy – 0.05µM and cisplatin – 0.3µM. N ≥ 2 ± SD, *p<0.05, **p<0.01.

Pt-NHC series

In the Pt-NHC series, we screened mononuclear, dinuclear and Pt-NHC complexes conjugated to the PDC G4 ligand for their radiosensitization potential in A2780 and T98G cell lines at their IC30 concentrations for 4 days treatments. The screening of some of the complexes was done with 5 days pretreatment instead of the 1 day pretreatment shown for the terpyridine series. This was done to have the desired inhibition at the end of 4 days and to reseed the cells with the good concentration of drugs for the screening.

In A2780 cell line, the two mononuclear and the four dinuclear complexes were able to induce a significant reduction in the D10 value from the survival curves. The same trend was observed in the T98G cell line for the dinuclear complex (C6) (figure 6 A, B & D). However, no radiosensitization was seen with the mononuclear and the Pt-NHC-PDC complexes (figure 6D). In the H1299 cell lines, the radiosensitization potential is currently performed by Dr. Tao Jia. The results seem to show that the mononuclear complexes inducing radiosensitization is not statistically significant; however, the dinuclear complexes show a sustained level of radiosensitization.

The screening shows that the ability of the Pt-NHC series to bind to G4s through the PDC ligand does not confer radiosensitization, stating that G4 selectivity is not necessary for radiosensitization and moreover revert the radiosensitizing effect of the NHC-Pt complex. This could be due to the proposed radioprotective nature of stabilized G4s [348]. The radiosensitization mechanism of NHC-Pt complexes remains to be established. It could depend on the nature of the DNA adduct they may form. While mononuclear Pt-NHC are capable *in vitro* of creating monoadducts, intrastrand crosslinks between two distant guanines (GTG, and GTTTG) and interstrand crosslinks (ICL), their dinuclear counterpart are capable of forming monoadducts, intrastrand crosslinks between two guanines over long distances (GTTTG), due to the presence of a linker chain between the two Pt-NHC complexes, and interstrand crosslinks more efficiently than mono nuclear Pt-NHC complexes [151].

In order to understand if the radiosensitization was dependent on the size of the linker chain, we compared the RS effect of a complex with a 4 membered chain and an 8 membered chain, along with the already two different 6 membered chain dinuclear Pt-NHC complex. The results show a length dependent radiosensitization trend where the C4 Pt-NHC dinuclear complex showed the highest potential followed by the C6 and C8 respectively. Moreover, in the C6 family, the nature of the NHC-Pt also influences its efficiency since C6cy seems less efficient that C6 (same linker chain but different substituent). Hence, the screening suggests that while a Pt-NHC (mono or dinuclear) is required for radiosensitization in A2780 cell lines, and that limiting the linker chain length in the dinuclear complex provides increased radiosensitization, probably by limiting the flexibility between both anchoring Pt atoms on DNA.

To decipher if Pt-NHC complexes are able to induce ICL, we performed a comet assay that can show ICL formation as described in the case of cisplatin treatments [353]. The ICL formation by a drug can be determined by determining the percentage decrease of the tail moment compared to non-drug treated cells. With time the crosslinks are repaired or 'unhooked' from the strands and the percentage decrease of tail moment goes back to basal non drug treated levels. However, we were not successful in our IC_{30} concentration condition. We need to repeat the experiment at higher concentrations.

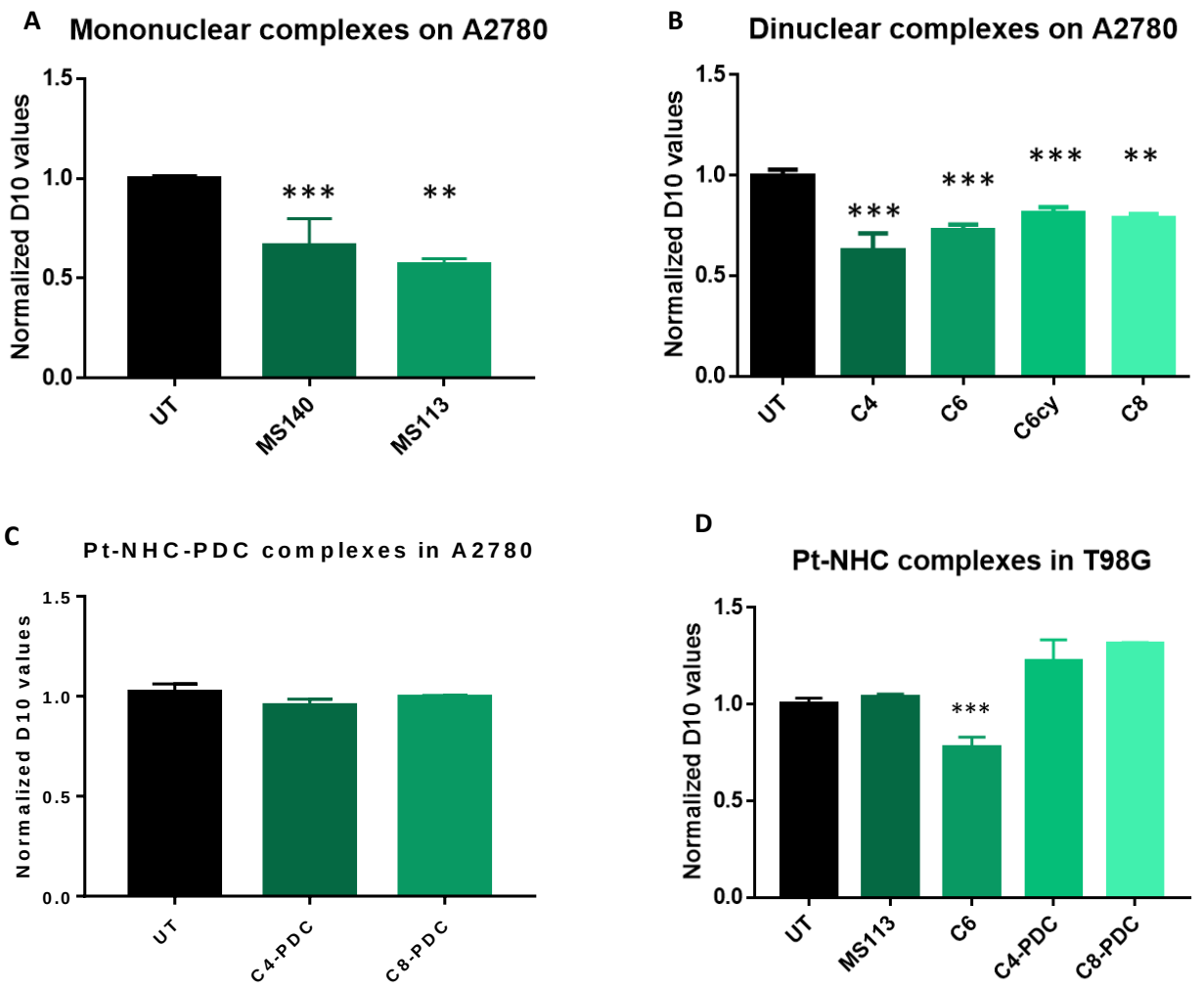

Figure 6: **Differential radiosensitization is induced by Pt-NHC series drugs**. Radiosensitization potential with 1day pretreatment of the Pt-NHC complexes at their IC_{30} concentration in A2780 cell lines are shown by comparing their D10 values normalized to the Untreated irradiated (UT) for (A) the two mononuclear complexes, (B) dinuclear complexes and (C) Pt-NHC-PDC complexes. Select complexes were tested for their radiosensitization potential in (D) T98G cell line. Concentrations of drugs used (IC_{30}): MS140 – 2µM, MS113 – 2µM, C4 – 0.75µM, C6 – 1µM, C6cy – 1.5µM and C8 – 1.2µM. N ≥ 2 ± SD, *p<0.05, **p<0.01, ***p<0.001

Salphen complexes

The Salphen complexes, C-Ni, S-Ni, S-Cu and S-V, were screened in both A2780 and T98G cell lines for their radiosensitization at their IC_{30} concentrations determined at 96 h treatment. The screening was done with 5 days preincubation conditions to determine the appropriate concentration of drugs for the screen. The results show that in A2780 cell line, S-Cu in capable of inducing radiosensitization. However, S-Cu cannot reproduce this potential with the T98G cell line. Interestingly, C-Ni and S-Ni, both with Ni metals, are capable of inducing radiosensitization in both T98G and A2780 cells. C-Ni could continue the trend in H1299 cell line as well (figure 7). The screening with the metal-salphen series suggests that the capability of a complex to induce radiosensitization in one cell line does not guarantee the same result in other cancer cell lines, except for the Ni complexes that was shown to radiosensitize the 3 cell lines tested here. It also re-iterates the point that radiosensitization is not dependent on the metal attached to the ligand.

Figure 7: **Differential radiosensitization is induced by Salphen series drugs**. Radiosensitization

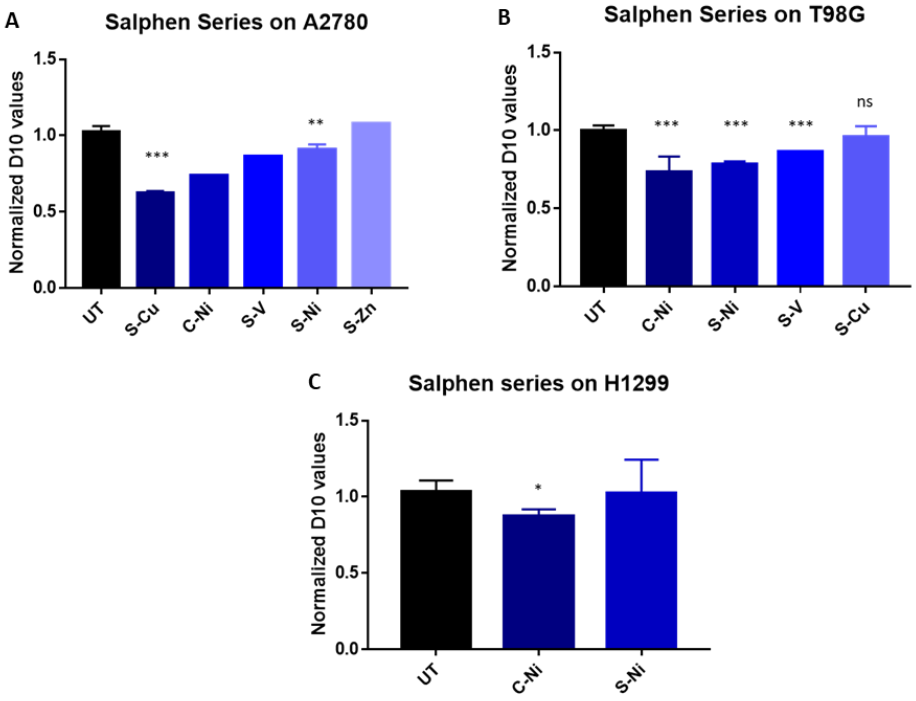

with 1day pretreatment by salphen series at their IC_{30} concentration are shown by comparing their D10 values normalized to the untreated irradiated (UT) cells in (A) A2780 cell line, (B) T98G cell line and (C) H1299 cell line. Concentration of drugs used (IC_{30}): S-Cu – 1µM, C-Ni – 1µM, S-Ni – 2µM, S-V – 2µM, S-Zn – 1µM. N ≥ 2 ± SD, *p<0.05, **p<0.01, ***p<0.001

Conclusion

Since the terpyridine complex Pt-ctpy had shown radiosensitization potential [143] in GBM and NSCLC cell lines, we wanted to see if all Pt metal complexes of the terpyridine series show radiosensitization. We observed that only Pt-ttpy and Pt-(A)tpy were able to induce radiosensitization in A2780 cell line, with only Pt-ttpy capable of inducing radiosensitization in two other, H1299 and T98G cell lines. This shows that Pt- metal complexes in the terpyridine series do not all have an intrinsic predisposition to induce radiosensitization and that the Pt-coordination to DNA for is not necessarily required.

In the normal cell line CCD19Lu, it is difficult to get a D10 value as the survival curves are not of the same character as the cancer cells, hence the comparison of irradiated cells and Pt-ttpy co-treated with irradiation was shown with the survival percentage at 4Gys. We see higher better survival with the Pt-ttpy co-treatment indicating radioprotection but it is difficult to claim without performing further experiments. Moreover, we checked for Pt-ttpy and some Pt-NHC complexes that the radiosensitizing effect can be detected only after a long time post irradiation, indicating that a number of cell doubling population needs to be performed. Since the doubling population of CCD19Lu is twice of our cancerous cell line, the cells divided half the number of times at the point of analysis for the radiosensitizing effect.

In the Pt-NHC complexes, we found that both mononuclear and dinuclear complexes show radiosensitization, however, when the Pt-NHC complex is conjugated to the G4 binding PDC molecule giving it a more targeted activity, the complexes lose their radiosensitization property. This implies that not only is the ability to bind to G4s not essential to induce radiosensitization, in certain condition, it can act in an inhibitory fashion. A recent paper showing the radioprotective effect of stabilized G4 structures by a phenomenon called hole trapping, could provide a possible explanation for our results [348]. In the dinuclear complexes with A2780 cell line, we also observe a trend of increasing radiosensitization potential with shorter linker chains, radiosensitization is highest for C4 > C6 > C8, while the length of the linker chains is the reverse. They are now protected by a DOI and are currently under the process of a patent.

In the G4 binding salphen series, we tested complexes with different metals and saw radiosensitization with a few of them (S-Cu, S-Ni, C-Ni and S-V). This confirmed once again that the presence of Pt-metal is not obligatory and other metal complexes can also induce radiosensitization [271]. Moreover, it also shows that radiosensitization can be cell line dependent and does not guarantee radiosensitization in all cell lines if the effect has been seen in one. This could be due to different efficiency of uptake, which could be checked by ICP-MS, or the status of the cells in terms of DNA damage signaling and cell death pathways (p53 status).

2: Understanding Radiosensitization

Metal- Terpyridine series –

2.1. Radiosensitization is dependent on the concentration of the drug

Pt-ttpy is already shown to be a radiosensitizer for A2780, H1299 and T98G cell lines. The primary effect of irradiation is to cause DNA damage, hence we hypothesized that if a drug is able to induce radiosensitization at a low concentration, there should be enhanced radiosensitization with increasing concentration of the drug, as was shown by Pt-ctpy in GBM and NSCLC cell lines [143].

Hence, we decided to test if Pt-ttpy can induce increased radiosensitization based on its increasing concentration in A2780 cells. The cells were incubated at concentrations of 1.5µM, 2µM, 2.5µM and 3µM, which correspond to a range from IC_{30} to IC_{70} of Pt-ttpy for 96 h treatment, overnight before irradiation. The proliferation assay at the end of 6 days show that even if there is a trend of increasing radiosensitization with increasing concentration of drugs, however, this is not significantly different from each other (figure 8A).

The results from the control drug, cisplatin also show an increasing trend of radiosensitization from concentrations ranging from IC_{20} to IC_{50}. However, this experiment needs to be repeated again (figure 8B).

The results seem to indicate that there exists a certain concentration which would initiate the radiosensitization process, after which increasing the concentration of the drug seems to have a slight increase of radiosensitization and the response is not proportional to the cytotoxic potential of the drug. Therefore, the effect is more efficient for low concentrations of Pt-ttpy, which is considered the best condition for radiosensitization (subtoxic concentrations).

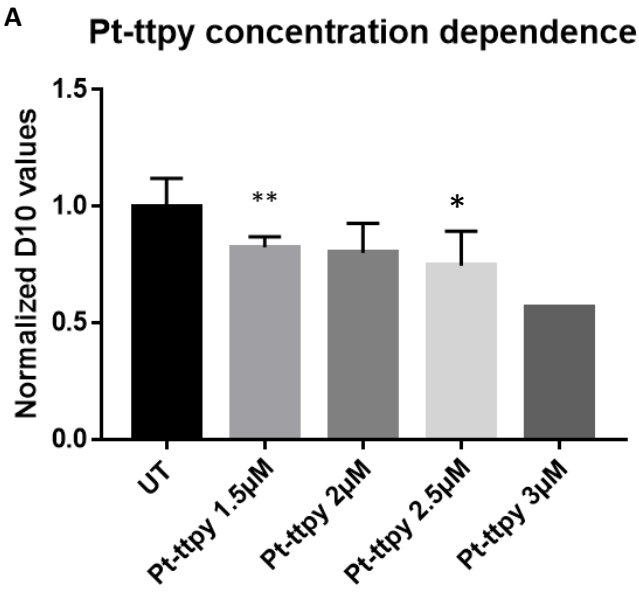

Pt-ttpy concentration (μM)	% Proliferation
1.5	70%
2	60%
2.5	50%
3	30%

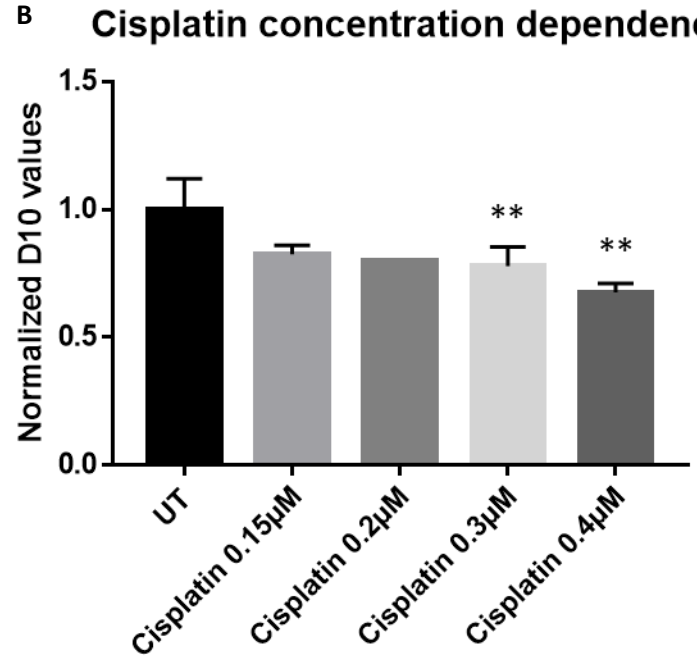

Cisplatin concentration (μM)	% Proliferation
0.15	80%
0.2	75%
0.3	70%
0.4	50%

Figure 8: **Radiosensitization potential is directly proportional to drug concentration**. Increasing radiosensitization potential is shown with increasing concentration of (A) Pt-ttpy from 1.5μM to 3μM and (B) cisplatin from 0.15μM to 0.4μM in A2780 cell line with 1 day pre-incubation conditions. The D10 values are normalized to the untreated irradiated (UT) cells. The percentage of proliferation with the drug concentrations are shown in a table for all drugs, which were calculated at the end of 7days in the absence of irradiation. N ≥ 2 ± SD, *p<0.05, **p<0.01, ***p<0.001

2.2. Radiosensitization is dependent on the duration of pre-treatment with the drug

We wanted to decipher if the amount of platinum bound to the genomic DNA would be a determining factor for the radiosensitization potential. In order to discern that, we need to find out if binding of the drug over different intervals can influence radiosensitization. Hence, we varied the duration of incubation of Pt-ttpy with the A2780 cell line prior to irradiation. 5day, 1 day and 10 minutes pre-incubation time was studied along with Pt-ttpy incubation 10 minutes post irradiation as well (figure 9A). The drug was present in the system for the subsequent 6 days after irradiation after which the cell count was taken and survival curves were drawn.

The D10 value is significantly reduced with longer pre-incubation time, indicating that radiosensitization effect is proportional to the time of incubation of Pt-ttpy (Figure 9C). No radiosensitization is observed when the drug is pre-incubated for just 10 min (almost no Pt bound to DNA) but radiosensitizing effect after 1 day pre-treatment is significant. However, the radiosensitization is highest with 5 days pre-incubation. This result may be explained in the context of the kinetics of Pt-ttpy bound to DNA over time that have been previously performed in the laboratory (Figure 9B) for their IC_{50} and IC_{80} doses, and that with more Pt-ttpy bound to the DNA at the point of irradiation, the higher is the radiosensitization.

In the case of cisplatin, it shows radiosensitization with 1day pre-treatment but no radiosensitization with 5day treatment. This could be because cisplatin shows a higher degree of binding to DNA in the first day compared to the fourth day (Figure 9B), a trend converse to that of Pt-ttpy. Hence, the results from cisplatin, although being the reverse trend from Pt-ttpy, still holds true of the hypothesis that increased amounts of drug bound to DNA at the point of irradiation leads to increased radiosensitization.

Interestingly, we notice that removal of Pt-ttpy post irradiation (Pt-ttpy 1day-) as shown in the figure 9C does not induce radiosensitization. However, the converse is seen for cisplatin. Hence, it can be hypothesized that Pt-ttpy is required post irradiation as it can have a direct effect on the DNA either by continuing to induce DNA damage or inhibit the DNA damage repair.

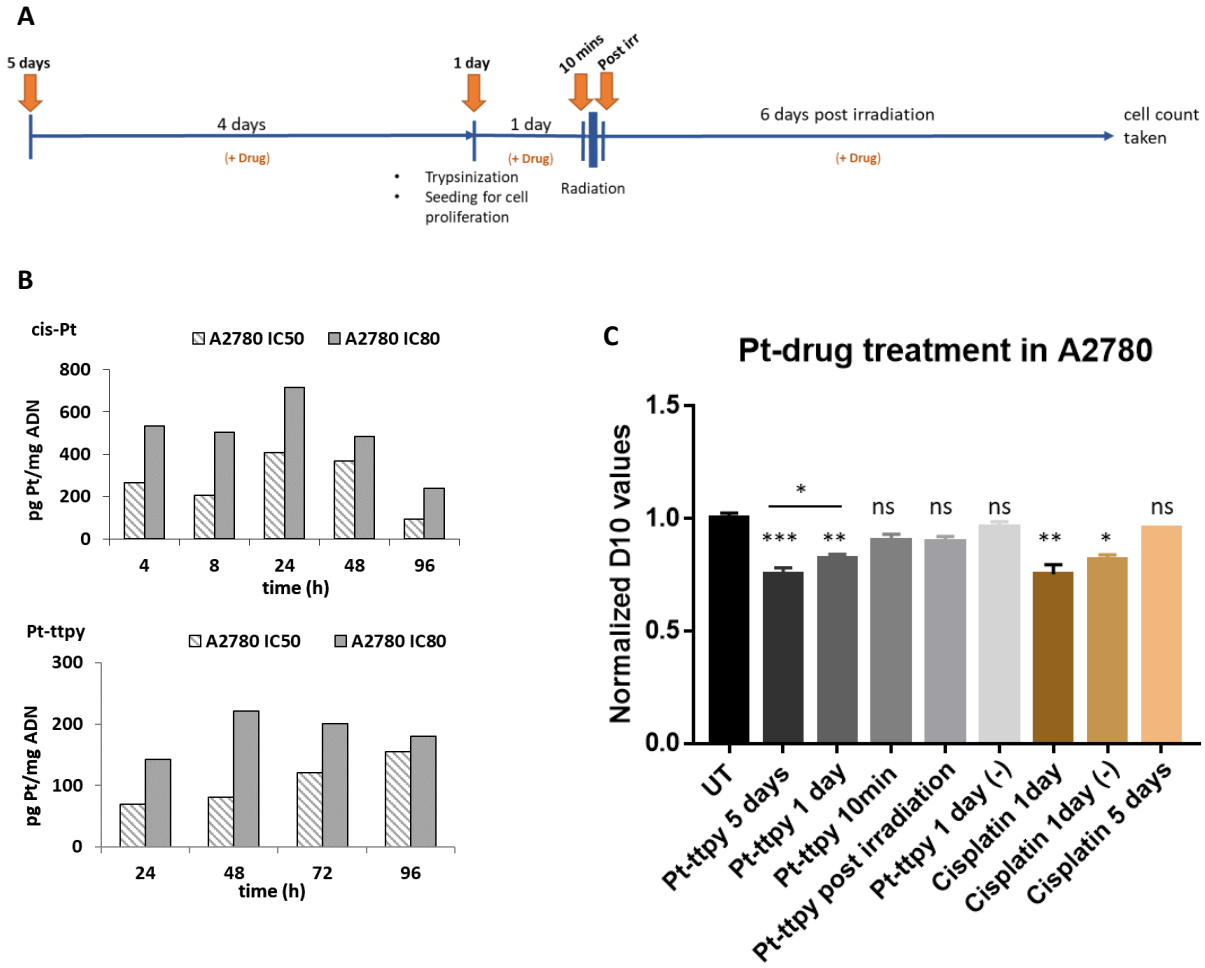

Figure 9: **Radiosensitization potential is directly proportional to pre-incubation time.** (A) Schematic representation of the different drug duration administered for this experiment. The amount of Pt bound to DNA is shown by (B) the amount of cisplatin and Pt-ttpy drug bound to DNA at their IC_{50} and IC_{80} concentration over a period of 96hours in A2780 cells. (C) The radiosensitization potential of Pt-ttpy (1.5µM) and cisplatin (0.3µM) are compared with different pre-incubation times using their normalized D10 values in A2780 cell line, N ≥ 3 ± SEM, *p<0.05, **p<0.01, ***p<0.001.

2.3. Cellular uptake and DNA binding of the drug at different time points of the radiosensitization assay

In order to comment in further detail regarding the effect of 'increased drug binding to DNA leads to higher radiosensitization', we have to check the amount of Pt present in the cells and bound to DNA at different time points based on their incubation time in our RS conditions. Indeed, we need to check the exact concentration of Pt-ttpy used in the RS experiments and to analyze if irradiation disturbs the uptake process and increases the binding of the drug to DNA. It has been shown from in vitro experiments that irradiation helps in the departure of Cl from cisplatin, increasing the concentration of active aqua species that can bind more easily to DNA [324].

IC_{30} concentration of Pt-ttpy was used to incubate A2780 cells for 5days, 1day with and without irradiation. Additional time points include 10 minutes pre-irradiation and 1day treatment of drug removed post irradiation. The cell pellets were collected 2h after irradiation. The results (Figure 10A) show that Pt-ttpy accumulation is still time dependent in cells as previously found for IC_{50} and IC_{80} concentrations (figure 21A) and there is not much increase in the amount of Pt uptake in the cells post irradiation compared to their non-irradiated counterparts indicating no influence of the radiations on the cellular uptake of Pt-ttpy. However, there seems to be a significant increase of Pt bound to the DNA post irradiation when compared with the non-irradiated controls (Figure 10B). This experiment needs to be confirmed a third time. This shows that irradiation has an effect on the binding capability of Pt-ttpy to DNA, as proposed for cisplatin [324]. Moreover, the binding of Pt-ttpy to DNA is also time dependent as expected from the previous figure and Pt-ttpy cellular uptake. This increased binding correlates with the increased radiosensitization suggesting that radiosensitization is indeed dependent on the amount of Pt-ttpy bound to DNA.

No significant difference in Pt-ttpy bound to DNA was seen between 1 day and 5 days pretreatment while the difference exists in term of radiosensitization. The difference seen between 1 day and 5 days treatment before irradiation is as expected but not for the samples post irradiation. The experiment was done twice but needs to be reproduced as there was some platinum contamination in some of the samples.

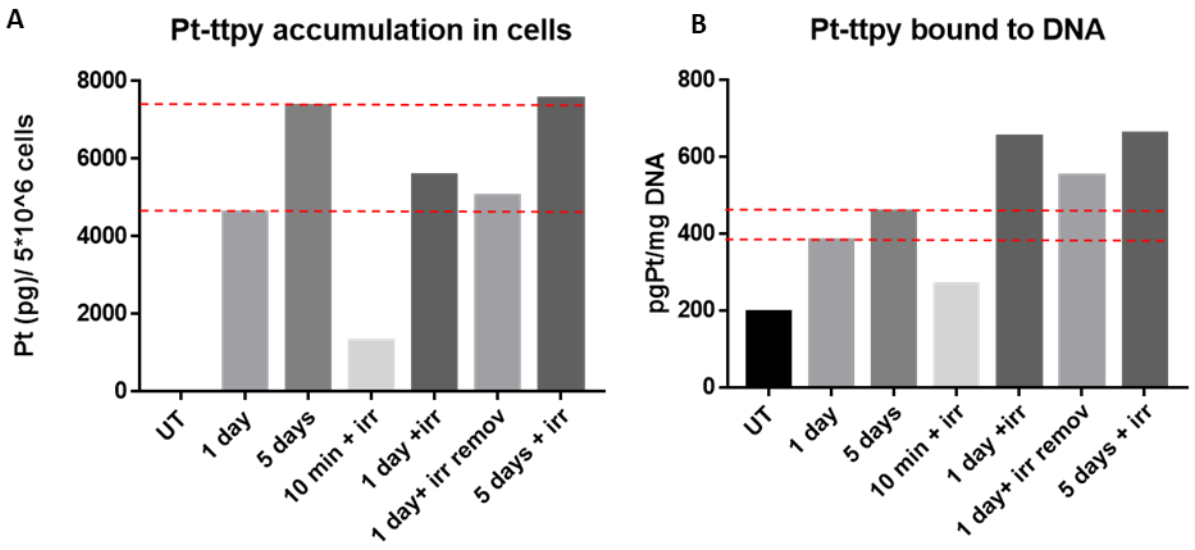

Figure 10: **Irradiation increases the binding of the drug to DNA**. (A) Graph shows the amount of Pt-ttpy accumulation in cells and (B) amount of Pt-ttpy bound to DNA when treated at its IC_{30} concentration (1.5µM) with varying pre-incubation times and conditions with and without irradiation in A2780 cells. The cells were collected 2h post irradiation and the data is collected through ICP-MS.

Conclusion

We wanted to understand if increased binding of the drug Pt-ttpy to DNA would have an effect on its radiosensitization potential, and therefore could be an essential element to explain the radiosensitizing effect. We observe that increasing the concentration of Pt-ttpy from IC_{30} to IC_{70} has a trend of increasing radiosensitization, however it is not a significant increase. In case of cisplatin, however, with increasing concentration from IC_{20} to IC_{50}, we saw an increase in radiosensitization. We cannot comment on the significance of the increase as the experiment needs to be repeated. However, these results seem to indicate that there could be a threshold of Pt-bound to DNA that can initiate the radiosensitization in the cell.

Dose and time relationships for a radiosensitizer drug can be manipulated to find the optimum schedule for radiosensitization. It has been shown for non DNA binding radiosensitizers as well as for DNA binding radiosensitizers such as 5-FU [354] and cisplatin [328]. In our study with Pt-ttpy in A2780 cell line, we find that Pt-ttpy needs at least 1day of pre-treatment to induce radiosensitization, however, an elongated time of pre-incubation would increase the radiosensitization slightly. The fact that 10 minutes pre-incubation and addition of the drug post irradiation shows no radiosensitization indicates that there is a need of Pt bound to DNA at the point of irradiation in order for radiosensitization to take place and increasing amount of Pt bound to DNA would increase its radiosensitization potential. In the case of cisplatin, the trend of incubation time dependent radiosensitization is reversed. However, the hypothesis still holds. It is shown that the amount of Pt bound to DNA with cisplatin treatment is much higher at 24hrs than it is at 4 days treatments. Hence, cisplatin still indicates that more Pt bound to DNA would involve increased radiosensitization. This needs to be confirmed by performing an ICP-MS on the cell treated with cisplatin at the RS and non-RS conditions.

We also note that for Pt-ttpy induced radiosensitization, it is absolutely necessary for the drug to be present post irradiation for the entire duration of the experiment. Removal of drug post irradiation does not induce radiosensitization. This is however, contrary to the radiosensitization observed with cisplatin. Removal of cisplatin post irradiation (with 1 day pretreatment) leads to a diminished but not significant radiosensitization. This phenomenon of radiosensitization by

cisplatin treatment pre irradiation followed by removal of the drug post irradiation has been shown before [328] on a different cell line, A549 and H460 (NSCLC cells). It indicates that Pt-ttpy, with its need to be present post irradiation, could be involved in inhibiting the repair process of irradiation induced damages. Cisplatin on the other hand, with no need to be present post irradiation uses a different mechanism of action than Pt-ttpy.

The Pt-ttpy accumulation in cells and the amount of Pt bound to DNA at different point in the radiosensitization assay, show that irradiation increased the amount of Pt bound to the DNA. There was a definite difference of Pt bound to DNA between 1 day and 5 day treatment, however, the jump in the amount of Pt bound to DNA 2h post irradiation clearly shows that irradiation has an effect on the binding of the drug to DNA. This could be explained with the *in vitro* results showing increased aquation of cisplatin post irradiation [324]. We need to test this theory by an experiment treating plasmid DNA with these complexes investigating if there is an increased binding of the drugs post-irradiation. Moreover, it also confirms to an extent that radiosensitization is dependent on the amount of Pt bound to DNA as non-radiosensitizing condition of 10min incubation shows very low amount of Pt on DNA.

Pt-NHC series

2.4. Radiosensitization by the complexes are concentration dependent

The hypothesis that increasing the drug concentration leads to better radiosensitization is also tested for the Pt-NHC complexes with 1 day pretreatment conditions. In the mononuclear complexes MS140 and MS113, we see a definite concentration dependent radiosensitization (figure 11A and B). In the case of MS140, the concentrations used ranged from the IC_{10} to IC_{40} in A2780 cell line for 96h treatments. For MS113, the concentration ranged from IC_{10} to IC_{60}.

In the dinuclear complexes, C4, C6 and C6cy, the concentration range was from IC_{10} to IC_{60}. The only exception being C8 which was tried with the range of IC_{20} to IC_{80}. However, none of the dinuclear complexes show any concentration dependent radiosensitization (figure 12 A, B, C and D).

Hence, it could be said that the mononuclear complexes tend to behave like cisplatin, with their concentration dependent radiosensitization probably due to their common ability to induce intra and interstrand crosslinks. Whereas the dinuclear complexes behave more like Pt-ttpy showing no significant concentration dependence for their radiosensitization.

Mononuclear complexes-

A

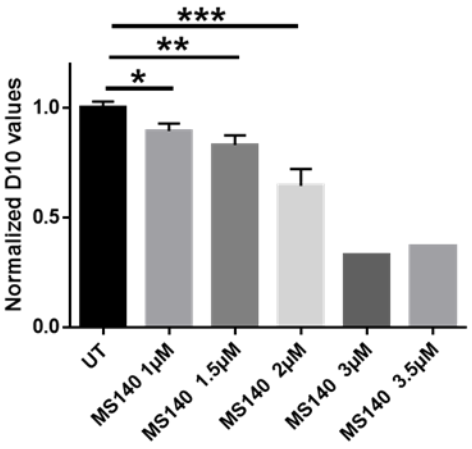

MS140 concentration (μM)	% Proliferation
1	90%
1.5	80%
2	70%
3	65%
3.5	60%

B

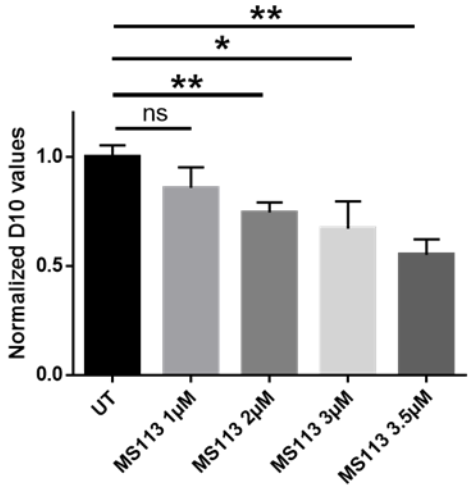

MS113 concentration (μM)	% Proliferation
1	90%
2	70%
3	50%
3.5	40%

Figure 11: **Radiosensitization is concentration dependent for mononuclear Pt-NHC complexes**. Graphs showing the D10 values of (A) MS140 and (B) MS113 complexes at increasing concentration demonstrates that radiosensitization is directly proportional to increasing concentration. The percentage of proliferation with the drug concentrations are shown in a table for all drugs, which were calculated at the end of 7days in the absence of irradiation, N ≥ 3 ± SD, *p<0.05, **p<0.01, ***p<0.001

Dinuclear complexes-

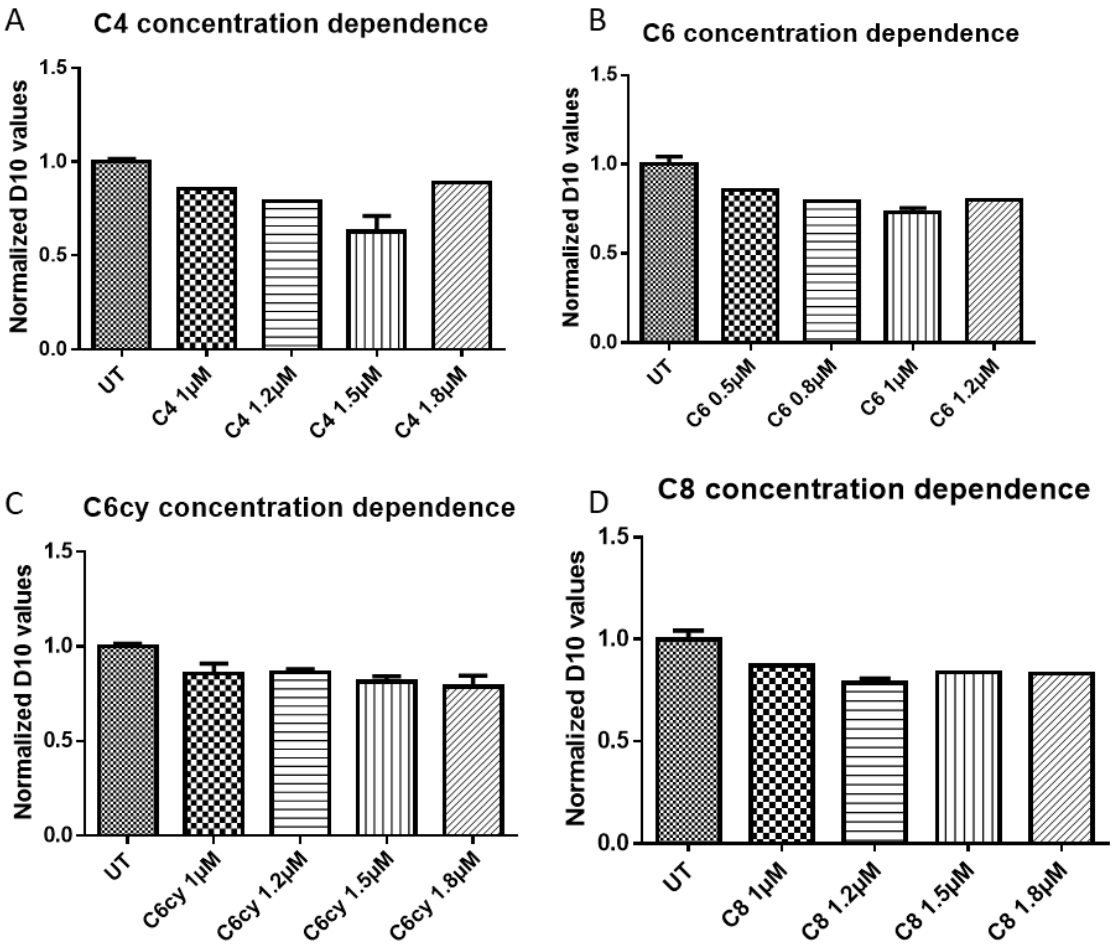

C4 (μM)	% proliferation	C6 (μM)	% proliferation	C6cy (μM)	% proliferation	C8 (μM)	% proliferation
1	90%	0.5	80%	1	90%	1	80%
1.2	80%	0.8	70%	1.2	80%	1.2	70%
1.5	60%	1	60%	1.5	70%	1.5	50%
1.8	40%	1.2	50%	1.8	50%	1.8	20%

Figure 12: **Radiosensitization is not concentration dependent for dinuclear Pt-NHC complexes**. Graphs showing the D10 values of (A) C4, (B) C6, (C) C6cy and (D) C8 complexes at increasing concentration indicates that radiosensitization is not dependent on increasing concentration. The percentage of proliferation with the drug concentrations are shown in a table for all drugs, which were calculated at the end of 7days in the absence of irradiation, N ≥ 3 ± SD, *p<0.05, **p<0.01, ***p<0.001.

2.5. Radiosensitization by the complexes depend on incubation time

Similar to Pt-ttpy, we wanted to decipher if the amount of platinum bound to the DNA would be a determining factor for the radiosensitization potential. Hence the dinuclear complexes were experimented with different time incubations of the drug was performed with A2780 cell line.

In the case of the drug C4, we observe a great radiosensitization effect with 1 day drug pre-treatment and interestingly we also see significant radiosensitization when the drug is removed post irradiation (figure 13A). This shows that the drug is not required to be present for the entire duration post irradiation hinting that its radiosensitization mechanism is very different from that of Pt-ttpy. We also observe radiosensitization with the longer 4 days pre-incubation and the short 10 minute pre-incubation but they need to be repeated for a significant analysis.

In C6cy, we observe the same trends as seen in C4, with significant radiosensitization only claimed by the 1day pre-incubation (figure 13B).

For C6 and C8, we observe radiosensitization with 1 day pre-treatment and when the drug is removed post irradiation, similar to C4 (figure 13C and D). We also see radiosensitization with the short term incubation of 10 minutes before irradiation, suggesting that presence of a huge amount of the drug within cells at the point of irradiation is not mandatory for their radiosensitization potential. But we need to quantify the amount of Pt at the time of irradiation to decipher the minimal amount needed to ensure radiosensitization.

These results show that the Pt-NHC dinuclear complexes are interesting Pt binding drugs that have a very different mechanism of radiosensitization than Pt-ttpy which needs to be further elucidated.

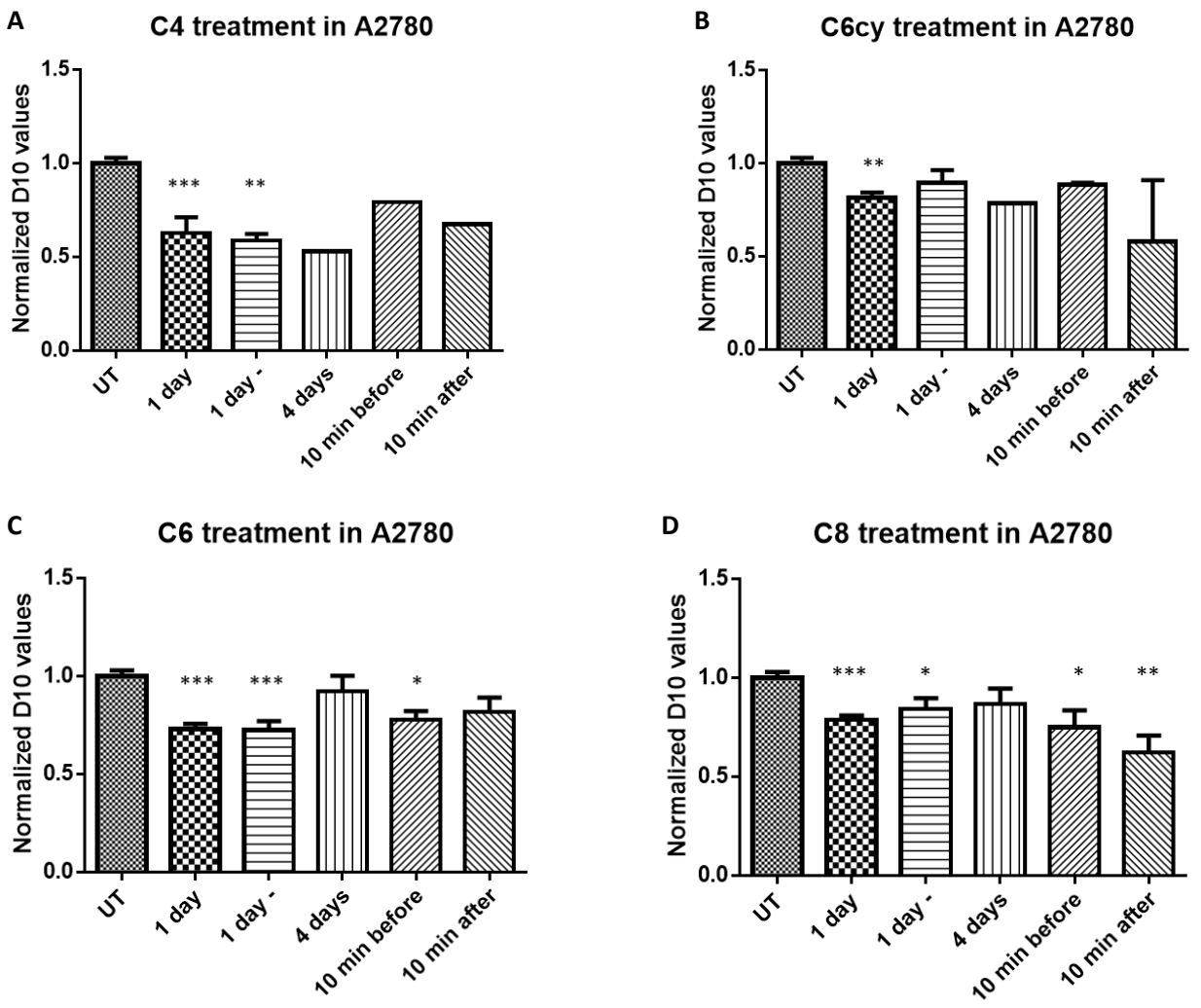

Figure 13: **Radiosensitization is dependent on drug incubation time**. The radiosensitization potential of (A) C4, (B) C6cy, (C) C6 and (D) C8 are shown with their D10 values normalized to the untreated (UT) condition, and compared across different pre-incubation times in A2780 cell line. The drugs are used at their IC_{30} concentration (C4- 0.75µM, C6cy- 1.5µM, C6- 1µM, C8- 1.2µM). N ≥ 3 ± SD, *p<0.05, **p<0.01, ***p<0.001.

Conclusion

The mononuclear Pt-NHC complexes are capable of inducing a strong concentration dependent radiosensitization, however, it is not the case for the dinuclear complexes. All four of the dinuclear complexes show no concentration based radiosensitization, hence, indicating that their mechanism of action is different from that of the mononuclear complexes. To an extent, the mononuclear and dinuclear complexes mimic the concentration dependence study of Pt-ttpy and cisplatin. Mononuclear complexes have an effect similar to cisplatin, probably due to its ability to form crosslinks, and dinuclear complexes mimic Pt-ttpy. This could suggest that the monoadducts formed by the di-nuclear complexes may be the governing reason for the radiosensitizing effect, instead of the ICL. Indeed, in the conditions used for the radiosensitizing effect, we did not detect any ICL by comet assay. Further studies need to be done in order to conclusively comment on the mechanism of action of these Pt-NHC complexes.

Regarding the incubation time dependent radiosensitization, there are a couple of interesting observations. Apart from C4, all the dinuclear complexes show radiosensitization with 1 day pretreatment and not with the 4 day pretreatment. It seems to follow the trend of cisplatin in that regard. Moreover, they all (apart from C6cy) show radiosensitization with the removal of drug post irradiation, again identical to cisplatin. Finally, C6 and C6 complexes could induce radiosensitization with 10 minutes pre-incubation, hinting that presence of a huge amount of Pt bound to DNA at the point of irradiation is not mandatory for these complexes to induce radiosensitization. However, this should be confirmed by Pt quantification by ICP-MS. This is a departure from the mechanism of action for Pt-ttpy, however, it is a useful quality for clinical purposes. Seeing that these complexes have been shown before to not be affected by cisplatin resistance, their mechanism of radiosensitization needs to be studied in greater detail in order to develop them into potent clinical radiosensitizers. The dinuclear complexes and their radiosensitizing effects have been protected by a DOI (declaration of Invention) and are now in progress towards a patent.

3: Radiosensitization and DNA Damage

3.1. Pt-ttpy induces a delay in early repair of DSB foci

Since the radiosensitization of Pt-ttpy can be correlated to the amount of the drug bound to DNA, we wanted to decipher 1) If the presence of the drug increases the number of DNA damage and/or 2) If the drug is capable of inhibiting the repair of IR-induced DNA damages since one of the major mechanism of action of radiosensitization by a DNA binding drug is its ability to inhibit repair of DNA post irradiation leading to cell death[143, 331, 344]. γH2AX foci is considered a marker of DSB damage. γH2AX is formed by the phosphorylation of the histone H2AX by ATM, ATR and DNA-PK and then recruited at the DBS. The γH2AX is formed minutes after the formation of the DSB and it rapidly spreads over large chromatin domains flanking the DNA breaks [199, 200]. Hence, we performed immunofluorescence assays to check the levels of γH2AX foci on A2780 cell line at 0.5h, 2h, 6h and 24h after irradiation in the presence and absence of Pt-ttpy. These time points were chosen as the cells post irradiation show a maximum of γH2AX foci at 30 minutes and then gradually keep decreasing till 24hrs post irradiation [355]. Post immunofluorescence we created a macro, with the help of the microscopy platform, to be able to determine the number of foci per cell, their area and their intensity.

The number of γH2AX foci induced by irradiation is similar to the number induced by the co-treatment of Pt-ttpy and irradiation at 30 minutes post irradiation (figure 14A). This disproves the first hypothesis. Now, for the second hypothesis, we clearly show a definite delay in the repair of DNA damage post irradiation in the presence of Pt-ttpy in the 2hour and 6hour time point. Both 5 day and 1 day pre-incubation conditions show a delay in repair (figure 14B and C). Pt-ttpy added post irradiation, which is a non radiosensitizing condition, is unable to induce a delay in repair. In addition, the non RS complex Cu-ttpy is also not able to induce a delay in repair. Hence, only Pt-ttpy in its radiosensitizing conditions is able to inhibit the repair of DSBs up to a period of 6hrs post irradiation.

Cisplatin is able to induce RS but is, however, seen to be unable to cause delay in repair in this condition. This suggests that the Pt-ttpy and cisplatin have different mechanisms of action for

radiosensitization and that the mandatory presence of the Pt-complex post-irradiation could be related to the delay in the repair of IR-induced DNA damage.

Another marker for DSB repair is the localization of 53BP1 protein on the damaged sites. 53BP1 is a non-enzymatic protein that binds to the broken DNA ends and helps promote NHEJ[215, 216]. It also helps recruit proteins involved in the repair of the DSBs, hence, it is a marker of DSBs. While there is a small increase of 53BP1 foci number with Pt-ttpy, Cu-ttpy and cisplatin co-treated with irradiation compared to irradiated cells alone (Figure 15C), the results for the kinetics of 53BP1 foci disappearance is not conclusive for any repair delay of DSB in terms of number.

We make an interesting observation that the area of the foci is increased at 2 and 6 hours post irradiation, as compared to irradiated but untreated cell. This increase of area in the 53BP1 foci is not seen in the case of cisplatin and the non radiosensitizing Cu-ttpy. We hypothesize that the increase of the area could be due to a cluster of DNA damages that are less efficiently repaired.

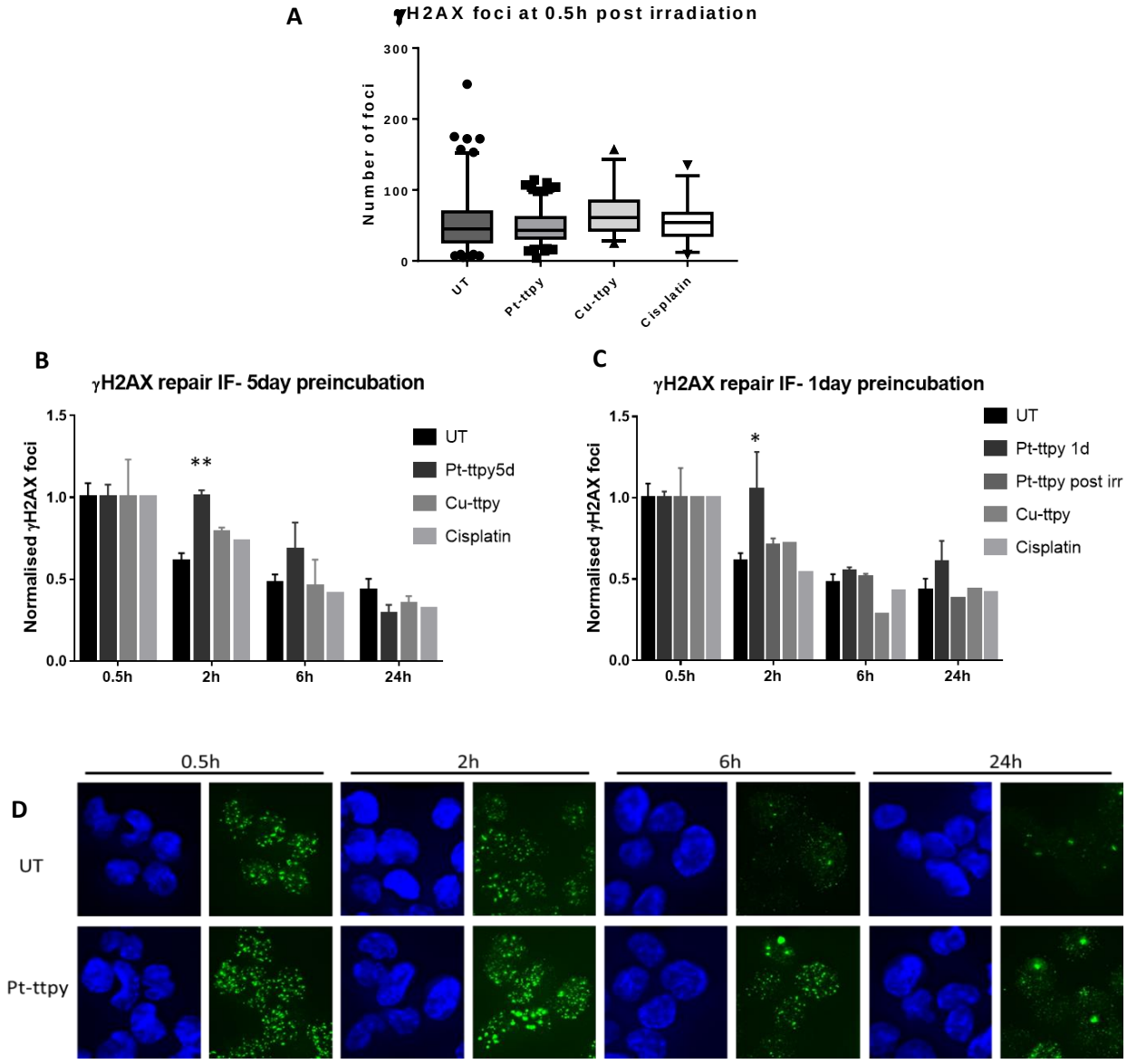

Figure 14: **Pt-ttpy induces delay in early disappearance of γH2AX foci**. The A2780 cells were treated with Pt-ttpy (1.5µM), Cu-ttpy (0.06µM) and Cisplatin (0.3µM) at their IC30 concentration with 1 day preincubation condition. Graph (A) shows the number of γH2AX foci formed after 0.5h of irradiation at 2Gys. Kinetics of DNA damage repair post 2Gy irradiation is shown through the number of γH2AX foci with (B) 5day pre-incubation and (C) 1day pre-incubation of A2780 cell line with Pt-ttpy, Cu-ttpy and cisplatin. (D) Immunofluorescence on A2780 cells showing the γH2AX foci at each time point post-irradiation with only irradiated (UT) and Pt-ttpy treated with 1 day pre-incubation. N ≥ 3 ± SEM, *p<0.05, **p<0.01, ***p<0.001.

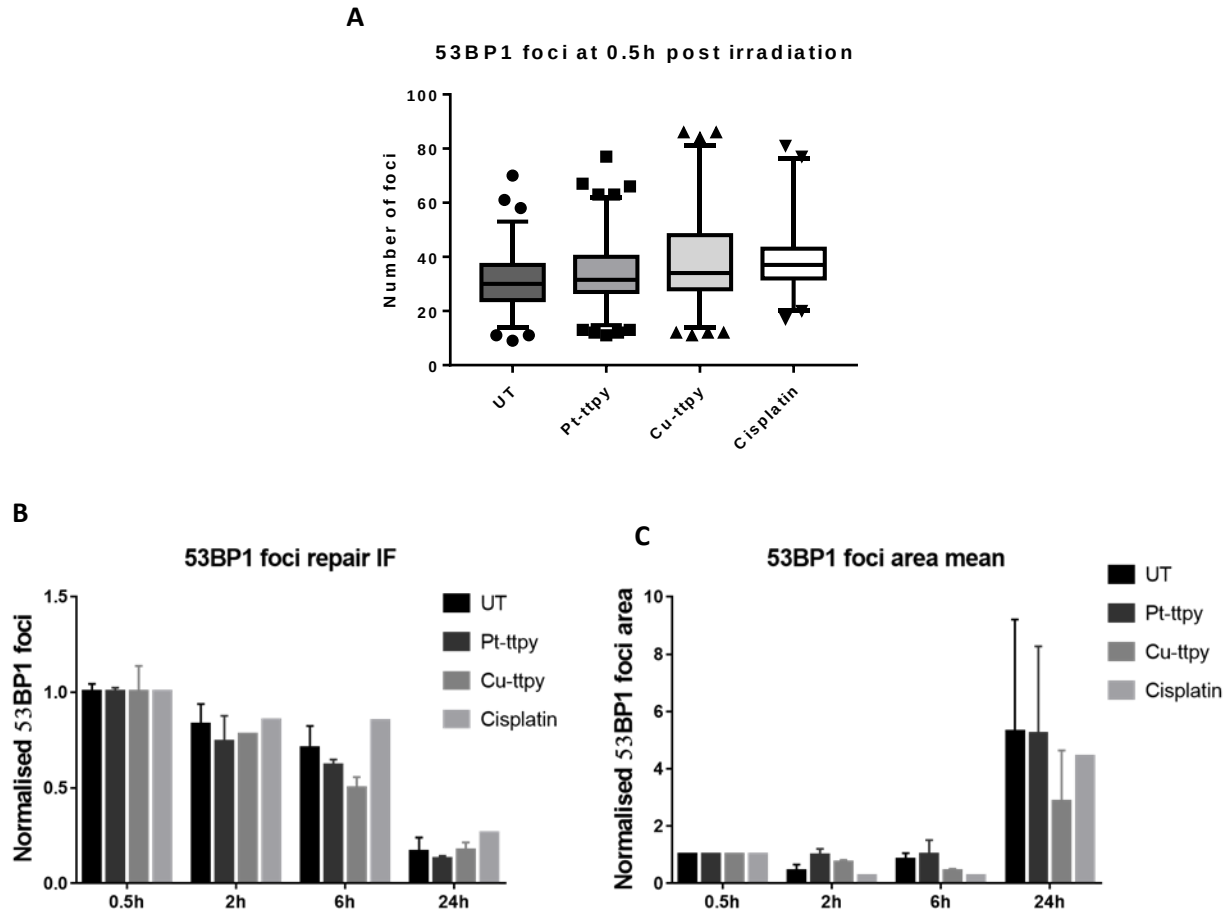

Figure 15: **Pt-ttpy induces an increase in area of 53BP1 foci.** The A2780 cells were treated with Pt-ttpy (1.5µM), Cu-ttpy (0.06µM) and Cisplatin (0.3µM) at their IC30 concentration with 1 day preincubation condition. Graph (A) shows the number of 53BP1 foci formed after 0.5h of irradiation at 2Gys. Kinetics of DNA damage repair post 2Gy irradiation is shown through the (B) Number of 53BP1 foci and (C) Area of 53BP1 foci in A2780 cell line after 1day pretreatment of Pt-ttpy, Cu-ttpy and cisplatin. N = 3 ± SEM.

3.2. Pt-ttpy induced radiosensitization is dependent on Telomeric dysfunction

Telomeric dysfunction as a reason of radiosensitization is hypothesized for two G4 binding ligands, RHPS4 and Pt-ctpy. As Pt-ttpy is a G4 binding ligand, it is mandatory to check if telomeric dysfunction is increased in the presence of both drug and radiation and if it can play a role in the radiosensitization potential of Pt-ttpy. Moreover, it is also necessary to check if the radiosensitization depends on telomeric dysfunction by the drug alone before irradiation.

The co-localization study done with the telomeric binding protein TRF1, which remains bound to telomeres during the Pt-ttpy treatment (pending publication, Annex 2) and γH2AX should give us a clear understanding of the importance of Telomeric dysfunction Induced Foci (TIFs) in radiosensitization. The results show that 1) no TIFs could be detected before irradiation, 2) irradiation does not induce the delocalization of TRF1 from telomeres and 3) A mild increase of TIFs is observed in the presence of Pt-ttpy 24h post irradiation (figure 16). This shows that the low IC_{30} concentration used for radiosensitization is able to induce some telomeric damage with irradiation, hence it can be a potential contributor to the mechanism of radiosensitization.

TIFs have already been shown for IC_{80} concentration after 96h treatment (publication pending). The possible reason for the absence of TIFs before irradiation could be the low concentration of drug used (IC_{30}) and the short time incubation (24h). Moreover, it is not surprising to see an absence of TIFs especially noting the kinetics of the drug binding to DNA (discussed before).

Regarding the small increase of TIFs produced post irradiation, since we don't see a significant increase of γH2AX foci at 24hrs with Pt-ttpy + irr compared to irradiation alone (shown before), we can comment that it's not the quantity of the remaining γH2AX foci but the quality of these foci that can push Pt-ttpy induced radiosensitization.

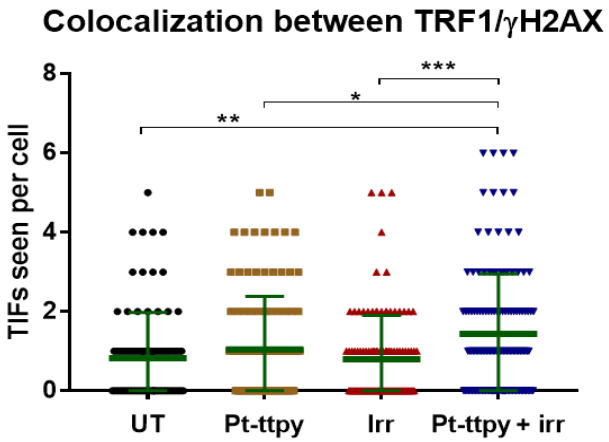

Figure 16: **Radiosensitization could be dependent on telomeric dysfunction**. Graph showing the number of TIFs induced 24 hours post irradiation by 1day pretreatment of Pt-ttpy alone (no irradiation), irradiation and the combination of Pt-ttpy and irradiation, compared to the untreated (UT) cells in a population of n>100, *p<0.05, **p<0.01, ***p<0.001.

3.3. Radiosensitization and the cell cycle

Radiosensitizing properties could also be associated with modifications of cell-cycle. It is known that the radiation could block the cell cycle in G2/M checkpoint [356], allowing the cells to repair the damages. The association of both irradiation and drugs could increase the blockage or induce the bypass of the blockade in G2/M, decreasing the time of repair and leading consequently to unrepaired DNA damage clusters.

Our results show that in the early hours post irradiation, 2h and 6h, there is an increase of cells in the G2M phase for irradiated cells without drugs (Figure 17C). Whereas, a significant decrease of cells in the G2/M phase was observed when cells were co-treated with Pt-ttpy indicating that Pt-ttpy abrogates this mandatory cell cycle arrest to allow repair to process. This could indicate the cells with Pt-ttpy treatment could in the early stages post irradiation have an impaired repair (as seen with the γH2AX foci kinetics disappearance) and pass through the G2/M block developing genomic instability leading to radiosensitization.

Regarding the effect of Pt-ttpy alone at their IC_{80} concentration with 1 day treatment, we see an increase of cells in G1 phase and a reduction of cells in S and G2-M phases (figure 17A, B and C). If there is a co-relation between the increased cells in G1 phase and the early apoptosis marker expression shown earlier, it is difficult to comment on due to the difference of drug concentration used and the time duration of the treatment. However, it could be an area to be focused on later.

Cisplatin is known to induce a block at G2/M [317, 318] and in our IC_{80} concentration condition still shows a trend of G2/M block. It also induces a block at the G2/M stage with irradiation but only at 24h when compared to the untreated cells. This is different from the cisplatin – irradiation co-treatment cell cycle results shown by Turchi [328], which shows a decrease of H460 cells in G2-M phase at 24 hours post irradiation compared to the only irradiated drugs. There is a clear difference in the results of the two drugs showing once again that both drugs have their separate mechanisms of action.

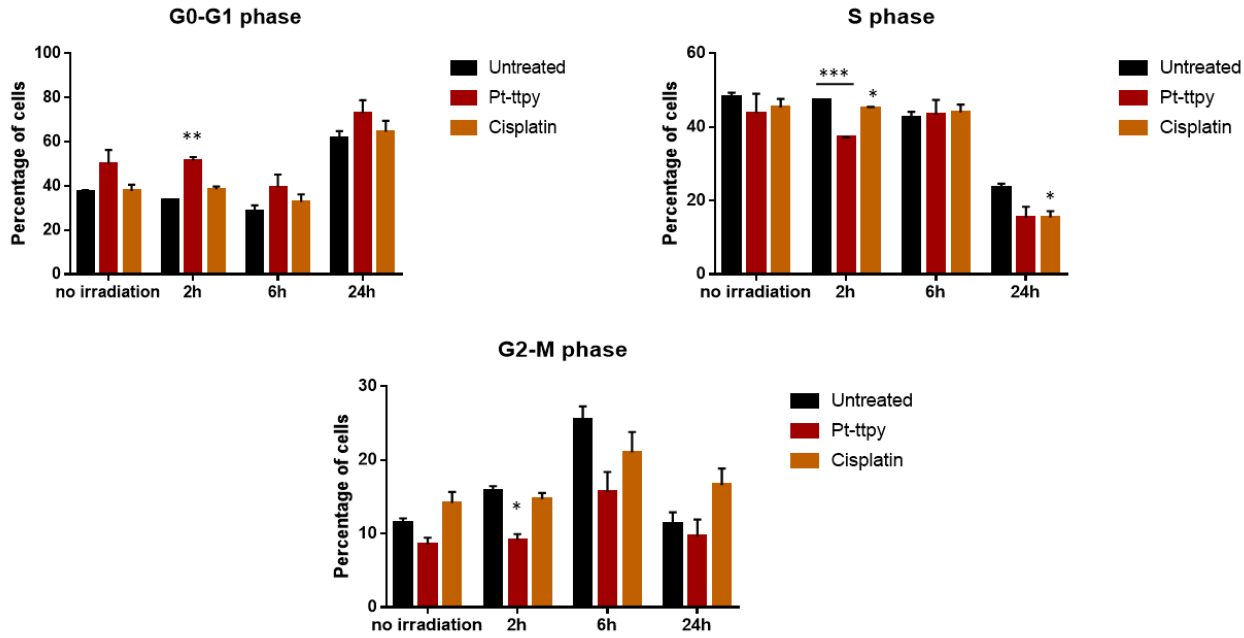

Figure 17: **Pt-ttpy induces an abrogation of G2-M cell cycle block post irradiation**. The percentage of A2780 cells in (A) G0-G1 phase, (B) S phase and (C) G2-M phase after 1 day pretreatment with Pt-ttpy (4µM) and cisplatin (0.6µM) and 2Gy irradiation, seen at different time points post irradiation. N ≥ 3 ± SEM, *p<0.05, **p<0.01, ***p<0.001.

3.4. Radiosensitization and ROS production

When cells are exposed to IR, water hydrolysis generates free radicals which attack nuclear and mitochondrial DNA and cause DNA damage in an indirect effect of irradiation [167]. The accumulation of damages in mitochondrial DNA represses mitochondrial function leading to the production of ROS inside the cell and then amplification of further damages to biomolecules. Since, the life time of ROS produced by IR is very short (less than 10^{-6} sec) the ROS production that is quantified is the one amplified through mitochondria [357]. Most of the irradiation induced DNA damages are by the indirect action with the help of ROS production [171]. Hence, the hypothesis is that if a drug can also induce ROS by itself or lengthen the time of the irradiation induced ROS production, it would be able to induce more DNA damages.

Hence, we tested whether Pt-ttpy, cisplatin and Pt-tpy can induce ROS production by themselves at their IC_{30} concentration and if it can change the ROS levels 24hours post irradiation. The experiment was done by using the CellRox Deep red probe as it measures total ROS present in the cell.

The results show that Pt-ttpy and Pt-tpy do not produce ROS by themselves (figure 18). We have already seen that Pt-ttpy does not produce ROS at its IC_{80} concentration and at 10µM concentration (see results 1.4, pending publication, Annex 2). In this experiment, we also see a slight ROS quenching when treated only with Pt-ttpy but that would have to be corroborated by repeating the experiment. Cisplatin on the other hand produces ROS by itself and in the presence of irradiation is able to enhance the ROS levels 24hrs after irradiation (figure 18). This reaffirms the hypothesis that Pt-ttpy and cisplatin have very different mechanism for inducing radiosensitization.

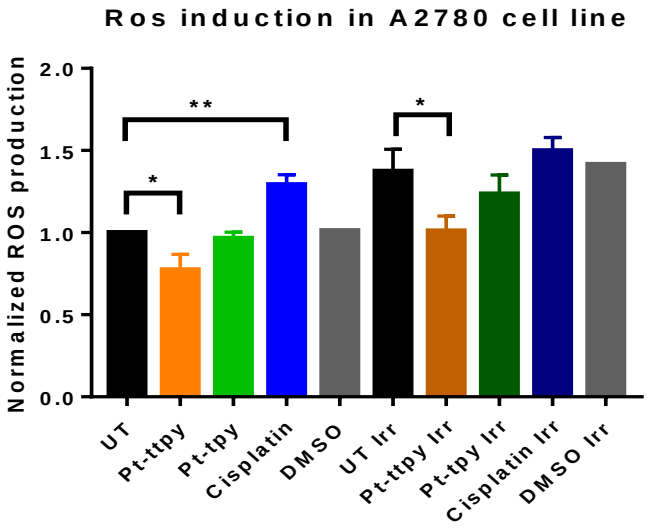

Figure 18: **Pt-ttpy helps quench ROS produced post irradiation**. Graph showing ROS production with 1 day pretreatment condition of Pt-ttpy (1.5µM), Pt-tpy (3µM) and cisplatin (0.3µM) alone and combined with 2Gy irradiation in A2780 cells 24h post irradiation normalized to UT (Untreated unirradiated). DMSO is also used as a control. N ≥ 3 ± SD, *p<0.05, **p<0.01

Conclusion

Delaying the repair of DSBs is seen to be one of the most characterized mechanism of action for DNA binding radiosensitizers. In fact, RHPS4 showed a delay in repair in a GBM cell line till 24hrs post irradiation [344]. For Pt-ctpy, an increase of DNA damage has been shown even at 0.5h post-irradiation that endures 24hours post irradiation [143]. Pt-ttpy is observed to delay DSB repair till 6hrs post irradiation. This delay of repair is important because the non radiosensitizing complex Cu-ttpy does not show such effect. Moreover, Pt-ttpy in its non radiosensitizing condition also shows no such effect, hence equating this particular DSB damage repair delay phenomenon with Pt-ttpy induced radiosensitization. Interestingly, cisplatin in its radiosensitizing condition also shows no delay in repair, even though in literature cisplatin also shows a delay in DNA repair till 24hrs post irradiation [328]. This can be construed as another example of its separate mechanism of action from Pt-ttpy in our RS condition. Regarding the 53BP1 foci, we don't see any delay in the disappearance of the foci number with any of the drugs, however, we see an interesting phenomenon concerning the size of the 53BP1 foci: it is increased at the same time points where the number of γ-H2AX foci were increased when treated with

irradiation and Pt-ttpy and is not seen for the other drugs. We hypothesize that this increase of size of the 53BP1 foci is due to the accumulation of DNA damages forming at cluster that is more difficult to repair and this could be related to the presence of Pt-DNA adducts in close proximity to the DSBs created by irradiation.

The radiosensitization of Pt-ttpy is shown to be independent of its telomeric damage formed before irradiation as we do not see any TIFs created by the drugs alone, probably due to its low concentration. However, there are a mild increase of TIFs for 24hrs post irradiation in the presence of Pt-ttpy. This is different from the mechanism of action of RHPS4 that show the importance of telomere damages before irradiation for its radiosensitization. Pt-ctpy focuses on the TIFs formed post irradiation with the presence of the drug, that could also be the case of Pt-ttpy. Since Pt-ttpy is shown to target telomeres at higher concentrations (publication pending from the lab and [144]), the targeting of telomeres was not surprising for radiosensitization. We can propose, that radiosensitization could also be connected to a delay in telomeric DNA damage, just as it is for genomic DNA damage.

Pt-ttpy is also seen to cause a blockage of cells in G1 phase of the cell cycle for the first 6 hours and has a reduced percent of cells at the G2-M phase. Since, post irradiation, cells are blocked at G2-M phase in order to repair as can be seen with our cells as well, the reduction of cells in this phase due to Pt-ttpy treatment can be hypothesized to lead to unrepaired damages inducing genomic instability. Cisplatin does not exhibit this behavior and apart from a small G2-M block at 24hrs post irradiation does not seem to have any stark effect. This is different from what has been observed in literature that shows a marked decrease of cells in G2-M phase post cisplatin and irradiation co-treatment [328], which could be dependent on the different drug concentration and time of treatment. Interestingly, for both drugs, the cell cycle arrest post-irradiation, seems to be governed by the drugs' inherent cell cycle arrest characteristic. This difference of mechanism of action of cisplatin is even more enhanced with the effect of ROS formation where it is the only drug to induce ROS by itself and in the presence of irradiation.

The final conclusion from these experiments is that Pt-ttpy seems to induce radiosensitization by causing a delay in DSB repair probably due to the formation of a complex DNA damage that is

difficult to repair, compounded by its escape from the G2-M block of the cell cycle. Cisplatin on the other hand seems to induce radiosensitization by enhancing and probably elongating the ROS production post irradiation.

4: Terpyridine complexes and mitochondria

Pt-ttpy- Importance in context

Pt-ttpy is a G4 binding metallo-organic complex. *In vitro* biophysical and biochemical analysis showed that Pt-ttpy is capable of binding to many G4 structures [142] (Annex 1) comprising of the telomeric and myc-22 (from the transcription regulatory element of the c-myc gene) G4 (figure 19). Moreover Pt-ttpy can irreversibly trap both G4s by platinating the loop adenine in the telomeric G4 structure [126] or the base residue at the 5'-end overhanging region of the c-myc G4 [141]. Interestingly, the *in vitro* properties have been consolidated *in cellulo* by showing that telomeres are effective targets of Pt-ttpy. In fact, in HT1080 cells, Pt-ttpy has shown to target linear Human Artificial Chromosome, HACs (containing telomeres), over circular HACs (without telomeres) and to induce a significant loss of chromosome for the linear HACs [144]. Moreover, in the laboratory with the use of ICP-MS, it is seen that Pt-ttpy is able to bind covalently to telomeres of A2780 cells, together with genomic DNA. A platination enrichment for telomeric DNA over the genomic DNA was observed for Pt-ttpy and its derivative Pt-tpy (non G4 ligand) when compared to cisplatin [127]. This suggests that while Pt-ttpy can bind covalently to telomeres *in cellulo*, it is probably due the differential accessibility or DNA repair efficiency of telomeric versus genomic DNA of cisplatin and terpyridin platinum complexes. Further experiments in the lab (pending publication, Annex 2) showed that Pt-ttpy and cisplatin (but not Pt-tpy) partially removed the telomere protective protein TRF2 from telomeres of A2780 and A2780cis cell lines but only Pt-ttpy showed signs of real telomeric DNA damage. Since neither cisplatin nor Pt-tpy are G4 ligand, this suggests that the G4 binding properties of Pt-ttpy could be at the origin of telomere targeting. In addition, Pt-ttpy was also capable of inducing DNA damage elsewhere in the genome.

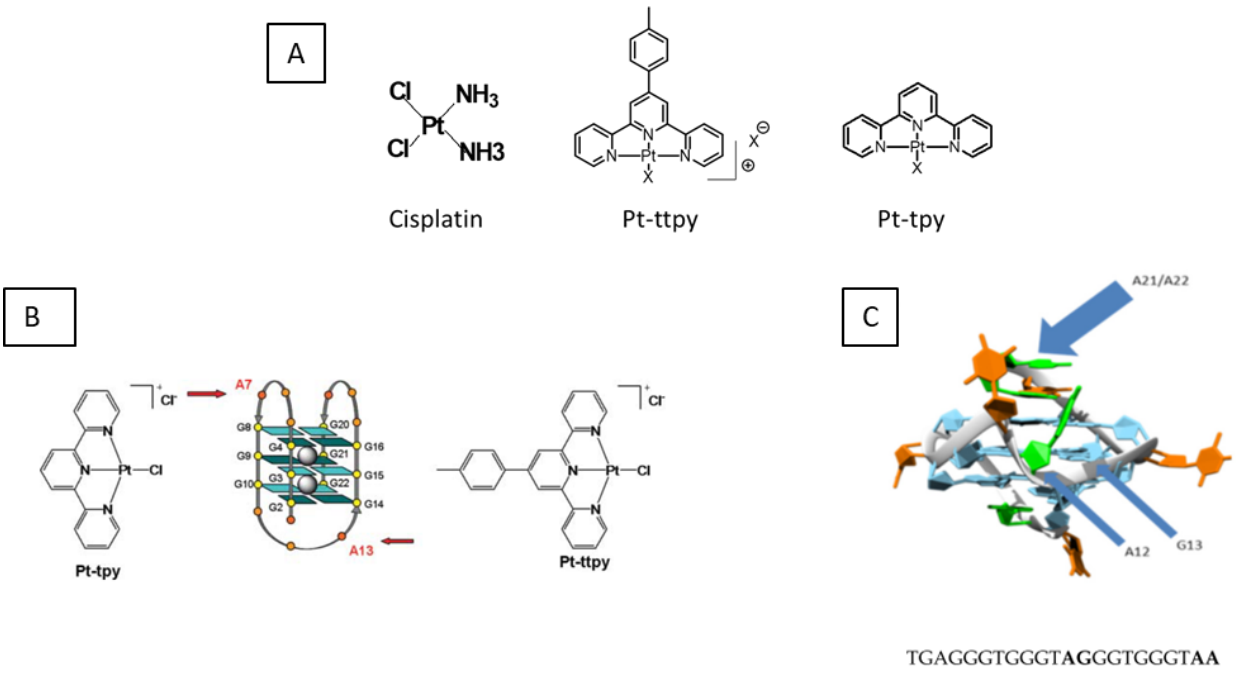

Figure 19: **Structure and binding sites of the drugs**. (A) The structure of the three metal complex drugs, cisplatin, Pt-ttpy and Pt-tpy. The platination site of (B) Pt-ttpy and Pt-tpy in telomeric G4 [126] and (C) Pt-ttpy in c-myc G4 sequence [142] (Annex 1).

Hence, in order to achieve a proper understanding of the genomic DNA target sites of Pt-ttpy, γ-H2AX ChIP-seq experiments was performed post treatment of Pt-ttpy and cisplatin in A2780 cells. In this publication (pending submission), Pt-ttpy showed preferential DNA damage in G and A rich tandemly repeated sequences, and not exclusively in G4 rich motifs of the genomic DNA. It is seen to accumulate in 6 chromosomes (chr 1, chr4, chr9, chr15, chr16, chr21) that are identical to that of cisplatin (figure 20). Interestingly, both cisplatin and Pt-ttpy show an enrichment of γ-H2AX domains in mitochondrial DNA. The question arises if the mitochondrial DNA enriched in γ-H2AX domains is the DNA from mitochondria or the Nuclear Mitochondrial Sequences (NUMTs) present in the genome. NUMTs are partial or whole mtDNA sequences that are present in the nuclear DNA [358]. While this question has been solved in the laboratory by showing that no γH2AX foci were localized within mitochondria, I personally investigated if Pt-ttpy, like other metal complexes including cisplatin[83, 359] and the G4 binding RHPS4 [82], can enter the mitochondria and if so, are they able to induce mitochondrial dysfunction.

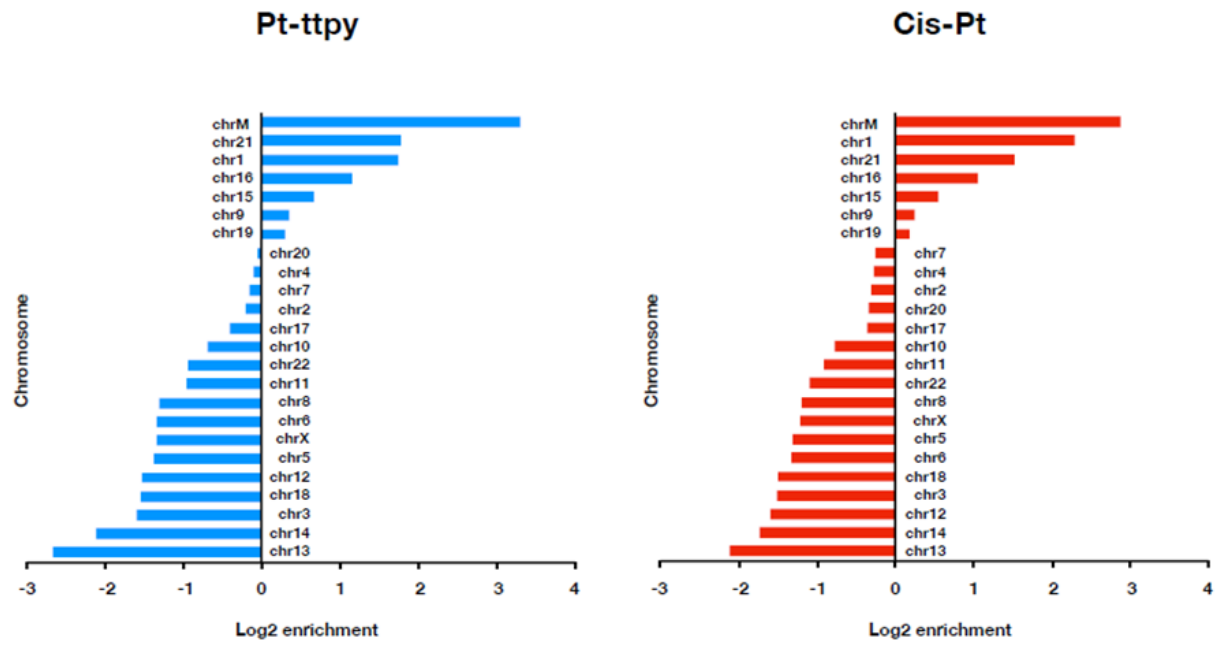

Figure 20: **γH2AX enrichment sites post treatment with Pt-ttpy and cisplatin**. γH2AX domains of cisplatin and Pt-ttpy are enriched in the same chromosomes, with a main enrichment in mitochondrial DNA. Their relative peak enrichment on each chromosome and chrM is shown for Pt-ttpy γ-H2AX peaks in blue and cisplatin γ-H2AX peaks in red (publication pending, Annex 2).

4.1. Pt-ttpy accumulates in mitochondria

Mitochondria is a cellular organelle that is responsible for the energy production of the cell [360], apart from other significant role [361]. Changes to the mitochondria such as OXPHOS uncoupling, mitochondrial Ca^{2+} modulation, Electron Transport Chain (ETC) inhibition and control of oxidative stress through increase or decrease of mitochondrial ROS accumulation can cause mitochondrial dysfunction and induce cell death [362]. Hence, it is a valued target for novel anti-cancer drugs. Mitochondria possesses its own DNA, 16kb of circular DNA present in multiple copies, that can be targeted by DNA binding drugs due to its insufficient DNA repair mechanism [363].

Various Pt-drugs have been shown to target mitochondria [83]. One such important drug to target mitochondria is cisplatin. Moreover, since G4 can be formed in mtDNA, a G4 binding ligand, RHPS4 has also been shown to target mitochondria. Hence, we wanted to see if Pt-ttpy is capable of targeting mitochondria and to which extent in terms of Pt complex accumulation.

Moreover, metal complex accumulation can lead to mitochondrial membrane potential loss and higher ROS formation which can induce mitochondrial dysfunction.

In order to test if Pt-ttpy is able to localize in mitochondria, we performed an ICP-MS quantification of the mitochondrial fraction isolated from A2780 cells treated with the drugs for 96h at their IC_{50} and IC_{80} concentration (the latter being the condition of ChIP-seq experiments). In addition, we performed the Pt quantification content on the total cell pellet and bound on its nuclear DNA. The results show that Pt-ttpy accumulates to mitochondria 12 fold more than cisplatin and 5 fold more than Pt-tpy (Figure 21). Pt-tpy also shows a 2fold increase in Pt accumulation in mitochondria compared to cisplatin. The Pt accumulation in mitochondria for cisplatin Pt-ttpy and Pt-tpy can be correlated to the drug accumulation within cells. This test shows that Pt-ttpy is able to accumulate to mitochondria better than cisplatin at iso-effect doses thereby giving certain insights into the mechanistic potency of Pt-ttpy as an anti-cancer drug.

Figure 21: **Pt-ttpy accumulates in cells and mitochondria more than cisplatin and Pt-tpy**. The

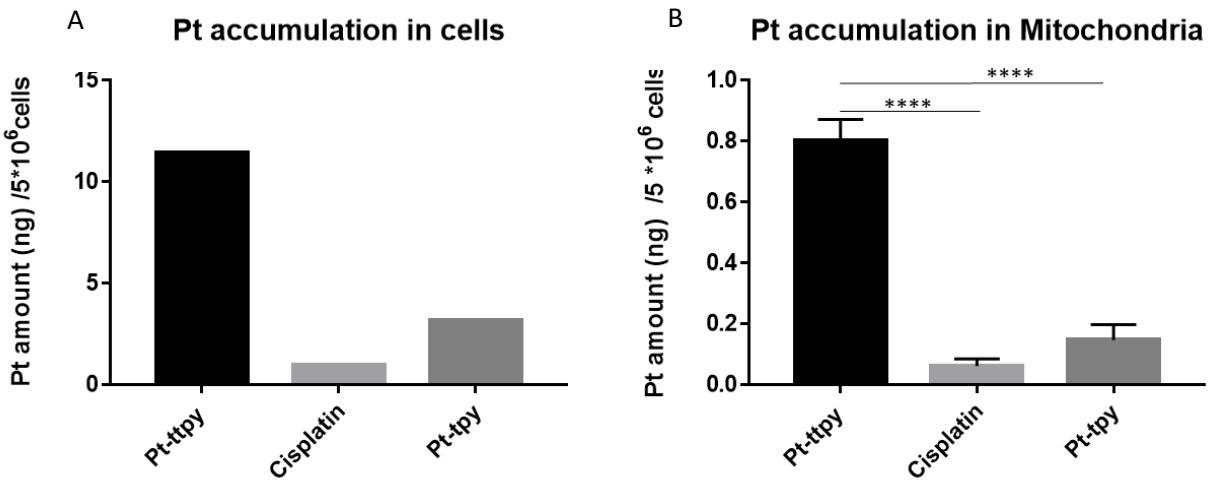

accumulation of platinum on (A) whole cells and (B) mitochondria after being treated by Pt-ttpy, cisplatin and Pt-tpy at their IC_{80} concentration for 96hours and quantified by ICP-MS.

4.2. Pt-ttpy can induce mitochondrial membrane potential loss

We need to find if the localization of Pt-ttpy in mitochondria is capable of causing deleterious effects on the organelle. Hence, it was important to test if Pt-ttpy was able to induce a mitochondrial membrane potential loss.

A2780 cells were treated with the drugs for 96hrs and then incubated with the JC-1 dye for 30 minutes at 37°C, following which the cells were analyzed using a flow cytometer. The change of mitochondrial membrane potential ($\Delta\psi_m$) was detected by JC-1 that accumulates into the mitochondrial membrane matrix space inversely proportional to the ($\Delta\psi_m$). JC-1 is a monomer emitting green fluorescence at low concentration, whereas at high concentration, its aggregation in mitochondria leads to red fluorescence. Hence a decrease of red fluorescence with the drug treatment would give us an indication of mitochondrial membrane potential loss. Calculating the percentage of cells in the quadrant with high green and low red fluorescence gives us an idea of the number of cells with mitochondrial potential loss. With the JC-1 assay study, we observed that Pt-ttpy has an increased ability to induce mitochondrial membrane potential loss (Figure 22). The percentage of cells with dysfunctional mitochondria with Pt-ttpy treatment at its IC_{80} concentration is significantly higher than that of the non-treated and cells treated with cisplatin and Pt-tpy (Figure 23A). Moreover, another way of analyzing the results is by computing the total red fluorescence emitted by the cells indicating the amount of intact mitochondria, we observe a significant drop of the red fluorescence when the cells are treated with Pt-ttpy at its IC80 compared to the other drugs (Figure 23B). We also observe a concentration dependent increase of mitochondrial dysfunction induced by Pt-ttpy. We also performed the experiment with the 10µM concentration of the drugs and we observe an increase of mitochondrial dysfunction by all the drugs (Pt-ttpy, cisplatin and Pt-tpy), though Pt-ttpy and cisplatin had the strongest effect with a 4 fold increase of cells with mitochondrial dysfunction (figure 23C).

This result proves that Pt-ttpy is significantly more capable of creating mitochondrial dysfunction when compared to cisplatin and Pt-tpy at their iso-effect concentration and iso-dose conditions at 10µM.

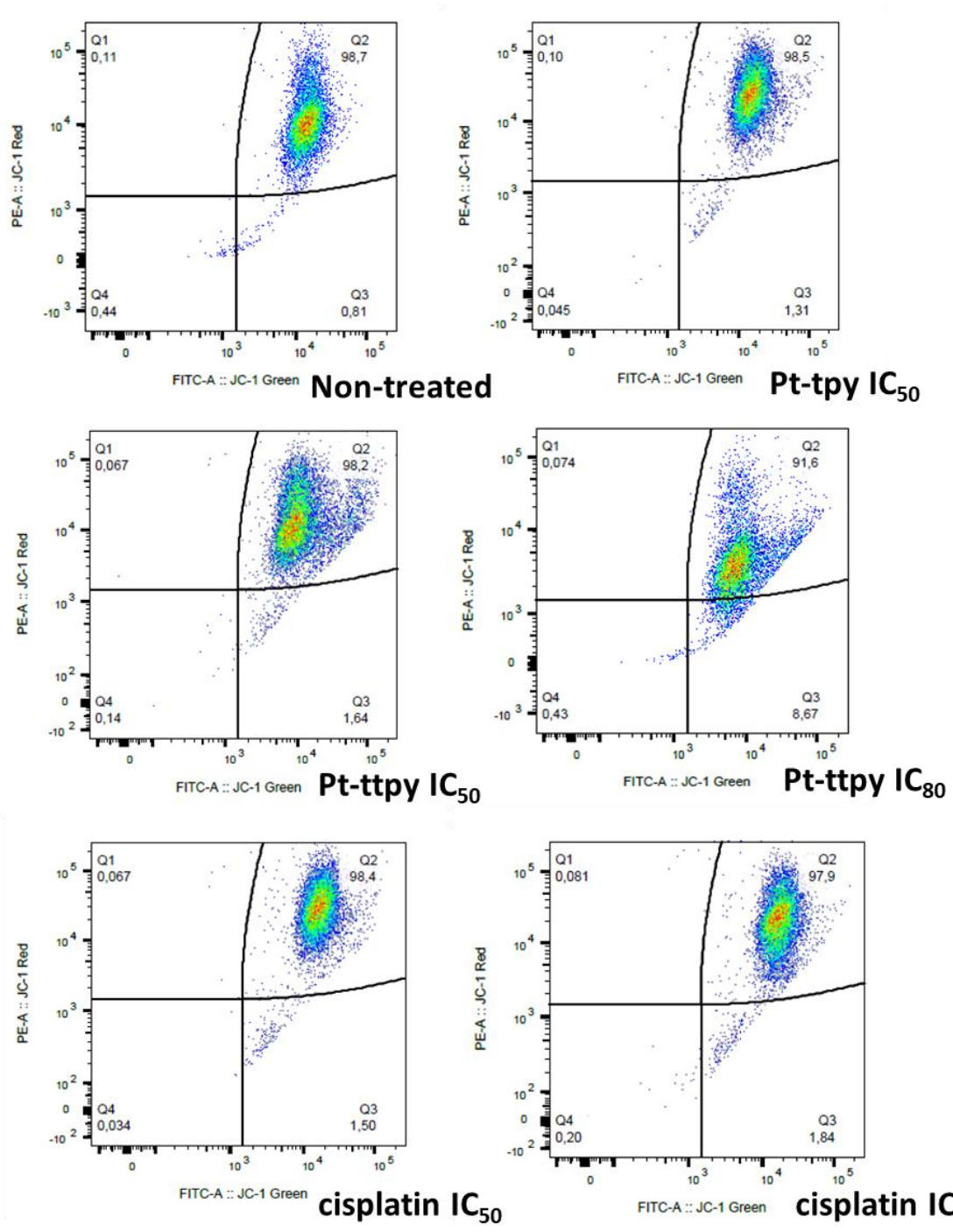

Figure 22: **Pt-ttpy induces mitochondrial membrane potential loss**. The JC-1 assay by flow cytometry shows cell population in different quadrants with Q3 representing mitochondrial membrane potential loss in Pt-tpy, Pt-ttpy and cisplatin treated cells at their IC_{50} and IC_{80} concentration for 96 hours in A2780 cells.

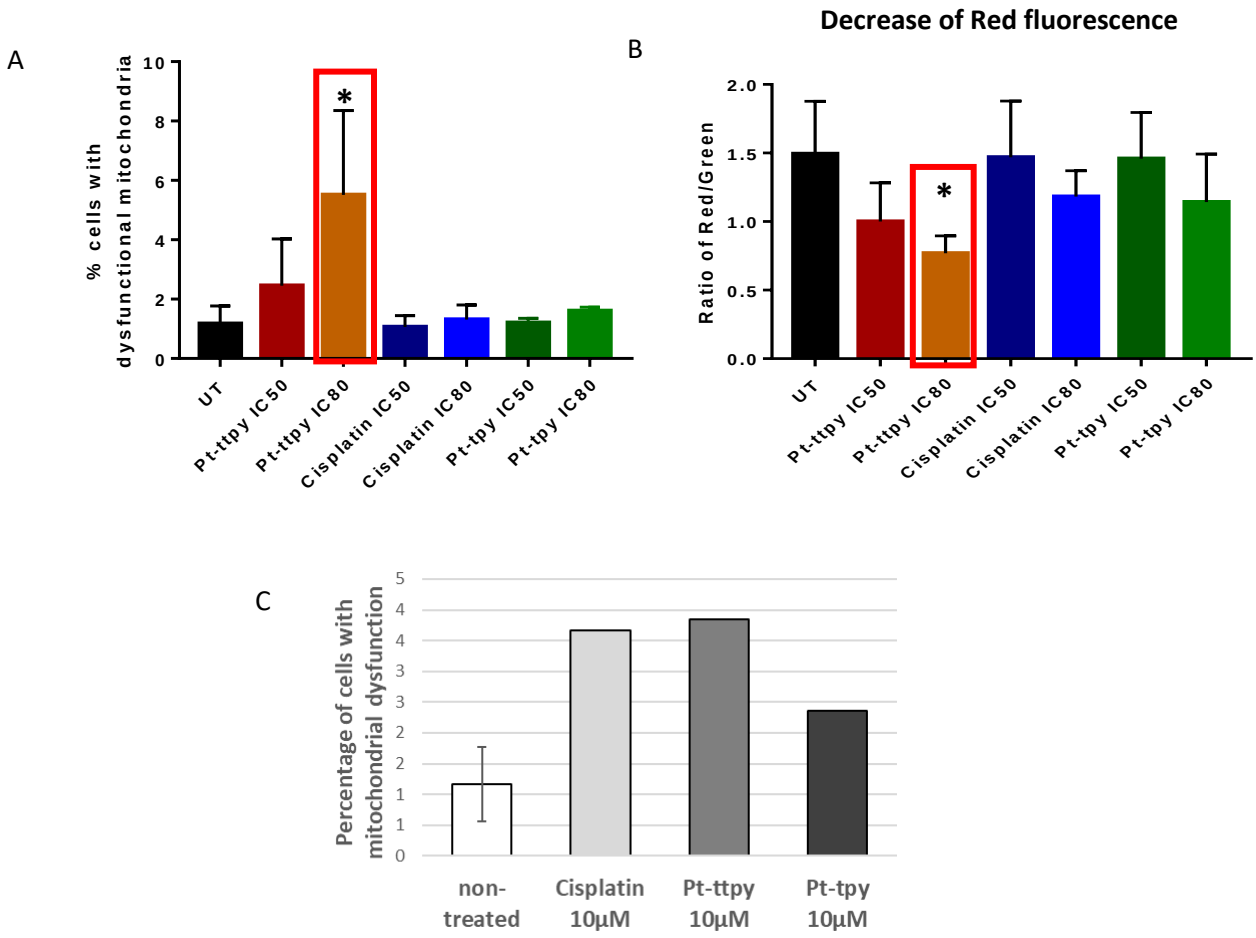

Figure 23: **Comparison of drugs inducing mitochondrial membrane potential loss**. (A) The percentage of cells with dysfunctional mitochondria is tabulated from the previous figure (figure 22) with the drug treatment of 96h at their IC_{50} and IC_{80} concentration in A2780 cells. (B) The ratio of red/green fluorescence detected from the cell population are tabulated as another form of representation of the flow cytometry data. $N \geq 3 \pm SD$, $^*p<0.05$ (C) The percentage of cells with mitochondrial dysfunction when treated with 10µM of the drugs overnight in A2780 cells is tabulated.

4.3. Pt-ttpy and the induction of early apoptosis markers

Pt-ttpy and cisplatin, both are capable of localizing to the mitochondria and Pt-ttpy is capable of inducing mitochondrial dysfunction. Since mitochondrial membrane loss can lead to apoptosis via the intrinsic apoptotic pathway [251], we wanted to test if Pt-ttpy treatment is capable of inducing apoptosis revealed by markers such as Annexin-V markers in parallel we used the fluorescent intercalator 7-AAD for marking dead cells. Apoptosis is divided into early apoptosis (Annexin V+/7-AAD-) and late apoptosis (Annexin V+/7-AAD+). The results show that with Pt-ttpy treatment at IC_{80} concentration, there is an increased signal for early apoptosis, compared to cisplatin and Pt-tpy (Figure 24A and 24B). However, there is no significant increase of late apoptotic cells with any of the drugs. When the concentration of the drug is increased to 10µM for an overnight treatment, we see a 1.7fold increase of cisplatin induced early apoptotic cells compared to non-treated cells. There was no increase of early apoptotic cells for Pt-ttpy.

Cisplatin in literature has shown a percentage of apoptotic cells depending on the amount of mitochondrial DNA within cells [364], and the results we obtained were similar to the ones of literature for the same cell line, classified as low mtDNA content. However, the condition of drug treatment in literature was very different with 10µM cisplatin being treated for 48 hours, compared to our IC_{80} treatment for 96 hours. In another example of mono-functional Pt complex, it has been shown that the complex can increase the percent of early apoptotic cells in a concentration dependent manner [365].

A

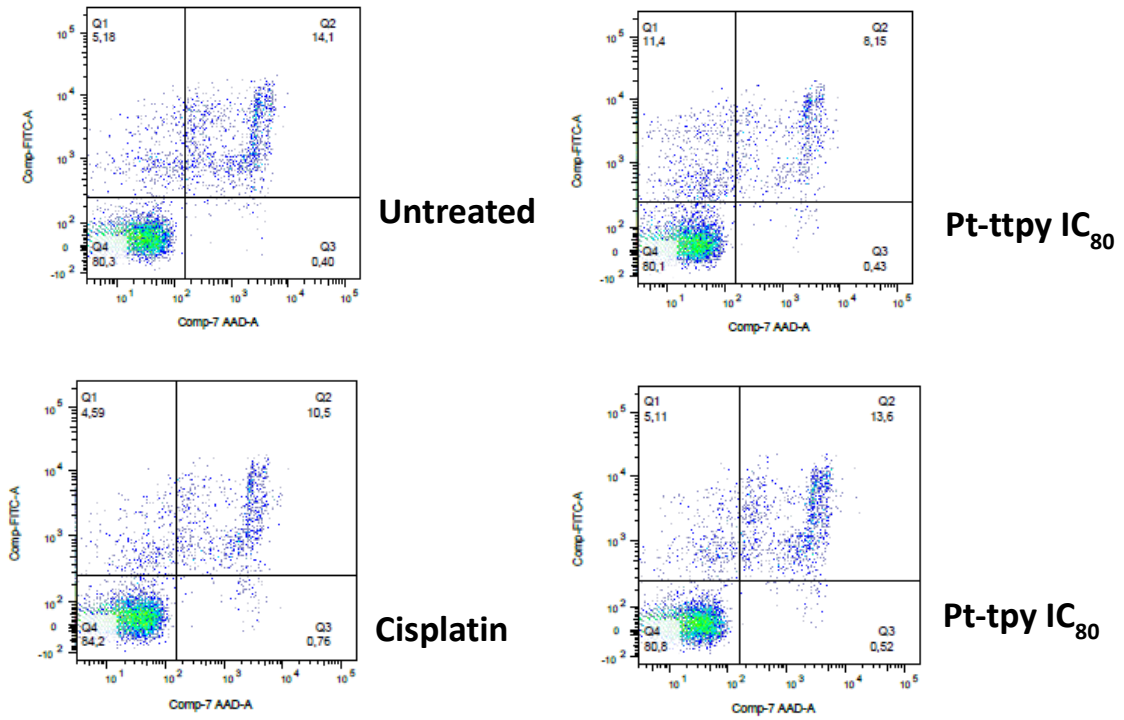

figure 24: **Pt-ttpy induces weak early apoptosis markers compared to other drugs**. (A) The

B

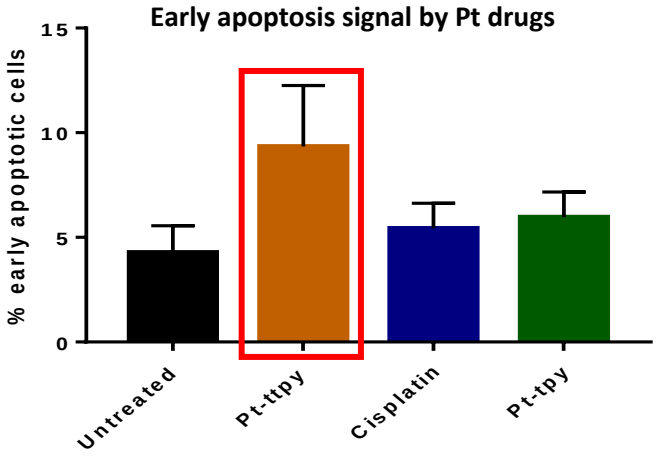

Annexin V apoptosis assay by flow cytometry showing an increase of cells in Q1 (FITC+/7-AAD-) for early apoptosis after treatment with Pt-ttpy (4µM), cisplatin (0.6µM) and Pt-tpy (6µM) for 96 hours. (B) Tabular representation of the percentage of early apoptotic cells after the drug treatment. N ≥ 3 ± SD.

4.4. Pt-ttpy and ROS formation

One of the important features of mitochondrial dysfunction is the formation of reactive oxygen species (ROS). Superoxide $O_2^{\bullet-}$ is released from the mitochondria in the event when the electron transport mechanism is compromised or the mitochondrial metabolism is disrupted due to mitochondrial dysfunction [366]. Hence, we wanted to test if there is an increase in the production of ROS post treatment of our drugs. We used CellROX deep red to measure the amount of total ROS present in the cell by incubating the cells for 1 hour with the probe, followed by flow cytometry analysis. The IC_{80} concentration for Pt-ttpy and cisplatin was used for a treatment of 96hrs for the experiment. We also did an experiment with 10µM concentration of the drugs incubated overnight.

The ROS quantification analysis showed that Pt-ttpy at its IC_{80} concentration is not able to induce ROS in the experimental conditions used, whereas cisplatin is able to show some ROS production (figure 25A). Moreover, in the 10µM concentration of drugs, there is again a definite increase of total ROS production by cisplatin, and once again, none is observed for Pt-ttpy (figure 25B). This shows that Pt-ttpy is not capable of ROS production by itself and follows a different mechanism of action to cisplatin.

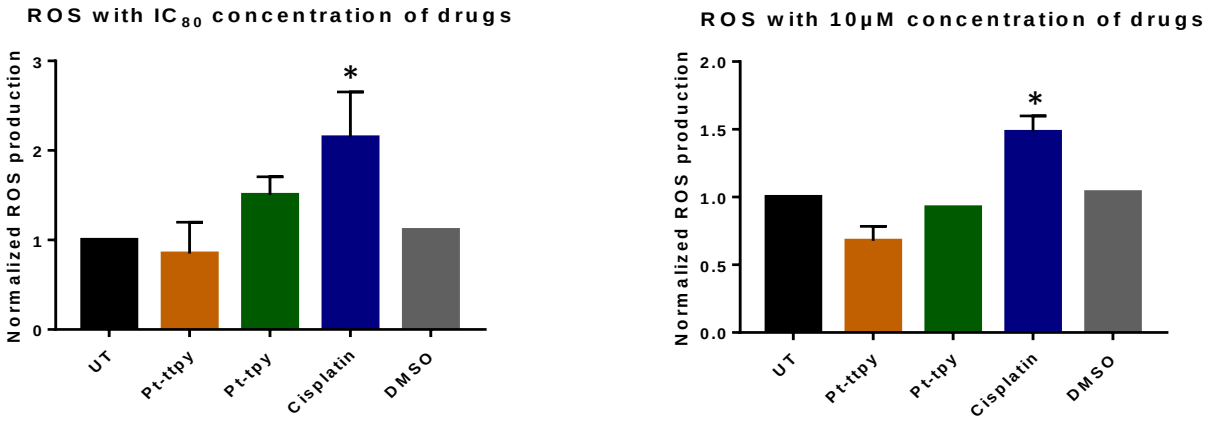

Figure 25: **Pt-ttpy does not induce ROS formation**. ROS production calculated in A2780 cells with (A) Pt-ttpy (4µM) and cisplatin (0.6µM) treatment for 96hours, N=3 ± SD, *p<0.05 and (B) 10µM concentration treatment for 18hours N=2 ± SD, *p<0.05, from the fluorescence of Cellrox Deep Red by flow cytometry. Cisplatin shows a significant increase of ROS production with both treatments.

Conclusion

Pt-ttpy is seen to accumulate in mitochondria more favorably than cisplatin or Pt-tpy at their iso-effect. It has been observed that Pt-ttpy accumulates ~12 times more than cisplatin in mitochondria and is proportional to its accumulation in the cell. This high accumulation of Pt-ttpy in mitochondria indicates that Pt-ttpy could play a vital role in mitochondrial dysfunction. Pt-tpy, on the other hand has double the amount of mitochondrial accumulation compared to cisplatin and is 5 fold lower than that of Pt-ttpy. Since mitochondrial accumulation is proportional to cellular accumulation, it does seem that mitochondrial accumulation is only dependent on the intracellular accumulation and not on the platinum structure.

The mitochondrial dysfunction assay with JC-1 concurs with the Pt-ttpy accumulation as only Pt-ttpy treatment is able to show a significantly higher fraction of cells with mitochondrial dysfunction compared to the other two drugs. Loss of membrane potential is an indicator of Mitochondrial Outer Membrane Permeabilization (MOMP) [367]. MOMP is a fundamental event that leads to apoptotic pathway initialization by the release of apoptotic factors such as cytochrome C, SMAC and Omi that can lead to caspase activation [251]. We observe that there is a weak but non-significant increase of Phosphatidylserine (PS) present in the outer cell membrane with Pt-ttpy treatment, which is a marker of early apoptosis [368]. Coupled with the fact that there is no increase of late apoptotic cells and no ROS induction, leads us to speculate that Pt-ttpy treated cells induce partial or incomplete MOMP (iMOMP). This could be because MOMP was induced in some but not all mitochondria in cells [251].

In A2780 cell line, cisplatin induced ROS production but showed loss of mitochondrial potential membrane only at high concentration treatment in agreement with the low mitochondrial content of this cell line [364]. This production of intracellular ROS has been shown in literature to be in parallel with mitochondrial superoxide formation and can be found elevated in non-apoptotic cells as well [369]. In contrast, Pt-ttpy accumulates in mitochondria at higher level than cisplatin, induces mitochondrial dysfunction by a loss of its potential membrane consequently leading to an increase in early apoptosis but without the induction of ROS. Hence, our work (pending publication in annex 2) suggests that Pt-ttpy could be an effective drug for 1) circumventing the resistance of cisplatin in cancerous cells with low mitochondrial content, such

as high malignant ovarian cancer cell lines, because it accumulates at higher rate and 2) inducing less secondary toxicities because of the absence of ROS production. The biological consequences of mitochondrial membrane potential reduction by Pt-ttpy and its higher mitochondrial accumulation rate need to be further studied.

We are current working to see if Pt-ttpy and cisplatin are able to induce lesions in the mtDNA, and its quantification would help us gauge if Pt-ttpy is able to induce mtDNA damage and consequently stop its DNA processing activities such as replication or transcription (currently ongoing under Dr. Tao Jia). Therefore, we would also need to investigate if Pt-ttpy can change the expression of mitochondrial proteins (13 proteins coded for the ETC complex) to further understand the mitochondrial dysfunction in detail.

5: Pt-ttpy and chemosensitization of DDR inhibitors

5.1. Pt-ttpy and Olaparib

Pt-ttpy is able to cause genomic DNA damage by binding to DNA in an irreversible way [126, 142] (Annex 1) which can lead to the formation of DNA lesions, highlighted by the formation of DSBs. Repair pathways are initiated after identification of DNA damage sites and cell-cycle DNA damage checkpoints. PARP proteins are shown to be involved in the excision repair pathways, SSB and DSB repair pathways [192]. Hence, we decided to check if Pt-ttpy can sensitize PARP inhibited cells.

First, we wanted to see the effect of the drug Pt-ttpy on PARP1 and PARP2 deleted cells of A2780 cell line. Deletion of both the PARP enzymes was achieved by proper shRNA treatment. This work of creating shRNA induced PARP deletion was done by Vincent Peneneach, Institute Curie (figure 26A).

Treatment of the PARP1/PARP2 deleted cells, in comparison with the cells treated by the shRNA empty vector with Pt-ttpy at IC_{30} concentration for 4days, 7days and 11days showed that there is a definite sensitization with the drug (figure 26B). Pt-ttpy is able to inhibit proliferation at a higher rate when the PARP enzymes are deleted. However, the cells with the empty vector also showed moderate sensitization. Hence it was difficult to comment whether the sensitivity seen is indeed because of the deletion of PARP1 and PARP2.

In order to really understand if PARP protein dysfunction can cause sensitivity of A2780 cells with Pt-ttpy, we also decided to use Olaparib. It is a clinically used PARP1 inhibitor and works by trapping the enzyme at the DNA damage site and inhibiting its catalytic activity [370]. Co-treatment of Olaparib with Pt-ttpy showed signs of definite sensitization over 7days incubation (figure 26C). Treatment of A2780 cells with Pt-ttpy 1.5µM (IC_{30} concentration) and increasing concentration of Olaparib show synergistic effect as calculated by the software CompuSyn [371] (figure 26D). At lower concentrations of Olaparib the combinatory indice (CI) values are above 1 showing that the interaction is antagonistic, which changes with increasing concentration of the

inhibitor as the CI values drop below 1, showing a synergistic effect. The results clearly show that the sensitization of the cells to Olaparib by Pt-ttpy is concentration dependent. Increasing the concentration of Pt-ttpy does not seem to have any additional effect. Pt-ttpy concentration of 1.5µM and 2µM shows synergistic effect from 2µM Olaparib.

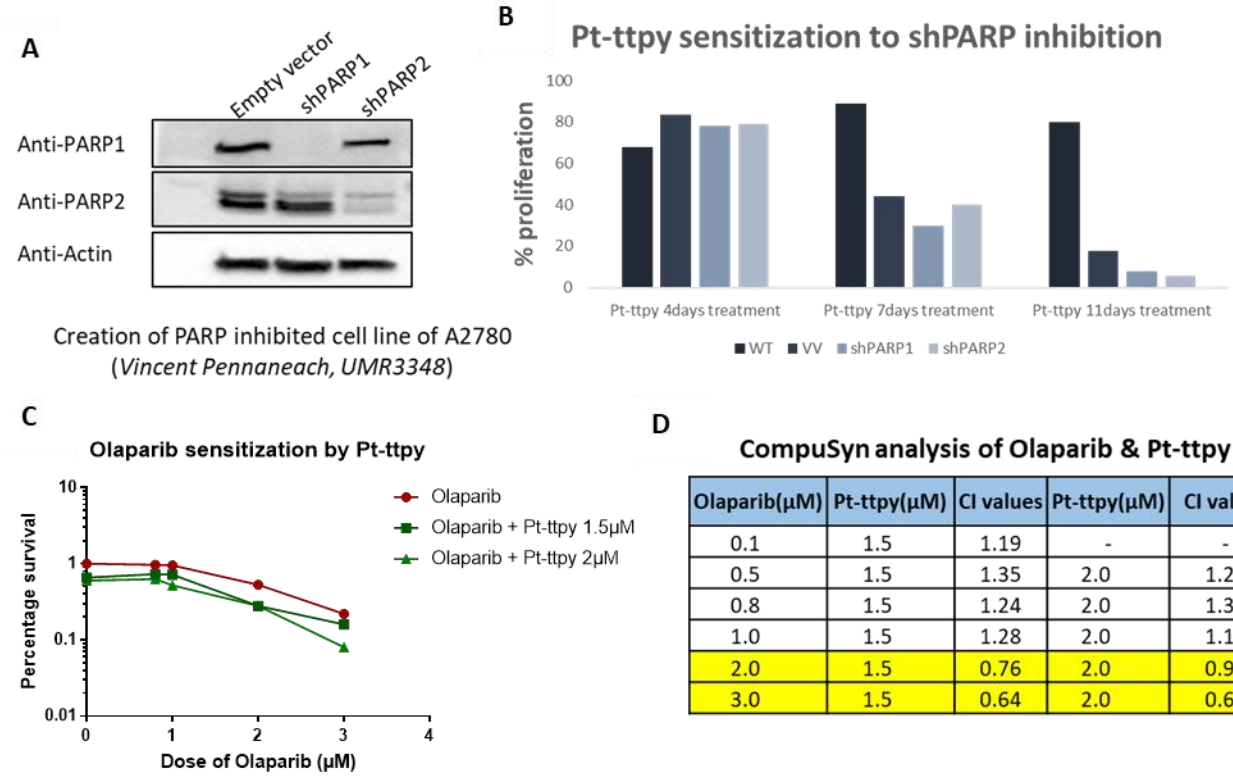

Olaparib(µM)	Pt-ttpy(µM)	CI values	Pt-ttpy(µM)	CI values
0.1	1.5	1.19	-	-
0.5	1.5	1.35	2.0	1.25
0.8	1.5	1.24	2.0	1.33
1.0	1.5	1.28	2.0	1.19
2.0	1.5	0.76	2.0	0.95
3.0	1.5	0.64	2.0	0.61

Figure 26: **Pt-ttpy induces chemosensitization of A2780 cells to PARP inhibitor**. (A) Western blots verifying the expression of PARP1 and PARP2 in shPARP1 and shPARP2 transfected A2780 cell line. (B) Percentage proliferation graph showing the sensitization of the A2780 cells to IC_{30} concentration of Pt-ttpy (1.5µM) when PARP proteins are deleted. (C) Survival curve showing the sensitization of A2780 cells when co-treated with increasing doses of Olaparib and 1.5µM and 2µM Pt-ttpy after 96h treatment. (D) Combinatory Index calculated from compusyn software of the Olaparib and Pt-ttpy co-treatment showing synergistic tendency (marked in yellow).

Olaparib is capable of inducing radiosensitization due to its capability in inhibiting DNA repair by blocking the catalytic activity of DNA damage sensor PARP1 [372]. Since, Olaparib is also capable of sensitizing A2780 cells to Pt-ttpy, it would be interesting to investigate if the combined treatment of irradiation + Pt-ttpy + Olaparib be more lethal than any of the individual combinations. Perhaps, the doses used for Olaparib were too high to allow detection of an increase in the sensitizing effect. Before concluding it could be necessary to reproduce the experiment at subtoxic doses of Olaparib

The radiosensitization potential assay is performed on A2780 cell line. As observed before, Pt-ttpy in the presence of irradiation shows radiosensitization, as does Olaparib. However, the combination of 3 does not show any additional sensitization than what was achieved with Olaparib (figure 27). This shows that either Pt-ttpy induced radiosensitization involves the inhibition of PARP activity or that the combination of 3 is extremely deleterious for the cells and radiosensitization cannot be pushed any further.

The chemosensitization of A2780 cells to Olaparib by Pt-ttpy, in addition to be a positive advance from a therapeutic point of view, indicates that the Pt-ttpy DNA adduct repair pathway involved the recruitment of PARP1. Since Pt-ttpy which is a mono-functional Pt complex, is only able to form a mono-adduct on DNA and not crosslinks as cisplatin, we can suggest that this adduct may be repaired by the BER pathway. But further experiments are needed for it to be confirmed.

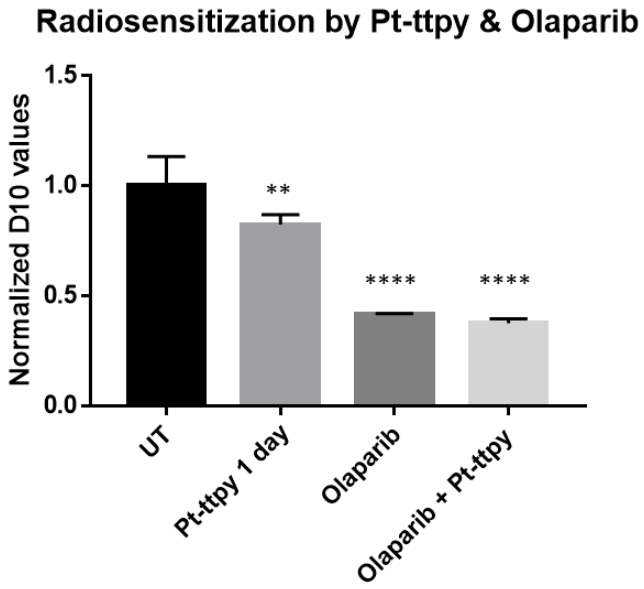

Figure 27: **Pt-ttpy is not able to induce additional radiosensitization of A2780 cells by Olaparib**. Radiosensitization potential of 1.5µM Pt-ttpy, 1µM Olaparib and their combined treatment with irradiation with 1 day pretreatment conditions in A2780 cells, normalized to the untreated irradiated (UT). N ≥ 2 + SD, *p<0.05, **p<0.01, ***p<0.001.

5.2. Pt-ttpy and ATM, ATR and DNA-PK inhibitors

Since Pt-ttpy induces DNA damage response for DSBs and recruits γ-H2AX to damage site, we wanted to know if cells could be sensitized by Pt-ttpy if any of the DDR signaling kinases would be inhibited. Hence we chose inhibitor of ATM, KU-60019; an inhibitor of ATR, AZD6738; and an inhibitor DNA-PK, NU7441.

The IC_{50} was observed for the 3 kinase inhibitors over a period of 7 days and are shown in Table 5. ATR inhibitor is the most sensitive with IC_{50} = 0.7µM. Pt-ttpy is able to sensitize all the DDR signaling inhibitors from a certain threshold inhibitor concentration. DNA-PK inhibitor and ATR inhibitor are more sensitized by Pt-ttpy than ATM inhibitor.

The cells were treated with Pt-ttpy at concentrations of 1.5µM and 2µM and with an increasing concentration of the DDR inhibitor. The cell proliferation assay at the end of 7 days was mapped as a survival curve and the chemosensitization was calculated using the Compusyn software

(figure 28). At lower concentrations of all the DDR inhibitors the CI values are above 1 showing that the interaction is antagonistic. This behavior changes with increasing concentration of the inhibitors as the CI values drop below 1, showing a synergistic effect. The results clearly show that the sensitization of the cells by Pt-ttpy to all the DDR signaling inhibitors is concentration dependent. The results also show that, while Pt-ttpy is able to sensitize the cells with all three of the DDR signaling inhibitors, DNA-PK inhibitor seems to be the most efficient inhibitor because its synergistic concentration is the closest to its IC_{50}.

DDR Inhibitors	IC50 (µM)
ATM inhibitor – KU-60019	2.8
DNA-PK inhibitor – NU7441	1.5
ATR inhibitor – AZD6738	0.7

Table 5: The IC_{50} (µM) of the three DDR signaling inhibitors calculated from the proliferation of A2780 cell line after 7 days treatment.

A

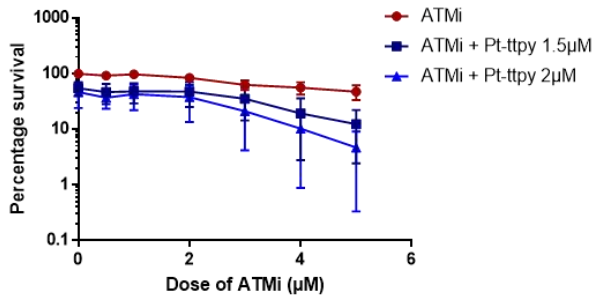

ATM inhibitor(μM)	Pt-ttpy(μM)	CI values	Pt-ttpy(μM)	CI values
0.5	1.5	1.22	2.0	1.32
1.0	1.5	1.35	2.0	1.64
2.0	1.5	1.64	2.0	1.76
3.0	1.5	1.34	2.0	1.24
4.0	1.5	0.97	2.0	0.90
5.0	1.5	0.76	2.0	0.67

B

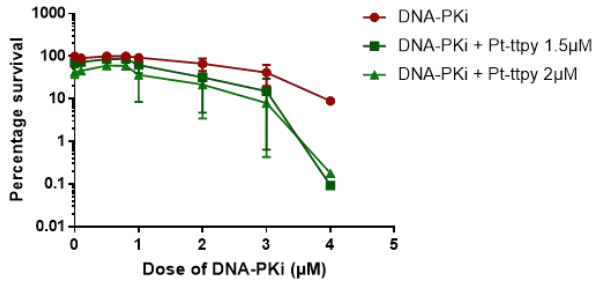

DNA-Pk inhibitor(μM)	Pt-ttpy(μM)	CI values	Pt-ttpy(μM)	CI values
0.5	1.5	1.16	2.0	1.09
0.8	1.5	1.22	2.0	1.09
1.0	1.5	1.24	2.0	1.01
2.0	1.5	0.80	2.0	0.86
3.0	1.5	0.56	2.0	0.57
4.0	1.5	0.33	2.0	0.46

C

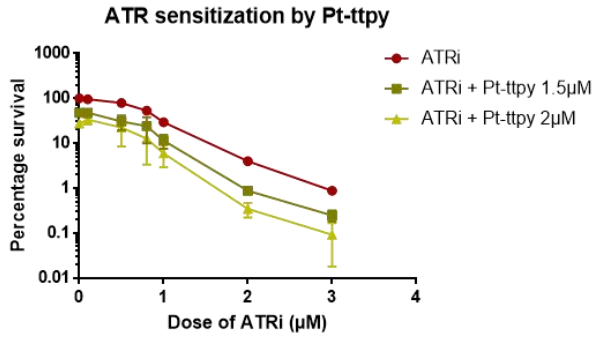

ATR inhibitor(μM)	Pt-ttpy(μM)	CI values	Pt-ttpy(μM)	CI values
0.1	1.5	1.17	2.0	1.24
0.5	1.5	1.39	2.0	1.57
0.8	1.5	1.64	2.0	1.54
1.0	1.5	1.33	2.0	1.29
2.0	1.5	0.99	2.0	0.88
3.0	1.5	0.88	2.0	0.53

Figure 28: **Pt-ttpy induces chemosensitization of A2780 cells to DDR inhibitors**. Survival curve showing the sensitization of A2780 cells when co-treated with increasing doses of (A) ATM inhibitor, (B) DNA-PK inhibitor and (C) ATR inhibitor with 1.5μM and 2μM Pt-ttpy after 96h treatment. CI values are also tabularized for each inhibitor showing the concentration from which the synergistic effect is seen (highlighted in yellow). N = 3 + SD.

Conclusion

Pt-ttpy is seen to sensitize the A2780 cells to PARP deletion and PARP inhibition. This phenomenon, apart from showing that PARP is involved in the repair of the DNA damage by Pt-ttpy, is useful for Pt-ttpy in a prospective clinical setting. As the current chemotherapeutic treatment regime has started involving a DNA damaging agent coupled with a repair inhibitor, Pt-ttpy coupled with Olaparib does seem to have a good potential for a combined chemotherapeutic treatment. Moreover, the radiosensitization potential of Pt-ttpy coupled with Olaparib is seen to be extremely high, though it should be expected as the cells are exposed to three different cytotoxic agents.

Pt-ttpy is also seen to be sensitizing the cells in the presence of all the three DDR signaling inhibitors. This could indicate that the DNA damage induced by Pt-ttpy are signaled, at different times, by all 3 of the DDR signaling pathways. Further work needs to be done in order to promote the importance of a combinatorial approach of treatment with Pt-ttpy and other DDR signaling inhibitors.

The synergy with the ATR inhibitor with Pt-ttpy treatment is a little bit surprising since in the laboratory only phosphorylation ChK2 was observed as expected from an activation of ATM following DNA damage, but not ChK1 which is a downstream target of ATR.

DISCUSSION & PERSPECTIVES

Discussion and Perspectives

Combined therapy is often used in clinic due to the fact that some drugs can induce synergistic effects when used at their subtoxic concentrations, thereby reducing their secondary toxic effects. Radiotherapy, which is one of the most used modality in clinic (in 50% of the cases) [165] is also one of the treatments which is frequently associated with chemotherapy in order to abrogate its limitations namely radioresistance of tumor cells and reactions in normal tissue around the tumor [169]. Hence, there is a need to identify and understand radiosensitizers that would improve the combination treatment modalities. Since radiotherapy is based on the induction of a large number of DNA damages that if not correctly repaired would induce cell death, combination therapy has been divided in several classes and are based on either impairing the DNA repair, the DNA signalling repair and the following pathways, or increasing the DNA damages. There are different classes of radiosensitizing drugs that have targets such as inhibition of repair pathways, cell cycle deregulation, enhancing ROS production in hypoxic cells, inhibition of prosurvival pathways, enhancing auger effects of high atomic number (Z) materials, etc, which are discussed in the introduction of the thesis (See chapter 4B). Certain drugs from each of these classes are now also involved in a clinical trial for their radiosensitization potential (see Table 1, chapter4C). There is another class of radiosensitizers, which is the focus of this thesis, that are DNA binding and damaging agents. In contrast to their extensive research as possible chemotherapeutic agents, their possible use as radiosensitizer has been largely ignored even though cisplatin is already used in clinic in combination with ionizing radiations. Since their mechanism of actions are not elucidated, a crucial need to decipher them is awaited. It is known that these DNA damaging agents also have detrimental effects in normal cells due to the fact they target DNA, but their associated with irradiation at their subtoxic doses may lead to the emergence of new treatments. They include two kinds of drugs from which some of them have already have shown radiosensitizing properties-

A. Metallic complexes[271] including platinum complexes that can bind irreversibly to DNA causing DNA damage which need to be processed by DNA repair pathways – example, cisplatin is able to induce a chelate between two adjacent guanines in the DNA and the DNA lesion requires the NER pathway to be repaired [309].
B. G4 ligands that can bind and stabilize G4s present in the genomic, telomeric and mitochondrial DNA. In the telomeric DNA, they can bind to the telomeric G4 inducing loss of shelterin proteins (TRF2 or POT1) that can lead to uncapping of telomeres and their dysfunction. This induces the shortening of the telomeric sequence, illegitimate repair of the chromosome ends that could lead to telomeric fusion and permanent cell growth arrest or cell death [44]. In the genomic DNA, they can induce replication stress, block R-loops which lead to the formation of DNA damage as well [68]. In mitochondrial DNA, G4 ligands induce inhibition of its DNA transcription, leading to respiratory complex depletion [82]. Three G4 ligands RHPS4, TAC and the metal complex Pt-ctpy were shown to have radiosensitizing properties with different mechanism of actions including possible involvement of telomere dysfunction in telomerase positive cancerous cell lines. In addition, in ATRX (serves to resolve G4s) deficient cell lines another G4 ligand CX-3543 was shown to be radiosensitizer leading to the conclusion that stabilization of G4 is significant in a cell line context [346].

The three cell lines used in this work, A2780 ovarian carcinoma, T98G Glioblastoma (GBM) and H1299 non small cell lung carcinoma (NSCLC) are chosen firstly to represent a diversity of cancer types in order to judge the efficacy of the drugs. Moreover, T98G and H1299 have an inherent radioresistance, as can be seen by their D10 values. A2780 is not as radioresistant as the other cell lines but its importance stems from the fact that ovarian carcinoma is predominantly treated by a platinum drug such as cisplatin [373]. Cisplatin resistance in these treatments occur in 25% of at the early stage and 80% at the advanced stage, hence in order to search for other platinum drugs that can overcome this resistance, A2780 cell line has been proven to be an effective choice for research.

The results from our screening failed to show any Structure Activity Relationship (SAR) with the G4/non G4 metal complexes and radiosensitization (RS). In the terpyridine series, only Pt-ttpy showed RS in all three cell lines independently of their p53 status. This showed that RS is not dependent on the terpyridine structure as other terpyridine complexes (including tolyterpyridine complexes) did not show RS. Moreover, it also showed that RS is not based on the Pt-atom as not all platinum complexes showed RS. In case of salphen series, S-Ni and C-Ni showed RS potential. While certain other complexes also showed a mild RS property, it was not consistent on all cell lines.

There was one interesting observation with the Pt-NHC series. All the complexes in the Pt-NHC series had shown RS potential in A2780 cell line. However, with the addition of the G4 ligand PDC, the Pt-NHC-PDC complexes lost their RS potential entirely. One of the Pt-NHC-PDC complex has been shown to target telomeres and uncap them via the loss of TRF2 proteins, but its genomic targeting has not been evaluated. The fact that G4 ligands that show RS have proposed their mechanism of action to be telomere targeting [143, 339, 344] coupled with a new theory that stabilization of the G4 structure can be radioprotective [348], suggests that the non-RS capability of the hybrid complex Pt-NHC-PDC could result from the binding of this complex on G4 within genomic DNA. Especially since it has been shown that the G4 ligand part targets telomeres in addition to genomic DNA [111]. However, to use this explanation for the phenomenon observed by the Pt-NHC-PDC complexes would need further work.

Hence in order to decipher the mechanism of action of radiosensitization induced by metal complexes, we choose Pt-ttpy which was the one able to radiosensitize different cell lines and for which the DNA targets has already been studied in the laboratory in absence of ionizing radiation. Moreover, this particular complex has got dual properties that can be involved in its radiosensitizing properties; G4 binding capability and Pt atom capable of inducing platination on telomeric and genomic DNA [127]. Nothing is concretely known from literature regarding the mechanism of action of the RS property of DNA binding drugs (both G4 and Pt-complex). Moreover, the knowledge gained is also inconsistent as can be seen in the case of cisplatin. The RS potential of cisplatin discussed in multiple papers seem to contradict each other and the RS observed seems to be dependent on multiple factors such as the cell line used, the concentration

used and the time duration and of the drug treatment, (see introduction chapter 4D.2) [327-329]. It is why we decided to also analyse the RS effect of cisplatin in our conditions.

Regarding the mechanism of action of G4 ligands inducing RS, there are multiple proposed theories:

1. The capability of the ligand to induce telomeric dysfunction post irradiation as is seen in the case of Pt-ctpy in GBM and NSCLC cell lines [143].
2. The capability of the ligand to induce telomeric dysfunction by itself independently before irradiation, as is seen in the case of RHPS4 in GBM cell lines [344].
3. The capability of the drug to induce a delay in DNA damage repair, seen in RHPS4 in GBM cell line but not in glioblastoma stem cells (GSCs) [345].
4. The capability of the drug to induce a dysregulation of ChK1 and RAD51, as seen in the case of RHPS4 in GSCs [345].
5. The capability of the drug to induce a cell cycle arrest in G2-M phase, as seen with RHPS4 [344] and Pt-ctpy [143].

Regarding the mechanism of action for cisplatin induced RS, the theories stated are:

1. Cisplatin induces a delay in the DNA damage repair [328]
2. Cisplatin causes a decrease of the amount of cells in G2-M phase 6hrs post irradiation [328]
3. Cisplatin DNA adducts can impede the translocation of Ku to the DSB *in vitro* which consequently inhibit the NHEJ repair pathway, possibly leading to radiosensitization [333, 335].
4. Unexpectedly, the effect of ROS production during the combined treatment of cisplatin with ionizing radiation has never been explored

In the case of Pt-ttpy, its RS in not dependant on the presence of telomeric damage pre-irradiation, unlike RHPS4 [344]. In addition, a mild telomeric effect was observed in the presence of the drug at its subtoxic concentration and irradiation. In fact, we saw a small rise in telomere dysfunction induced foci (TIFs) with the co-treatment whereas no TIFs were seen with either drug or irradiation separately. Hence, we cannot eliminate the possibility of telomere targeting by Pt-

ttpy in the presence of irradiation as a RS mechanism of action, as it has been proposed for RHPS4 and Pt-ctpy [143, 344]. However, the experiment needs to be repeated and further experiments need to be performed such as a dependence of TIFs formation with increasing drug concentration and dose of irradiation for example, in order to comment on this phenomenon. Moreover, Pt-ttpy was shown to induce damages on genomic DNA in G- rich regions, but not specifically in G4 forming sequences, as seen with the γH2AX ChIP-seq. Hence, we need to be cautious when attributing the RS effect only on DNA G4 selectivity.

In regards to the hypothesis of Pt-ttpy induced radiosensitizing effect depends on its DNA platination properties, we obtained results supporting the hypothesis. We noted that the RS by Pt-ttpy is possible with at least one day preincubation before irradiation. There is no RS observed when the drug is administered 10 minutes before irradiation or after. Moreover, with an extended preincubation of 5days, we saw an even better RS. This leads us to believe that the amount of Pt-ttpy bound to DNA could correlate to the level of RS induced by the drug. This hypothesis stays true when compared for cisplatin even though the trend is reversed. Cisplatin induces RS with one day preincubation but not with the longer 5 day preincubation, but it has been seen in the lab that the amount of Pt bound to DNA after 1 day treatment with cisplatin is actually higher than 4 day treatment. Though this DNA-drug binding kinetics is done at IC_{50} and IC_{80} concentrations, the trend can be assumed to be true for IC_{30} as well. Hence, the hypothesis of increased DNA platination at the point of irradiation holds true for both these complexes. In addition, we saw that irradiation increases the amount of Pt-ttpy bound to DNA in the hours following irradiation. This effect, if confirmed, could explain at least one part of RS by Pt-ttpy. It then needs to be demonstrated by *in vitro* assays on a plasmid system that irradiation can indeed increase the platination kinetics, as was shown for cisplatin. It has been proposed that irradiation could increase the rate of Pt-Cl cleavage bond which is the rate limiting step of platination [324].

Pt-ttpy, in contrast to cisplatin, needs to be present post irradiation for the RS effect. This led us to believe that radiosensitization by Pt-ttpy might have a role to play in the repair of DNA damage induced by irradiation. We observe that both 5 day and 1 day preincubation condition show a delay in DSB repair up to 6 hrs post irradiation. Interestingly, non RS complex Cu-ttpy and non RS conditions of Pt-ttpy (drug added post irradiation) do not show any delay of DSB repair, indicating

that this repair delay might be a reason of radiosensitization. In contrast, cisplatin does not show any delay in DSB repair indicating a difference in RS mechanism of action from that of Pt-ttpy. Remarkably, the number of DNA damages as seen by γH2AX foci (a molecular marker of DSB) is not increased 30 min after irradiation, which is the time point when maximum DSBs are formed post irradiation [355], in the presence of Pt-ttpy or cisplatin, in contrast to Pt-ctpy[143]. This indicates that the presence of Pt-ttpy or cisplatin bound to DNA does not increase the number of DSBs at the time of irradiation. Consequently, the DNA strand breaks produced on plasmids containing cisplatin adducts under ionizing radiations are not relevant in our conditions [325]. All together our results show that the RS of Pt-ttpy could be linked to the delay in repair of the DSBs.

This delay in DSB repair has been confirmed by the increase of 53BP1 foci area only for the Pt-ttpy combined to irradiation and not for cisplatin. 53BP1 is a transducer protein in DDR that is recruited at DSBs and plays a critical role in choosing the DSB repair pathway [214]. It will be of interest to analyse the co-localisation of both proteins since it has been shown that IR induced a higher yield of γH2AX than 53BP1 [374]. These results are in line with the cell cycle arrest seen with the co-treatment of Pt-ttpy and irradiation in their RS condition. As expected, ionizing radiation increase the number of cells in G2-M phase [356]. The presence of Pt-ttpy decreases the number of cells blocked in the G2-M phase until 6hours post irradiation, consequently reducing the time for repair of their DNA damage. In addition, the increased blockade in G1 could help in the promotion of heterochromatin DSB repair by 53BP1 by recruiting ATM [375]. In contrast, cisplatin which induces by itself a G2-M block does not modify the cell cycle arrest induced by IR.

We propose a model for the radiosensitization seen by Pt-ttpy based on our results (figure 1). When irradiation induced DSBs are produced near a Pt-ttpy DNA adduct, these DSBs are more difficult to repair due to the physical inference from the Pt complex leading to the formation of clustered damages, as can be revealed by the accumulation of 53BP1. The need of continuous Pt-ttpy treatment post-irradiation sustains the necessity of continuous Pt-ttpy-DNA adduct formation to continue producing this effect.

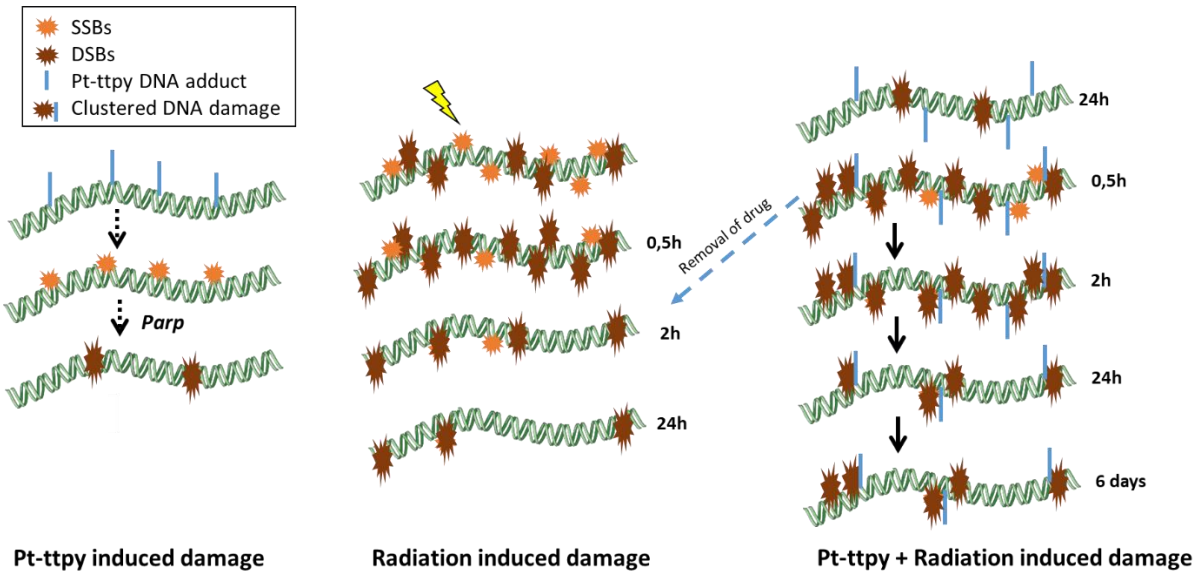

Figure 1: Schematic representation of the proposed model of DNA damage by Pt-ttpy alone, irradiation alone and the combination between Pt-ttpy and irradiation.

Hence, Pt-ttpy and cisplatin do not share the same mechanisms for radiosensitization in a number of conditions:

1. The need of drug post-irradiation treatment for Pt-ttpy and not cisplatin
2. The delay in DBS break repair in our RS condition with Pt-ttpy but not cisplatin, even though it has been shown in literature that cisplatin induces a delay in DSB repair in other RS conditions [328]
3. The decrease of cells in G2-M phase in our condition with Pt-ttpy and not cisplatin, even though a decrease of cells in G2-M phase at 6 hours has been shown in literature [328].

One other important feature of cisplatin to discuss is its ability to induce ROS by itself and in combination with irradiation in A2780 cells. This leads us to hypothesize that the ROS production could be a mechanism of action for cisplatin induced RS. This is completely reverse in the case of Pt-ttpy, which does not produce ROS by itself at IC_{80} concentration and even at a 10µM concentration. Moreover, in combination with irradiation, it also does not show any ROS production and interestingly, hints at a reduction of ROS levels in irradiated cells. This shows, once again, the divergence of the mechanism of action for both cisplatin and Pt-ttpy induced RS.

An important thing to take into account is that ROS production by cisplatin has been shown to be dependent on mitochondria content (amount) with a range of high grade serious ovarian cancer and their respective capacity to produce ROS. A2780 cell line, with low mitochondrial content, is one of the less sensitive cell lines to cisplatin and the one that produces less ROS [364]. Therefore, in this A2780 cell line, combining cisplatin treatment with a ROS producer as IR would explain this synergistic effect between both treatments. In the case of Pt-ttpy however, even though it accumulates in mitochondria at a higher rate than cisplatin and is able to cause mitochondrial dysfunction, there is no production of ROS. Pt-ttpy does not show an increase in ROS production even when combined to irradiation, indicating that ROS production is not involved in Pt-ttpy induced RS. It however, does not exclude the effect of Pt-ttpy in mitochondrial dysfunction driven by mt-DNA lesions, mt-DNA deletions, mitochondrial mass, the mitochondrial membrane potential change, the mitochondrial oxidative phosphorylation activity and ATP production. Indeed, next to their central role in ROS production, mitochondria also plays a role in apoptosis signalling pathway and are the source of ATP and importantly, treatments can modify some of these functions [82, 376]. Hence, the effect of mitochondria in Pt-ttpy induced RS needs to be further investigated

Altogether the results show that Pt-ttpy has got its own mechanisms of action in the absence of irradiation such as, telomere targeting and partial TRF2 uncapping, mitochondrial targeting and non-production of ROS. In combination with irradiation we note that Pt-ttpy induces a delay in DSB repair of the induced IR-DNA damage and a decrease in the amount of cells in G2-M cell cycle, for up to 6 hours post irradiation. In addition, there is a mild telomere dysfunction, an increased platination to genomic DNA that could also contribute to the RS of Pt-ttpy but no extra production of ROS. The mechanism of action for Pt-ttpy (drug alone and in combination with irradiation) differs clearly from cisplatin, which is a good indication in order to circumvent the resistance or acquired resistance to cisplatin. Interestingly, Pt-ttpy also shows sensitization potential in combination with DNA repair inhibitors and DDR signalling inhibitors, particularly with the PARP inhibitor Olaparib which is already used in clinic. This synergistic effect shows that, in addition to Pt-ttpy-DNA adducts that may interfere with the repair of DSBs, its own repair may involve the PARP1 pathway. Results of combination treatment of Pt-ttpy with irradiation and

inhibitors of DNA repair pathways clearly indicate that the major pathway leading to the cytotoxicity of Pt-ttpy is governed by its interaction with DNA.

The family of Pt-NHC was shown to induce efficient RS. The SAR in this family showed that for the dinuclear complexes, the shorter linker chain helps induce better RS. However, the structure of this new series cannot be shown because a patent is currently being filed. This series is important because their structure is different from that of cisplatin, being trans geometry instead of the cis geometry of cisplatin, which allows the complexes to create different DNA adducts. They have been shown to mainly create monoadducts that can over time turn into intrastand crosslinks between remote bases as well as interstrand crosslinks [151]. This new type of DNA adducts allows the complexes to bypass the resistance of cisplatin as has been shown for some of the complexes [150, 151] and more interestingly, can interfere with the repair differently (and perhaps more efficiently) than the cisplatin adducts. Moreover, some of these complexes were shown to induce apoptosis though AIF translocation from mitochondria to nucleus and cytosol in caspase 3 and 7 independent pathways suggesting the involvement of a mitochondrial pathway, which would need to be further clarified.

In combination with irradiation we recently have shown that Pt-NHC complexes interfere with the repair mechanism of IR-induced DSB since a delay in kinetics in DNA DSB repair has been observed (data not shown, work of Dr. Tao Jia). Moreover, it seems that they increase the number of DSBs formed immediately post irradiation, unlike Pt-ttpy and cisplatin. Length of preincubation time (from 1day - 5 days) does not change the RS effect, while a weak RS has been observed when cells are pre-treated 15 min before irradiation. The need of continuous treatment is also not mandatory to their RS effect. Since the complexes are able to induce bulky DNA adducts compared to cisplatin, these adducts should either be more efficient to impede the repair of DSBs located next to them or could help to the formation of DSBs by increasing the accessibility of ROS due to DNA distortion (as has been proposed for cisplatin [377]). Hence, before making final conclusions, we need to quantify the amount of platinum bound to DNA in each treatment to see if a correlation exits between the amount of Pt-DNA adducts and RS, as in the case of Pt-ttpy and identify the role of mitochondria. All these questions need to be answered in order to decipher in more detail the RS mechanism of action of these new complexes.

In conclusion, in this thesis we have-

- Screened different series of metal complexes belonging to G4 ligands and some not, for their RS activity. No SAR could be given from this screening.
- Promoted a new class of platinum complexes that are now under patent for their novelty of structure and their radiosensitizing effect.
- Developed some insights in the mechanism of RS by Pt-ttpy complex, a G4 ligand highlighted from the screening. As shown from its own activity in absence of radiation, Pt-ttpy differs from cisplatin which could be associated in part to its G4 property. Its high mitochondrial targeting needs to be further studied. In regards to its RS activity Pt-ttpy also behaves differently from cisplatin, Pt-ctpy and RHPS4, showing its own properties that combine G4 ligand and platination properties.

This study of Pt-ttpy should help us understand the importance of G4 binding metal complex ligands in the context of cancer therapeutics and hopefully, lead to the discovery of platinum complex exhibiting various mechanisms of action different from cisplatin. In addition, the discovery of the Pt-NHC complexes with RS properties, clearly show that the field of Pt-complexes still has a lot to offer in the realm of cancer pharmacology and one of these complexes can go further in translational studies and have an impact in a clinical setting.

MATERIALS & METHODS

Materials and Methods

Cell lines

The cells used in this work are A2780 ovarian cancer cells, which exist in two cell lines: the sensitive A2780-S line (ECACC catalogue No. 93112519) and the cis-platinum resistant line A2780-R (ECACC-catalog No. 93112517); H1299 Non Small Cell Lung Carcinoma (ATCC® CRL-5803™) and T98G Glioblastoma Multiforme (ATCC® CRL-1690™). We also used the CCD19Lu cell (ATCC® CCL-210™) line which are human normal lung fibroblast cells that are capable of 8-9 population doublings.

Chemical compounds

The chemical compounds used in this work from the terpyridine family are Pt-ttpy, Pt-ctpy, Pt-tpy, Pt-(A)tpy, Pt-BisQ, Pt-cpym, Pt-vypm, Cu-ttpy and Pd-ttpy. These molecules were synthesized in the laboratory of Dr. M-P Teulade Fichou (Institut Curie, Orsay). All the terpyridine complexes except Pt-ttpy and Cu-ttpy were prepared at a concentration of 1mM in water, and Pt-ttpy as well as Cu-ttpy was prepared at a concentration of 6mM in DMSO, then diluted in water at a concentration of 100µMand 10µM respectively. The treatment solutions were then further diluted in water from these solutions.

The chemical compounds from the salphen series are S-Cu, S-V, S-Zn, S-Ni and C-Ni. These molecules were synthesized from the lab of Dr. Ramon Vilar (Imperial College London).

The chemical compounds from the Pt-NHC series are MS113, MS140, C4, C6, C6cy, C8, C4-PDC and C8-PDC which were synthesized from the lab of Dr. J.F. Betzer and Dr. Angela Marinetti from Institut de Chimie des Substances Naturelles.

Cell culture

The A2780 cell lines were cultured in RPMI medium supplemented with 10% fetal calf serum, in the presence of penicillin and streptomycin. H1299 cell line was grown in RPMI medium supplemented with 10% fetal calf serum, 1% HEPES, 1% Sodium Pyruvate in the presence of penicillin and streptomycin. T98G cell line was grown in MEM medium supplemented with 10% fetal calf serum, in the presence of penicillin and streptomycin.

1. Drug toxicity assay

The cell lines A2780, T98G and H1299 were seeded in their medium at a concentration of $0.2*10^5$ cells/ml in 24-well (1ml) plates. The cells are cultured in an incubator at 37°C in a humid atmosphere enriched with CO2 (5%). The drug is added 2hours later at their desired concentration and the cells are incubated again for a period of 4 or 7 days. They are then washed with PBS, treated with 100µL of trypsin and reseeded in an adequate volume of culture medium and counted with a cell counter (Coulter Z2, Beckman).

For the chemosensitization experiments, the A2780 cells are co-treated with Pt-ttpy and the other drug (PARP inhibitor, ATM inhibitor, ATR inhibitor and DNA-PK inhibitor) concurrently and incubated for 7 days after which they are counted and compared to the control condition of the inhibitor only treated cells. The chemosensitization is determined by using the software CompuSyn which gives a CI value of >1 for antagonistic interaction, =1 for additive and <1 for synergistic interaction between two drugs.

2. Radiosensitization assay

Make dilution of cells at $0.2*10^5$ cells/ml in 6 well plates. Add the IC_{30} of the drugs in duplicate wells after 2 hours of cell seeding. Incubate the cells with the drug at 37°C for 4 days. Trypsinize and count the cells for each drug treatment and collect in a 15ml falcon. Next we can either do a proliferation assay or a clonogenic assay.

For the proliferation assay, make new dilution of $0.08*10^5$ cells/ml with the drug treated cells. The 5 ml from the new dilution is poured onto each well of a 6 well plate, labelled correctly. The same concentration of drugs is added 2 hours after cell seeding and incubated at 37°C. Irradiation is done the next day at the desired Gys for the cell line using GSR D1 irradiator (gamma-ray, 662 keV). The cells are left to grow for 6days in the incubator (in the presence of drug) – atleast 5 population doublings. Cell count of each well is taken and a graph is plotted with the percentage survival of each treatment of cells with its control (0 Gy).

For the clonogenic assay, volume containing 400 drug treated cells or higher (according to the experiment) are added to 3ml media present in each well of a 6 well plate. The same concentration of drugs is added 2 hours after cell seeding and incubated at 37°C. Irradiation is

done the next day at the desired Gys for the cell line using using GSR D1 irradiator (gamma-ray, 662 keV). The cells are left to grow for 7-10 days (till colonies are over 50 cells in number). The cells are washed with PBS and fixed by adding 1ml 100% ethanol and leaving for 15 minutes. The ethanol is aspirated and wait for the wells to dry. Coomassie blue (10X diluted with dilution buffer to 1X) is added to the cells, enough to cover the cell colonies. The cells are left for 1hr and the coomassie dye is aspirated from the wells. The cells are washed with rinsing solution to remove the excess coomassie from the wells. The number of colonies with more than 50 cells in the colony are counted.

The survival plot is made in a KaleidaGraph software where the linear quadratic fit model: $S(D)/S(0) = \exp(-\alpha D - \beta D^2)$ is used to make the curve. The D10 value (dose of Gy at which only 10% cells survive) is noted from the curve.

Immunofluorescence Assays

1. DNA damage repair Immunofluorescence

The principle of immunofluorescence consists of labelling with a primary antibody (anti γ-H2AX or anti-53BP1) then with a secondary fluorescent antibody (Alexa). Thanks to fluorescence, we can quantify the number, area and intensity of the foci (γH2AX or 53BP1) in samples of treated and untreated cells.

For 5day preincubation condition with the drugs, the cells are incubated at $0.2*10^5$ cells/ml in 6 well plates. Add the IC30 of the drugs in duplicate wells after 2 hours of cell seeding. Incubate the cells with the drug at 37°C for 4 days. Trypsinize and count the cells for each drug treatment and reseed the cells in a LAB-TEK at a concentration of 1*10^5 cells/ml. For 1day preincubation with the drugs, the A2780 cells are seeded directly at a concentration of 1*10^5 cells/ml on LAB-TEK slides and the IC30 concentration of the drugs are added after 2hours. The slides are incubated at 37°C for 1day. The slides are irradiated at a dose of 2Gys and then fixed with 4% paraformaldehyde in PBS for 15minutes at room temperature, at time intervals of 0.5h, 2h, 6h and 24h from the point of irradiation.

The cells are then washed with PBS and permeabilized for 15 minutes at 37°C by the permeabilization buffer (Tris-HCl 20mM pH8, NaCl 50mM, MgCl2 3mM, Sucrose 300mM, TritonX-100 0.5%). The cells are blocked for 2h at room temperature with a 5% BSA solution in PBS and incubated with the primary anti- γ-H2AX (mouse clone JBW30, Millipore) antibody at room temperature for 2h. After 3 washes with PBS, the cells are incubated with secondary antibody Alexa 488 (anti-mouse) at room temperature for 45 minutes in the dark. After 3 washes with PBS the coverslips are mounted on slides with a drop of vectashield mounting solution containing DAPI.

labelling with anti-53BP1 antibody (mouse ab10579) was also performed using the same procedure.

Cell images were acquired using an upright 3D deconvolution epifluorescence microscope at 63X magnification from the imaging platform of the Institut Curie, Orsay. The experiments were performed at least thrice and about 100 cells were analyzed each time.

2. Co-location of damage at the telomeric DNA

This method consists of double labelling with an antibody against the shelterin protein TRF1 which binds at the telomeres and the anti-γ-H2AX antibody which binds at the double-stranded DNA breaks.

The cells were seeded on LAB-TEK slides containing 8 compartments at a concentration of $1*10^5$cells/ml with 400µl/well for untreated cells and cells treated with IC_{30} dose of Pt-ttpy.

They are then permeabilized with the following buffer (20mM Tris-HCl pH8, 50mM NaCl, 3mM MgCl2, 300mM Sucrose, 0.5% TritonX-100) at 37°C for 15 min and then washed with PBS. They are then blocked by a 5% BSA solution in PBS for 1 hour. Then they are incubated with the anti-γ-H2AX antibody (phosphor S139, rabbit polyclonal) and anti-TRF1 antibody (TRF-78, mouse monoclonal). After washing, the cells are incubated with the secondary Alexa 488 (anti-rabbit) and Alexa 555 (anti-mouse) antibody and washed with PBS. Finally, the slides are mounted on slides with a drop of Vectashield mounting solution containing DAPI.

Cell images were acquired using an upright 3D deconvolution epifluorescence microscope at 63X magnification from the imaging platform of the Institut Curie, Orsay. The colocalization analysis was performed using the ImageJ plugin JACoP.

Quantification of platinum complexes incorporated into cells and fixed on genomic DNA

1. Preparation of pellets and DNA:

A2780 cells were seeded in 75 cm^2 flasks at a concentration of $0.2*10^5$cells/ml (40ml), respectively, and were treated with IC80 doses for each complex (Pt-ttpy, Pt-tpy and cisplatin) for the indicated treatment times. At the end of each treatment, cells were recovered and aliquoted by $5*10^6$ cells. For each treatment condition, one pellet of $5*10^6$ cells will be used for the intracellular platinum assay and another pellet will be used for DNA extraction using the DNesay ® kit (blood and tissue Kit, Qiagen) and will be used for the assay of platinum bound to DNA. The concentration of the extracted DNA is then evaluated using a Nano-drop. It is then dried in a water bath at 96°C and mineralized by adding 50µl of 0.1 M HNO_3. The pellets are mineralized by adding 50µl of 2.8M HNO_3 and heated to 80°C.

2. Extraction of DNA

DNA extraction is performed on the pellets of $5*10^6$ cells frozen in liquid nitrogen and stored at -80C° by the DNeasy Kit (Blood and tissue Kit, Qiagen). The pellet is resuspended in 200µl of fresh PBS to which 4µl of Rnase 100mg/ml (Qiagen) and 20µl of proteinase K are added. The cells are lysed with 200 µl of AL buffer and incubated at 70°C for 10 minutes. The DNA is precipitated by adding 200µl of fresh alcohol and deposited on a DNeasy column which fixes the DNA. The columns are washed by centrifugation with buffers AW1 and then AW2. The DNA is eluted with 260 µl of elution buffer AE for 5 minutes. The concentration of the DNA is determined using the Nano-drop.

The platinum assay was performed by ICP-MS (Inductively Coupled Plasma Mass Spectrometry) in collaboration with Dr. J. Poupon at the toxicology laboratory he runs at the Lariboisière Hospital.

3. Mitochondrial extraction

The mitochondrial extraction is performed on the pellets of $5*10^6$ cells frozen in liquid nitrogen and stored at -80C°. Four pellet were used for the mitochondrial extraction of one sample. The kit used was 'Mitochondria Isolation Kit for Cultured cells' (Thermo Scientific). The 4 pellets are are suspended in Reagent A from the kit and kept on ice for 2 minutes followed by addition of 10µL Reagent B and incubation in ice or homogenization using a dounce. 800µl of Reagent C is then added to the cells are centrifuged at 700xg for 10 minutes at 4°C. The supernatant is collected and centrifuged again at 12000xg for 15 minutes at 4°C. The supernatant is removed, the pellet washed with 500µl of Reagent C. Finally, the solution is centrifuged again at 12000xg for 5 minutes at 4°C.

JC-1 assay

The A2780 cells are cultured with the initial concentration of $0.2*10^5$ cells/ml in a 6 well plate with the IC_{50} and IC_{80} concentration of the drug. After 96 hours of treatment, we use the JC-1 Mitochondrial Membrane Potential Detection Kit (Biotium) to label the cells. We remove cells from the substrate to generate a single cell suspension before staining. The transfer 0.5 mL cell suspension to a centrifuge tube. Pellet cells by centrifugation for 5 minutes at room temperature at 400 xg. Remove the supernatant and resuspend cells in 0.5 mL 1X JC-1 Reagent working solution. Incubate the cells in a 37°C cell culture incubator for 15 minutes. Centrifuge for 5 minutes at 400 xg and remove supernatant, then wash the cells by resuspending the cell pellet in 2 mL PBS or cell culture medium followed by centrifugation. Remove the supernatant and repeat once more. Resuspend the cell pellet in 0.5 mL PBS or cell culture medium. Cells are now ready for flow cytometry analysis.

Mitochondria containing red JC-1 aggregates in healthy cells are detectable in the PE or PI channel (FL2), and green JC-1 monomers in apoptotic cells are detectable in FITC channel (FL1)

ROS Detection assay

The A2780 cells are cultured with the initial concentration of $0.2*10^5$ cells/ml in a 6 well plate with the desired concentration of the drug. After the treatment duration, add the CellROX Deep Red (Molecular Probes) at the final concentration of 500-1000nM to the cells and incubate at 37°C cell culture incubator for 30-60 minutes protected from light. Wash the cells with PBS once and analyze using the flow cytometry. Use the 635nm excitation for the CellROX Deep Red reagent.

Apoptosis Detection Assay

The A2780 cells are cultured with the initial concentration of $0.2*10^5$ cells/ml in a 6 well plate with the desired concentration of the drug. The labelling of the Apoptosis marker is done by the FITC Annexin V Apoptosis Detection Kit I (BD Pharmingen). The cells are washed with PBS and suspended in 1X binding buffer at a concentration of $1*10^6$cells/ml. 100µl is transferred to a 5ml culture tube and add 5µl of FITC Annexin V and 5µl PI. We gently vortex the cells and incubate at RT for 15 minutes in the dark. Add 400µl of 1X binding buffer to each tube and analyze by flow cytometry.

Cell cycle analysis

The A2780 cells are cultured with the initial concentration of $1*10^5$ cells/ml in a 6 well plate with the desired concentration of the drug with or without irradiation. The staining is done with the APC BrdU Flow Kit –Part A (BD Pharmingen). First, fix and permeabilize the cells with BD Cytofix/Cytoperm Buffer. Then we resuspend the cells in 100 µL of BD Cytofix/Cytoperm Buffer per tube. Incubate the cells for 15 to 30 minutes at room temperature or on ice. After, we wash the cells with 1 mL of 1X BD Perm/Wash Buffer and centrifuge for 5 minutes at 200 to 300g and discard the supernatant. Next we resuspend the cells in 100 µL of BD Cytoperm Permeabilization Buffer Plus per tube. Incubate the cells for 10 minutes on ice and wash the cells in 1 mL of 1X BD Perm/Wash Buffer. Resuspend the cells in 100 µL of BD Cytofix/ Cytoperm Buffer per tube and

incubate the cells for 5 minutes at room temperature or on ice. Wash the in 1 mL of 1X BD Perm/Wash Buffer. Then we treat the cells to DNase by resuspending the cells in 100 µL of diluted DNase (diluted to 300 µg/mL in DPBS) per tube, (ie,30 µg of DNase/106 cells) and incubate cells for 1 hour at 37°C. Wash the cells in 1 mL of 1X BD Perm/Wash Buffer. Next, Resuspend the cells in 50 µL of BD Perm/Wash Buffer containing diluted fluorescent anti-BrdU and/or antibodies specific for intracellular antigens and incubate the cells for 20 minutes at room temperature. Wash the cells again. Finally, resuspend the cells in 1 mL of staining buffer and acquire the stained cells on a flow cytometer. For optimal resolution, acquire using a low flow rate.

RÉSUMÉ THÈSE

Résumé de l'introduction

Quatre guanines forment un quartet de G, ces quartets sont ensuite empilés pour former un G-quadruplex (G4). Le quartet G est une structure plane qui est stabilisée dans une certaine mesure par le réseau de liaisons hydrogènes. La stabilité thermodynamique du quartet nécessite un cation monovalent tel que Na+ ou K+. Dans le motif de séquence $G_{\geq}3N_x\ G_{\geq}3N_x\ G_{\geq}3N_x\ G_{\geq}3$ [3, 4], les nucléotides Nx constituent les boucles de la structure G4. Un G4 parallèle est un G4 où la direction de tous les brins est dans la même direction, tandis qu'un G4 antiparallèle a au moins un des quatre brins antiparallèles aux autres.

L'importance des G4 dans la physiologie cellulaire réside dans

Protection des télomères - Les télomères sont des structures nucléoprotéiques qui protègent l'extrémité des chromosomes linéaires. L'ADN télomérique est constitué de répétitions en tandem de séquences riches en G avec des répétitions (TTAGGG)n que l'on trouve chez l'homme et qui peuvent former des G4 [40].. Afin de protéger l'extrémité des chromosomes reconnus comme une cassure d'ADN double brin (DSB) et d'empêcher les fusions chromosomiques, les télomères protègent leurs extrémités à l'aide d'un complexe de protéines appelé complexe Shelterin [41]. Il s'agit d'un conglomérat de 6 protéines TRF1, TRF2, RAP1, POT1, TIN2 et TPP1. Les molécules se liant aux G4 (ligands de G4) peuvent induire un dysfonctionnement télomérique soit en inhibant la fonction de la télomérase, soit en déprotégeant la structure télomérique.

Régulation des gènes - Plus de 40% des gènes humains contiennent des pG4 (G4 potentiels) à proximité de leurs régions promotrices, en particulier des oncogènes, ce qui suggère leur rôle dans la régulation de l'expression de ces gènes [3]. On constate que les structures G4s se forment dans la chromatine active lors de la transcription dans les cellules humaines. Outre leur rôle dans la régulation de la transcription, les G4 jouent également un rôle dans la régulation de la traduction. Les G4 sont connus pour se former dans les ARNm et sont présents dans les régions 3' ou 5' UTR qui peuvent ainsi réguler leur capacité à exprimer des protéines [67].

Instabilité génétique - Les G4 se forment lorsque des brins d'ADN sont exposés pendant la réplication ou la transcription, ce qui peut provoquer un blocage de la réplication et nécessiter la présence d'une hélicase G4. L'implication de l'ADN G4 dans l'instabilité génomique et les

dommages spécifiques à l'ADN a conduit à suggérer qu'une combinaison de ligands G4 avec des inhibiteurs de la réparation de l'ADN ou des voies associées pourrait être utilisée pour le traitement futur des tumeurs [33] [36].

Mitochondries - On a constaté que l'ADN mitochondrial possède des sites potentiels de formation de G4. Le génome mitochondrial des mammifères présente une asymétrie significative dans la composition des brins, avec un double enrichissement en guanines sur un brin. Cet enrichissement en guanines contribue à une densité PQS plus élevée de l'ADN mitochondrial par rapport au génome nucléaire. Dans une étude in silico récente, le PQS par kb dans l'ADN mitochondrial humain est estimé être 2,4 à 3,6 fois plus élevé que dans l'ADN nucléaire [18]. Pendant la réplication et la transcription, le brin d'ADN riche en séquences PQS est temporairement monocaténaire, ce qui suggère une possibilité accrue de former des structures G4.

Les médicaments qui se lient aux G4 sont des composés capables de cibler les G4 avec une spécificité et une sélectivité plus élevée que l'ADN duplex. Il existe plusieurs classifications parmi les G4, mais nous allons nous concentrer sur les complexes métalliques des G4. Dans les ligands comportant un complexe métallique, l'atome de métal est le locus central qui aide à organiser les ligands selon une géométrie spécifique telle qu'octaédrique, pyramidale à base carrée, plane carrée, etc. et une orientation pour une liaison G4 efficace. Il existe différentes séries de métaux en fonction de la structure de leurs ligands -

1. **Métal - série Salphen** - ce sont des structures planes et leur espacement approprié fait de ces complexes métalliques des stabilisateurs G4 très efficaces. Ex : S-Cu, S-V, S-Zn. [133]

2. **Métal - série Terpyridine** - Ce sont des stabilisateurs G4 qui peuvent avoir différents atomes de métal tels que Cu, Pt, Pd, Zn et Ru [137-140]. La présence d'un atome de Pt possédant au moins un ligand labile, entraîne une coordination directe du composé avec l'ADN G4, ce qui fournit un ancrage supplémentaire. Ex : Pt-ttpy, Cu-ttpy.

3. **Complexes Pt-G4 hybrides** - Ce sont des complexes où un métal, comme le platine, est attaché à un ligand G4 déjà établi. Cela pourrait contribuer à l'efficacité biologique du complexe. Ex : Pt-MPQ, Pt-NHC-PDC [128] [148].

La radiothérapie (RT) est l'utilisation de l'irradiation pour tuer les cellules cancéreuses. Elle est souvent accompagnée d'une autre forme de traitement, soit la chimiothérapie, soit la chirurgie. Les rayonnements utilisés en médecine pour le traitement du cancer appartiennent à la catégorie des rayonnements ionisants [165]. Les rayonnements ionisants sont un type d'énergie libérée par les atomes qui se déplacent sous forme d'ondes électromagnétiques (rayons gamma ou X) ou de particules (neutrons, bêta ou alpha). Nous nous concentrerons sur les rayonnements à faible TLE tels que les rayonnements gamma. Elle peut endommager l'ADN de deux façons, la première étant l'action directe où la particule chargée (électron ou ion) est capable d'ioniser la molécule d'ADN sur son chemin. La deuxième façon d'endommager l'ADN est l'action indirecte, où la particule chargée est capable d'ioniser les molécules d'eau autour de l'ADN, ce qui entraîne la formation de radicaux libres tels que OH●, qui réagissent ensuite avec l'ADN [174]. Une dose de 1Gy de rayons X est capable d'induire environ 3000 bases endommagées, 1000 SSB et 40DSB dans une cellule [171].

Les rayonnements ionisants ne sont pas sans limites. Il existe deux grandes directions dans lesquelles l'index thérapeutique des radiations peut être élargi : 1) augmenter la radiosensibilité des cellules tumorales et/ou 2) augmenter la radioprotection des tissus normaux qui l'entourent [169]. La radiosensibilisation peut être définie comme la capacité d'un médicament à diminuer la quantité de rayonnement nécessaire à l'inhibition irréversible de la prolifération. La capacité de radiosensibilisation d'un composé est généralement étudiée in vitro par des essais clonogéniques ou des essais de prolifération cellulaire. Les médicaments peuvent être radiosensibilisants en ciblant la réparation de l'ADN, le cycle cellulaire, les voies de signalisation cellulaire, l'augmentation des ROS dans les cellules hypoxiques et le microenvironnement tumoral [294][297-299]. Les médicaments de ces catégories font déjà l'objet d'essais cliniques.

Certains complexes métalliques ont montré une radiosensibilisation dans les cellules cancéreuses

1. **Cisplatine** - Il peut créer des adduits à l'ADN en formant des liaisons de coordination avec le site N7 des bases puriques, ce qui conduit à la formation de pontages sur l'ADN intrabrin ou interbrin. Il peut provoquer une radiosensibilisation en inhibant la voie de réparation NHEJ et en

bloquant le cycle cellulaire [271]. Mais son effet radiosensibilisant semble dépendant des lignées cellulaires et des conditions de traitement.

2. **Pt-ctpy** - Il s'agit d'un complexe de terpyridine et il est démontré qu'il s'agit d'un ligand de liaison G4. Il induit une radiosensibilisation dans les glioblastomes et une réduction de la croissance tumorale chez les souris [143]. Le mécanisme d'action possible de la radiosensibilisation par Pt-ctpy a été montré être lié à un dysfonctionnement télomérique après irradiation.

Il est également démontré que certains autres complexes non métalliques se liant au G4 induisent une radiosensibilisation, tels que le RHPS4 (par un dysfonctionnement télomérique pré-irradiation et un retard dans la cinétique de réparation de l'ADN) et le TAC (par un retard dans la cinétique de réparation de l'ADN et un blocage du cycle cellulaire).

Résumé des objectifs

Le premier objectif était d'identifier si d'autres ligands complexes métalliques pouvaient provoquer une radiosensibilisation (RS) dans plusieurs lignées de cellules cancéreuses et d'étudier leur relation structure-activité. Nous voulions déterminer si la structure du ligand (série terpyridine G4, série salphen G4 et série Pt-NHC (*trans*-(*bis*-NHC)[PtX_2(amine)]$_2$, N-hétérocycle carbène)) joue un rôle dans la radiosensibilisation ; ensuite, si l'atome de métal (Pt, Ni, Cu, V, Zn) est capable de fournir un avantage pour la radiosensibilisation et enfin, si le ciblage du G4 était essentiel pour la radiosensibilisation. Nous avons donc effectué un criblage de plusieurs complexes métalliques de différentes familles (ciblage G4 ou non) et différant par la nature de leur métal.

Le second objectif était de déchiffrer le mécanisme d'action du complexe sélectionné à partir du criblage effectué, Pt-ttpy. Nous voulions d'abord voir les effets de la drogue seule et identifier ses sites de dommages à l'ADN, puis son mécanisme d'action pour la RS. Il y a de multiples raisons pour lesquelles les médicaments peuvent induire une radiosensibilisation [271], c'est pourquoi nous avons exploré si l'effet radiosensibilisant de Pt-ttpy était dû à l'efficacité accrue de sa liaison à l'ADN après irradiation, à un retard dans la réparation des dommages à l'ADN, à une

modification de la progression du cycle cellulaire, à la production de ROS et/ou à un dysfonctionnement des télomères avant ou après irradiation.

Résumé des résultats

1. Dépistage de la radiosensibilisation

Série terpyridine -

La cytotoxicité des complexes de terpyridine (ligands ou non des G4) (Pt-ttpy, Pt-tpy, Pt(PA)-tpy, Pt-vpym, Pt-cpym, Pt-BisQ, Cu-ttpy et Pd-ttpy) présente une IC50 dans la gamme µM, sauf pour Pt-(A)tpy qui se situe dans la gamme nM pour les lignées cellulaires de cancer d'ovaire A2780. A l'exception de Pt(PA)-tpy et Pt-tpy, ces complexes métalliques sont tous ligands de G4 in vitro. Plus important encore, ils sont capables de surmonter la résistance du cisplatine dans la lignée cellulaire A2780cis.

Comme le complexe terpyridine Pt-ctpy avait montré dans la littérature un potentiel de radiosensibilisation dans les lignées cellulaires de glioblastome et de cancer de poumons non à petites cellules (GBM et NSCLC), nous avons voulu voir si d'autres complexes métalliques de la série terpyridine présentaient également des propriétés de radiosensibilisation à leur concentration subtoxique (IC30). Nous avons observé que seuls Pt-ttpy et Pt-(A)tpy étaient capables d'induire une radiosensibilisation dans la lignée cellulaire A2780 et que seul Pt-ttpy étant capable d'induire une radiosensibilisation dans deux autres lignées cellulaires, H1299 (NSCLC) et T98G (Glioblastome). Cela montre que les complexes métalliques de Pt dans la série des terpyridines n'ont pas tous une prédisposition intrinsèque à induire une radiosensibilisation et que la coordination du Pt à l'ADN n'est pas nécessairement nécessaire, vu que Pt-(A)tpy, ne possédant pas de ligands labiles, n'est pas capable de se lier par coordination à l'ADN.

Série Pt-NHC -

Les complexes Pt-NHC (2 mononucléaires - MS140, MS113 et 4 dinucléaires - C4, C6, C6cy, C8) font maintenant l'objet d'un brevet déposé suite au travail de thèse, car ce sont de nouveaux complexes de Pt non publiés encore, efficaces pour inhiber la prolifération des cellules cancéreuses (ovaire, poumons, glioblastome), de l'ordre du µM , qui peuvent également surmonter la résistance au cisplatine dans les cellules A2780cis, se lier à l'ADN par coordination et avoir des propriétés radiosensibilisantes dans différentes lignées de cellules cancéreuses .

Dans les complexes Pt-NHC, nous avons constaté que les complexes mononucléaires et dinucléaires présentent tous des propriétés de radiosensibilisation à leurs concentrations subtoxiques. Cependant, lorsque le complexe Pt-NHC est conjugué au ligand de G4 PDC (Pyridodicarboxamide), ce qui lui confère une activité plus ciblée, les complexes perdent leur propriété de radiosensibilisation. Cela implique que non seulement la capacité de liaison aux G4 n'est pas essentielle pour induire une radiosensibilisation, mais que dans certaines conditions, elle peut agir de manière inhibitrice. Pour les complexes dinucléaires dans la lignée cellulaire A2780, nous observons une tendance à l'augmentation du potentiel de radiosensibilisation pour les complexes possédant des chaînes de liaison plus courtes entre les deux atomes de platine, la radiosensibilisation étant la plus élevée pour C4 > C6 > C8, alors que la longueur des chaînes de liaison est l'inverse.

Série Salphen -

Les séries métal-salphène sont des complexes ligands de G4 qui peuvent être cytotoxiques pour les cellules cancéreuses. Leur IC50 a été déterminée pour 5 complexes métal-salphène différents dans 3 lignées cellulaires différentes (A2780, T98G et H1299) et s'est révélée être de l'ordre du µM.

Dans la série des salphènes reconnaissant les G4, nous avons testé des complexes avec différents métaux et constaté une radiosensibilisation avec quelques-uns d'entre eux (S-Cu, S-Ni, C-Ni et S-V) à leurs concentrations subtoxiques. Cela a confirmé une fois de plus que la présence du centre métallique Pt n'est pas obligatoire et que d'autres complexes métalliques peuvent également induire une radiosensibilisation [271]. De plus, nous avons également vu que la

radiosensibilisation peut dépendre de la lignée cellulaire et ne garantit pas la radiosensibilisation de toutes les lignées cellulaires si l'effet a été observé sur l'une d'entre elles.

2. Comprendre la radiosensibilisation

Le Pt-ttpy a été choisi comme complexe de choix pour comprendre son mécanisme de radiosensibilisation dans les cellules de cancer d'ovaire A2780. Nous observons que l'augmentation de la concentration de Pt-ttpy de l'IC30 à l'IC70 (concentrations de l'ordre du µM) qui inhibe la prolifération cellulaire de 30% et 70% respectivement en absence d'irradiation, augmente également le potentiel de radiosensibilisation, mais de façon non significative. Cependant, dans le cas du cisplatine, avec l'augmentation de la concentration de l'IC20 à l'IC50, nous avons constaté une augmentation significative de la radiosensibilisation proportionnelle à la concentration en cisplatine (concentrations de l'ordre du µM).

Nous constatons que le Pt-ttpy nécessite au moins une journée de prétraitement pour induire une radiosensibilisation, cependant, un temps de pré-incubation prolongé augmente légèrement son effet radiosensibilisant. Le fait que 10 minutes de pré-incubation et l'ajout du complexe après l'irradiation ne montrent aucune radiosensibilisation indique qu'il y a nécessité 1) d'une accumulation de complexe intracellulaire et 2) probablement de complexe lié à l'ADN au moment de l'irradiation pour induire la radiosensibilisation : ceci laisse supposer qu'une quantité croissante de complexe lié à l'ADN augmenterait son potentiel de radiosensibilisation. Dans le cas du cisplatine, la tendance de la radiosensibilisation dépendant du temps d'incubation est inversée. Nous notons également que pour la radiosensibilisation induite par le Pt-ttpy, il est absolument nécessaire que le complexe soit présent après l'irradiation pendant toute la durée de l'expérience. L'élimination du complexe après l'irradiation n'induit pas de radiosensibilisation.

La quantification de l'accumulation de Pt-ttpy dans les cellules et leur quantité liée à l'ADN lors des différents tests de radiosensibilisation montrent qu'effectivement l'irradiation augmente d'un facteur 2 la quantité de complexe lié à l'ADN sans modifier son accumulation intracellulaire.

3. Radiosensibilisation et dommages à l'ADN

On observe que le Pt-ttpy retarde la réparation des cassures d'ADN double brin (DSB) jusqu'à 6 heures après l'irradiation (indiqué par le nombre de foyers H2AX, un marqueur moléculaire des DSB). Ce délai de réparation est important car il peut participer au mécanisme de radiosensibilisation. En effet, le complexe non radiosensibilisant Cu-ttpy ne présente pas un tel effet. De plus, Pt-ttpy dans les conditions de traitement où il n'induit pas de radiosensibilisation ne présente pas non plus un tel effet. Cette observation permet de relier ce délai de la cinétique de réparation des dommages au phénomène de radiosensibilisation induit par Pt-ttpy. Il est intéressant de noter que le cisplatine, dans les conditions de traitement où il induit une radiosensibilisation, ne montre pas de retard dans la réparation des DSB, suggérant un mécanisme différent de radiosensibilisation pour les 2 complexes de platine.

La radiosensibilisation du Pt-ttpy est indépendante des dommages télomériques (TIFs) formés avant l'irradiation, car nous ne voyons pas de TIF créés par le complexe seul, en raison de leur faible concentration (IC30). Cependant, on observe une légère augmentation des TIFs 24 heures après l'irradiation en présence de Pt-ttpy comparé aux traitements seuls.

On observe également que le Pt-ttpy provoque un blocage des cellules en phase G1 du cycle cellulaire pendant les 6 premières heures post-irradiation et qu'il diminue le nombre de cellules en phase G2-M. Comme, après l'irradiation, les cellules sont bloquées en phase G2-M afin de permettre de réparer leur ADN, on peut supposer que la réduction du nombre des cellules dans cette phase suite au traitement par Pt-ttpy post-irradiation entraîne la persistance de dommages non réparés, ce qui est cohérent avec le retard dans la réparation des DSB et la formation de cluster de foyers de 53BP1 (grosse accumulation de 53PB1).

Le traitement des cellules par Pt-ttpy n'induit pas la formation de ROS (espèces réactives d'oxygène), même lorsqu'il est testé à des concentrations plus élevées, contrairement au cisplatine. Les cellules irradiées produisent des ROS, comme attendu, le co-traitement avec Pt-ttpy ne modifie pas le taux de ROS. Au contraire, la présence du cisplatine exacerbe la taux de ROS 24 h post-irradiation soulignant une fois de plus un mode d'action différent pour les deux complexes.

4. Pt-ttpy et mitochondries

On constate que Pt-ttpy s'accumule dans les mitochondries plus favorablement que le cisplatine ou Pt-tpy à leur concentration produisant une inhibition de prolifération de 80% (IC80) (iso-effet). Il a été observé que Pt-ttpy s'accumule ~12 fois plus que le cisplatine dans les mitochondries : cette accumulation est cependant proportionnelle à son accumulation intracellulaire.

Le test de dysfonctionnement mitochondrial avec la sonde JC-1 concorde avec l'accumulation de Pt-ttpy car seul le traitement par Pt-ttpy est capable de montrer une fraction significativement plus élevée de cellules présentant un dysfonctionnement mitochondrial par rapport aux deux autres complexes.

Pt-ttpy s'accumule dans les mitochondries à un niveau plus élevé que le cisplatine, induit un dysfonctionnement mitochondrial par une perte de son potentiel membranaire, entraînant ainsi une augmentation de l'apoptose précoce mais sans production de ROS. Ceci suggère que Pt-ttpy pourrait être un complexe efficace pour 1) contourner la résistance du cisplatine dans les cellules cancéreuses à faible contenu mitochondrial, comme les lignées cellulaires de cancer d'ovaire, parce qu'il s'y accumule à un taux plus élevé et 2) induire moins de toxicité secondaire en raison de l'absence de production de ROS.

5. Pt-ttpy et chimiosensibilisation des inhibiteurs DDR

Pt-ttpy sensibilise les cellules A2780 à la délétion et à l'inhibition de PARP, une enzyme fortement impliquée dans la réparation des cassures d'ADN. En effet, Pt-ttpy associé à l'Olaparib (inhibiteur de PARP) a montré un bon potentiel pour un traitement chimiothérapeutique combiné. De plus, le potentiel de radiosensibilisation de Pt-ttpy couplé à l'Olaparib en a été exacerbé. Pt-ttpy sensibilise également les cellules traitées par trois inhibiteurs de signalisation DDR (DNA damage response, ATR, ATM et PK). Cela indique que les dommages à l'ADN induits par Pt-ttpy sont signalés, à différents moments, par les trois voies de signalisation DDR.

Résumé des discussions

La thérapie combinée est souvent utilisée en clinique car certains médicaments peuvent induire des effets synergiques lorsqu'ils sont utilisés ensemble à leurs concentrations sous-toxiques, réduisant ainsi leurs effets toxiques secondaires. La radiothérapie, qui est l'une des modalités les plus utilisées en clinique (dans 50% des cas) [165], est également l'un des traitements fréquemment associés à la chimiothérapie afin d'abroger ses limites, à savoir la radiorésistance des cellules tumorales et les réactions dans les tissus normaux autour de la tumeur [169]. Il est donc nécessaire d'identifier de nouveaux radiosensibilisateurs et d'en comprendre les mécanismes d'action, ce qui permettraient d'améliorer les modalités de traitement combiné.

Il existe une autre classe de radiosensibilisateurs, qui est le centre d'intérêt de cette thèse, qui sont des agents de liaison à l'ADN et des agents intrinsèquement cytotoxiques. Contrairement aux recherches approfondies en tant qu'agents chimiothérapeutiques possibles, leur utilisation éventuelle comme radiosensibilisateurs a été largement ignorée, même si le cisplatine est déjà utilisé en clinique en combinaison avec des radiations ionisantes. Comme leurs mécanismes d'action ne sont pas élucidés, on attend un besoin crucial de les déchiffrer. On sait que ces agents endommageant l'ADN ont également des effets néfastes sur les cellules normales du fait qu'ils ciblent l'ADN, mais leur association avec l'irradiation à des doses subtoxiques peut conduire à l'émergence de nouveaux traitements. Ils comprennent deux types de médicaments dont certains ont déjà montré des propriétés radiosensibilisantes - (A) les complexes métalliques [271], y compris les complexes de platine qui peuvent se lier de manière irréversible à l'ADN, causant des dommages à l'ADN qui doivent être traités par des voies de réparation de l'ADN endommagé [309]. (B) les ligands de G4 qui peuvent se lier et stabiliser les G4 présents dans l'ADN génomique, l'ADN télomérique et l'ADN mitochondrial. Ils peuvent entraîner un dysfonctionnement télomérique, un stress génomique et un dysfonctionnement mitochondrial.

Les résultats de notre criblage n'ont montré aucune relation structure-activité (SAR) entre les complexes métalliques G4/non G4 et la radiosensibilisation (RS). Dans la série des terpyridines, seul Pt-ttpy a montré une RS dans les trois lignées cellulaires, indépendamment de leur statut p53. Cela a montré que la RS ne dépend pas de la structure de la terpyridine ou de l'atome Pt, car les autres complexes de terpyridine ne présentaient pas de RS.

Pt-ttpy a été choisi pour étudier l'effet de radiosensibilisation dans la lignée cellulaire A2780, car ce complexe particulier possède une double propriété qui peut être impliquée dans ses propriétés radiosensibilisantes : la capacité de reconnaissance et de liaison aux G4 et l'atome Pt capable d'induire la platination sur l'ADN télomérique et génomique [127].

La RS induite par Pt-ttpy ne dépend pas de la présence de dommages télomériques présents avant irradiation, contrairement au RHPS4 [344]. Cependant, l'apparition significative de dommages à l'ADN télomérique , même s'ils demeurent faibles , a été observé dans le traitement combinatoire de Pt-ttpy et de l'irradiation alors qu'il n'est pas observé pour les deux traitements isolés. Par conséquent, le ciblage des télomères par Pt-ttpy en présence des rayonnements ionisants peut être proposé comme un des mécanismes d'action participant à la RS, comme cela a été proposé pour deux autres ligands de G4, RHPS4 et le Pt-ctpy [143, 344].

En ce qui concerne l'hypothèse selon laquelle l'effet radiosensibilisant induit par Pt-ttpy dépend de ses propriétés de fixation sur l'ADN, les résultats montrent que la RS induite par ce complexe, peut être également corrélée avec sa quantité liée à l'ADN génomique. On a montré qu'une préincubation d'au moins un jour est nécessaire pour la RS et qu'une préincubation plus longue de cinq jours entraîne une augmentation du potentiel de la RS, la quantité de complexe fixée sur l'ADN augmentant avec le temps de pré-incubation. D'autre part, nous avons vu que l'irradiation augmente la quantité de Pt-ttpy lié à l'ADN dans les heures qui suivent l'irradiation. Cette hypothèse reste vraie lorsque l'on compare avec les résultats de RS en présence de cisplatine, même si la tendance est inversée. En effet, le cisplatine induit une RS avec une préincubation d'un jour mais pas avec la préincubation plus longue de 5 jours, et dans ce cas la quantité de cisplatine lié à l'ADN après un jour de traitement est supérieure à celle d'un traitement de 4 jours.

Nous observons que les deux conditions de préincubation avec Pt-ttpy (5 jours et de 1 jour) montrent un retard dans la réparation des DSB jusqu'à 6 heures après l'irradiation. Il est intéressant de noter que les traitements par Cu-ttpy et ou Pt-ttpy ajouté juste après l'irradiation (conditions non radiosensibilisantes) ne présentent aucun retard dans la réparation des cassures de l'ADN induites par l'irradiation, ce qui indique que ce retard pourrait être un des mécanismes impliqués dans la RS par Pt-ttpy. En revanche, le cisplatine ne présente aucun retard dans la

réparation des DSB, ce qui indique une différence dans le mécanisme d'action du RS par rapport à celui du Pt-ttpy. Il est remarquable de noter que ni Pt-ttpy, ni le cisplatine n'augmente le nombre de lésions de l'ADN, 30 minutes après l'irradiation, temps où le maximum de DSB sont formés après l'irradiation [355], contrairement à Pt-ctpy [143] et aux complexes NHC-Pt étudiés dans cette thèse. De plus, le retard de la réparation des DSB est cohérent avec l'augmentation de la surface des foyers 53BP1 puisqu'il apparait uniquement pour le traitement combiné Pt-ttpy /irradiation. 53BP1 est une protéine transductrice dans la DDR qui est recrutée dans les DSB et joue un rôle essentiel dans le choix de la voie de réparation des DSB [214]. Une accumulation de cette protéine est donc un signe d'accumulation de dommages non réparés.

Ces résultats sont cohérents avec l'arrêt du cycle cellulaire observé lors du co-traitement Pt-ttpy/irradiation. Comme prévu, les rayonnements ionisants augmentent le nombre de cellules bloquées en phase G2-M [356]. La présence de Pt-ttpy diminue le nombre de cellules bloquées dans la phase G2-M jusqu'à 6 heures après l'irradiation, réduisant ainsi le temps nécessaire aux cellules pour réparer des dommages causés à leur ADN. De plus, le blocage accru en G1 pourrait contribuer à promouvoir la réparation des DSB par 53BP1 en recrutant ATM [375], ce qui expliquerait l'apparition des clusters de foyers 53BP1. En revanche, le cisplatine qui induit par lui-même un bloc G2-M ne modifie pas l'arrêt du cycle cellulaire induit par l'IR.

Nous proposons un modèle de radiosensibilisation par Pt-ttpy sur la base de nos résultats. Lorsque les DSB induits par l'irradiation sont produites à proximité d'un adduit de Pt-ttpy sur l'ADN, ces DSB sont plus difficiles à réparer en raison de l'inférence physique du complexe de Pt qui conduit à un retard dans la réparation de ces lésions (délai dans la disparition des foyers γ-H2AX) et par conséquence l'accumulation de foyers de réparation de dommages, (accumulation de 53BP1 dans un même foyer). La nécessité d'un traitement continu du Pt-ttpy après l'irradiation soutient la nécessité de la formation continue d'un adduit Pt-ttpy-ADN pour continuer à produire cet effet.

Le Pt-ttpy et le cisplatine ne partagent pas les mêmes mécanismes de radiosensibilisation car ils divergent sur un grand nombre de points :

1. La nécessité d'un traitement post-irradiation pour le Pt-ttpy et non pour le cisplatine

2. Le retard dans la réparation des cassures de DSB avec Pt-ttpy, uniquement dans les conditions de traitement où il induit la RS, mais pas avec le cisplatine, même s'il a été démontré dans la littérature que le cisplatine peut induire un retard dans la réparation des DSB dans d'autres conditions de RS [328].

3. La diminution des cellules en phase G2-M avec Pt-ttpy uniquement en condition de RS et non avec le cisplatine, même si une diminution des cellules en phase G2-M à 6 heures a été démontrée dans la littérature pour ce dernier dans d'autres conditions [328].

4. Aucune augmentation des ROS en présence de Pt-ttpy après irradiation, contrairement au cisplatine.

Il a été démontré que la famille du Pt-NHC induit une RS efficace. La SAR de cette famille a montré que pour les complexes dinucléaires, une chaîne de liaison plus courte en tre les 2 centres métalliques, permet d'induire une meilleure RS. Cependant, la structure de cette nouvelle série ne peut être démontrée car un brevet a été déposé afin de protéger les structures et leurs propriétés radiosensibilisantes. Il a été démontré qu'ils créent principalement des monoadduits qui peuvent, avec le temps, se transformer en pontages intra-brins entre des bases éloignées dans la séquence d'ADN ainsi que des pontages inter-brins, puisqu'ils possèdent deux ligands labiles [151]. Ce nouveau type de d'adduits sur l'ADN permet aux complexes de contourner la résistance du cisplatine, comme cela a été démontré pour certains des complexes de cette même famille [150, 151]. En combinaison avec l'irradiation, nous avons également récemment montré au laboratoire que les complexes Pt-NHC interfèrent avec le mécanisme de réparation des DSB induits par l'IR puisqu'un retard dans la cinétique de leur réparation a été observé (données non montrées, travaux du Dr. Tao Jia). De plus, il semble qu'ils augmentent le nombre de DSB formés immédiatement après l'irradiation, contrairement au Pt-ttpy et au cisplatine. La durée de la préincubation (de 1 à 5 jours) ne modifie pas leur propriété de RS. La nécessité d'un traitement continu post-irradiation n'est pas non plus obligatoire. Comme les complexes sont capables d'induire des adduits d'ADN volumineux par rapport au cisplatine, ces adduits devraient être plus efficaces pour empêcher la réparation des DSB situées à leur proximité et/ou pourraient

contribuer à l’augmentation des DSB en augmentant l'accessibilité des ROS en raison de la distorsion de l’ADN [377].

Cette étude de Pt-ttpy devrait nous aider à comprendre l'importance des complexes métalliques ligands de G4 dans le contexte thérapeutique du cancer et, espérons-le, conduire à la découverte d'un complexe de platine présentant divers mécanismes d'action différents de ceux du cisplatine. En outre, la découverte des complexes Pt-NHC avec des propriétés de RS, montrent clairement que le domaine des complexes de Pt a encore beaucoup à offrir dans le domaine de la pharmacologie du cancer et que l'un de ces complexes peut aller plus loin dans les études translationnelles et avoir un impact dans un cadre clinique.

BIBLIOGRAPHY

Bibliography

1. Arnott, S., R. Chandrasekaran, and C.M. Marttila, *Structures for polyinosinic acid and polyguanylic acid.* Biochemical Journal, 1974. **141**(2): p. 537-543.
2. Zimmerman, S.B., G.H. Cohen, and D.R. Davies, *X-ray fiber diffraction and model-building study of polyguanylic acid and polyinosinic acid.* J Mol Biol, 1975. **92**(2): p. 181-92.
3. Huppert, J.L. and S. Balasubramanian, *Prevalence of quadruplexes in the human genome.* Nucleic Acids Res, 2005. **33**(9): p. 2908-16.
4. Todd, A.K., M. Johnston, and S. Neidle, *Highly prevalent putative quadruplex sequence motifs in human DNA.* Nucleic acids research, 2005. **33**(9): p. 2901-2907.
5. Lane, A.N., et al., *Stability and kinetics of G-quadruplex structures.* Nucleic Acids Res, 2008. **36**(17): p. 5482-515.
6. Collie, G.W. and G.N. Parkinson, *The application of DNA and RNA G-quadruplexes to therapeutic medicines.* Chem Soc Rev, 2011. **40**(12): p. 5867-92.
7. Burge, S., et al., *Quadruplex DNA: sequence, topology and structure.* Nucleic Acids Res, 2006. **34**(19): p. 5402-15.
8. Kwok, C.K. and C.J. Merrick, *G-Quadruplexes: Prediction, Characterization, and Biological Application.* Trends Biotechnol, 2017. **35**(10): p. 997-1013.
9. Parkinson, G.N., M.P. Lee, and S. Neidle, *Crystal structure of parallel quadruplexes from human telomeric DNA.* Nature, 2002. **417**(6891): p. 876-80.
10. Lin, C. and D. Yang, *Human Telomeric G-Quadruplex Structures and G-Quadruplex-Interactive Compounds.* Methods Mol Biol, 2017. **1587**: p. 171-196.
11. Murat, P. and S. Balasubramanian, *Existence and consequences of G-quadruplex structures in DNA.* Curr Opin Genet Dev, 2014. **25**: p. 22-9.
12. Spiegel, J., S. Adhikari, and S. Balasubramanian, *The Structure and Function of DNA G-Quadruplexes.* Trends in Chemistry, 2020. **2**(2): p. 123-136.
13. Paramasivan, S., I. Rujan, and P.H. Bolton, *Circular dichroism of quadruplex DNAs: applications to structure, cation effects and ligand binding.* Methods, 2007. **43**(4): p. 324-31.
14. Mergny, J.L., A.T. Phan, and L. Lacroix, *Following G-quartet formation by UV-spectroscopy.* FEBS Lett, 1998. **435**(1): p. 74-8.
15. Han, H., L.H. Hurley, and M. Salazar, *A DNA polymerase stop assay for G-quadruplex-interactive compounds.* Nucleic Acids Res, 1999. **27**(2): p. 537-42.
16. Williamson, J.R., M.K. Raghuraman, and T.R. Cech, *Monovalent cation-induced structure of telomeric DNA: the G-quartet model.* Cell, 1989. **59**(5): p. 871-80.
17. Kwok, C.K., et al., *rG4-seq reveals widespread formation of G-quadruplex structures in the human transcriptome.* Nat Methods, 2016. **13**(10): p. 841-4.
18. Bedrat, A., L. Lacroix, and J.L. Mergny, *Re-evaluation of G-quadruplex propensity with G4Hunter.* Nucleic Acids Res, 2016. **44**(4): p. 1746-59.

19. Kikin, O., L. D'Antonio, and P.S. Bagga, *QGRS Mapper: a web-based server for predicting G-quadruplexes in nucleotide sequences.* Nucleic Acids Research, 2006. **34**(Web Server): p. W676-W682.
20. Eddy, J. and N. Maizels, *Gene function correlates with potential for G4 DNA formation in the human genome.* Nucleic Acids Res, 2006. **34**(14): p. 3887-96.
21. Yadav, V.K., et al., *QuadBase: genome-wide database of G4 DNA--occurrence and conservation in human, chimpanzee, mouse and rat promoters and 146 microbes.* Nucleic Acids Res, 2008. **36**(Database issue): p. D381-5.
22. Schaffitzel, C., et al., *In vitro generated antibodies specific for telomeric guanine-quadruplex DNA react with Stylonychia lemnae macronuclei.* Proc Natl Acad Sci U S A, 2001. **98**(15): p. 8572-7.
23. Isalan, M., et al., *Selection of zinc fingers that bind single-stranded telomeric DNA in the G-quadruplex conformation.* Biochemistry, 2001. **40**(3): p. 830-6.
24. Scholz, O., S. Hansen, and A. Pluckthun, *G-quadruplexes are specifically recognized and distinguished by selected designed ankyrin repeat proteins.* Nucleic Acids Res, 2014. **42**(14): p. 9182-94.
25. Fernando, H., R. Rodriguez, and S. Balasubramanian, *Selective recognition of a DNA G-quadruplex by an engineered antibody.* Biochemistry, 2008. **47**(36): p. 9365-71.
26. Biffi, G., et al., *Quantitative visualization of DNA G-quadruplex structures in human cells.* Nat Chem, 2013. **5**(3): p. 182-6.
27. Henderson, A., et al., *Detection of G-quadruplex DNA in mammalian cells.* Nucleic Acids Res, 2014. **42**(2): p. 860-9.
28. Kazemier, H.G., K. Paeschke, and P.M. Lansdorp, *Guanine quadruplex monoclonal antibody 1H6 cross-reacts with restrained thymidine-rich single stranded DNA.* Nucleic acids research, 2017. **45**(10): p. 5913-5919.
29. Hansel-Hertsch, R., et al., *G-quadruplex structures mark human regulatory chromatin.* Nat Genet, 2016. **48**(10): p. 1267-72.
30. Chambers, V.S., et al., *High-throughput sequencing of DNA G-quadruplex structures in the human genome.* Nat Biotechnol, 2015. **33**(8): p. 877-81.
31. Biffi, G., et al., *Visualization and selective chemical targeting of RNA G-quadruplex structures in the cytoplasm of human cells.* Nature Chemistry, 2013. **6**(1): p. 75-80.
32. Law, M.J., et al., *ATR-X syndrome protein targets tandem repeats and influences allele-specific expression in a size-dependent manner.* Cell, 2010. **143**(3): p. 367-78.
33. Gray, L.T., et al., *G quadruplexes are genomewide targets of transcriptional helicases XPB and XPD.* Nature Chemical Biology, 2014. **10**(4): p. 313-318.
34. Kanoh, Y., et al., *Rif1 binds to G quadruplexes and suppresses replication over long distances.* Nature structural & molecular biology, 2015. **22**(11): p. 889.
35. Paeschke, K., J.A. Capra, and V.A. Zakian, *DNA replication through G-quadruplex motifs is promoted by the Saccharomyces cerevisiae Pif1 DNA helicase.* Cell, 2011. **145**(5): p. 678-691.
36. Rodriguez, R., et al., *Small-molecule-induced DNA damage identifies alternative DNA structures in human genes.* Nat Chem Biol, 2012. **8**(3): p. 301-10.
37. Lam, E.Y., et al., *G-quadruplex structures are stable and detectable in human genomic DNA.* Nat Commun, 2013. **4**: p. 1796.

38. Piazza, A., et al., *Short loop length and high thermal stability determine genomic instability induced by G-quadruplex-forming minisatellites.* EMBO J, 2015. **34**(12): p. 1718-34.
39. Kouzine, F., et al., *Permanganate/S1 nuclease footprinting reveals non-B DNA structures with regulatory potential across a mammalian genome.* Cell Systems, 2017. **4**(3): p. 344-356. e7.
40. Ourliac-Garnier, I., R. Charif, and S. Bombard, *Telomeres and telomerase: potential targets for platinum complexes.* Metal Complex-DNA Interactions. Wiley, 2009: p. 209-235.
41. Giraud-Panis, M.J., et al., *One identity or more for telomeres?* Front Oncol, 2013. **3**: p. 48.
42. Palm, W. and T. de Lange, *How shelterin protects mammalian telomeres.* Annu Rev Genet, 2008. **42**: p. 301-34.
43. Smogorzewska, A. and T. de Lange, *Regulation of telomerase by telomeric proteins.* Annual review of biochemistry, 2004. **73**(1): p. 177-208.
44. De Lange, T., *Shelterin: the protein complex that shapes and safeguards human telomeres.* Genes & development, 2005. **19**(18): p. 2100-2110.
45. Griffith, J.D., et al., *Mammalian telomeres end in a large duplex loop.* Cell, 1999. **97**(4): p. 503-514.
46. Karlseder, J., *p53- and ATM-Dependent Apoptosis Induced by Telomeres Lacking TRF2.* Science, 1999. **283**(5406): p. 1321-1325.
47. Van Steensel, B., A. Smogorzewska, and T. De Lange, *TRF2 protects human telomeres from end-to-end fusions.* Cell, 1998. **92**(3): p. 401-413.
48. Celli, G.B., E.L. Denchi, and T. de Lange, *Ku70 stimulates fusion of dysfunctional telomeres yet protects chromosome ends from homologous recombination.* Nature cell biology, 2006. **8**(8): p. 885-890.
49. Denchi, E.L. and T. de Lange, *Protection of telomeres through independent control of ATM and ATR by TRF2 and POT1.* Nature, 2007. **448**(7157): p. 1068-1071.
50. Sfeir, A., et al., *Mammalian telomeres resemble fragile sites and require TRF1 for efficient replication.* Cell, 2009. **138**(1): p. 90-103.
51. Colgin, L.M., et al., *Human POT1 facilitates telomere elongation by telomerase.* Current biology, 2003. **13**(11): p. 942-946.
52. Hockemeyer, D., et al., *Telomere protection by mammalian Pot1 requires interaction with Tpp1.* Nature structural & molecular biology, 2007. **14**(8): p. 754-761.
53. Wang, F., et al., *The POT1–TPP1 telomere complex is a telomerase processivity factor.* Nature, 2007. **445**(7127): p. 506-510.
54. Takahama, K., et al., *Regulation of telomere length by G-quadruplex telomere DNA- and TERRA-binding protein TLS/FUS.* Chem Biol, 2013. **20**(3): p. 341-50.
55. Takahama, K., et al., *Identification of Ewing's sarcoma protein as a G-quadruplex DNA- and RNA-binding protein.* Febs j, 2011. **278**(6): p. 988-98.
56. Biffi, G., D. Tannahill, and S. Balasubramanian, *An intramolecular G-quadruplex structure is required for binding of telomeric repeat-containing RNA to the telomeric protein TRF2.* J Am Chem Soc, 2012. **134**(29): p. 11974-6.

57. Zhang, M., et al., *Mammalian CST averts replication failure by preventing G-quadruplex accumulation.* Nucleic Acids Res, 2019. **47**(10): p. 5243-5259.
58. Vannier, J.B., et al., *RTEL1 dismantles T loops and counteracts telomeric G4-DNA to maintain telomere integrity.* Cell, 2012. **149**(4): p. 795-806.
59. Riou, J.F., et al., *Cell senescence and telomere shortening induced by a new series of specific G-quadruplex DNA ligands.* Proc Natl Acad Sci U S A, 2002. **99**(5): p. 2672-7.
60. Zahler, A.M., et al., *Inhibition of telomerase by G-quartet DNA structures.* Nature, 1991. **350**(6320): p. 718-20.
61. Moye, A.L., et al., *Telomeric G-quadruplexes are a substrate and site of localization for human telomerase.* Nat Commun, 2015. **6**: p. 7643.
62. Zhang, M.L., et al., *Yeast telomerase subunit Est1p has guanine quadruplex-promoting activity that is required for telomere elongation.* Nat Struct Mol Biol, 2010. **17**(2): p. 202-9.
63. Zhou, G., et al., *Telomere targeting with a novel G-quadruplex-interactive ligand BRACO-19 induces T-loop disassembly and telomerase displacement in human glioblastoma cells.* Oncotarget, 2016. **7**(12): p. 14925-39.
64. Berardinelli, F., et al., *Targeting telomerase and telomeres to enhance ionizing radiation effects in in vitro and in vivo cancer models.* Mutat Res, 2017. **773**: p. 204-219.
65. Rhodes, D. and H.J. Lipps, *G-quadruplexes and their regulatory roles in biology.* Nucleic Acids Research, 2015. **43**(18): p. 8627-8637.
66. David, A.P., et al., *G-quadruplexes as novel cis-elements controlling transcription during embryonic development.* Nucleic Acids Res, 2016. **44**(9): p. 4163-73.
67. Arora, A., et al., *Inhibition of translation in living eukaryotic cells by an RNA G-quadruplex motif.* RNA, 2008. **14**(7): p. 1290-6.
68. Varshney, D., et al., *The regulation and functions of DNA and RNA G-quadruplexes.* Nat Rev Mol Cell Biol, 2020.
69. London, T.B., et al., *FANCJ is a structure-specific DNA helicase associated with the maintenance of genomic G/C tracts.* J Biol Chem, 2008. **283**(52): p. 36132-9.
70. Leonetti, C., et al., *G-quadruplex ligand RHPS4 potentiates the antitumor activity of camptothecins in preclinical models of solid tumors.* Clin Cancer Res, 2008. **14**(22): p. 7284-91.
71. Aggarwal, M., et al., *Inhibition of helicase activity by a small molecule impairs Werner syndrome helicase (WRN) function in the cellular response to DNA damage or replication stress.* Proc Natl Acad Sci U S A, 2011. **108**(4): p. 1525-30.
72. Besnard, E., et al., *Unraveling cell type-specific and reprogrammable human replication origin signatures associated with G-quadruplex consensus motifs.* Nat Struct Mol Biol, 2012. **19**(8): p. 837-44.
73. Berbenetz, N.M., C. Nislow, and G.W. Brown, *Diversity of Eukaryotic DNA Replication Origins Revealed by Genome-Wide Analysis of Chromatin Structure.* PLoS Genetics, 2010. **6**(9): p. e1001092.
74. Valton, A.L. and M.N. Prioleau, *G-Quadruplexes in DNA Replication: A Problem or a Necessity?* Trends Genet, 2016. **32**(11): p. 697-706.
75. Falabella, M., et al., *Potential Roles for G-Quadruplexes in Mitochondria.* Curr Med Chem, 2019. **26**(16): p. 2918-2932.

76. Anderson, S., et al., *Sequence and organization of the human mitochondrial genome.* Nature, 1981. **290**(5806): p. 457-65.
77. Kang, E., et al., *Mitochondrial replacement in human oocytes carrying pathogenic mitochondrial DNA mutations.* Nature, 2016. **540**(7632): p. 270-275.
78. Alexeyev, M., et al., *The maintenance of mitochondrial DNA integrity--critical analysis and update.* Cold Spring Harb Perspect Biol, 2013. **5**(5): p. a012641.
79. Kaasik, A., et al., *Regulation of mitochondrial matrix volume.* Am J Physiol Cell Physiol, 2007. **292**(1): p. C157-63.
80. Dong, D.W., et al., *Association of G-quadruplex forming sequences with human mtDNA deletion breakpoints.* BMC Genomics, 2014. **15**: p. 677.
81. Bharti, S.K., et al., *DNA sequences proximal to human mitochondrial DNA deletion breakpoints prevalent in human disease form G-quadruplexes, a class of DNA structures inefficiently unwound by the mitochondrial replicative Twinkle helicase.* J Biol Chem, 2014. **289**(43): p. 29975-93.
82. Falabella, M., et al., *G-quadruplex dynamics contribute to regulation of mitochondrial gene expression.* Sci Rep, 2019. **9**(1): p. 5605.
83. Erxleben, A., *Mitochondria-Targeting Anticancer Metal Complexes.* Curr Med Chem, 2019. **26**(4): p. 694-728.
84. Sun, D., et al., *Inhibition of human telomerase by a G-quadruplex-interactive compound.* J Med Chem, 1997. **40**(14): p. 2113-6.
85. Lemarteleur, T., et al., *Stabilization of the c-myc gene promoter quadruplex by specific ligands' inhibitors of telomerase.* Biochemical and Biophysical Research Communications, 2004. **323**(3): p. 802-808.
86. Hansel-Hertsch, R., M. Di Antonio, and S. Balasubramanian, *DNA G-quadruplexes in the human genome: detection, functions and therapeutic potential.* Nat Rev Mol Cell Biol, 2017. **18**(5): p. 279-284.
87. Nakanishi, C. and H. Seimiya, *G-quadruplex in cancer biology and drug discovery.* Biochemical and Biophysical Research Communications, 2020.
88. Campbell, N.H., et al., *Structural basis of DNA quadruplex recognition by an acridine drug.* J Am Chem Soc, 2008. **130**(21): p. 6722-4.
89. Read, M., et al., *Structure-based design of selective and potent G quadruplex-mediated telomerase inhibitors.* Proc Natl Acad Sci U S A, 2001. **98**(9): p. 4844-9.
90. White, E.W., et al., *Structure-specific recognition of quadruplex DNA by organic cations: influence of shape, substituents and charge.* Biophys Chem, 2007. **126**(1-3): p. 140-53.
91. Cheng, M.-K., et al., *Antitumor Polycyclic Acridines. 20. Search for DNA Quadruplex Binding Selectivity in a Series of 8,13-Dimethylquino[4,3,2-kl]acridinium Salts: Telomere-Targeted Agents.* Journal of Medicinal Chemistry, 2008. **51**(4): p. 963-975.
92. Sharon M. Gowan, et al., *Potent Inhibition of Telomerase by Small-Molecule Pentacyclic Acridines Capable of Interacting with G-Quadruplexes.* Molecular Pharmacology, 2001. **60**(5): p. 8.
93. Rizzo, A., et al., *Identification of novel RHPS4-derivative ligands with improved toxicological profiles and telomere-targeting activities.* J Exp Clin Cancer Res, 2014. **33**: p. 81.

94. Berardinelli, F., et al., *The G-quadruplex-stabilising agent RHPS4 induces telomeric dysfunction and enhances radiosensitivity in glioblastoma cells.* DNA Repair (Amst), 2015. **25**: p. 104-15.
95. Berardinelli, F., et al., *The G-quadruplex-stabilizing ligand RHPS4 enhances sensitivity of U251MG glioblastoma cells to clinical carbon ion beams.* FEBS J, 2018. **285**(7): p. 1226-1236.
96. Berardinelli, F., et al., *G-quadruplex ligand RHPS4 radiosensitizes glioblastoma xenograft in vivo through a differential targeting of bulky differentiated- and stem-cancer cells.* J Exp Clin Cancer Res, 2019. **38**(1): p. 311.
97. Shin-ya, K., et al., *Telomestatin, a novel telomerase inhibitor from Streptomyces anulatus.* J Am Chem Soc, 2001. **123**(6): p. 1262-3.
98. Kim, M.Y., et al., *Telomestatin, a potent telomerase inhibitor that interacts quite specifically with the human telomeric intramolecular g-quadruplex.* J Am Chem Soc, 2002. **124**(10): p. 2098-9.
99. Kim, M.-Y., et al., *The Different Biological Effects of Telomestatin and TMPyP4 Can Be Attributed to Their Selectivity for Interaction with Intramolecular or Intermolecular G-Quadruplex Structures.* Cancer research, 2003. **63**: p. 3247-56.
100. Agrawal, S., R.P. Ojha, and S. Maiti, *Energetics of the human Tel-22 quadruplex-telomestatin interaction: a molecular dynamics study.* J Phys Chem B, 2008. **112**(22): p. 6828-36.
101. Rosu, F., et al., *Cation involvement in telomestatin binding to g-quadruplex DNA.* J Nucleic Acids, 2010. **2010**.
102. Tahara, H., et al., *G-Quadruplex stabilization by telomestatin induces TRF2 protein dissociation from telomeres and anaphase bridge formation accompanied by loss of the 3' telomeric overhang in cancer cells.* Oncogene, 2006. **25**(13): p. 1955-66.
103. Hasegawa, D., et al., *G-quadruplex ligand-induced DNA damage response coupled with telomere dysfunction and replication stress in glioma stem cells.* Biochem Biophys Res Commun, 2016. **471**(1): p. 75-81.
104. Tauchi, T., et al., *Telomerase inhibition with a novel G-quadruplex-interactive agent, telomestatin: in vitro and in vivo studies in acute leukemia.* Oncogene, 2006. **25**(42): p. 5719-25.
105. Minhas, G.S., et al., *Synthesis and G-quadruplex stabilizing properties of a series of oxazole-containing macrocycles.* Bioorg Med Chem Lett, 2006. **16**(15): p. 3891-5.
106. Iida, K., et al., *G-quadruplex recognition by macrocyclic hexaoxazole (6OTD) dimer: greater selectivity than monomer.* Chem Commun (Camb), 2009(42): p. 6481-3.
107. Monchaud, D. and M.P. Teulade-Fichou, *A hitchhiker's guide to G-quadruplex ligands.* Org Biomol Chem, 2008. **6**(4): p. 627-36.
108. Doi, T., et al., *Total Synthesis of (R)-Telomestatin.* Organic Letters, 2006. **8**(18): p. 4165-4167.
109. Pilch, D.S., et al., *Targeting human telomeric G-quadruplex DNA with oxazole-containing macrocyclic compounds.* Biochimie, 2008. **90**(8): p. 1233-49.
110. Tian, T., et al., *G-Quadruplex: A Regulator of Gene Expression and Its Chemical Targeting.* Chem, 2018. **4**(6): p. 1314-1344.

111. Granotier, C., et al., *Preferential binding of a G-quadruplex ligand to human chromosome ends.* Nucleic Acids Res, 2005. **33**(13): p. 4182-90.
112. Pennarun, G., et al., *Apoptosis related to telomere instability and cell cycle alterations in human glioma cells treated by new highly selective G-quadruplex ligands.* Oncogene, 2005. **24**(18): p. 2917-28.
113. Pennarun, G., et al., *Role of ATM in the telomere response to the G-quadruplex ligand 360A.* Nucleic Acids Res, 2008. **36**(5): p. 1741-54.
114. Gauthier, L.R., et al., *Rad51 and DNA-PKcs are involved in the generation of specific telomere aberrations induced by the quadruplex ligand 360A that impair mitotic cell progression and lead to cell death.* Cell Mol Life Sci, 2012. **69**(4): p. 629-40.
115. De Cian, A., et al., *Highly efficient G-quadruplex recognition by bisquinolinium compounds.* J Am Chem Soc, 2007. **129**(7): p. 1856-7.
116. Saha, A., et al., *Nucleolin Discriminates Drastically between Long-Loop and Short-Loop Quadruplexes.* Biochemistry, 2020. **59**(12): p. 1261-1272.
117. Piazza, A., et al., *Genetic instability triggered by G-quadruplex interacting Phen-DC compounds in Saccharomyces cerevisiae.* Nucleic Acids Res, 2010. **38**(13): p. 4337-48.
118. Reznichenko, O., et al., *Novel cationic bis (acylhydrazones) as modulators of Epstein–Barr virus immune evasion acting through disruption of interaction between nucleolin and G-quadruplexes of EBNA1 mRNA.* European journal of medicinal chemistry, 2019. **178**: p. 13-29.
119. Lista, M.J., et al., *Nucleolin directly mediates Epstein-Barr virus immune evasion through binding to G-quadruplexes of EBNA1 mRNA.* Nature communications, 2017. **8**(1): p. 1-13.
120. Rodriguez, R., et al., *A Novel Small Molecule That Alters Shelterin Integrity and Triggers a DNA-Damage Response at Telomeres.* Journal of the American Chemical Society, 2008. **130**(47): p. 15758-15759.
121. Marchand, A., et al., *Ligand-induced conformational changes with cation ejection upon binding to human telomeric DNA G-quadruplexes.* J Am Chem Soc, 2015. **137**(2): p. 750-6.
122. Müller, S., et al., *Pyridostatin analogues promote telomere dysfunction and long-term growth inhibition in human cancer cells.* Organic & biomolecular chemistry, 2012. **10**(32): p. 6537-6546.
123. Cao, Q., et al., *G-quadruplex DNA targeted metal complexes acting as potential anticancer drugs.* Inorganic Chemistry Frontiers, 2017. **4**(1): p. 10-32.
124. Vilar, R., *Nucleic Acid Quadruplexes and Metallo-Drugs.* Met Ions Life Sci, 2018. **18**.
125. Sigel, A., et al., *Historical Development and Perspectives of the Series Metal Ions in Life Sciences.* 2018: p. vii-viii.
126. Bertrand, H., et al., *Exclusive platination of loop adenines in the human telomeric G-quadruplex.* Org Biomol Chem, 2009. **7**(14): p. 2864-71.
127. Saker, L., et al., *Platinum Complexes Can Bind to Telomeres by Coordination.* Int J Mol Sci, 2018. **19**(7).
128. Bertrand, H., et al., *A platinum-quinacridine hybrid as a G-quadruplex ligand.* J Biol Inorg Chem, 2007. **12**(7): p. 1003-14.

129. Shi, D.-F., et al., *Quadruplex-interactive agents as telomerase inhibitors: Synthesis of porphyrins and structure− activity relationship for the inhibition of telomerase.* Journal of medicinal chemistry, 2001. **44**(26): p. 4509-4523.
130. Dixon, I.M., et al., *A G-quadruplex ligand with 10000-fold selectivity over duplex DNA.* Journal of the American Chemical Society, 2007. **129**(6): p. 1502-1503.
131. Sabater, L., et al., *The nickel(II) complex of guanidinium phenyl porphyrin, a specific G-quadruplex ligand, targets telomeres and leads to POT1 mislocalization in culture cells.* J Biol Inorg Chem, 2015. **20**(4): p. 729-38.
132. Seenisamy, J., et al., *Design and synthesis of an expanded porphyrin that has selectivity for the c-MYC G-quadruplex structure.* Journal of the American Chemical Society, 2005. **127**(9): p. 2944-2959.
133. Reed, J.E., et al., *Stabilization of G-Quadruplex DNA and Inhibition of Telomerase Activity by Square-Planar Nickel(II) Complexes.* Journal of the American Chemical Society, 2005. **128**(18): p. 5992-5993.
134. Arola-Arnal, A., et al., *Effects of Metal Coordination Geometry on Stabilization of Human Telomeric Quadruplex DNA by Square-Planar and Square-Pyramidal Metal Complexes.* Inorganic Chemistry, 2008. **47**(24): p. 11910-11919.
135. Campbell, N.H., et al., *Molecular Basis of Structure–Activity Relationships between Salphen Metal Complexes and Human Telomeric DNA Quadruplexes.* Journal of Medicinal Chemistry, 2012. **55**(1): p. 209-222.
136. Leczkowska, A., et al., *Binding Studies of Metal-Salphen and Metal-Bipyridine Complexes towards G-Quadruplex DNA.* Chemistry, 2018. **24**(45): p. 11785-11794.
137. Wei, C., L. Ren, and N. Gao, *Interactions of terpyridines and their Pt(II) complexes with G-quadruplex DNAs and telomerase inhibition.* Int J Biol Macromol, 2013. **57**: p. 1-8.
138. Gama, S., et al., *Anthracene-terpyridine metal complexes as new G-quadruplex DNA binders.* J Inorg Biochem, 2016. **160**: p. 275-86.
139. Wang, P., et al., *Structure-based design of platinum(II) complexes as c-myc oncogene down-regulators and luminescent probes for G-quadruplex DNA.* Chemistry, 2010. **16**(23): p. 6900-11.
140. Bertrand, H., et al., *The importance of metal geometry in the recognition of G-quadruplex-DNA by metal-terpyridine complexes.* Org Biomol Chem, 2007. **5**(16): p. 2555-9.
141. Trajkovski, M., et al., *Interactions of Pt-ttpy with G-Quadruplexes Originating from Promoter Region of the c-myc Gene Deciphered by NMR and Gel Electrophoresis Analysis.* Chemistry, 2015. **21**(21): p. 7798-807.
142. Morel, E., et al., *Selectivity of Terpyridine Platinum Anticancer Drugs for G-quadruplex DNA.* Molecules, 2019. **24**(3): p. 404.
143. Merle, P., et al., *Highly efficient radiosensitization of human glioblastoma and lung cancer cells by a G-quadruplex DNA binding compound.* Sci Rep, 2015. **5**: p. 16255.
144. Lee, H.S., et al., *Systematic Analysis of Compounds Specifically Targeting Telomeres and Telomerase for Clinical Implications in Cancer Therapy.* Cancer Res, 2018. **78**(21): p. 6282-6296.

145. Rao, L. and U. Bierbach, *Kinetically favored platination of adenine in the g-rich human telomeric repeat.* Journal of the American Chemical Society, 2007. **129**(51): p. 15764-15765.
146. Rao, L., et al., *Interactions of a platinum-modified perylene derivative with the human telomeric G-quadruplex.* The Journal of Physical Chemistry B, 2011. **115**(46): p. 13701-13712.
147. Charif, R., et al., *Association of a Platinum Complex to a G-Quadruplex Ligand Enhances Telomere Disruption.* Chem Res Toxicol, 2017. **30**(8): p. 1629-1640.
148. Skander, M., et al., *N-heterocyclic carbene-amine Pt(II) complexes, a new chemical space for the development of platinum-based anticancer drugs.* J Med Chem, 2010. **53**(5): p. 2146-54.
149. Cohen, S.M. and S.J. Lippard, *Cisplatin: from DNA damage to cancer chemotherapy.* Prog Nucleic Acid Res Mol Biol, 2001. **67**: p. 93-130.
150. Betzer, J.F., et al., *Linking of Antitumor trans NHC-Pt(II) Complexes to G-Quadruplex DNA Ligand for Telomeric Targeting.* Bioconjug Chem, 2016. **27**(6): p. 1456-70.
151. Chtchigrovsky, M., et al., *Antitumor trans-N-heterocyclic carbene-amine-Pt(II) complexes: synthesis of dinuclear species and exploratory investigations of DNA binding and cytotoxicity mechanisms.* J Med Chem, 2013. **56**(5): p. 2074-86.
152. Carvalho, J., et al., *G-quadruplex, Friend or Foe: The Role of the G-quartet in Anticancer Strategies.* Trends Mol Med, 2020.
153. Hu, M.-H., et al., *New substituted quinoxalines inhibit triple-negative breast cancer by specifically downregulating the c-MYC transcription.* Nucleic acids research, 2019. **47**(20): p. 10529-10542.
154. Hu, M.-H., et al., *Discovery of a new four-leaf clover-like ligand as a potent c-MYC transcription inhibitor specifically targeting the promoter G-quadruplex.* Journal of medicinal chemistry, 2018. **61**(6): p. 2447-2459.
155. Dutta, D., et al., *Cell penetrating thiazole peptides inhibit c-MYC expression via site-specific targeting of c-MYC G-quadruplex.* Nucleic acids research, 2018. **46**(11): p. 5355-5365.
156. Pattanayak, R., et al., *Porphyrins to restrict progression of pancreatic cancer by stabilizing KRAS G-quadruplex: In silico, in vitro and in vivo validation of anticancer strategy.* European Journal of Pharmaceutical Sciences, 2018. **125**: p. 39-53.
157. Carvalho, J., et al., *Fluorescent light-up acridine orange derivatives bind and stabilize KRAS-22RT G-quadruplex.* Biochimie, 2018. **144**: p. 144-152.
158. Miglietta, G., et al., *RNA G-quadruplexes in Kirsten ras (KRAS) oncogene as targets for small molecules inhibiting translation.* Journal of Medicinal Chemistry, 2017. **60**(23): p. 9448-9461.
159. Drygin, D., et al., *Anticancer activity of CX-3543: a direct inhibitor of rRNA biogenesis.* Cancer research, 2009. **69**(19): p. 7653-7661.
160. Xu, H., et al., *CX-5461 is a DNA G-quadruplex stabilizer with selective lethality in BRCA1/2 deficient tumours.* Nature communications, 2017. **8**(1): p. 1-18.
161. Salvati, E., et al., *PARP1 is activated at telomeres upon G4 stabilization: possible target for telomere-based therapy.* Oncogene, 2010. **29**(47): p. 6280-93.

162. McLuckie, K.I., et al., *G-quadruplex DNA as a molecular target for induced synthetic lethality in cancer cells.* Journal of the American Chemical Society, 2013. **135**(26): p. 9640-9643.
163. Zimmer, J., et al., *Targeting BRCA1 and BRCA2 Deficiencies with G-Quadruplex-Interacting Compounds.* Mol Cell, 2016. **61**(3): p. 449-460.
164. Begg, A.C., F.A. Stewart, and C. Vens, *Strategies to improve radiotherapy with targeted drugs.* Nat Rev Cancer, 2011. **11**(4): p. 239-53.
165. Delaney, G., et al., *The role of radiotherapy in cancer treatment: estimating optimal utilization from a review of evidence-based clinical guidelines.* Cancer, 2005. **104**(6): p. 1129-37.
166. Chen, H.H.W. and M.T. Kuo, *Improving radiotherapy in cancer treatment: Promises and challenges.* Oncotarget, 2017. **8**(37): p. 62742-62758.
167. Beyzadeoglu, M., G. Ozyigit, and C. Ebruli, *Radiobiology.* 2010: p. 71-144.
168. Hall, E. and A. Giaccia, *Radiobiology for the radiobiologist*. Vol. 6. 2006.
169. Maier, P., et al., *Cellular Pathways in Response to Ionizing Radiation and Their Targetability for Tumor Radiosensitization.* Int J Mol Sci, 2016. **17**(1).
170. Mohan, R. and D. Grosshans, *Proton therapy - Present and future.* Adv Drug Deliv Rev, 2017. **109**: p. 26-44.
171. Hall, E. and A. Giaccia, *Radiobiology for the radiobiologist.* 2012. **7th edition**.
172. Brady, L.W., *Textbook of Radiotherapy.* JAMA, 1974. **228**(11): p. 1434-1434.
173. Beyzadeoglu, M., G. Ozyigit, and C. Ebruli, *Radiobiology*, in *Basic Radiation Oncology*. 2010. p. 71-144.
174. Hall, E.J., *Radiation biology for pediatric radiologists.* Pediatr Radiol, 2009. **39 Suppl 1**: p. S57-64.
175. Lewanski, C.R. and W.J. Gullick, *Radiotherapy and cellular signalling.* Lancet Oncol, 2001. **2**(6): p. 366-70.
176. Dahm-Daphi, C.S.W.A.J., *Comparison of biological effects of DNA damage induced by ionizing radiation and hydrogen peroxide in CHO cells.* International Journal of Radiation Biology, 2000. **76**(1): p. 67-75.
177. Asaithamby, A. and D.J. Chen, *Mechanism of cluster DNA damage repair in response to high-atomic number and energy particles radiation.* Mutation research, 2011. **711**(1-2): p. 87-99.
178. Povirk, L.F., *Biochemical mechanisms of chromosomal translocations resulting from DNA double-strand breaks.* DNA Repair (Amst), 2006. **5**(9-10): p. 1199-212.
179. Atamna, H., I. Cheung, and B.N. Ames, *A method for detecting abasic sites in living cells: age-dependent changes in base excision repair.* Proc Natl Acad Sci U S A, 2000. **97**(2): p. 686-91.
180. Matt, S. and T.G. Hofmann, *The DNA damage-induced cell death response: a roadmap to kill cancer cells.* Cellular and Molecular Life Sciences, 2016. **73**(15): p. 2829-2850.
181. Hanahan, D. and R.A. Weinberg, *Hallmarks of cancer: the next generation.* Cell, 2011. **144**(5): p. 646-74.
182. Blackford, A.N. and S.P. Jackson, *ATM, ATR, and DNA-PK: The Trinity at the Heart of the DNA Damage Response.* Mol Cell, 2017. **66**(6): p. 801-817.

183. Zhou, B.B. and S.J. Elledge, *The DNA damage response: putting checkpoints in perspective.* Nature, 2000. **408**(6811): p. 433-9.
184. D'Amours, D., et al., *Poly(ADP-ribosyl)ation reactions in the regulation of nuclear functions.* Biochem J, 1999. **342 (Pt 2)**: p. 249-68.
185. Ossovskaya, V., et al., *Upregulation of Poly (ADP-Ribose) Polymerase-1 (PARP1) in Triple-Negative Breast Cancer and Other Primary Human Tumor Types.* Genes Cancer, 2010. **1**(8): p. 812-21.
186. Ba, X. and N.J. Garg, *Signaling mechanism of poly(ADP-ribose) polymerase-1 (PARP-1) in inflammatory diseases.* Am J Pathol, 2011. **178**(3): p. 946-55.
187. Huambachano, O., et al., *Double-stranded DNA binding domain of poly(ADP-ribose) polymerase-1 and molecular insight into the regulation of its activity.* J Biol Chem, 2011. **286**(9): p. 7149-60.
188. Isabelle, M., et al., *Investigation of PARP-1, PARP-2, and PARG interactomes by affinity-purification mass spectrometry.* Proteome Sci, 2010. **8**: p. 22.
189. Gagne, J.P., et al., *Proteome-wide identification of poly(ADP-ribose) binding proteins and poly(ADP-ribose)-associated protein complexes.* Nucleic Acids Res, 2008. **36**(22): p. 6959-76.
190. Jungmichel, S., et al., *Proteome-wide identification of poly(ADP-Ribosyl)ation targets in different genotoxic stress responses.* Mol Cell, 2013. **52**(2): p. 272-85.
191. Krietsch, J., et al., *Reprogramming cellular events by poly(ADP-ribose)-binding proteins.* Mol Aspects Med, 2013. **34**(6): p. 1066-87.
192. Ray Chaudhuri, A. and A. Nussenzweig, *The multifaceted roles of PARP1 in DNA repair and chromatin remodelling.* Nat Rev Mol Cell Biol, 2017. **18**(10): p. 610-621.
193. Carney, J.P., et al., *The hMre11/hRad50 protein complex and Nijmegen breakage syndrome: linkage of double-strand break repair to the cellular DNA damage response.* Cell, 1998. **93**(3): p. 477-86.
194. Uziel, T., et al., *Requirement of the MRN complex for ATM activation by DNA damage.* Embo j, 2003. **22**(20): p. 5612-21.
195. Lee, J.H. and T.T. Paull, *ATM activation by DNA double-strand breaks through the Mre11-Rad50-Nbs1 complex.* Science, 2005. **308**(5721): p. 551-4.
196. Shiotani, B. and L. Zou, *Single-stranded DNA orchestrates an ATM-to-ATR switch at DNA breaks.* Mol Cell, 2009. **33**(5): p. 547-58.
197. Awasthi, P., M. Foiani, and A. Kumar, *ATM and ATR signalling at a glance.* Journal of Cell Science, 2016(128): p. 4255-4262.
198. Tanaka, T., et al., *Cytometry of ATM activation and histone H2AX phosphorylation to estimate extent of DNA damage induced by exogenous agents.* Cytometry. Part A : the journal of the International Society for Analytical Cytology, 2007. **71**(9): p. 648-661.
199. Meier, A., et al., *Spreading of mammalian DNA-damage response factors studied by ChIP-chip at damaged telomeres.* Embo j, 2007. **26**(11): p. 2707-18.
200. Savic, V., et al., *Formation of dynamic gamma-H2AX domains along broken DNA strands is distinctly regulated by ATM and MDC1 and dependent upon H2AX densities in chromatin.* Mol Cell, 2009. **34**(3): p. 298-310.
201. Stewart, G.S., et al., *MDC1 is a mediator of the mammalian DNA damage checkpoint.* Nature, 2003. **421**(6926): p. 961-6.

202. Lee, M.S., et al., *Structure of the BRCT repeat domain of MDC1 and its specificity for the free COOH-terminal end of the gamma-H2AX histone tail.* J Biol Chem, 2005. **280**(37): p. 32053-6.
203. Stucki, M., et al., *MDC1 directly binds phosphorylated histone H2AX to regulate cellular responses to DNA double-strand breaks.* Cell, 2005. **123**(7): p. 1213-26.
204. Lou, Z., et al., *MDC1 maintains genomic stability by participating in the amplification of ATM-dependent DNA damage signals.* Mol Cell, 2006. **21**(2): p. 187-200.
205. Dvir, A., et al., *Ku autoantigen is the regulatory component of a template-associated protein kinase that phosphorylates RNA polymerase II.* Proc Natl Acad Sci U S A, 1992. **89**(24): p. 11920-4.
206. Gottlieb, T.M. and S.P. Jackson, *The DNA-dependent protein kinase: requirement for DNA ends and association with Ku antigen.* Cell, 1993. **72**(1): p. 131-42.
207. Jiang, W., et al., *Differential phosphorylation of DNA-PKcs regulates the interplay between end-processing and end-ligation during nonhomologous end-joining.* Mol Cell, 2015. **58**(1): p. 172-85.
208. Chapman, J.R., M.R. Taylor, and S.J. Boulton, *Playing the end game: DNA double-strand break repair pathway choice.* Mol Cell, 2012. **47**(4): p. 497-510.
209. Price, B.D. and A.D. D'Andrea, *Chromatin remodeling at DNA double-strand breaks.* Cell, 2013. **152**(6): p. 1344-54.
210. Iliakis, G., T. Murmann, and A. Soni, *Alternative end-joining repair pathways are the ultimate backup for abrogated classical non-homologous end-joining and homologous recombination repair: Implications for the formation of chromosome translocations.* Mutat Res Genet Toxicol Environ Mutagen, 2015. **793**: p. 166-75.
211. Hsu, P.D., E.S. Lander, and F. Zhang, *Development and applications of CRISPR-Cas9 for genome engineering.* Cell, 2014. **157**(6): p. 1262-78.
212. Betermier, M., P. Bertrand, and B.S. Lopez, *Is non-homologous end-joining really an inherently error-prone process?* PLoS Genet, 2014. **10**(1): p. e1004086.
213. van Schendel, R., et al., *Polymerase Theta is a key driver of genome evolution and of CRISPR/Cas9-mediated mutagenesis.* Nat Commun, 2015. **6**: p. 7394.
214. Marechal, A. and L. Zou, *DNA damage sensing by the ATM and ATR kinases.* Cold Spring Harb Perspect Biol, 2013. **5**(9).
215. Feng, L., et al., *Cell cycle-dependent inhibition of 53BP1 signaling by BRCA1.* Cell Discovery, 2015. **1**(1): p. 15019.
216. Guo, X., et al., *Acetylation of 53BP1 dictates the DNA double strand break repair pathway.* Nucleic Acids Research, 2018. **46**(2): p. 689-703.
217. Zimmermann, M. and T. de Lange, *53BP1: pro choice in DNA repair.* Trends Cell Biol, 2014. **24**(2): p. 108-17.
218. Yaneva, M. and S. Jhiang, *Expression of the Ku protein during cell proliferation.* Biochim Biophys Acta, 1991. **1090**(2): p. 181-7.
219. Deng, S.K., H. Chen, and L.S. Symington, *Replication protein A prevents promiscuous annealing between short sequence homologies: Implications for genome integrity.* Bioessays, 2015. **37**(3): p. 305-13.

220. Baumann, P. and S.C. West, *Role of the human RAD51 protein in homologous recombination and double-stranded-break repair.* Trends Biochem Sci, 1998. **23**(7): p. 247-51.
221. San Filippo, J., P. Sung, and H. Klein, *Mechanism of eukaryotic homologous recombination.* Annu Rev Biochem, 2008. **77**: p. 229-57.
222. Haber, J.E., *DNA Repair: The Search for Homology.* BioEssays : news and reviews in molecular, cellular and developmental biology, 2018. **40**(5): p. e1700229-e1700229.
223. Daley, J.M., et al., *Regulation of DNA pairing in homologous recombination.* Cold Spring Harbor perspectives in biology, 2014. **6**(11): p. a017954-a017954.
224. Maloisel, L., F. Fabre, and S. Gangloff, *DNA polymerase delta is preferentially recruited during homologous recombination to promote heteroduplex DNA extension.* Molecular and cellular biology, 2008. **28**(4): p. 1373-1382.
225. Wu, L. and I.D. Hickson, *The Bloom's syndrome helicase suppresses crossing over during homologous recombination.* Nature, 2003. **426**(6968): p. 870-874.
226. Li, M. and X. Yu, *Function of BRCA1 in the DNA damage response is mediated by ADP-ribosylation.* Cancer Cell, 2013. **23**(5): p. 693-704.
227. Schwertman, P., S. Bekker-Jensen, and N. Mailand, *Regulation of DNA double-strand break repair by ubiquitin and ubiquitin-like modifiers.* Nat Rev Mol Cell Biol, 2016. **17**(6): p. 379-94.
228. Hu, Y., et al., *PARP1-driven poly-ADP-ribosylation regulates BRCA1 function in homologous recombination-mediated DNA repair.* Cancer Discov, 2014. **4**(12): p. 1430-47.
229. Bryant, H.E., et al., *Specific killing of BRCA2-deficient tumours with inhibitors of poly(ADP-ribose) polymerase.* Nature, 2005. **434**(7035): p. 913-7.
230. Farmer, H., et al., *Targeting the DNA repair defect in BRCA mutant cells as a therapeutic strategy.* Nature, 2005. **434**(7035): p. 917-21.
231. Karanam, K., et al., *Quantitative live cell imaging reveals a gradual shift between DNA repair mechanisms and a maximal use of HR in mid S phase.* Mol Cell, 2012. **47**(2): p. 320-9.
232. Jette, N. and S.P. Lees-Miller, *The DNA-dependent protein kinase: A multifunctional protein kinase with roles in DNA double strand break repair and mitosis.* Prog Biophys Mol Biol, 2015. **117**(2-3): p. 194-205.
233. Graham, T.G., J.C. Walter, and J.J. Loparo, *Two-Stage Synapsis of DNA Ends during Non-homologous End Joining.* Mol Cell, 2016. **61**(6): p. 850-8.
234. Moshous, D., et al., *Artemis, a novel DNA double-strand break repair/V(D)J recombination protein, is mutated in human severe combined immune deficiency.* Cell, 2001. **105**(2): p. 177-86.
235. Hammel, M., et al., *Ku and DNA-dependent protein kinase dynamic conformations and assembly regulate DNA binding and the initial non-homologous end joining complex.* J Biol Chem, 2010. **285**(2): p. 1414-23.
236. Malu, S., et al., *Artemis C-terminal region facilitates V(D)J recombination through its interactions with DNA Ligase IV and DNA-PKcs.* J Exp Med, 2012. **209**(5): p. 955-63.
237. Li, Z., et al., *The XRCC4 gene encodes a novel protein involved in DNA double-strand break repair and V(D)J recombination.* Cell, 1995. **83**(7): p. 1079-89.

238. Ahnesorg, P., P. Smith, and S.P. Jackson, *XLF interacts with the XRCC4-DNA ligase IV complex to promote DNA nonhomologous end-joining.* Cell, 2006. **124**(2): p. 301-13.
239. Grawunder, U., et al., *Activity of DNA ligase IV stimulated by complex formation with XRCC4 protein in mammalian cells.* Nature, 1997. **388**(6641): p. 492-5.
240. Ochi, T., et al., *DNA repair. PAXX, a paralog of XRCC4 and XLF, interacts with Ku to promote DNA double-strand break repair.* Science, 2015. **347**(6218): p. 185-188.
241. Ruscetti, T., et al., *Stimulation of the DNA-dependent protein kinase by poly(ADP-ribose) polymerase.* J Biol Chem, 1998. **273**(23): p. 14461-7.
242. Spagnolo, L., et al., *Visualization of a DNA-PK/PARP1 complex.* Nucleic Acids Res, 2012. **40**(9): p. 4168-77.
243. Rybanska, I., et al., *PARP1 and DNA-PKcs synergize to suppress p53 mutation and telomere fusions during T-lineage lymphomagenesis.* Oncogene, 2013. **32**(14): p. 1761-71.
244. Luijsterburg, M.S., et al., *PARP1 Links CHD2-Mediated Chromatin Expansion and H3.3 Deposition to DNA Repair by Non-homologous End-Joining.* Mol Cell, 2016. **61**(4): p. 547-562.
245. Cheng, Q., et al., *Ku counteracts mobilization of PARP1 and MRN in chromatin damaged with DNA double-strand breaks.* Nucleic Acids Res, 2011. **39**(22): p. 9605-19.
246. Wang, M., et al., *PARP-1 and Ku compete for repair of DNA double strand breaks by distinct NHEJ pathways.* Nucleic Acids Res, 2006. **34**(21): p. 6170-82.
247. Wray, J., et al., *PARP1 is required for chromosomal translocations.* Blood, 2013. **121**(21): p. 4359-65.
248. Sfeir, A. and T. de Lange, *Removal of shelterin reveals the telomere end-protection problem.* Science, 2012. **336**(6081): p. 593-7.
249. Haince, J.F., et al., *PARP1-dependent kinetics of recruitment of MRE11 and NBS1 proteins to multiple DNA damage sites.* J Biol Chem, 2008. **283**(2): p. 1197-208.
250. Ceccaldi, R., et al., *Homologous-recombination-deficient tumours are dependent on Poltheta-mediated repair.* Nature, 2015. **518**(7538): p. 258-62.
251. Kalkavan, H. and D.R. Green, *MOMP, cell suicide as a BCL-2 family business.* Cell Death & Differentiation, 2018. **25**(1): p. 46-55.
252. Karnitz, L.M. and L. Zou, *Molecular Pathways: Targeting ATR in Cancer Therapy.* Clinical Cancer Research, 2015. **21**(21): p. 4780.
253. Zeman, M.K. and K.A. Cimprich, *Causes and consequences of replication stress.* Nat Cell Biol, 2014. **16**(1): p. 2-9.
254. Zou, L. and S.J. Elledge, *Sensing DNA damage through ATRIP recognition of RPA-ssDNA complexes.* Science, 2003. **300**(5625): p. 1542-8.
255. Lam, M.H. and J.M. Rosen, *Chk1 versus Cdc25: chking one's levels of cellular proliferation.* Cell Cycle, 2004. **3**(11): p. 1355-7.
256. Caldecott, K.W., et al., *An interaction between the mammalian DNA repair protein XRCC1 and DNA ligase III.* Mol Cell Biol, 1994. **14**(1): p. 68-76.
257. Marintchev, A., et al., *Domain specific interaction in the XRCC1-DNA polymerase beta complex.* Nucleic Acids Res, 2000. **28**(10): p. 2049-59.
258. Caldecott, K.W., *Single-strand break repair and genetic disease.* Nat Rev Genet, 2008. **9**(8): p. 619-31.

259. Oei, S.L. and M. Ziegler, *ATP for the DNA ligation step in base excision repair is generated from poly(ADP-ribose).* J Biol Chem, 2000. **275**(30): p. 23234-9.
260. Dantzer, F., et al., *Base excision repair is impaired in mammalian cells lacking Poly(ADP-ribose) polymerase-1.* Biochemistry, 2000. **39**(25): p. 7559-69.
261. Pachkowski, B.F., et al., *Cells deficient in PARP-1 show an accelerated accumulation of DNA single strand breaks, but not AP sites, over the PARP-1-proficient cells exposed to MMS.* Mutat Res, 2009. **671**(1-2): p. 93-9.
262. Vodenicharov, M.D., et al., *Base excision repair is efficient in cells lacking poly(ADP-ribose) polymerase 1.* Nucleic Acids Res, 2000. **28**(20): p. 3887-96.
263. Reynolds, P., et al., *Disruption of PARP1 function inhibits base excision repair of a sub-set of DNA lesions.* Nucleic Acids Res, 2015. **43**(8): p. 4028-38.
264. Rocha, C.R.R., et al., *DNA repair pathways and cisplatin resistance: an intimate relationship.* Clinics (Sao Paulo), 2018. **73**(suppl 1): p. e478s.
265. Marteijn, J.A., et al., *Understanding nucleotide excision repair and its roles in cancer and ageing.* Nat Rev Mol Cell Biol, 2014. **15**(7): p. 465-81.
266. Kapetanaki, M.G., et al., *The DDB1-CUL4ADDB2 ubiquitin ligase is deficient in xeroderma pigmentosum group E and targets histone H2A at UV-damaged DNA sites.* Proc Natl Acad Sci U S A, 2006. **103**(8): p. 2588-93.
267. Wang, H., et al., *Histone H3 and H4 ubiquitylation by the CUL4-DDB-ROC1 ubiquitin ligase facilitates cellular response to DNA damage.* Mol Cell, 2006. **22**(3): p. 383-94.
268. Pines, A., et al., *PARP1 promotes nucleotide excision repair through DDB2 stabilization and recruitment of ALC1.* J Cell Biol, 2012. **199**(2): p. 235-49.
269. Robu, M., et al., *Role of poly(ADP-ribose) polymerase-1 in the removal of UV-induced DNA lesions by nucleotide excision repair.* Proc Natl Acad Sci U S A, 2013. **110**(5): p. 1658-63.
270. King, B.S., et al., *Poly(ADP-ribose) contributes to an association between poly(ADP-ribose) polymerase-1 and xeroderma pigmentosum complementation group A in nucleotide excision repair.* J Biol Chem, 2012. **287**(47): p. 39824-33.
271. Gill, M.R. and K.A. Vallis, *Transition metal compounds as cancer radiosensitizers.* Chem Soc Rev, 2019. **48**(2): p. 540-557.
272. Steel, G.G. and M.J. Peckham, *Exploitable mechanisms in combined radiotherapy-chemotherapy: the concept of additivity.* Int J Radiat Oncol Biol Phys, 1979. **5**(1): p. 85-91.
273. Huang, R.-y., et al., *Isobologram Analysis: A Comprehensive Review of Methodology and Current Research.* Frontiers in Pharmacology, 2019. **10**(1222).
274. Wilson, G.D., S.M. Bentzen, and P.M. Harari, *Biologic basis for combining drugs with radiation.* Semin Radiat Oncol, 2006. **16**(1): p. 2-9.
275. Verhagen, C.V., et al., *Extent of radiosensitization by the PARP inhibitor olaparib depends on its dose, the radiation dose and the integrity of the homologous recombination pathway of tumor cells.* Radiother Oncol, 2015. **116**(3): p. 358-65.
276. de Haan, R., et al., *Study protocols of three parallel phase 1 trials combining radical radiotherapy with the PARP inhibitor olaparib.* BMC Cancer, 2019. **19**(1): p. 901.
277. Tu, X., et al., *ATR Inhibition Is a Promising Radiosensitizing Strategy for Triple-Negative Breast Cancer.* Mol Cancer Ther, 2018. **17**(11): p. 2462-2472.

278. Biau, J., et al., *[Dbait: An innovative concept to inhibit DNA repair and treat cancer].* Bull Cancer, 2016. **103**(3): p. 227-35.
279. Quanz, M., et al., *Small-molecule drugs mimicking DNA damage: a new strategy for sensitizing tumors to radiotherapy.* Clin Cancer Res, 2009. **15**(4): p. 1308-16.
280. Le Tourneau, C., et al., *First-in-human phase I study of the DNA-repair inhibitor DT01 in combination with radiotherapy in patients with skin metastases from melanoma.* Br J Cancer, 2016. **114**(11): p. 1199-205.
281. Pawlik, T.M. and K. Keyomarsi, *Role of cell cycle in mediating sensitivity to radiotherapy.* Int J Radiat Oncol Biol Phys, 2004. **59**(4): p. 928-42.
282. Wahl, A.F., et al., *Loss of normal p53 function confers sensitization to Taxol by increasing GZ/M arrest and apoptosis.* NATURE MEDICINE, 1996. **2**(1): p. 8.
283. Werner, M.E., et al., *Preclinical evaluation of Genexol-PM, a nanoparticle formulation of paclitaxel, as a novel radiosensitizer for the treatment of non-small cell lung cancer.* Int J Radiat Oncol Biol Phys, 2013. **86**(3): p. 463-468.
284. Seiwert, T.Y., J.K. Salama, and E.E. Vokes, *The concurrent chemoradiation paradigm—general principles.* Nature Clinical Practice Oncology, 2007. **4**(2): p. 86-100.
285. De Ridder, M., et al., *Hypoxic tumor cell radiosensitization through nitric oxide.* Nitric Oxide, 2008. **19**(2): p. 164-9.
286. Wang, H., et al., *Hypoxic Radioresistance: Can ROS Be the Key to Overcome It?* Cancers (Basel), 2019. **11**(1).
287. O'Connor, L.J., et al., *Design, synthesis and evaluation of molecularly targeted hypoxia-activated prodrugs.* Nature Protocols, 2016. **11**(4): p. 781-794.
288. Bonner, J.A., et al., *Radiotherapy plus cetuximab for locoregionally advanced head and neck cancer: 5-year survival data from a phase 3 randomised trial, and relation between cetuximab-induced rash and survival.* Lancet Oncol, 2010. **11**(1): p. 21-8.
289. Bonner, J.A., et al., *Enhancement of Cetuximab-Induced Radiosensitization by JAK-1 Inhibition.* BMC Cancer, 2015. **15**: p. 673.
290. Graham, J., M. Muhsin, and P. Kirkpatrick, *Cetuximab.* Nat Rev Drug Discov, 2004. **3**(7): p. 549-50.
291. Maity, A. and E.J. Bernhard, *Modulating tumor vasculature through signaling inhibition to improve cytotoxic therapy.* Cancer Res, 2010. **70**(6): p. 2141-5.
292. Kobayashi, K., et al., *Enhancement of radiation effect by heavy elements.* Mutat Res, 2010. **704**(1-3): p. 123-31.
293. Wang, H., et al., *Cancer Radiosensitizers.* Trends Pharmacol Sci, 2018. **39**(1): p. 24-48.
294. Buckley, A.M., et al., *Targeting hallmarks of cancer to enhance radiosensitivity in gastrointestinal cancers.* Nature Reviews Gastroenterology & Hepatology, 2020. **17**(5): p. 298-313.
295. Ferreira, S. and M. Dutreix, *DNA repair inhibitors to enhance radiotherapy: Progresses and limitations.* Cancer Radiother, 2019. **23**(8): p. 883-890.
296. Ghadjar, P., et al., *Concomitant cisplatin and hyperfractionated radiotherapy in locally advanced head and neck cancer: 10-year follow-up of a randomized phase III trial (SAKK 10/94).* Int J Radiat Oncol Biol Phys, 2012. **82**(2): p. 524-31.
297. Tharmalingham, H. and P. Hoskin, *Clinical trials targeting hypoxia.* The British journal of radiology, 2019. **92**(1093): p. 20170966-20170966.

298. Hamming, L.C., et al., *The clinical application of angiostatic therapy in combination with radiotherapy: past, present, future.* Angiogenesis, 2017. **20**(2): p. 217-232.
299. Verry, C., et al., *Treatment of multiple brain metastases using gadolinium nanoparticles and radiotherapy: NANO-RAD, a phase I study protocol.* BMJ Open, 2019. **9**(2): p. e023591.
300. Baggaley, E., J.A. Weinstein, and J.A.G. Williams, *Lighting the way to see inside the live cell with luminescent transition metal complexes.* Coordination Chemistry Reviews, 2012. **256**(15-16): p. 1762-1785.
301. Agostinis, P., et al., *Photodynamic therapy of cancer: an update.* CA Cancer J Clin, 2011. **61**(4): p. 250-81.
302. Linam, J. and L.-X. Yang, *Recent Developments in Radiosensitization.* Anticancer Research, 2015(35): p. 7.
303. Karges, J., et al., *Rationally designed ruthenium complexes for 1-and 2-photon photodynamic therapy.* Nature Communications, 2020. **11**(1): p. 1-13.
304. Hammerer, F., et al., *Synthesis and characterization of glycoconjugated porphyrin triphenylamine hybrids for targeted two-photon photodynamic therapy.* J Org Chem, 2014. **79**(3): p. 1406-17.
305. Achelle, S., et al., *Carbohydrate-Porphyrin Conjugates with Two-Photon Absorption Properties as Potential Photosensitizing Agents for Photodynamic Therapy.* European Journal of Organic Chemistry, 2011. **2011**(7): p. 1271-1279.
306. Candelaria, M., et al., *Radiosensitizers in cervical cancer. Cisplatin and beyond.* Radiation oncology (London, England), 2006. **1**: p. 15-15.
307. Sculier, J.-P., et al., *A phase III randomised study of concomitant induction radiochemotherapy testing two modalities of radiosensitisation by cisplatin (standard versus daily) for limited small-cell lung cancer.* Annals of oncology, 2008. **19**(10): p. 1691-1697.
308. Ma, S., et al., *Platinum single-agent vs. platinum-based doublet agent concurrent chemoradiotherapy for locally advanced cervical cancer: A meta-analysis of randomized controlled trials.* Gynecologic oncology, 2019.
309. Wang, D. and S.J. Lippard, *Cellular processing of platinum anticancer drugs.* Nat Rev Drug Discov, 2005. **4**(4): p. 307-20.
310. Jung, Y. and S.J. Lippard, *Direct cellular responses to platinum-induced DNA damage.* Chemical reviews, 2007. **107**(5): p. 1387-1407.
311. Douple, E.B., et al., *Carboplatin as a potentiator of radiation therapy.* Cancer Treat Rev, 1985. **12 Suppl A**: p. 111-24.
312. Kjellstrom, J., E. Kjellen, and A. Johnsson, *In vitro radiosensitization by oxaliplatin and 5-fluorouracil in a human colon cancer cell line.* Acta Oncol, 2005. **44**(7): p. 687-93.
313. Xue, R., et al., *The efficacy of concurrent weekly carboplatin with radiotherapy in the treatment of cervical cancer: A meta-analysis.* Gynecol Oncol, 2018. **150**(3): p. 412-419.
314. Wewala, N.T. and M.B. Jameson, *The Role of Oxaliplatin in Chemoradiotherapy for Rectal Cancer.* Asia Pac J Clin Oncol, 2017. **13**(6): p. 341-342.
315. Fuertes, M.A., et al., *Novel concepts in the development of platinum antitumor drugs.* Curr Med Chem Anticancer Agents, 2002. **2**(4): p. 539-51.

316. Wexselblatt, E., E. Yavin, and D. Gibson, *Cellular interactions of platinum drugs.* Inorganica chimica acta, 2012. **393**: p. 75-83.
317. Siddik, Z.H., *Cisplatin: mode of cytotoxic action and molecular basis of resistance.* Oncogene, 2003. **22**(47): p. 7265-79.
318. Mueller, S., et al., *Cell-cycle progression and response of germ cell tumors to cisplatin in vitro.* Int J Oncol, 2006. **29**(2): p. 471-9.
319. Furuta, T., et al., *Transcription-coupled nucleotide excision repair as a determinant of cisplatin sensitivity of human cells.* Cancer Res, 2002. **62**(17): p. 4899-902.
320. Madan, R., *Radiosensitizers and Radioprotectors*, in *Practical Radiation Oncology*. 2020, Springer. p. 179-183.
321. Dong, Y., et al., *Chemoradiation Cancer Therapy: Molecular Mechanisms of Cisplatin Radiosensitization.* The Journal of Physical Chemistry C, 2017. **121**(32): p. 17505-17513.
322. Zheng, Y., et al., *Role of secondary low-energy electrons in the concomitant chemoradiation therapy of cancer.* Phys Rev Lett, 2008. **100**(19): p. 198101.
323. Rousseau, J., et al., *Efficacy of intracerebral delivery of cisplatin in combination with photon irradiation for treatment of brain tumors.* Journal of Neuro-Oncology, 2010. **98**(3): p. 287-295.
324. Kopyra, J., et al., *A single slow electron triggers the loss of both chlorine atoms from the anticancer drug cisplatin: implications for chemoradiation therapy.* Angew Chem Int Ed Engl, 2009. **48**(42): p. 7904-7.
325. Rezaee, M., L. Sanche, and D.J. Hunting, *Cisplatin enhances the formation of DNA single- and double-strand breaks by hydrated electrons and hydroxyl radicals.* Radiation research, 2013. **179**(3): p. 323-331.
326. Myint, W.K., C. Ng, and G.P. Raaphorst, *Examining the non-homologous repair process following cisplatin and radiation treatments.* Int J Radiat Biol, 2002. **78**(5): p. 417-24.
327. Gorodetsky, R., et al., *Combination of cisplatin and radiation in cell culture: effect of duration of exposure to drug and timing of irradiation.* Int J Cancer, 1998. **75**(4): p. 635-42.
328. Sears, C.R., et al., *DNA damage response (DDR) pathway engagement in cisplatin radiosensitization of non-small cell lung cancer.* DNA Repair, 2016. **40**: p. 35-46.
329. Toulany, M., et al., *Cisplatin-mediated radiosensitization of non-small cell lung cancer cells is stimulated by ATM inhibition.* Radiother Oncol, 2014. **111**(2): p. 228-36.
330. Dolling, J.A., et al., *Cisplatin-modification of DNA repair and ionizing radiation lethality in yeast, Saccharomyces cerevisiae.* Mutat Res, 1999. **433**(2): p. 127-36.
331. Boeckman, H.J., K.S. Trego, and J.J. Turchi, *Cisplatin sensitizes cancer cells to ionizing radiation via inhibition of nonhomologous end joining.* Mol Cancer Res, 2005. **3**(5): p. 277-85.
332. Turchi, J.J. and K. Henkels, *Human Ku autoantigen binds cisplatin-damaged DNA but fails to stimulate human DNA-activated protein kinase.* J Biol Chem, 1996. **271**(23): p. 13861-7.
333. Turchi, J.J., K.M. Henkels, and Y. Zhou, *Cisplatin-DNA adducts inhibit translocation of the Ku subunits of DNA-PK.* Nucleic Acids Res, 2000. **28**(23): p. 4634-41.
334. Diggle, C.P., et al., *Inhibition of double-strand break non-homologous end-joining by cisplatin adducts in human cell extracts.* Nucleic Acids Res, 2005. **33**(8): p. 2531-9.

335. Sears, C.R. and J.J. Turchi, *Complex cisplatin-double strand break (DSB) lesions directly impair cellular non-homologous end-joining (NHEJ) independent of downstream damage response (DDR) pathways.* J Biol Chem, 2012. **287**(29): p. 24263-72.
336. Bertrand, H., et al., *The importance of metal geometry in the recognition of G-quadruplex-DNA by metal-terpyridine complexes.* Organic & Biomolecular Chemistry, 2007. **5**(16): p. 2555.
337. Gomez, D., et al., *Resistance to senescence induction and telomere shortening by a G-quadruplex ligand inhibitor of telomerase.* Cancer Res, 2003. **63**(19): p. 6149-53.
338. Smogorzewska, A., et al., *Control of human telomere length by TRF1 and TRF2.* Mol Cell Biol, 2000. **20**(5): p. 1659-68.
339. Merle, P., et al., *Telomere targeting with a new G4 ligand enhances radiation-induced killing of human glioblastoma cells.* Mol Cancer Ther, 2011. **10**(10): p. 1784-95.
340. Wong, K.K., et al., *Telomere dysfunction impairs DNA repair and enhances sensitivity to ionizing radiation.* Nature genetics, 2000. **26**(1): p. 85.
341. Ayouaz, A., et al., *Telomeres: hallmarks of radiosensitivity.* Biochimie, 2008. **90**(1): p. 60-72.
342. Leonetti, C., et al., *Biological activity of the G-quadruplex ligand RHPS4 (3,11-difluoro-6,8,13-trimethyl-8H-quino[4,3,2-kl]acridinium methosulfate) is associated with telomere capping alteration.* Mol Pharmacol, 2004. **66**(5): p. 1138-46.
343. Salvati, E., et al., *Telomere damage induced by the G-quadruplex ligand RHPS4 has an antitumor effect.* J Clin Invest, 2007. **117**(11): p. 3236-47.
344. Berardinelli, F., et al., *The G-quadruplex-stabilising agent RHPS4 induces telomeric dysfunction and enhances radiosensitivity in glioblastoma cells.* DNA Repair (Amst), 2014. **25**: p. 104-15.
345. Berardinelli, F., et al., *G-quadruplex ligand RHPS4 radiosensitizes glioblastoma xenograft in vivo through a differential targeting of bulky differentiated- and stem-cancer cells.* Journal of Experimental & Clinical Cancer Research, 2019. **38**(1).
346. Wang, Y., et al., *G-quadruplex DNA drives genomic instability and represents a targetable molecular abnormality in ATRX-deficient malignant glioma.* Nat Commun, 2019. **10**(1): p. 943.
347. Koschmann, C., et al., *ATRX loss promotes tumor growth and impairs nonhomologous end joining DNA repair in glioma.* Sci Transl Med, 2016. **8**(328): p. 328ra28.
348. Kumari, N., et al., *G-quadruplex Structures Contribute to Differential Radiosensitivity of the Human Genome.* iScience, 2019. **21**: p. 288-307.
349. Henkels, K.M. and J.J. Turchi, *Cisplatin-induced apoptosis proceeds by caspase-3-dependent and-independent pathways in cisplatin-resistant and-sensitive human ovarian cancer cell lines.* Cancer research, 1999. **59**(13): p. 3077-3083.
350. Li, N., et al., *MiR-130a and MiR-374a function as novel regulators of cisplatin resistance in human ovarian cancer A2780 cells.* PloS one, 2015. **10**(6): p. e0128886.
351. Uehara, T., et al., *Metformin potentiates the anticancer effects of cisplatin under normoxic conditions in vitro.* Oncol Rep, 2015. **33**(2): p. 744-50.
352. Galluzzi, L., et al., *Molecular mechanisms of cisplatin resistance.* Oncogene, 2012. **31**(15): p. 1869-83.

353. Wynne, P., et al., *Enhanced repair of DNA interstrand crosslinking in ovarian cancer cells from patients following treatment with platinum-based chemotherapy.* British Journal of Cancer, 2007. **97**(7): p. 927-933.
354. Ojima, E., et al., *The optimal schedule for 5-fluorouracil radiosensitization in colon cancer cell lines.* Oncol Rep, 2006. **16**(5): p. 1085-91.
355. Mariotti, L.G., et al., *Use of the γ-H2AX assay to investigate DNA repair dynamics following multiple radiation exposures.* PloS one, 2013. **8**(11): p. e79541-e79541.
356. Bernhard, E.J., et al., *Effects of ionizing radiation on cell cycle progression. A review.* Radiat Environ Biophys, 1995. **34**(2): p. 79-83.
357. Kawamura, K., F. Qi, and J. Kobayashi, *Potential relationship between the biological effects of low-dose irradiation and mitochondrial ROS production.* Journal of radiation research, 2018. **59**(suppl_2): p. ii91-ii97.
358. Tsuji, J., et al., *Mammalian NUMT insertion is non-random.* Nucleic acids research, 2012. **40**(18): p. 9073-9088.
359. Wang, K., et al., *Restraining Cancer Cells by Dual Metabolic Inhibition with a Mitochondrion-Targeted Platinum (II) Complex.* Angewandte Chemie International Edition, 2019. **58**(14): p. 4638-4643.
360. Wallace, D.C., W. Fan, and V. Procaccio, *Mitochondrial Energetics and Therapeutics.* Annual Review of Pathology: Mechanisms of Disease, 2010. **5**(1): p. 297-348.
361. Smith, R.A., et al., *Mitochondrial pharmacology.* Trends in pharmacological sciences, 2012. **33**(6): p. 341-352.
362. Fulda, S., L. Galluzzi, and G. Kroemer, *Targeting mitochondria for cancer therapy.* Nature reviews Drug discovery, 2010. **9**(6): p. 447-464.
363. Wallace, D.C., *Mitochondria and cancer.* Nature Reviews Cancer, 2012. **12**(10): p. 685-698.
364. Kleih, M., et al., *Direct impact of cisplatin on mitochondria induces ROS production that dictates cell fate of ovarian cancer cells.* Cell Death Dis, 2019. **10**(11): p. 851.
365. Wang, F.Y., et al., *Mitochondria-targeted platinum(II) complexes induce apoptosis-dependent autophagic cell death mediated by ER-stress in A549 cancer cells.* Eur J Med Chem, 2018. **155**: p. 639-650.
366. Murphy, M.P., *How mitochondria produce reactive oxygen species.* The Biochemical journal, 2009. **417**(1): p. 1-13.
367. Luna-Vargas, M.P.A., et al., *Mitochondrial Isolation and Real-Time Monitoring of MOMP.* Methods in molecular biology (Clifton, N.J.), 2019. **1877**: p. 121-130.
368. Wlodkowic, D., et al., *Apoptosis and beyond: cytometry in studies of programmed cell death.* Methods in cell biology, 2011. **103**: p. 55-98.
369. Marullo, R., et al., *Cisplatin induces a mitochondrial-ROS response that contributes to cytotoxicity depending on mitochondrial redox status and bioenergetic functions.* PloS one, 2013. **8**(11): p. e81162.
370. Murai, J., et al., *Trapping of PARP1 and PARP2 by Clinical PARP Inhibitors.* Cancer Res, 2012. **72**(21): p. 5588-99.
371. Chou, T. and N. Martin, *CompuSyn for drug combinations: PC software and user's guide: a computer program for quantitation of synergism and antagonism in drug*

combinations, and the determination of IC50 and ED50 and LD50 values. ComboSyn, Paramus, NJ, 2005.
372. Senra, J.M., et al., *Inhibition of PARP-1 by olaparib (AZD2281) increases the radiosensitivity of a lung tumor xenograft.* Mol Cancer Ther, 2011. **10**(10): p. 1949-58.
373. Muggia, F.M., M.G. Jimenez, and P. Murthy, *Platinum compounds: Their continued impact on ovarian cancer treatment.* Inorganica Chimica Acta, 2019. **496**: p. 119037.
374. Ding, D., et al., *γ-H2AX/53BP1/pKAP-1 foci and their linear tracks induced by in vitro exposure to radon and its progeny in human peripheral blood lymphocytes.* Scientific reports, 2016. **6**(1): p. 1-11.
375. Baldock, R.A., et al., *ATM localization and heterochromatin repair depend on direct interaction of the 53BP1-BRCT2 domain with γH2AX.* Cell reports, 2015. **13**(10): p. 2081-2089.
376. Tondera, D., et al., *SLP-2 is required for stress-induced mitochondrial hyperfusion.* The EMBO journal, 2009. **28**(11): p. 1589-1600.
377. Bellon, S.F., J.H. Coleman, and S.J. Lippard, *DNA unwinding produced by site-specific intrastrand crosslinks of the antitumor drug cis-diamminedichloroplatinum (II).* Biochemistry, 1991. **30**(32): p. 8026-8035.

ANNEXES

PAPER 1

Selectivity of Terpyridine Platinum Anticancer Drugs for G-quadruplex DNA

Certain metal complexes have shown a high affinity and selectivity towards a DNA secondary structure called G-quadruplexes. In this paper, we use different Platinum metal complexes synthesized in the lab (Unit of Chemistry and Modelling for the biology of cancer, Institut Curie) belonging to the Terpyridine family of metal complexes, to investigate if changing the structure of the ligand leads to a change in their affinity and selectivity for G-quadruplexes.

I wanted to investigate further and determine if changing the skeletal structure of the terpyridine platinum complexes, has an effect on the cytotoxicity of the drug. I also sought to examine if there is a significant cross-resistance with cisplatin by using two ovarian carcinoma cell lines A2780 and its cisplatin resistant counterpart A2780cis.

Determination of the cytotoxicity profile of these Platinum terpyridine complexes are important in order to decide the concentration of the drug to be used for the screening of their radiosensitization potential. Since, the target concentration for identifying radiosensitization potential is set for 70% cell proliferation, the survival curves of these complexes are extremely important for identifying the optimal concentration.

molecules

MDPI

Article

Selectivity of Terpyridine Platinum Anticancer Drugs for G-quadruplex DNA

Elodie Morel [1,2,†], Claire Beauvineau [1,2,†], Delphine Naud-Martin [1,2], Corinne Landras-Guetta [1,2], Daniela Verga [1,2], Deepanjan Ghosh [1,2], Sylvain Achelle [1,2,3], Florence Mahuteau-Betzer [1,2], Sophie Bombard [1,2,*] and Marie-Paule Teulade-Fichou [1,2,*]

1 Institut Curie, PSL Research University, CNRS-UMR 9187, INSERM U1196, F-91405 Orsay, France; emc.morel@gmail.com (E.M.); Claire.Beauvineau@curie.fr (C.B.); Delphine.Naud@curie.fr (D.N.-M.); Corinne.guetta@curie.fr (C.L.-G.); Daniela.Verga@curie.fr (D.V.); Deepanjan.ghosh@curie.fr (D.G.); sylvain.achelle@univ-rennes1.fr (S.A.); Florence.Mahuteau@curie.fr (F.M.-B.)

2 Université Paris Sud, Université Paris-Saclay, CNRS-UMR 9187, INSERM U1196, F-91405 Orsay, France

3 University Rennes, CNRS, ISCR-UMR 6226, F-35000 Rennes, France

* Correspondence: sophie.bombard@curie.fr (S.B.); marie-paule.teulade-fichou@curie.fr (M.-P.T.-F.); Tel.: +33-169-863-189 (S.B.); +33-169-863-086 (M.-P.T.-F.)

† These authors contributed equally to this work.

Academic Editor: Danzhou Yang

Received: 14 December 2018; Accepted: 22 January 2019; Published: 23 January 2019

Abstract: Guanine-rich DNA can form four-stranded structures called G-quadruplexes (G4s) that can regulate many biological processes. Metal complexes have shown high affinity and selectivity toward the quadruplex structure. Here, we report the comparison of a panel of platinum (II) complexes for quadruplex DNA selective recognition by exploring the aromatic core around terpyridine derivatives. Their affinity and selectivity towards G4 structures of various topologies have been evaluated by FRET-melting (Fluorescence Resonance Energy Transfert-melting) and Fluorescent Intercalator Displacement (FID) assays, the latter performed by using three different fluorescent probes (Thiazole Orange (TO), TO-PRO-3, and PhenDV). Their ability to bind covalently to the c-myc G4 structure in vitro and their cytotoxicity potential in two ovarian cancerous cell lines were established. Our results show that the aromatic surface of the metallic ligands governs, in vitro, their affinity, their selectivity for the G4 over the duplex structures, and platination efficiency. However, the structural modifications do not allow significant discrimination among the different G4 topologies. Moreover, all compounds were tested on ovarian cancer cell lines and normal cell lines and were all able to overcome cisplatin resistance highlighting their interest as new anticancer drugs.

Keywords: terpyridine platinum complexes; G-quadruplex

1. Introduction

Among the clinically relevant anticancer drugs, cisplatin is the most frequently used chemotherapeutic drug particularly employed for the treatment of testicular, ovarian, lung, head, and neck cancers. However, undesirable side effects, as well as the emergence of intrinsic or acquired resistances, currently limit its use and drive the design and development of more effective and less toxic analogues [1–3]. One of the considered strategies is to induce different DNA lesions and to target specific DNA structures as G-quadruplexes (G4) [4]. G4 consists in the stacking of G-quartets formed by four guanines linked together by reverse-Hoogsteen hydrogen bonds involving their N7. G4s arise from DNA (or RNA) sequences that contain at least four runs of guanines and are stabilized by physiological concentrations of alkali metal cations. A large amount of data provides evidence that such structures could form in cells and may play important roles in biology, such as genomic

stability, replication, transcription, translation, and telomere maintenance [5,6]. Bioinformatics [7,8], cellular imaging [9–13], as well as high throughput sequencings of genomic DNA or RNA [14–16] have contributed to identifying G4 prevalence at specific key genomic sequences such as telomere and promoter regions of oncogenes. So far, they have been identified as potential drug targets, especially in cancer [17–19]. Consequently, a large number of G4 binders based on organic planar structures [20] have been synthesized, including metal complexes [21–29]. As an example, RHPS4 was one of the first proof-of-concept drugs for the application of G-quadruplex-binding DNA molecules in anticancer therapies [30]. Among metal complexes, platinum complexes have been extensively studied (for review see References [23,24]). Moreover, platinum (II) can also form coordinate bonds with DNA, and very stable adducts may result [3]. Besides double-stranded DNA, numerous examples indicate that G4 can be covalently coordinated in vitro by platinum complexes either on adenines (N1 or N7) located within the loops or on the guanines (N7) belonging to external G-quartets that transiently open [31–36]. Moreover, some of them were shown to target telomeres in cellulo by inducing their uncapping [33], loss [37], dysfunction [38], and platination [39] while other complexes were shown to target c-myc oncogene [40,41]. Despite the large body of data, the mechanism of action and the determinants that drive the in vitro and cellular target recognitions of G4-platinum complexes are not yet established. Metal-terpyridine complexes were shown to have good affinity towards G4 structures, due to their square planar and square-based pyramidal geometries [21,29,36]: it is assumed that the metal ion increases the ability of the ligand to display π–π stacking interactions with the external G-tetrad and can replace a metal cation involved in the G-tetrad stabilization. The family of terpyridine platinum complexes offers the opportunity to analyze in detail a potential structure–activity relationship. Some of them have already been shown to stabilize and metallate in vitro human telomeric and c-myc G4s via selective platination of adenine residues on the loops [31,42,43]. An NMR structure of **Pt-ttpy** complexed with a G4 originating from the promoter region of c-myc oncogene suggests that the predominant interaction occurs through the stacking of **Pt-ttpy** to the outer G-quartet and drives the platination of the adenine residue at the 5′-end overhanging region [42]. All these data suggest that this ligand is well suited for both G4 recognition and metal coordination. In addition, it is important to underline that **Pt-ttpy** has been shown to be able to modify the structure of telomeres of cancerous cell lines by inducing their loss and direct metalation [37,39]. Moreover, one of its derivatives, **Pt-ctpy**, exhibits promising radiosensitization properties in human glioblastoma and lung cancer cells [44]. In conclusion, the terpyridine platinum complexes are, therefore, promising compounds employed for cancer treatment alone or in combination with radiation.

These encouraging properties prompted us to explore the aromatic core around the Pt-terpyridine motif to raise new properties in terms of G4 affinity and selectivity for drug discovery in comparison with **Pt-ttpy** that has already been evaluated on the human telomeric and c-myc G4s [29,31,36,43]. The binding properties of these complexes towards G4s were studied with a panel of oligonucleotides (G4 of various topologies and duplex DNA) using FRET-melting assay and Fluorescent Intercalator Displacement (FID), the latter being performed in the presence of three different probes, namely Thiazole Orange (TO) [45], TO-PRO-3 [46], and PhenDV [47], to determine the key elements for G4 affinity and selectivity. In parallel, platination selectivity and efficiency in competition conditions with duplex DNA have been studied. At last, the potential of these Pt(II)-complexes as antitumor agents has been evaluated by studying their effects on the growth of cisplatin-sensitive and cisplatin-resistant cell lines.

2. Results

2.1. Panel of Platinum Complexes

Terpyridine (**tpy**) scaffold is a well-used metal ligand and has been extensively derivatized by Vilar et al. to stabilize G4 [22] yet shows poor selectivity toward duplex DNA. To overcome this selectivity issue, the extension of the aromatic surface of the Pt-complexes was successfully

proposed. Both **Pt-BisQ** and **Pt-ttpy**, bearing respectively two quinoline moieties or a tolyl group, display higher affinity and selectivity towards telomeric G4 by limiting duplex DNA intercalation [29,31,36]. Our group synthesized **Pt-ctpy**, based on the **Pt-ttpy** scaffold, by adding a short in situ protonable chain [29]. This chain increases the water solubility and the affinity towards telomeric G4 by adding supplementary electrostatic interactions with the G4-DNA [48]. To assess a structure–activity-relationship study, we extended our panel of platinum complexes (Scheme 1).

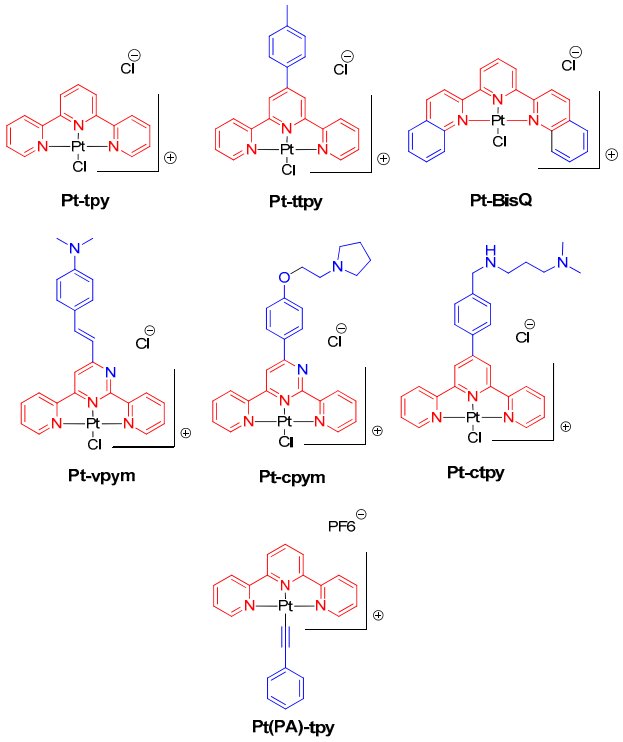

Scheme 1. The panel of metal complexes used in this study.

We changed the central pyridine of the terpyridine to a pyrimidine obtaining compounds **Pt-cpym** and **Pt-vpym**. The ligand **cpym** was prepared by a three-step synthesis starting from the already described pyrimidine 1 (Scheme 2) [49].

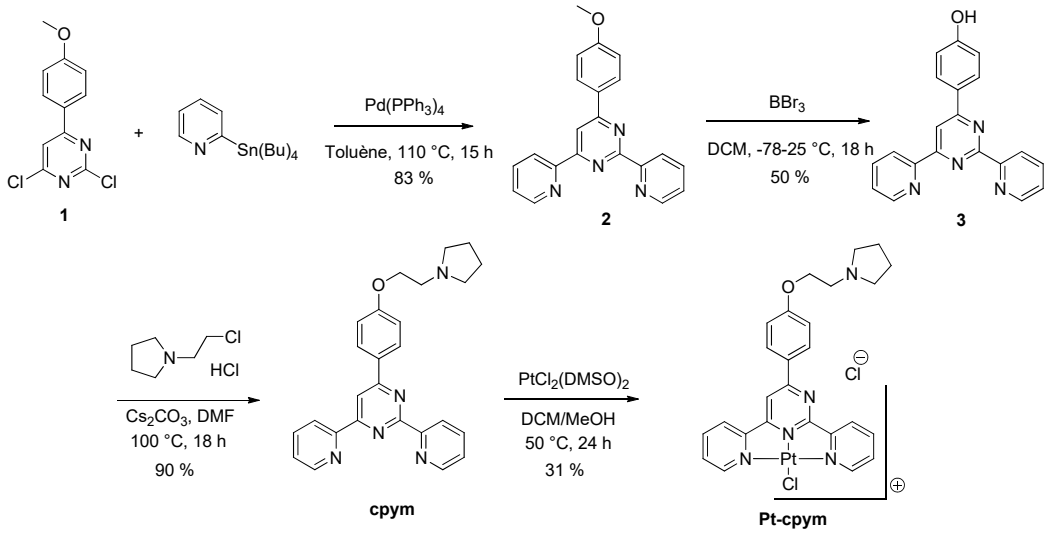

Scheme 2. The synthesis of **Pt-cpym**.

A double Stille coupling of dichloropyrimidine **1** afforded compound **2** in very good yield. Deprotection of the phenol group followed by O-alkylation allowed the formation of **cpym**. Compound **vpym**, bearing a vinyl linker, was prepared as described in the literature [50]. Both **vpym** and **cpym** ligands were platinated using $PtCl_2(DMSO)_2$. In addition, the aromatic surface of the complexes has also been extended on the metal center by replacing the labile ligand (Cl^-) on **Pt-tpy** by a phenylacetylene group (Figure S1). This complex was obtained by transmetallation of the in situ generated copper (I) phenylacetylide on the **Pt-tpy**. **Pt(PA)-tPy** does not contain any labile ligand and consequently is not able to metallate the DNA bases anymore.

2.2. Interaction Measurements

Binding properties towards G4 structures of the synthesized complexes were evaluated by performing biophysical assays, such as FRET-melting and G4-FID assays, in the presence of several G4-forming oligonucleotides representative of different folding topologies: 22AG human telomeric sequence (polymorphic), 21CTA human telomeric sequence variant (antiparallel), CEB25-WT minisatellite sequence (parallel with a central long propeller loop), and c-myc protooncogene sequence (parallel with short propeller loops).

The affinity and selectivity for G4-DNA of our panel of platinum complexes have been evaluated by FRET-melting [51] and G4-FID assays [45].

The ligand-induced stabilization measured by FRET-melting experiments (ΔT_m) is plotted for all compounds in Figure 1A–E, and the benchmark compound PhenDC3 was used as the control compound. Most importantly, **Pt-BisQ**, **Pt-ctpy**, and **Pt-ttpy** emerge as the best G4 stabilizers of the series, with ΔT_m values ranging from 10 to 25 °C for all G4-DNA structures (Figure 1A and Table S1). **Pt-vpym**, **Pt-cpym**, and **Pt-tpy** exhibit lower stabilizing capacities towards G4s while **Pt(PA)-tpy** shows a complete lack of stabilization properties. Among the different topologies exhibiting a similar melting temperature (around 60 °C), all complexes show similar stabilizing properties for 22AG, CEB25-WT, and 21CTA, as compared to c-myc that tends to be less stabilized by the different complexes. In addition, the selectivity of the compounds towards G4s vs. duplex DNA has been evaluated by carrying out competition experiments in the presence of 10 equivalents of ds26 (Figure 1B–E): all complexes show moderate selectivity since their ΔT_m is partially affected by the presence of ds26. One exception is represented by **Pt-vpym** which has stabilizing properties towards 21CTA and c-myc that increased in the presence of ds26 for a reason that is not yet elucidated but that is likely an artefact.

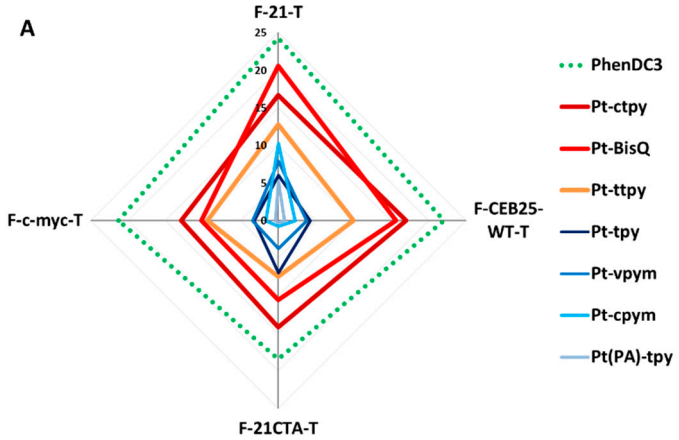

Figure 1. *Cont.*

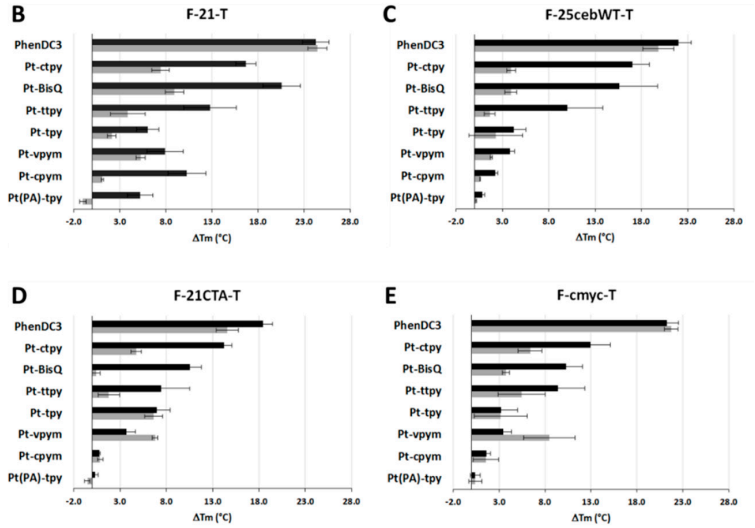

Figure 1. (**A**) A radar plot representing ΔT_m values obtained from FRET-melting experiments in the presence of various terpyridine-Pt complexes: **Pt-ctpy**, **Pt-BisQ**, **Pt-ttpy**, **Pt-tpy**, **Pt-vpym**, **Pt-cpym**, and **Pt(PA)-tpy** and PhenDC3, used as a control. ΔT_m of (**B**) F-21-T, (**C**) F-CEB25-WT-T, (**D**) F-21CTA-T, and (**E**) F-c-myc-T in the presence of 0 (black bars) or 10 μM (grey bars) of duplex DNA(ds26) used as the competitor in a K^+1 buffer, except for F-21-T (K^+10 buffer). The values are given in Table S1.

Since all these complexes (except for **Pt(PA)-tpy**) are susceptible to induce platination reactions, they can be exacerbated by a high temperature and by an increased number of nucleophilic sites which are exposed during unfolding (increased N7 G free sites); we wonder if such a reaction could occur during FRET-melting experiments and to what extent. Therefore, we followed the extent of platination reactions of c-myc and 22AG (same sequences as those used for FRET-melting but without fluorophore labeling) as a function of the melting temperature using ^{32}P-labelled oligonucleotides and denaturing gel electrophoresis (Figure 2). **Pt-ttpy**, **Pt-tpy**, and **Pt-BisQ** clearly platinate c-myc and 22AG (except for **Pt-BisQ**) during melting temperature experiments and the extent of platination depends both on the sequence (c-myc (60%) > 22AG (20%)) and on the complex (**Pt-ttpy** > **Pt-tpy** > **Pt-BisQ**). These results suggest that these platination reactions may therefore bias the melting temperature value. **Pt-ctpy**, **Pt-vpym**, and **Pt-cpym** do not give any defined platination product, and thus, they were not evaluated in this melting temperature condition (see Section 2.3. Quadruplex Platination).

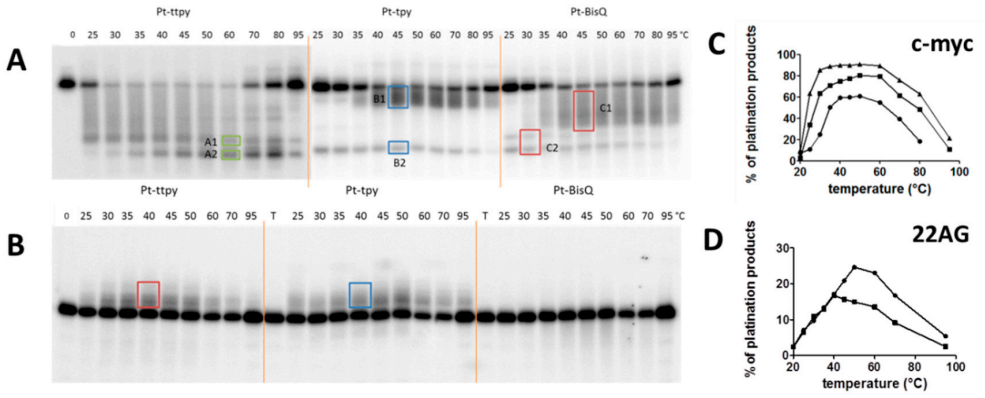

Figure 2. The denaturing gel of the platination reactions of (**A**) c-myc and (**B**) 22AG (0.2 μM) in the presence of **Pt-ttpy** (square), **Pt-tpy** (triangle), and **Pt-BisQ** (circle) (1 μM, 5 eq) and the quantification of the platination products for (**C**) c-myc and (**D**) 22AG were conducted under FRET-melting conditions: A temperature gradient of 25 °C for 5 min and then 0.5 °C/min up to 95 °C using K^+1 and K^+ 10 buffers, respectively. An example of the quantified platination products are highlighted in both (**A**) and (**B**) by colored squares.

Consequently, the relative binding ability of the complexes for the various G4s should be determined in the conditions that are less favorable to platination reaction, the room temperature and short incubation time: all these conditions are gathered in a G4-FID assay. A G4-FID assay is generally performed in the presence of thiazole orange (TO) as an on–off fluorescent probe for DNA structures [48]. TO-G4-FID allowed us to evaluate the binding properties for all the platinum complexes (Figure 3A, Figure S2 and Table S2), except **Pt-vpym** which had spectral properties that are incompatible with TO (Figure S3). The metallic complexes can be ranked in two groups: the first group, including **Pt-BisQ**, **Pt-ctpy**, and **Pt-ttpy**, efficiently displaces TO from all the G4 (>80% displacement at 1 μM) as compared to the duplex ds26 (<20% displacement) (Figures S2 and S4), whereas the second group, including **Pt-cpym**, **Pt-tpy**, and **Pt(PA)-tpy**, displaces less efficiently TO (<60%). For all of them, only a small displacement of the probe is observed in the presence of duplex ds26 (Figures S2 and S4). As the binding constants of TO for all the tested G4s are in the same range (~10^6 M^{-1}), we could assess that none of the metal complexes has a clear preference for a G4 structure.

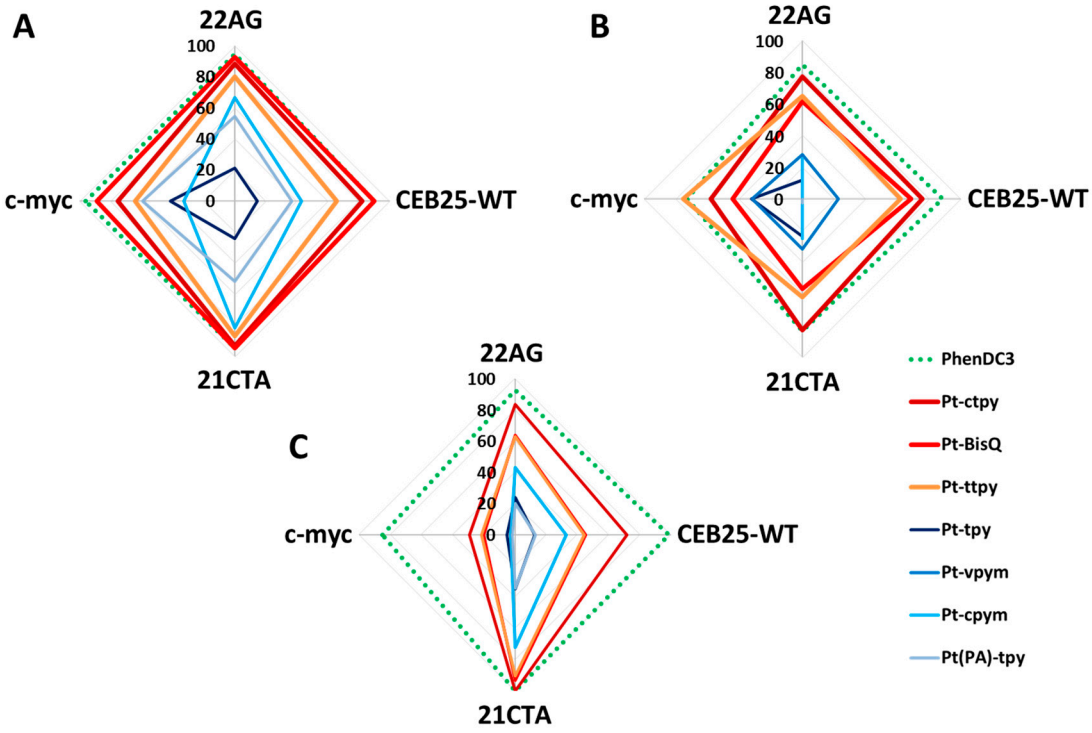

Figure 3. The radar plot representing the percent of the probe displacement at 1 μM of the Pt(II) complexes (**Pt-ctpy**, **Pt-BisQ**, **Pt-ttpy**, **Pt-tpy**, **Pt-vpym**, **Pt-cpym**, and **Pt(PA)-tpy**) and the PhenDC3 used as control for the G4-FID assay. The experiments are performed in the presence of 22AG, c-myc, 21CTA, and CEB25-WT with (**A**) Thiazole Orange (TO) (2 eq.), (**B**) TO-PRO-3 (2 eq.), or (**C**) Phen DV (1.5 eq.) in K^+100 buffer. The values are given in Tables S2–S4.

However, in order to evaluate **Pt-vpym**, we used the TO-PRO-3-G4-FID assay developed in our group [48] to compare the entire panel of ligands. Of interest, TO and TO-PRO-3 exhibit similar affinity constants towards all the tested G4s structures (*Ka* ~10^6 M^{-1}) [48]. The TO-PRO-3-G4-FID assay shows that **Pt-vpym** displays a moderate affinity for G4 structures (30% displacement) with poor selectivity vs. duplex DNA (Figure 3B, Figures S2 and S4 and Table S3) in contrast to **Pt-BisQ**, **Pt-ctpy**, and **Pt-ttpy** (>60% displacement). Of note, only a weak displacement for **Pt-tpy**, **Pt-cpym**, and **Pt(PA)-tpy** has been observed.

In addition, we tested our complexes in a G4-FID assay using PhenDV which is an off–on probe developed in our laboratory [47]. This probe improves the sensitivity of the G4-FID assay, as the read out, different from the two previous reported FID assays, relies on increased fluorescence: PhenDV

fluorescence is strongly quenched when it is bound to G4 DNA and fully restored when it is displaced by the ligand. Different from TO and TO-PRO-3, PhenDV displays a higher affinity towards G4 [47] (Table 1) and does not interact with duplex DNA. Thus, the displacement assays were carried on only with G4 sequences. In contrast to TO and TO-PRO-3, the binding constants of PhenDV are largely spread from 10^6 M^{-1} to 6×10^7 M^{-1} (Table 1). For 21CTA and 22AG, for which PhenDV displays the same affinity, the dye displacement is very similar for each metal complex. At the opposite, as PhenDV is much more affine than TO for CEB25-WT (10^7 M^{-1} versus 10^6 M^{-1}) and for c-myc (6×10^7 M^{-1} versus 5×10^6 M^{-1}), the dye displacement by the complexes are less efficient, especially in the case of c-myc. However, as for TO and TO-PRO-3, the same complex ranking has been observed: **Pt-ctpy**, **Pt-BisQ**, and **Pt-ttpy** are the most affine ligands, and the least affine are **Pt-cpym**, **Pt-tpy**, and **Pt(PA)-tpy** (Figure 3C and Table S4). In conclusion, FID experiments led to more similar rankings than the FRET experiments for the evaluated metal complexes on the different tested G4.

Table 1. The PhenDV and TO affinity constants measured in the presence of 22AG, c-myc, 21CTA, and CEB25-WT G4 structures.

DNA	Sequence (5′ to 3′)	PhenDV		TO	
		K_A (M^{-1})	Dye:DNA	K_A (M^{-1})	Dye:DNA
22AG	$AG_3T_2AG_3T_2AG_3T_2AG_3$	3×10^6 [a]	2:1	1×10^6 [a]	1:1
c-myc	$TGAG_3TG_3TAG_3TG_3TA_2$	6×10^7	4:1	5×10^6 [b]	1:1
21CTA	$AG_3CTAG_3CTAG_3CTAG_3$	1×10^6	3:1	1×10^6 [b]	1:1
CEB25-WT	$AG_3TG_3TG_3TG_3T$	1×10^7 [a]	4:1	1×10^6 [a]	1:1

[a] Determined in Reference [47]. [b] Determined in Reference [48].

2.3. Quadruplex Platination

Previous studies led by Bertrand et al. have shown that the terpyridine platinum complexes **Pt-tpy** and **Pt-ttpy** were also able to react with the human telomeric G4 (22AG) exclusively with adenines located within the loops whereas **Pt-BisQ** was not able to metallate 22AG [31]. As well, **Pt-ttpy** was found to platinate at the 3′-end exclusively in the proximity of the external G-quartet of 22AG; meanwhile, **Pt-tpy** metallates the most accessible nucleophilic base of 22AG [35], suggesting no tetrad interaction. It has been hypothesized that the **Pt-ttpy** coordination to DNA is, therefore, being driven by its affinity for the G4 structure, a hypothesis that has been supported by the demonstration of the stacking of **Pt-ttpy** on the external quartet of the c-myc derived G4 [42].

The platination reaction of the c-myc oncogene in the presence of our set of candidates (**Pt-tpy**, **Pt-ttpy**, **Pt-BisQ**, **Pt-ctpy**, **Pt-vpym**, and **Pt-cpym**) bearing a labile ligand was followed by gel electrophoresis and the binding sites identified by 3′-exonuclease digestion experiments.

The five platinum complexes were incubated for 18 h at 32 °C with pre-folded 5′-end ^{32}P radiolabeled c-myc DNA (10 or 100 μM) and loaded on denaturing polyacrylamide gel electrophoresis (Figure 4).

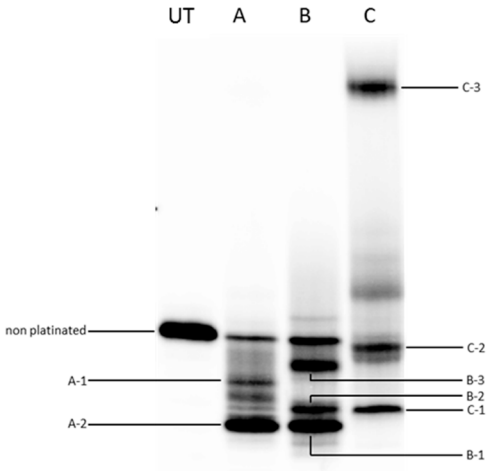

Figure 4. The denaturating gel electrophoresis (15% acrylamide) of platination adducts generated by (**A**) **Pt-ttpy**, (**B**) **Pt-tpy**, and (**C**) **Pt-BisQ** in the presence of c-myc (10 μM for (**A**) and (**B**) and 100 μM for (**C**)) in K^+100 buffer after 18 h incubation at 32 °C. UT is untreated.

Two main accelerated bands (A1 and A2) were detected for **Pt-ttpy** and three were detected for **Pt-tpy** (B1, B2, and B3) in the presence of 10 μM of DNA. However, for **Pt-BisQ**, two accelerated bands (C1 and C2) and one retarded band (C3) were only detected at higher DNA concentration (100 μM). It is noteworthy that c-myc platination products migrate faster that the non-platinated G4, resulting in a stark contrast if compared to 22AG in which platination products migrate slower (Figure 2): this is due to the presence of the still folded G4 structures that resist to denaturation, as already found [42]. Non-defined platination products were detected for **Pt-ctpy**, **Pt-cpym**, and **Pt-vpym** on gel electrophoresis at 100 μM of DNA (Figure S5), suggesting that the structure unfolds during platination giving rise to many platinated products. The platination sites of **Pt-ttpy**, **Pt-tpy**, and **Pt-BisQ** were determined by 3′-exonuclease digestion, which stops at the platinated base, followed by a de-platination treatment of the digested fragments with NaCN (Figures S6 and S7). The exact length of the digested de-platinated fragment was deduced from its migration compared with the one of a digestion ladder of the c-myc sequence on a denaturating gel electrophoresis.

Pt-ttpy forms a platination adduct on the 3′-end of the oligonucleotide, mainly on A21/A22 bases but also, to a lesser extent, on the inner loop of the quadruplex structure, on A12/G13 bases (Figure 5A). In addition, the less affine complex **Pt-tpy** can also form adducts on both flanking sequences of the G4 structure, on T20/A21 at the 3′-end and on G2/A3 on the 5′-end, while the larger aromatic complex **Pt-BisQ** forms exclusively a 3′-end adduct on G19/T20 bases with c-myc (Figure 5B).

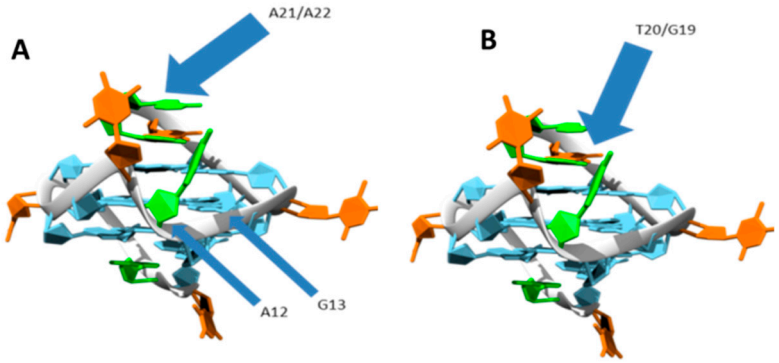

Figure 5. A schematic representation of the platination sites for (**A**) **Pt-ttpy** and (**B**) **Pt-BisQ** on c-myc G4. The platination sites are in indicated in bold.

2.4. Kinetics and Selectivity Studies

The selectivity of c-myc platination produced by **Pt-ttpy** and **Pt-tpy**, the two complexes able to produce efficient platination products at low G4 concentration, was finally assessed by gel electrophoresis by employing the same concentrations used for the FRET-melting experiments. The formation of the platinated products was followed as a function of time (Figures S8 and S9) on two ^{32}P-radiolabeled DNA, c-myc* and ds26*. **Pt-ttpy** is able to metallate a large amount of G4 DNA c-myc* within 120 min of incubation (Figure 6).

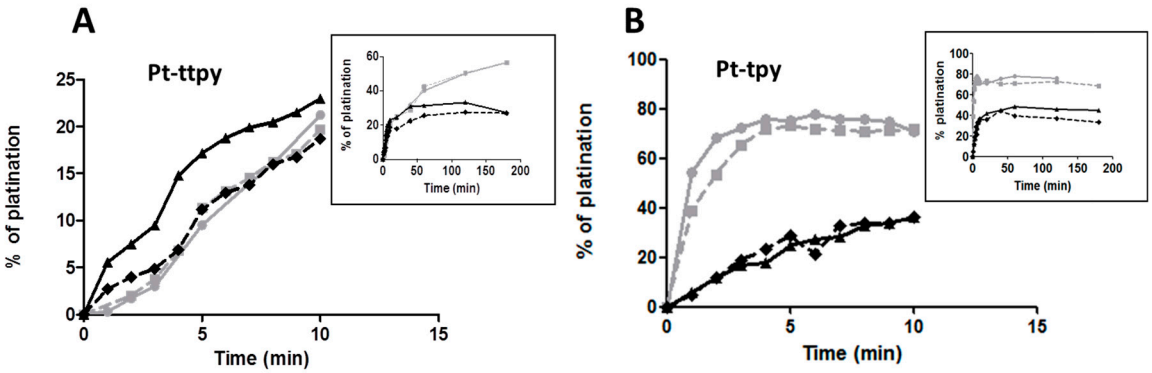

Figure 6. The kinetics of the formation of the platination products on ^{32}P radiolabelled c-myc* (0.2 μM) with (grey square) or without (grey circle) cold duplex competitor DNA ds26 (10 μM) or on ^{32}P radiolabelled ds26* (10 μM) with (black triangle) or without (black diamond) cold c-myc competitor (0.2 μM) in the presence of (**A**) **Pt-ttpy** or (**B**) **Pt-tpy** in a K^+10 buffer quantified from the denaturing acrylamide gel electrophoresis (Figures S8 and S9).

When adding an excess of duplex DNA (ds26) as a competitor, neither the amount of platinated products nor platination kinetics are affected. In contrast, when c-myc was added as a competitor, the platination kinetic of ds26* was affected. These results confirm the high selectivity of the platination reaction performed by **Pt-ttpy** with G4 DNA structures.

In contrast, the platination of c-myc* by **Pt-tpy** is more affected by the presence of the duplex competitor whereas the platination of ds26* is not affected by the addition of c-myc. These results confirm the low binding selectivity of **Pt-tpy** for G4. The amount of G4 adducts obtained with **Pt-tpy** is higher than with **Pt-ttpy**, confirming that **Pt-tpy** can react easily with all the accessible nucleophilic sites of the structure without previous stacking to the external tetrad. In contrast, the reactivity of **Pt-ttpy** is limited to the residues in the vicinity of the external G-quartets which have been shown by NMR to be its main binding sites [42].

2.5. In Vitro Cytotoxicity

Finally, we evaluated the effect of the complexes on the growth of two ovarian cancer cell lines A2780 and A2780cis, which are respectively sensitive and resistant to the antitumor drug cisplatin, and one normal lung cell line CCD19Lu. All cell lines have been treated for 96 h with increasing doses of complexes. Platinum complexes show cytotoxicity in the μM range (IC_{50} from 0.08 to 6 μM) as a function of their structure and can be classified as follows: **Pt(PA)-tpy** > **Pt-vpym** > **cisplatin** > **Pt-ttpy** ≥ **Pt-tpy** ≥ **Pt-ctpy** > **Pt-cpym** > **Pt-BisQ** (Table 2). Moreover, none of the platinum complexes show a significant cross-resistance to cisplatin since no significant differences between cisplatin-sensitive and resistant cell lines could be highlighted (IC_{50}ratio A2780cis/A2780 < 1.6). However, all of them show no specificity for cancer cell lines, similar to the clinical anticancer drug cisplatin.

Table 2. The IC_{50} (μM) of the various platinum complexes calculated from the proliferation of A2780, A2780cis, and CCD19Lu cell lines after 96 h treatments and their resistance factor (IC_{50}ratio A2780cis/A2780).

	A2780	A2780 cis	Resistance Factor	CCD19Lu
Pt-BisQ	4.00	6.00	1.5	4.10
Pt-ctpy	4.60	5.00	1.1	5.20
Pt-ttpy	2.50	2.50	1.0	1.75
Pt-cpym	3.80	5.00	1.3	1.80
Pt-vpym	0.70	0.40	0.6	0.70
Pt-tpy	3.00	5.00	1.6	3.00
Pt(PA)-tpy	0.08	0.05	0.6	0.12
cisplatin	0.33	3.00	9.1	0.20

3. Discussion

In this study, we explored the chemical space around the terpyridine aromatic core to put in evidence the key elements that drive affinity and selectivity for various G4-DNA exhibiting polymorphic (22AG), antiparallel (21CTA), long looped parallel (CEB25-WT), and short looped parallel (c-myc) topologies. The FRET-melting assays pointed out three ligands exhibiting higher binding inducing stabilization independently from the G4 topology (Figure 1A), namely **Pt-BisQ**, **Pt-ctpy**, and **Pt-ttpy** ($\Delta T_m > 10$ °C). Whereas **Pt-vpym**, **Pt-cpym**, and **Pt-tpy** showed less stabilizing capacities ($\Delta T_m < 10$ °C), and no stabilization was observed for **Pt(PA)-tpy**. However, their selectivity for G4 over duplex DNA is moderate since their ΔT_m decreases significantly in the presence of competitor duplex DNA (Figure 1B–E). This trend was then confirmed by FID assays. Interestingly, PhenDV was a better probe than TO-PRO-3 and TO able to discriminate the relative affinity of the complexes for each G4 topology. Indeed PhenDV, which displays higher binding constants for all of the evaluated G4s, was shown to discriminate more significantly among high affinity G4 ligands [47]. None of the complexes was able to displace PhenDV from c-myc in contrast to TO and TO-PRO-3, the exception represented by the benchmark l ligand, $PhenDC_3$. This is consistent with the particularly high affinity of PhenDV for the c-myc structure (Table 1) which induces a harsh competition as compared to the other markers, thereby leading to the selection of only very high affinity ligands (e.g., PhenDC3). Alternatively, other binding sites cannot be excluded for the platinum complexes in the presence of PhenDV.

It is quite surprising that the relative binding properties of the complexes determined from FRET-melting and FID experiments are consistent despite the formation of non-negligible amounts of platinum adducts (up to 50%) during the FRET-meting experiments (Figure 2). This suggests that the platination of the bases already accessible within the loops or released from the G-quartets during the thermal denaturation conditions does not shift significantly the equilibrium towards the unfolded state in FRET conditions. Nevertheless, it could explain the lower ΔT_m observed on c-myc versus 22AG independently from the metal complex since the amount of platination products is more important for c-myc than 22AG in these conditions. Of note, these FRET-melting experiments, done in thermal-denaturing conditions, lead to an irreversible process. Indeed, the N7 platination of guanines would prevent the formation of the G-quartets and consequently the folding in G4 [52] in thermal renaturation conditions.

Altogether the data highlight the need of different and complementary methods for the determination of the relative affinity of ligands for G4.

Considering the structure–activity relationship, our data show that the extension of the aromatic core modifies the affinity of the complexes for the G4-DNA structures. Since **Pt(PA)-tpy** did not show any affinity for G4, it can be claimed that introducing a phenylacetylene group on the platinum may support a decrease in affinity for the G4. While extending the terpyridine by a tolyl (**Pt-ttpy**), a tolyl with a protonable side chain (**Pt-ctpy**), or replacing the terpyridine core by a bisquinoline (**Pt-BisQ**) increase the affinity of all the complexes for G4-DNA, modifying the terpyridine core (**Pt-vpym** and **Pt-cpym**) reduces the affinity for G4. Interestingly, **Pt-ttpy** showed a high affinity for 22AG. This could

be related to the recent results showing that one of the cellular targets of **Pt-ttpy** is indeed telomeric DNA [37,39,44]. Noteworthily, while the selectivity of the present complexes for G4 over duplex DNA is moderate in vitro (Figure 2B–E), the example of **Pt-ttpy** indicates that low selective ligands can reach their cellular target even in the presence of genomic DNA.

One expected property of these complexes is to form mono-adducts with DNA. Our in vitro data show that the relative platination of c-myc G4 over duplex DNA by **Pt-ttpy** and **Pt-tpy** is correlated to the relative affinity for both structures, suggesting that the platination events are driven by the recognition of the DNA structures. However, the relative affinity of present complexes for G4 is not correlated to their platination efficiency. In this regard, **Pt-BisQ**, one of the most relevant complexes, is less susceptible to induce platination of c-myc G4 in vitro if compared to **Pt-ttpy**, **Pt-ctpy**, and **Pt-tpy** and does not show any alkylation on 22AG G4 [31]. This behavior can be explained by i) slow exchange kinetics of the chloride, mandatory for the direct coordination of Pt(II) to the nucleophilic site [53], and ii) the effect produced by the extension of the terpyridine core that can mask the nucleophilic sites of the G4 and/or the accessibility of Pt(II) [42]: indeed, the platinated bases depend on the nature of the complexes (A12, G13, A21, and A22) for **Pt-ttpy** and G19 for **Pt-BisQ**.

Finally and importantly, the IC_{50} of the complexes are in the μM range, except for **Pt(PA)-tpy** which is active at nM concentration in A2780 cell lines. However, all the complexes overcome the cisplatin resistance in A2780cis cell lines, providing new interesting anticancer drug candidates. This suggests that they may enter cells via a pathway independent from the copper carrier proteins used by cisplatin [54]. Among them, **Pt(PA)-tpy** is the most efficient complex despite its inability to form DNA adducts. Therefore, our results pointed out that the cellular efficiency of a panel of platinum complexes is not strictly related to their affinity for the various G4-DNA structures or their capacity to platinate in vitro DNA structures. Many other factors, in addition to their cellular target, must be taken into account, such as their cellular uptake and their binding to genomic DNA, as already shown for other platinum complexes [33,55]. For example, previous studies showed that the genomic DNA binding of **Pt-tpy** and **Pt-ttpy** is less efficient than the one of cisplatin, as compare to their cellular uptake.

In conclusion, the modulation of the terpyridine core of platinum complexes may greatly influence their in vitro affinity for G4 and their capacity to induce specific metallation of G4 in vitro and may be promising as future anticancer drugs overcoming the resistance to cisplatin. The identification of the cellular targets, which is ongoing, could definitely indicate if they also represent potential drugs targeting G4 in cellulo.

4. Materials and Methods

4.1. Materials

Oligonucleotides purified by reversed-phase HPLC were purchased from Eurogentec (Angers, France). The dual fluorescently labeled oligonucleotides were purchased from Eurogentec. The donor fluorophore was 6-carboxyfluorescein (FAM) and the acceptor fluorophore was 6-carboxytetramethylrhodamine (TAMRA).

PhenDV was synthesized as already described [47].

Stock solutions of the ligands (2 mM in DMSO) were used for G4-FID, FRET-melting assay, and fluorimetric titration, unless otherwise stated, and were stored at −20 °C. TO, TO-PRO-3, and cacodylic acid were purchased from Aldrich and used without further purification. Stock solutions of TO (2 mM in DMSO), PhenDV (2 mM in DMSO), and TO-PRO-3 (1 mM in DMSO) were used for the G4-FID assay. Fluorescent probe powders and solutions were stored and used, protected from light, and used as aliquots to avoid freeze–thaw cycles.

The FRET-melting measurements are performed on a 7900HT Fast Real-Time PCR System (Applied Biosystems, Foster City, CA, USA) with a Microamp Fast optical 96-well reaction plate (Applied Biosystems). HT-G4-FID measurements were performed on a FLUOstar Omega microplate reader (BMG Labtech, Champigny-sur-Marne, France) with 96-well Non-Binding Surface black

with black bottom polystyrene microplates (Corning). Fluorescence measurements (i.e., fluorimetric titration) were performed on a Cary Eclipse Fluorescence spectrophotometer (Agilent Technologies, Les Ulis, France).

4.2. Organic Synthesis

^{1}H and ^{13}C spectra were recorded at 300 MHz and 75 MHz on a Bruker Avance 300 spectrometer and at 500 MHz and 126 MHz on a bruker Avance 500 spectrometer (at the NMR service of ICSN) using TMS as the internal standard (Figure S1). DMSO-d_6 and $CDCl_3$ were purchased from SDS. Proton chemical shifts are reported in ppm (δ) with the solvent reference as the internal standard (DMSO-d_6, δ 2.50 ppm; $CDCl_3$, δ 7.26 ppm). Data are reported as follows: chemical shift (multiplicity (singlet (s), doublet (d), triplet (t), and multiplet (m)), coupling constants (Hz), and integration). LC-MS spectra (ESI in the positive ion mode) were performed with a Waters ZQ instrument (source voltage 50–75 kV). High resolution mass spectrometry (HR-MS) was performed at the Small Molecule Mass Spectrometry platform of IMAGIF (Centre de Recherche de Gif, Gif-sur-Yvette, France). Analytical thin-layer chromatography (TLC) was performed using silica gel 60 Å UV254 precoated plates (0.20 mm thickness) from Macherey Nagel (Hoerdt, France). Visualization was accomplished by irradiation with a UV lamp. Preparative flash chromatography was carried on a CombiFlash Companion) from Teledyne Isco(Lincoln, NE, USA) equipped with packed silica cartridges from Interchim (Montluçon, France). Starting materials were purchased from Sigma-Aldrich (Lyon, France), Alfa Aesar (Karlsruhe, Germany), and Acros (Geel, Belgium). The 2,4-dichloro-6-(4-methoxyphenyl)pyrimidine (CAS [154499-86-2]) [49], vpym (CAS [1297529-36-2]) [50] were prepared as described in the literature.

4-(4-Methoxyphenyl)-2,6-bis(pyridin-2-yl)pyrimidine (**1**). ^{1}H-NMR (300 MHz, $CDCl_3$): δ (ppm) 8.91 (d, *J* = 3.0 Hz, 1H), 8.76 (m, 4H), 8.39 (d, *J* = 9.0 Hz, 2H), 7.92 (m, 2H), 7.58–7.38 (t, *J* = 8.0 Hz, 2H), and 7.06 (d, *J* = 9.0 Hz, 2H), 3.91 (s, 3H); ^{13}C-NMR (75 MHz, DMSO-d_6): *δ* (ppm) 165.2, 163.9, 163.6, 162.1, 155.6, 154.4, 150.1, 149.4, 137.1, 136.8, 129.5, 129.2, 125.6, 124.6, 124.1, 122.4, 114.2, 111.1, and 55.4; and LR-MS (ESI-MS) m/z = 341.13 $[M + H]^+$.

In a dry round-bottomed flask, 2,4-dichloro-6-(4-methoxyphenyl)pyrimidine (677 mg, 2.65 mmol, 1.0 eq) and $Pd(Ph_3)_4$ (460 mg, 0,39 mmol, 0.15 eq) are introduced under argon atmosphere. Dry toluene (20 mL) is added, and a cooling system is installed. The mixture is degassed for 10 min before the addition of 2-(tributylstannyl)pyridine (2.1 mL, 6.63 mmol, 2.5 eq) and heated at reflux (110 °C) for 15 h. Then, 30 mL of water is added. The crude mixture is filtrated on a pad of celite and washed with ethyl acetate, followed by extraction. The combined organic phase is dried over $MgSO_4$, filtered and concentrated to dryness. The product is purified by column chromatography (Al_2O_3—cyclohexane/AcOEt 50/50) to afford the expected product (749 mg, 83%).

4-(2,6-Bis(pyridin-2-yl)pyrimidin-4-yl)phenol (**2**). ^{1}H-NMR (300 MHz, DMSO-d_6): *δ* (ppm) 10.15 (s, 1H), 8.84 (s, 2H), 8.74 (s, 1H), 8.65 (t, *J* = 7.5 Hz, 2H), 8.29 (d, *J* = 7.0 Hz, 2H), 8.07 (dt, *J* = 14.0, 7.0 Hz, 2H), 7.76–7.51 (m, 2H), and 6.99 (d, *J* = 9.0 Hz, 2H); ^{13}C-NMR (75 MHz, DMSO-d_6): *δ* (ppm) 165.3, 163.0, 161.6, 156.2, 151.8, 149.5, 147.5, 146.9, 143.4, 138.6, 129.9, 128.9, 126.9, 126.1, 125.7, 122.8, 116.1, and 111.9; and LR-MS (ESI-MS) m/z = 327.31 $[M + H]^+$.

Compound (**1**) (200 mg, 0.58 mmol, 1.0 eq) is dissolved in anhydrous CH_2Cl_2 (10 mL) under argon atmosphere. The mixture is cooled down to −78 °C, and BBr_3 (200 µL, 2.11 mmol, 3.6 eq) is added dropwise. After cooling back to room temperature, the mixture is stirred for one night and quenched by ice addition. The red solid is filtered, washed, and crystallized in methanol (96 mg, 50%).

2,4-Di(pyridin-2-yl)-6-(4-(2-(pyrrolidin-1-yl)ethoxy)phenyl)pyrimidine (**cpym**). ^{1}H-NMR (300 MHz, $CDCl_3$): *δ* (ppm) 8.86 (m, 1H), 8.71 (m, 4H), 8.32 (d, *J* = 9.0 Hz, 2H), 7.85 (m, 2H), 7.37 (m, 2H), 7.02 (d, *J* = 9.0 Hz, 2H), 4.15 (t, *J* = 6.0 Hz, 2H), 2.89 (t, *J* = 6.0 Hz, 2H), 2.60 (m, 4H), and 1.77 (m, 4H); ^{13}C-NMR (75 MHz, $CDCl_3$): *δ* (ppm) 165.3, 164.0, 163.7, 161.5, 155.7, 154.5, 150.1, 149.5, 137.3, 137.0, 129.6, 129.3, 125.5,

124.8, 124.2, 122.5, 114.9, 111.3, 77.6, 77.2, 76.7, 67.3, 55.1, 54.9, and 23.6; LR-MS (ESI-MS) m/z = 424 [M + H]$^+$; HR-MS (ESI+) m/z = 424.2137; and found, 424.2125.

In a round-bottomed flask under argon atmosphere, 4-(2,6-bis(pyridin-2-yl)pyrimidin-4-yl)phenol (50 mg, 0.15 mmol, 1.0 eq), N-(2-chloroethyl)pyrrolidine hydrochloride (26 mg, 0.15 mmol, 1.0 eq), and cesium carbonate (149 mg, 0.46 mmol, 3 eq) are introduced with DMF (2 mL). The mixture is stirred overnight at 100 °C. The solvent is removed under vacuum. Ethyl acetate (20 mL) and water (20 mL) are added for extraction. The combined organic phase is dried over $MgSO_4$, filtered, and concentrated to dryness to afford the compound **cpym** (58 mg, 89%).

Chloro-(2,4-di(pyridin-2-yl)-6-(4-(2-(pyrrolidin-1-yl)ethoxy)phenyl)pyrimidine)-platinum(II) Chloride (**Pt-cpym**). ^{1}H-NMR (300 MHz, DMSO-d_6): δ (ppm) 9.25 (s, 1H), 9.04 (d, J = 8.0 Hz, 1H), 8.75 (dd, J = 10.0, 5.5 Hz, 2H), 8.67–8.40 (m, 5H), 7.96 (dd, J = 12, 5.5 Hz, 2H), 7.16 (d, J = 9.0 Hz, 2H), 4.31 (t, J = 4.5 Hz, 2H), 3.02 (s, 2H), 2.74 (m, 4H), and 1.78 (m, 4H); ^{13}C-NMR (126 MHz, DMSO-d_6): δ 166.2, 163.4, 161.8, 159.5, 156.5, 154.6, 151.8, 151.5, 143.0, 142.7, 131.0, 130.94, 130.7, 127.7, 127.2, 126.5, 115.5, 113.1, 54.1, 53.8, 29.2, and 23.1; LR-MS (ESI-MS) m/z = 654 [M + H]$^+$; HR-MS (ESI+): m/z = 653.1395 calculated for $C_{26}H_{25}N_5OClPt$; and found, 653.1367.

In a round-bottomed flask under argon atmosphere, cpym (40 mg, 0.09 mmol, 1.0 eq) is dissolved in a minimal amount of CH_2Cl_2 (3 mL). Platinum catalyst $Pt(DMSO)_2Cl_2$ (40 mg, 0.09 mmol, 1.0 eq) is introduced dropwise with methanol (3 mL). The mixture is stirred at 50 °C for 20 h. The crude product is filtered on membrane, washed with a mixture of MeOH/CH_2Cl_2/acetone, and dried by Et_2O. **Pt-cpym** is obtained as a dark powder (20 mg, 31%).

Chloro-(E)-4-(2-(2,6-di(pyridin-2-yl)pyrimidin-4-yl)vinyl)-N,N-dimethylaniline-platinum(II) Chloride (**Pt-vpym**). ^{1}H-NMR (500 MHz, DMSO-d_6): δ 8.93 (d, J = 5.0 Hz, 1H), 8.90 (d, J = 5.0 Hz, 1H), 8.65 (d, J = 7.5 Hz, 1H), 8.60–8.50 (m, 3H), 8.48 (d, J = 7.5 Hz, 1H), 8.24 (d, J = 15.5 Hz, 1H), 8.05–7.99 (m, 2H), 7.58 (d, J = 9.0 Hz, 2H), 7.05 (d, J = 15.5 Hz, 1H), 6.72 (d, J = 9.0 Hz, 2H), and 3.04 (s, 6H);^{13}C-NMR (126 MHz, DMSO-d_6): δ 166.6, 161.6, 157.9, 156.8, 155.2, 152.5, 151.8, 151.6, 144.8, 142.8, 142.5, 131.1, 130.7, 130.3, 126.7, 126.6, 122.0, 118.4, 114.2, 112.1, and 45.7; LR-MS (ESI-MS) calculated for [$C_{24}H_{21}N_5ClPt$]$^+$, m/z = 610.22 [M + H]$^+$; HR-MS (ESI+): m/z = 609.1133; and found, 609.1140.

In a dry round-bottomed flask under argon atmosphere, **vpym** (50 mg, 0.13 mmol, 1.0 eq) is dissolved in the minimal amount of CH_2Cl_2 (3 mL). Platinum catalyst $Pt(DMSO)_2Cl_2$ (55.9 mg, 0.13 mmol, 1.0 eq) is introduced dropwise with methanol (3 mL). The dark reaction mixture is stirred overnight at room temperature. The crude product is filtrated on nylon membrane, washed with a mixture of MeOH/CH_2Cl_2/acetone, and dried by Et_2O. **Pt-vpym** is obtained as a dark purple solid (54 mg, 74%).

Phenylethylny-(2,6-bis(pyridin-2-yl)pyridine)-platinum(II) Hexafluorophosphate (**Pt(PA)-tpy**). ^{1}H-NMR (300 MHz, DMSO-d_6): δ 9.05 (d, J = 4.8 Hz, 1H), 8.77–8.31 (m, 6H), 8.01–7.73 (m, 2H), 7.48 (d, J = 7.1 Hz, 2H), and 7.44–7.08 (m, 5H); and LR-MS (ESI+): m/z = 529.9 [M + H]$^+$.

Pt-tpy (100 mg, 0.216 mmol), phenylacetylene (47.5 μL, 0.431 mmol), copper iodide (4.11 mg, 0.022 mmol), and triethylamine (30.0 μL, 0.216 mmol) were dissolved in DMF (10 mL) to give a bright red suspension. The reaction was stirred with a magnetic stir bar at room temperature under argon for 3 days. The solution slowly turned dark green. An aqueous saturated solution of NH_4PF_6 was added. The dark green precipitate was filtered and washed with water and plenty of diethyl ether (yellow filtrate) until the filtrate turned black and was finally dried to afford a green powder (42.3 mg, 0.080 mmol, 37.1% yield).

4.3. Oligonucleotides

For FI, fluorimetric, and gel electrophoresis experiments,

22AG	5′-A GGGTTAGGGTTAGGGTTAGGG-3′
c-myc (myc22)	5′-TGAGGGTGGGTAGGGTGGGTAA-3′
ds26	5′-CAATCGGATCGAATTCGATCCGATTG-3′
21CTA	AGGGCTAGGGCTAGGGCTAGGG
CEB25-WT	AAGGGTGGGTGTAAGTGTGGGTGGGT

For FRET experiments,

F-21-T	5′-*FAM*-GGG TTA GGG TTA GGG TTA GGG-*TAMRA*-3′
F-myc-T	5′-*FAM*-TGA GGG T GGG TA GGG T GGG TAA-*TAMRA*-3′
F-21CTA-T	5′-*FAM*-AGGGCTAGGGCTAGGGCTAGGG- *TAMRA*-3′
F-CEB25-WT-T	5′-*FAM*-AGGGTGGGTGTAAGTGTGGGTGGGT- *TAMRA*-3′

4.4. Preparation of Oligonucleotides

For the G4-FID assay, the oligonucleotides were dissolved in K^+100 buffer (10 mM lithium cacodylate buffer pH 7.3, 100 mM KCl, 1% DMSO). Oligonucleotide concentrations were determined on the basis of their absorbance at 260 nm. For the fluorimetric titration, the oligonucleotides were dissolved in K^+100 buffer without DMSO. For the FRET-melting assay, the oligonucleotides were dissolved in K^+1 buffer (10 mM lithium cacodylate buffer pH 7.3, 1 mM KCl, 99 mM LiCl) except for F-21-T. F-21-T was dissolved in K^+10 buffer (10 mM lithium cacodylate buffer pH 7.3, 10 mM KCl, 90 mM LiCl).

Prior to use, all oligonucleotides were pretreated by heating at 95 °C for 5 min, then rapidly cooled to 4 °C to favor the intramolecular folding by kinetic trapping. Duplex-DNA ds26 was prepared by heating the self-complementary strand at 90 °C for 5 min in K^+1 buffer followed by a slow cooling over 6 h.

4.5. FRET-Melting Experiments

The stabilization of the compounds with a quadruplex-structure was monitored via FRET-melting assay performed in 96-well plates on a real-time PCR apparatus 7900HT Fast Real-Time PCR System as follows: 5 min at 25 °C and then an increase of 0.5 °C every minute until 95 °C. Each experimental condition was tested and replicated in a volume of 25 μL for each sample. The FRET-melting assay was performed with three dual fluorescently labeled DNA oligonucleotide sequences oligonucleotides. The donor fluorophore was 6-carboxyfluorescein, FAM, and the acceptor fluorophore was 6-carboxytetramethylrhodamine, TAMRA. The 96-well plates (Applied Biosystems) were prepared by aliquoting the annealed DNA (0.2 μM in K^+1 or K^+10 buffer) into each well, followed by 1 μL of the ligand (100 μM (5 eq) in DMSO). For competition experiments, duplex competitors were added to 200 nM quadruplex sequences at final concentrations of 3.0 μM (15 eq) and 10.0 μM (50 eq), with a total reaction volume of 25 μL, with the labeled oligonucleotide (0.2 μM) and the ligand (1 μM). Measurements were made with excitation at 492 nm and detection at 516 nm. The change in the melting temperature at 1.0 μm compound concentration, ΔTm (1.0 μM), was calculated from at least two experiments by subtraction of the blank from the averaged melting temperature of each compound (1.0 μM). The final analysis of the data was carried out using Origin Pro 8.6 data analysis.

4.6. HT-G4-FID Assay

Each G4-FID assay was performed in a 96-well Non-Binding Surface black with black bottom polystyrene microplates (Corning). Every ligand was tested on a line of the microplate, in duplicate. The microplate was filled with (a) K^+100 solution (qs for 200 μL), (b) 10 μL of a solution of pre-folded oligonucleotides (5 μM) and fluorescent probe (TO/TO-PRO-3 (10 μM—2 eq) or PhenDV (7.5 μM—1.5 eq)), and (c) an extemporaneously prepared 5 μM ligand solution in K^+100 buffer (0 to 100 μL) along the line of the microplate, i.e., from column A to column H: 0, 0.125, 0.25, 0.375, 0.5,

0.625, 0.75, 1.0, 1.25, 1.5, 2.0, and 2.5 μM. After 5 min of orbital shaking at 500 rpm, fluorescence is measured using the following experimental parameters: positioning delay of 0.5 s, 20 flashes per well, emission/excitation filters for TO at 485/520, TO-PRO-3 at 620/670, and PhenDV at 355/520 gain adjusted at 80% of the fluorescence from the most fluorescent well (i.e., a well from column A for TO and a well from column H).

The percentage of TO displacement is calculated from the fluorescence intensity (F), using

$$\% \; TO \; displacement = 1 - \frac{F}{F_0} \tag{1}$$

where F_0 is the fluorescence from the fluorescent probe bound to DNA without added ligand.

In the case of PhenDV, the fluorescence of the unbound probe is not negligible. The percentage of displacement becomes

$$\% \; PhenDV \; Displacement = \frac{F - F_0}{F_{ligand+probe} - F_0} \tag{2}$$

The PhenDV displacement is calculated from the fluorescence intensity F; $F_{(ligand+probe)}$, which refers to the fluorescence of the probe in presence of the ligand (without G4); and F_0, which is the fluorescence without added ligand. The term $F_{(ligand+probe)}$ is necessary as the ligand can quench the fluorescence of the probe. The percentage of displacement is then plotted as a function of the concentration of the added ligand. The DNA affinity was evaluated by the concentration of ligand required to decrease the fluorescence of the probe by 50%, was noted DC50, and was determined after non-linear fitting of the displacement curve.

4.7. Fluorimetric Titrations for Affinity Constant Evaluation Reported in Table 1

A temperature of 20 °C was kept constant with a thermostated cell holder. Each titration was performed in a 1 mL quartz cell in K^+100-buffer in a total volume of 1 mL. Titrations were performed with a solution of the fluorescent probe (TO; 0.5 μM or PhenDV; 1 μM) in the corresponding buffer in which gradual addition of oligonucleotides was carried out (up to 10 molar equivalents). After each addition, a fluorescence emission spectrum was recorded at 501 or 387 nm excitation wavelength, respectively. The fluorescence emission area was measured between 510–750 or 397–700 nm, respectively, with 1.0 nm increments, a 0.1 s integration time, and 3/3 nm (excitation/emission) slits. The titration curves were obtained by plotting the fluorescence emission area enhancement against the oligonucleotide concentration. Fluorimetric titrations were performed according to published procedures [56], and the binding constants were determined by fitting of the experimental data to the theoretical model:

$$\frac{I}{I_0} = 1 + \frac{Q-1}{2}\left(A + xn + 1 - \sqrt{(A + xn + 1)^2 - 4xn}\right) \tag{3}$$

where $Q = I_\infty / I_0$ is the minimal fluorescence intensity in the presence of excess ligand; n is the number of independent binding sites per quadruplex; $A = 1/(K_b \times c_L)$; and $x = c_{G4}/c_L$ is the titration variable.

4.8. Gel Electrophoresis

The oligonucleotides were 5′-end-labelled using a polynucleotide kinase and (γ^{32}P)-ATP (Perkin Helmer). The reaction products were purified by electrophoresis on 20% denaturing gel. Sample platinations were prepared by folding a mixture of 5′-end-radiolabeled DNA and 10 μM or 100 μM of non-radiolabeled material in 100 mM $KClO_4$ or 100 mM KCl solution except for the platination reaction in the denaturing temperature conditions. The folding was achieved by heating the samples at 90 °C for 5 min, followed by slow cooling to room temperature over the course of 2 h to induce the formation of the quadruplex structure. It was then incubated with platinum complexes, and platinated products were separated by electrophoresis on 15% denaturing gel. They were then eluted

from gel, precipitated, treated by 3'-exonuclease at 37 °C for 30 min, and loaded on a 20% denaturing gel. The digested fragments were eluted from this gel precipitated, treated over night by NaCN 0.2M, precipitated, and loaded once again on a 20% denaturing gel. Gels were scanned using a STORM860 (Molecular Dynamics).

4.9. Cell Culture

The ovarian carcinoma cell lines and human normal lung cells were purchased from ATCC and were grown in complete RPMI medium (ovarian) and DMEM (human lung cells) supplemented with 10% fetal calf serum, in the presence of penicillin, streptomycin. The resistance of A2780cis cells to cisplatin was maintained by monthly treatment with 1 μM cisplatin for 4 days. Concentrated stock solutions of complexes were conserved at −20 °C (DMSO/Water) and freshly diluted in water just before the experiments. Cells were treated with various concentrations of platinum complexes at 37 °C under humidity and 5% CO_2 conditions for 96 h. Cellular growth was quantified using the particle counter MOXI (VWR).

Supplementary Materials: The supplementary materials are available online.

Author Contributions: Conceptualization, M.-P.T.-F., S.B., and F.M.-B.; methodology and investigation, E.M., C.B., D.N.-M., C.L.-G., D.G., and S.A.; writing—original draft preparation, E.M., S.B., F.M.-B., and M.-P.T.-F.; writing—review and editing, S.B., F.M.-B., C.B., D.V., and M.-P.T.-F.; supervision, S.B., F.M.-B., and M.-P.T.-F.; funding acquisition, S.B., and M.-P.T.-F.

Funding: This research was funded by the Association pour la Recherche contre le Cancer (ARCgrant 4835), the Institut National du Cancer INCA, (2010-1-PLBIO)04-UP5-14835 grant.

Conflicts of Interest: The authors declare no conflict of interest.

References

1. Kelland, L. The resurgence of platinum-based cancer chemotherapy. *Nat. Rev. Cancer* **2007**, *7*, 573–584. [CrossRef] [PubMed]
2. Reedijk, J. New clues for platinum antitumor chemistry: Kinetically controlled metal binding to DNA. *Proc. Natl. Acad. Sci. USA* **2003**, *100*, 3611–3616. [CrossRef] [PubMed]
3. Jung, Y.; Lippard, S.J. Direct cellular responses to Platinum-induced DNA damage. *Chem. Rev.* **2007**, *107*, 1387–1407. [CrossRef] [PubMed]
4. Burge, S.; Parkinson, G.N.; Hazel, P.; Todd, A.K.; Neidle, S. Quadruplex DNA: Sequence, topology and structure. *Nucleic Acids Res.* **2006**, *34*, 5402–5415. [CrossRef] [PubMed]
5. Maizels, N. G4-associated human diseases. *EMBO Rep.* **2015**, *16*, 910–922. [CrossRef] [PubMed]
6. Rhodes, D.; Lipps, H.J. G-quadruplexes and their regulatory roles in biology. *Nucleic Acids Res.* **2015**, *43*, 8627–8637. [CrossRef] [PubMed]
7. Huppert, J.L.; Balasubramanian, S. G-quadruplexes in promoters throughout the human genome. *Nucleic Acids Res.* **2007**, *35*, 406–413. [CrossRef] [PubMed]
8. Bedrat, A.; Lacroix, L.; Mergny, J.L. Re-evaluation of G-quadruplex propensity with G4Hunter. *Nucleic Acids Res.* **2016**, *44*, 1746–1759. [CrossRef]
9. Schaffitzel, C.; Berger, I.; Postberg, J.; Hanes, J.; Lipps, H.J.; Pluckthun, A. In vitro generated antibodies specific for telomeric guanine-quadruplex DNA react with Stylonychia lemnae macronuclei. *Proc. Natl. Acad. Sci. USA* **2001**, *98*, 8572–8577. [CrossRef]
10. Biffi, G.; Tannahill, D.; McCafferty, J.; Balasubramanian, S. Quantitative visualization of DNA G-quadruplex structures in human cells. *Nat. Chem.* **2013**, *5*, 182–186. [CrossRef]
11. Amor, S.; Yang, S.Y.; Wong, J.M.Y.; Monchaud, D. Cellular Detection of G-Quadruplexes by Optical Imaging Methods. *Curr. Protoc. Cell Biol.* **2017**, *76*, 4–33. [CrossRef] [PubMed]
12. Shivalingam, A.; Vysniauskas, A.; Albrecht, T.; White, A.J.; Kuimova, M.K.; Vilar, R. Trianguleniums as optical probes for G-quadruplexes: A photophysical, electrochemical, and computational study. *Chem. Eur. J.* **2016**, *22*, 4129–4139. [CrossRef] [PubMed]

13. Granotier, C.; Pennarun, G.; Riou, L.; Hoffschir, F.; Gauthier, L.R.; De Cian, A.; Gomez, D.; Mandine, E.; Riou, J.F.; Mergny, J.L.; et al. Preferential binding of a G-quadruplex ligand to human chromosome ends. *Nucleic Acids Res.* **2005**, *33*, 4182–4190. [CrossRef] [PubMed]
14. Lam, E.Y.; Beraldi, D.; Tannahill, D.; Balasubramanian, S. G-quadruplex structures are stable and detectable in human genomic DNA. *Nat. Commun.* **2013**, *4*, 1796. [CrossRef] [PubMed]
15. Chambers, V.S.; Marsico, G.; Boutell, J.M.; Di Antonio, M.; Smith, G.P.; Balasubramanian, S. High-throughput sequencing of DNA G-quadruplex structures in the human genome. *Nat. Biotechnol.* **2015**, *33*, 877. [CrossRef]
16. Hansel-Hertsch, R.; Beraldi, D.; Lensing, S.V.; Marsico, G.; Zyner, K.; Parry, A.; Di Antonio, M.; Pike, J.; Kimura, H.; Narita, M.; et al. G-quadruplex structures mark human regulatory chromatin. *Nat. Genet.* **2016**, *48*, 1267–1272. [CrossRef] [PubMed]
17. Neidle, S. Quadruplex Nucleic Acids as Novel Therapeutic Targets. *J. Med. Chem.* **2016**, *59*, 5987–6011. [CrossRef]
18. Müller, S.; Rodriguez, R. G-quadruplex interacting small molecules and drugs: From bench toward bedside. *Expert Rev. Clin. Pharmacol.* **2014**, *7*, 663–679. [CrossRef]
19. Hansel-Hertsch, R.; Di Antonio, M.; Balasubramanian, S. DNA G-quadruplexes in the human genome: Detection, functions and therapeutic potential. *Nat. Rev. Mol. Cell Biol.* **2017**, *18*, 279–284. [CrossRef]
20. Monchaud, D.; Teulade-Fichou, M.P. A hitchhiker's guide to G-quadruplex ligands. *Org. Biomol. Chem.* **2008**, *6*, 627–636. [CrossRef]
21. Georgiades, S.N.; Abd Karim, N.H.; Suntharalingam, K.; Vilar, R. Interaction of metal complexes with G-Quadruplex DNA. *Angew. Chem. Int. Ed. Engl.* **2010**, *49*, 4020–4034. [CrossRef]
22. Stafford, V.S.; Suntharalingam, K.; Shivalingam, A.; White, A.J.P.; Mann, D.J.; Vilar, R. Syntheses of polypyridyl metal complexes and studies of their interaction with quadruplex DNA. *Dalton Trans.* **2015**, *44*, 3686–3700. [CrossRef] [PubMed]
23. Cao, Q.; Li, Y.; Freisinger, E.; Qin, P.Z.; Sigel, R.K.O.; Mao, Z.-W. G-quadruplex DNA targeted metal complexes acting as potential anticancer drugs. *Inorg. Chem. Front.* **2017**, *4*, 10–32. [CrossRef]
24. Vilar, R. Nucleic Acid Quadruplexes and Metallo-Drugs. *Met. Ions Life Sci.* **2018**, *18*, 325. [CrossRef]
25. Pradines, V.; Pratviel, G. Interaction of cationic manganese porphyrin with G-quadruplex nucleic acids probed by differential labeling of the two faces of the porphyrin. *Angew. Chem. Int. Ed. Engl.* **2013**, *52*, 2185–2188. [CrossRef] [PubMed]
26. Reed, J.E.; Neidle, S.; Vilar, R. Stabilisation of human telomeric quadruplex DNA and inhibition of telomerase by a platinum–phenanthroline complex. *Chem. Commun.* **2007**, *42*, 4366–4368. [CrossRef]
27. Reed, J.E.; Arnal, A.A.; Neidle, S.; Vilar, R. Stabilization of G-Quadruplex DNA and Inhibition of Telomerase Activity by Square-Planar Nickel(II) Complexes. *J. Am. Chem. Soc.* **2006**, *128*, 5992–5993. [CrossRef]
28. Leczkowska, A.; Gonzalez-Garcia, J.; Perez-Arnaiz, C.; Garcia, B.; White, A.J.P.; Vilar, R. Binding studies of metal-salphen and metal-bipyridine complexes towards G-Quadruplex DNA. *Chem. Eur. J.* **2018**, *24*, 11785–11794. [CrossRef]
29. Bertrand, H.; Monchaud, D.; De Cian, A.; Guillot, R.; Mergny, J.-L.; Teulade-Fichou, M.-P. The importance of metal geometry in the recognition of G-quadruplex-DNA by metal-terpyridine complexes. *Org. Biomol. Chem.* **2007**, *5*, 2555–2559. [CrossRef]
30. Rizzo, A.; Iachettini, S.; Zizza, P.; Cingolani, C.; Porru, M.; Artuso, S.; Stevens, M.; Hummersone, M.; Biroccio, A.; Salvati, E.; et al. Identification of novel RHPS4-derivative ligands with improved toxicological profiles and telomere-targeting activities. *J. Exp. Clin. Cancer Res.* **2014**, *33*, 81. [CrossRef]
31. Bertrand, H.; Bombard, S.; Monchaud, D.; Talbot, E.; Guédin, A.; Mergny, J.-L.; Grünert, R.; Bednarski, P.J.; Teulade-Fichou, M.-P. Exclusive platination of loop adenines in the human telomeric G-quadruplex. *Org. Biomol. Chem.* **2009**, *7*, 2864. [CrossRef] [PubMed]
32. Bertrand, H.; Bombard, S.; Monchaud, D.; Teulade-Fichou, M.P. A Platinum-Quinacridine Hybrid as G-Quadruplex Ligand. *J. Biol. Inorg. Chem.* **2007**, *12*, 1003–1014. [CrossRef] [PubMed]
33. Betzer, J.F.; Nuter, F.; Chtchigrovsky, M.; Hamon, F.; Kellermann, G.; Ali, S.; Calméjane, M.A.; Roque, S.; Poupon, J.; et al. Linking of antitumour trans NHC-Pt(II) complexes to G-quadruplex DNA ligand for telomeric targeting. *Bioconjug. Chem.* **2016**, *27*, 1456. [CrossRef] [PubMed]
34. Rao, L.; Bierbach, U. Kinetically favored platination of adenine in the g-rich human telomeric repeat. *J. Am. Chem. Soc.* **2007**, *129*, 15764–15765. [CrossRef] [PubMed]

35. Ourliac-Garnier, I.; Elizondo-Riojas, M.A.; Redon, S.; Farrell, N.P.; Bombard, S. Cross-links of quadruplex structures from human telomeric DNA by dinuclear platinum complexes show the flexibility of both structures. *Biochemistry* **2005**, *44*, 10620–10634. [CrossRef] [PubMed]
36. Largy, E.; Hamon, F.; Rosu, F.; Gabelica, V.; De Pauw, E.; Guédin, A.; Mergny, J.-L.; Teulade-Fichou, M.-P. Tridentate N-donor Palladium(II) complexes as efficient coordinating quadruplex DNA binders. *Chemistry* **2011**, *17*, 13274–13283. [CrossRef] [PubMed]
37. Lee, H.S.; Carmena, M.; Liskovykh, M.; Peat, E.; Kim, J.H.; Oshimura, M.; Masumoto, H.; Teulade-Fichou, M.P.; Pommier, Y.; Earnshaw, W.C.; et al. Systematic analysis of compounds specifically targeting telomeres and telomerase for clinical implications in cancer therapy. *Cancer Res.* **2018**, *78*, 6282–6296. [CrossRef]
38. Charif, R.; Granotier-Beckers, C.; Bertrand, H.C.; Poupon, J.; Ségal-Bendirdjian, E.; Teulade-Fichou, M.P.; Boussin, F.D.; Bombard, S. Association of a platinum complex to a G-quadruplex ligand enhances the telomere disruption. *Chem. Res. Tox.* **2017**, *38*, 1629–1640. [CrossRef]
39. Saker, L.; Ali, S.; Masserot, C.; Kellermann, G.; Poupon, J.; Teulade-Fichou, M.P.; Segal-Bendirdjian, E.; Bombard, S. Platinum complexes can bind to telomeres by coordination. *Int. J. Mol. Sci.* **2018**, *19*, 1951. [CrossRef]
40. Wei, Z.Z.; Qin, Q.P.; Meng, T.; Deng, C.X.; Liang, H.; Chen, Z.F. 5-Bromo-oxoisoaporphine platinum(II) complexes exhibit tumor cell cytotoxcicity via inhibition of telomerase activity and disruption of c-myc G-quadruplex DNA and mitochondrial functions. *Eur. J. Med. Chem.* **2018**, *145*, 360–369. [CrossRef]
41. Qin, Q.P.; Qin, J.L.; Chen, M.; Li, Y.L.; Meng, T.; Zhou, J.; Liang, H.; Chen, Z.F. Chiral platinum (II)-4-(2,3-dihydroxypropyl)- formamide oxo-aporphine (FOA) complexes promote tumor cells apoptosis by directly targeting G-quadruplex DNA in vitro and in vivo. *Oncotarget* **2017**, *8*, 61982–61997. [CrossRef] [PubMed]
42. Trajkovski, M.; Morel, E.; Hamon, F.; Bombard, S.; Teulade-Fichou, M.-P.; Plavec, J. Interactions of Pt-ttpy with G-quadruplexes originating from promoter region of the c-myc Gene deciphered by NMR and gel electrophoresis analysis. *Chemistry* **2015**, *21*, 7798–7807. [CrossRef] [PubMed]
43. Morel, E.; Poyer, F.; Vaslin, L.; Bombard, S.; Teulade-Fichou, M.P. Photoactivatable platinum(II) terpyridine derivatives for G-quadruplex DNA double anchoring. *Inorg. Chim. Acta* **2016**, *452*, 152–158. [CrossRef]
44. Merle, P.; Gueugneau, M.; Teulade-Fichou, M.-P.; Müller-Barthélémy, M.; Amiard, S.; Chautard, E.; Guetta, C.; Dedieu, V.; Communal, Y.; Mergny, J.-L.; et al. Highly efficient radiosensitization of human glioblastoma and lung cancer cells by a G-quadruplex DNA binding compound. *Sci. Rep.* **2015**, *5*, 16255. [CrossRef] [PubMed]
45. Yang, P.; De Cian, A.; Teulade-Fichou, M.-P.; Mergny, J.-L.; Monchaud, D. Engineering Bisquinolinium/Thiazole Orange Conjugates for Fluorescent Sensing of G-Quadruplex DNA. *Angew. Chem. Int. Ed. Engl.* **2009**, *48*, 2188–2191. [CrossRef] [PubMed]
46. Wood, E.J. Molecular probes: Handbook of fluorescent probes and research chemicals: By R P Haugland. pp 390. Interchim (Molecular Probes Inc, PO Box 22010 Eugene, OR 97402-0414, USA, or 15 rue des Champs, 92600 Asnieres, Paris). 1992–1994. $15. *Biochem. Educ.* **1994**, *22*, 83. [CrossRef]
47. Beauvineau, C.; Guetta, C.; Teulade-Fichou, M.P.; Mahuteau-Betzer, F. PhenDV, a turn-off fluorescent quadruplex DNA probe for improving the sensitivity of drug screening assays. *Org. Biomol. Chem.* **2017**, *15*, 7117–7121. [CrossRef] [PubMed]
48. Largy, E.; Hamon, F.; Teulade-Fichou, M.-P. Development of a high-throughput G4-FID assay for screening and evaluation of small molecules binding quadruplex nucleic acid structures. *Anal. Bioanal. Chem.* **2011**, *400*, 3419–3427. [CrossRef]
49. Peng, Z.-H.; Journet, M.; Humphrey, G. A highly regioselective amination of 6-Aryl-2,4-dichloropyrimidine. *Org. Lett.* **2006**, *8*, 395–398. [CrossRef]
50. Hadad, C.; Achelle, S.; García-Martinez, J.C.; Rodríguez-López, J. 4-Arylvinyl-2,6-di(pyridin-2-yl)pyrimidines: Synthesis and optical properties. *J. Org. Chem.* **2011**, *76*, 3837–3845. [CrossRef]
51. Mergny, J.-L.; Maurizot, J.-C. Fluorescence resonance energy transfer as a probe for G-quartet formation by a telomeric repeat. *ChemBioChem* **2001**, *2*, 124–132. [CrossRef]
52. Heringova, P.; Kasparkova, J.; Brabec, V. DNA adducts of antitumor cisplatin preclude telomeric sequences from forming G quadruplexes. *J. Biol. Inorg. Chem.* **2009**, *14*, 959–968. [CrossRef] [PubMed]

53. Cummings, S.D. Platinum complexes of terpyridine: Interaction and reactivity with biomolecules. *Coord. Chem. Rev.* **2009**, *253*, 1495–1516. [CrossRef]
54. Galluzzi, L.; Senovilla, L.; Vitale, I.; Michels, J.; Martins, I.; Kepp, O.; Castedo, M.; Kroemer, G. Molecular mechanisms of cisplatin resistance. *Oncogene* **2012**, *31*, 1869–1883. [CrossRef] [PubMed]
55. Chtchigrovsky, M.; Eloy, L.; Jullien, H.; Saker, L.; Segal-Bendirdjian, E.; Poupon, J.; Bombard, S.; Cresteil, T.; Retailleau, P.; Marinetti, A. Antitumor trans-N-heterocyclic carbene-amine-Pt(II) complexes: Synthesis of dinuclear species and exploratory investigations of DNA binding and cytotoxicity mechanisms. *J. Med. Chem.* **2013**, *56*, 2074–2086. [CrossRef] [PubMed]
56. Jager, K.; Bats, J.W.; Ihmels, H.; Granzhan, A.; Uebach, S.; Patrick, B.O. Polycyclic azoniahetarenes: Assessing the binding parameters of complexes between unsubstituted ligands and G-quadruplex DNA. *Chem. Eur. J.* **2012**, *18*, 10903–10915. [CrossRef]

Sample Availability: Samples of the compounds are available from the authors.

PAPER 2

Pt-ttpy, a G-quadruplex binding platinum complex, induces telomere dysfunction, G-rich regions DNA damage and mitochondrial toxicity

Pt-ttpy is the complex chosen from the screening for radiosensitization potential of metal complexes. While we studied the molecular mechanism of action for Pt-ttpy induced radiosensitization, it is also important to explore the effect of the drug by itself in the absence of irradiation. In this paper, Pt-ttpy, a G-quadruplex binding metal complex is shown to target telomeres, G- and A- rich tandemly repeated sequences and mitochondria in A2780 ovarian carcinoma cell lines. The work done by Dr. Samar Ali shows the displacement of TRF2 (shelterin protein found in telomeric ends) from telomeres and the telomeric damages induced due to the treatment of Pt-ttpy. A γH2AX – ChIP assay was performed to determine the genomic DNA damage sites induced by Pt-ttpy and the results were analyzed by Dr. Emilia Puig Lombardi.

I was interested in the effect of Pt-ttpy at mitochondria, hence I was involved in the experiments exploring this relationship. We investigated the accumulation of the drug in mitochondria, and its ability to induce mitochondrial damage by estimating the mitochondrial membrane potential loss, ability to induce ROS production and evaluating the amount of DNA lesions formed in mitochondrial DNA template using real time Q-PCR.

Pt-ttpy, a G-quadruplex binding platinum complex, induces telomere dysfunction, G-rich regions DNA damage and mitochondrial toxicity

Samar Ali[1], Emilia Puig Lombardi[2], Deepanjan Ghosh[3,4], Tao Jia[3,4], Géraldine Vitry[1], Lina Saker[1], Joël Poupon[5], Marie-Paule Teulade-Fichou[3,4], Alain Nicolas[2], Arturo Londono-Vallejo[2] and Sophie Bombard[3,4*]

[1,] INSERM UMRS 1007, Université de Paris, 75006 Paris
[2] Telomeres and Cancer Laboratory, CNRS, Sorbonne Université, Université PSL, Institut Curie, 75248 Paris Cedex 05, France
[3] Institut Curie, CNRS UMR9187-INSERMU1196, CMBC, 91405 Orsay, France
[4] Institut Curie, CNRS UMR9187-INSERMU1196, Université Paris-Saclay, 91405 Orsay, France
[5] Hôpital Laboratoire de Toxicologie Biologique, Hôpital Lariboisière, 2 rue Ambroise Paré, 75475 Paris, France

**Corresponding author* : sophie.bombard@curie.fr

Abstract

Pt-ttpy (tolyl terpyridin-Pt complex) covalently binds to G-quadruplex (G4) structures *in vitro* and to telomeres *in cellulo* via its Pt moiety. Here, we identified its targets in the human genome, in comparison to **Pt-tpy,** its derivative without G4 affinity, and cisplatin. **Pt-ttpy**, but not **Pt-tpy,** induces the release of the shelterin protein TRF2 from telomeres concomitantly to the formation of DNA damage foci at telomeres but also at other chromosomal locations. γ-H2AX chromatin immunoprecipitation (ChIP-seq) after treatment with **Pt-ttpy** or cisplatin revealed accumulation in G- and A-rich tandemly repeated sequences, but not particularly in potential G4 forming sequences. In addition **Pt-ttpy** efficiency accumulates in mitochondria accompanied with mitochondrial membrane potential reduction and mitochondrial DNA lesions. Collectively, **Pt-ttpy** presents dual targeting efficiency on DNA by inducing telomere dysfunction and genomic DNA damage at specific loci, and on mitochondria.

Key words

G-quadruplex, platinum complexes, telomere dysfunction, DNA damage, mitochondria targeting,

Introduction

G-quadruplexes (G4) are stable nucleic acid secondary structures that are formed in DNA and RNA containing several G-runs [1]. They consist of the stacking of G-tetrads stabilized by the presence of physiological concentrations of monovalent cations. Substantial evidence shows that G4 DNA and RNA structures form *in vivo.* Bioinformatics analyses have predicted that the human genome contains 350,000 to 650,000 potential G4 forming sequences [2-4]. While 700,000 G4s have been identified from DNA cellular extracts using in vitro polymerase stop assay [5], BG4 ChIP-seq experiments have led to the identification of 10,000 G4s in HaCaT cells, where they have been shown to be mainly located in regulatory regions of DNA [6]. These were unevenly distributed and mostly found in promoter of genes, particularly those of several oncogenes. In addition, G4 formation has been intensively studied at telomeres, which are particularly predisposed to form such structures due to their G-richness organized in TTAGGG tandem repeats [7, 8]. Telomeres constitute the essential and specialized nucleoprotein structure that is located at the end of chromosomes and functions as a specialized DNA "cap", protecting chromosome ends from degradation and eliciting DNA repair activities [9, 10]. A complex of six proteins called shelterin ensures the protection of telomeres [11]. Among them, TRF1 and TRF2 (telomeric repeat binding factors 1 and 2) and POT1 (Protection of Telomere 1) are directly bound to telomeric DNA. Telomere uncapping by release of TRF2 or POT1 induces telomere dysfunction and cell senescence or death [12], thus making telomeric DNA and its shelterin promising targets for anticancer therapy [13]. In all, it is well established that G4s play important roles in a broad range of biological processes [14, 15], including telomere maintenance [16], replication [17], transcription and translation [18] as well as regulation of mitochondrial homeostasis [19]. Therefore, a large number of G4-interacting molecules [20, 21], including metallic complexes[22, 23], have been developed and many of them have been shown to reduce cancer growth [24-26].

Platinum complexes bearing a leaving group (typically Cl^- or I^-) are able to bind covalently *in vitro* to G4s by coordinating N_7 or N_1 of adenines or N_7 of guanines [27-32]. Among these, the tolyl-terpyridin-Platinum complex (**Pt-ttpy**) (scheme 1) preferentially stabilizes G4s *in vitro* with regard to

duplex DNA [33, 34] by stacking to external G-tetrads [35] and is also able to efficiently trap G4s covalently by direct coordination to loop bases [30, 35]. **Pt-ttpy** displays potent anti-tumor activity [34] and one of its derivative, Pt-ctpy, was shown to have promising radiosensitizing properties [36]. In line with its potential G4-sequence targeting ability, **Pt-ttpy** has been shown to bind covalently to telomeric DNA *in cellulo* [37], and to induce chromosome loss and ultrafine bridges formation that may be correlated with telomere dysfunctions [38]. Moreover, emerging evidence indicated that certain metal complexes present dual-targeting efficiency on both nuclear and mitochondrial DNA, which may induce additional DNA toxicity and may potentiate their anticancer activity [39]. In addition, it is likely that mitochondria also play a role in mediating cellular sensitivity to cisplatin [40]. Mitochondria are organelles that generate energy via ATP and play an essential role in mediating apoptosis [41]. Mitochondrial modifications such as respiratory chain injury or membrane depolarization lead to mitochondrial dysfunctions [42] and to cell death [43]. In addition, the mitochondrial DNA comprised of 16.5kb is more susceptible to damage than nuclear DNA due to insufficient DNA repair mechanism [44]. Collectively, targeting mitochondria provides a promising approach not only for designing anti-cancer drugs but also for circumventing drug resistance [45].

Since **Pt-ttpy** combines G4 stabilization, metal complex and direct DNA-metal coordination properties, it appears of great interest to identify its molecular targets and decipher its mechanism of action. We tested whether the biological activity of **Pt-ttpy** could be related to its G4-binding properties, using as controls two platinum complexes with poor or no affinity for G4s, **Pt-tpy** [34] and the anticancer drug cisplatin (Scheme 1) [46]. **Pt-ttpy** and **Pt-tpy** form monofunctional DNA adducts [30], whereas cisplatin forms mainly bifunctional DNA adducts between two adjacent guanines (1,2 intrastrand cross-links) [47, 48]. Here, we show that **Pt-ttpy** targets simultaneously telomeres and mitochondria, induces DNA damage preferentially at G- and A-rich regions, and appeared as a more potent agent than cisplatin, as it is able to overcome cisplatin resistance.

Results

Antiproliferative properties of Pt-ttpy compared to Pt-tpy and cisplatin

We examined the cell growth inhibition of **Pt-ttpy** and **Pt-tpy** for a 96h-treatment compared to cisplatin on the ovarian cell line A2780 and its counterpart cisplatin-resistant, A2780cis. This allowed determining the IC_{80}, a dose that inhibits 80% proliferation, conditions that were used for the subsequent experiments. In A2780, the IC_{80} of **Pt-ttpy** and **Pt-tpy** (Figure 1 and Table 1) are similar (4 and 5.5 µM, respectively) but 7-fold higher than that of cisplatin (0.66µM), which is consistent with the reported IC_{50} values (2.5, 3 and 0.3µM, respectively) [34]. To note, while the IC_{80} values of **Pt-ttpy** are the same for A2780 and A2780cis cell lines and those of **Pt-tpy** are only slightly higher in A2780cis when compared to A2780, the IC_{80} of cisplatin increases in A2780cis by a factor of 10, as expected. These results indicate that the two terpyridine complexes show no (or almost no) cross-resistance with cisplatin (factor resistance of 1-1.7, Table 1). Therefore, **Pt-ttpy** becomes more efficient than cisplatin (4µM versus 7µM at IC_{80}) in A2780cis. The viability of remaining adherent cells was then evaluated using the acridine orange/Propidium iodide viability assay after treatment with the drugs at IC_{80} for 96h. Detection of green fluorescence by microscopy indicated that nearly 95% of the cells are alive (Figure S1A). Further analysis by Annexin V-FITC/PI assay confirms the absence of dead cells (late apoptotic cells) but evidenced an induction of early apoptotic cells restricted to **Pt-ttpy** treatment (Figures S1B-C).

Cellular uptake and genomic DNA binding of platinum complexes

The discrepancy of the three complexes in anti-proliferative activity between both cell lines might result from their difference in cellular uptake and/or genomic DNA binding efficiency, since platinum DNA-adducts have been recognized as the ultimate event generated in cells [48, 49]. To explore the cellular fate of the three platinum drugs, we determined their cellular uptake and distribution using the inductively-coupled plasma mass spectrometry (ICP-MS) method [50, 51], which allows to quantify the amount of Pt in whole cells and that bound to genomic DNA. The cellular accumulation of the three complexes and their binding to DNA are time- and dose-dependent (Figure S2). For the 96h-treatment,

the accumulation of both **Pt-ttpy** and **Pt-tpy** is stronger than the one of cisplatin in A2780 cells (9 or 7.4 times more at IC_{80}, respectively, Figure2A and Table 2), however their binding to DNA is quite similar (Figure2B and Table 1). This suggests that anti-proliferative activity in A2780 cells is to be linked to their ability to bind DNA rather than to their cellular uptake. In A2780cis cells, as compared to A2780 cells, cellular uptake and DNA binding are slightly increased for both **Pt-ttpy** and **Pt-tpy** with regard to cisplatin**.** We observe a large increase in cisplatin uptake and DNA binding (7 times) in agreement with the increase of the IC_{50}/IC_{80} [52]. These results are in agreement with the ones obtained when cells were treated at equimolar concentrations of drugs [37] and indicate that the influx/efflux of **Pt-ttpy** and **Pt-tpy** are not altered in A2780cis cells, contrary to cisplatin [53, 54]. For cisplatin, both the cellular accumulation and amount bound to DNA in A2780cis cells are slightly higher than those reported in previous studies [40, 55], which may be attributed to different incubation conditions.

Given that all complexes show similar binding efficiency to DNA, we decided to explore their binding specificity for various DNA loci (telomeres, genomic G4 sequences) and evaluated their distribution in subcellular compartments such as mitochondria, a well-known target of cationic metal complexes [39].

TRF2 displacement from telomeres is induced upon treatment with Pt-tty and cisplatin but not with Pt-tpy.

G4 ligands can induce telomere dysfunction by dissociating some shelterin proteins (especially TRF2 and POT1) from telomeres, leading to telomere uncapping and degradation [56-63], thus resulting in telomere-end fusions [63-65]. Therefore, we investigated and compared the capacity of **Pt-ttpy**, **Pt-tpy** and cisplatin to induce telomere dysfunction by quantifying the amount of TRF2, TRF1 and POT1 bound to telomeres after a 96h-treatment at an IC_{80} dose. Histone H3, a non-telomere specific DNA binding protein, was used as control.

Immunostaining of TRF2 revealed that **Pt-ttpy** and cisplatin induced a significant loss of TRF2 foci (47 to 78% remaining foci) in both A2780 (Figures 3A-B) and A2780cis cells (Figure 3C), whereas **Pt-tpy** had no impact. Since TRF2 foci are not exclusively localized at telomeres [66], we performed Chromatin Immunoprecipitation (ChIP) experiments using telomeric probes for the detection and

quantification of DNA, which confirmed the immunostaining results. Indeed, 50 to 58% of TRF2 remained bound to telomeres in A2780 cells treated with cisplatin or **Pt-ttpy,** respectively, whereas TRF2 remained fully bound upon **Pt-tpy** treatment (Figure 4A-D). In A2780cis cells, 56 to 68% of TRF2 remained bound to telomeres by cisplatin and **Pt-ttpy** treatments, respectively, whereas for **Pt-tpy** treatment TRF2 remained fully bound (Figure 4E)**.** In contrast, TRF1, POT1 and H3 were not affected and remained fully bound, irrespective of the platinum complex used.

Since the release of TRF2 from telomeres can also result from a decrease in TRF2 expression due to the stabilisation of the G4 structure located within its 5'UTR mRNA region [67], the amount of protein TRF2 was analysed by Western blot. TRF2 expression was not significantly affected by **Pt-ttpy**, **Pt-tpy** or cisplatin treatments (Figures 5A-B).

Absence of telomere shortening upon TRF2 displacement from telomeres

Since the release of TRF2 from telomeres can induce telomere shortening, we investigated the platinum complexes effects on telomere length by Southern blot and qPCR of telomeric DNA in A2780 cells. Southern blot analysis of the mean value of TRF (Telomere Restriction Fragments) and qPCR showed that **Pt-ttpy**, **Pt-tpy,** and cisplatin did not induce telomere shortening (Figures 5B and 5C).

Only Pt-ttpy induced telomeric damages

TRF2 uncapping from telomeres induce telomeric DNA damage, as assessed by telomere dysfunction-induced foci (TIFs) quantification [68]. We tested platinum complexes effects on DNA damage response by γ-H2AX immunostaining (γ-H2AX foci), a well-defined marker of DNA damage [69]. Cisplatin, **Pt-ttpy** and **Pt-tpy** induced a large amount of γ-H2AX foci formation (40-80 foci) (Figures 6A, 6B and S3A). Specific damage to telomeres was further assessed by the quantification of γ-H2AX foci using a telomeric specific targeting PNA probe. Co-localisation analysis of the DNA damage signals with telomeres staining (Figure 6A) showed that only **Pt-ttpy** induced significant telomere damage (24% of cells comprising 3-5 TIF per cells) (Figure 6C). Since the binding of platinum complexes to

telomeric DNA could partially impede the hybridization of telomeric probes to telomeres [37], **Pt-ttpy**-induced TIFs were confirmed by the co-localisation of the DNA damage signals with the telomeric protein TRF1 (Figure S3A), which is not released from telomeres upon the various treatments (as seen in Figure 4). As shown in Figure S3B, 35% of cells treated by **Pt-ttpy** contain 3 to 8 telomeric damages per cell (average 2 TIFs per cell). These results are in agreement with the TIFs analyses following other cell line treatment by **Pt-ttpy** using TRF2 as a telomeric probe [38], even if this protein is partly delocalized from telomeres during such a treatment.

Pt-ttpy preferentially induced damage at genomic G-rich sequences but not exclusively at predicted G4 motifs

Beside telomeres, γ-H2AX foci induce upon drug treatment localize in other chromosomal regions (Figures 6 and S3). In order to determine these sites, we conducted chromatin immunoprecipitation of cells treated with **Pt-ttpy** using an antibody against γ-H2AX followed by Next-Generation sequencing (ChIP-seq), in comparison with cisplatin-treated and non-treated cells.

We identified a total of 25,788, 17,682 and 10,050 peaks from treatments with cisplatin, **Pt-ttpy** and untreated cells, respectively (Figure 7A). Cisplatin and **Pt-ttpy** IPs were then analyzed over the untreated IPs, revealing 11 744 common peaks (Figure 7A). Interestingly, the γ-H2AX domains are unevenly distributed among chromosomes (Figure 7B). Indeed, γ-H2AX preferentially accumulates on six chromosomes, with the highest enrichment detected in chr1≥ chr21>chr16> chr15> chr9> chr19 (Figure 7C). Notably, this distribution is identical for cisplatin and **Pt-ttpy**. Of note, the bioinformatics analyses of the ChIP-seq data revealed also multiple reads that mapped onto mitochondrial DNA (chrM). Mitochondrial DNA exists in a closed-circular double-stranded form in high copy numbers in mitochondria within the cells as well as remnants of partial or whole copies within the nuclear genome, known as Nuclear Mitochondrial sequences (NUMTs) [70]. The ChIP-seq peaks that mapped on chrM covered almost the entire mitochondrial DNA. Thus, it was not possible to decipher whether the enriched signal originates from NUMTs or from mitochondria. Moreover, even if some histones like

H2A and H2AX were reported in mitochondria and that the decreased expression of H2AX could lead to mitochondrial toxicity [71], no detectable γ-H2AX has been reported within mitochondria, even under ionizing radiation [72]. Likewise, our immunofluorescence analyses did not show any γ-H2AX signal outside from the nucleus upon drug treatments (Figures 6A and S3A). These data suggest that chrM chipped by γ-H2AX originates from the nucleus and not from mitochondria.

We observed that the preferred DNA damage domains are G- and A-rich tandemly repeated sequences, comprising satellite DNA, rDNA and pseudogene regions (Figure 8A). We then analyzed the enrichment of DNA damage sites in regions containing potential G4-forming sequences (G4L1-12 and G4L1-7 motifs, matching the regular expressions $G_{3-5}N_{1-7}G_{3-5}N_{1-7}G_{3-5}N_{1-7}G_{3-5}$ or $G_{3-5}N_{1-12}G_{3-5}N_{1-12}G_{3-5}N_{1-12}G_{3-5}$; see Material and Methods) in gene promoters, telomeric sequences ($[TTAGGG]_n$ repeats) and in GG and GNG sites that are preferentially crosslinked by cisplatin [48] (Figure 8B). Except for GNG-containing sequences, none of these domains, including G4 genomic motifs, are prominent damage domains of **Pt-ttpy**. Even if telomeric damages have been evidenced by confocal microscopy, we did not detect any telomeric enrichment in peaks from our sequencing data. However, since assigning telomeric reads with high confidence using ChIP-seq data is not possible (specialized software designed for WGS data, repetitive nature of the telomeric regions, long stretches of unknown nucleotides at the ends of most chromosomes in the human reference genome assembly), this quantification has not be taken into account in our analysis. For cisplatin, enrichment in γ-H2AX domains containing GG and GNG was observed. To note, our genome wide pattern of γ-H2AX domains of cisplatin treatments differs significantly from the maps obtained from cisplatin-DNA adducts and cisplatin DNA damage and repair sequencing of the human genome at single-nucleotide resolution [73, 74]. Indeed, in our study, the γ-H2AX domains do not correlate with the density of GG (Figure S4) and no enrichment has been observed in promoter regions. Most interestingly, the analysis of prominent peak regions highlights that six consensus motif sequences (60% of the peaks) were significantly enriched after **Pt-ttpy** treatment and are different from those observed after cisplatin treatment (Figure S5). In all, **Pt-ttpy** induced preferentially DNA damage in G- and A-rich tandemly repeated sequences in A2780 cells

comprising satellite DNA, rDNA and pseudogene regions, and was not restricted to sites with G4-forming potential.

Pt-ttpy shows mitochondria-targeted efficiency

Since some platinum complexes have been shown to accumulate within mitochondria and to induce mitochondrial dysfunction [39, 40, 75, 76], we then studied the cellular uptake and mitochondria targeting efficiency of **Pt-ttpy**, as compared with **Pt-tpy** and cisplatin. We quantified the amount of platinum accumulated in mitochondria using ICP-MS, following a 96h-treatment of A2780 cells with **Pt-ttpy, Pt-tpy** and cisplatin at their IC_{80} doses. Remarkably, **Pt-ttpy** accumulates more than 12 and 5 times in mitochondria than cisplatin and **Pt-tpy**, respectively (Figure 9A), in correlation to their cellular accumulation (Figure 2A, Table 2).

Next, we studied the consequence of a large differential accumulation of different platinum complexes on mitochondrial function by measuring mitochondrial membrane potential, one of the hallmarks of mitochondrial damage. The change of mitochondrial membrane potential ($\Delta\psi_m$) was detected by JC-1 that accumulates into the mitochondrial membrane matrix space inversely proportional to $\Delta\psi_m$. JC-1 is a monomer emitting green fluorescence at low concentration, whereas at high concentration, its aggregation leads to red fluorescence. The percentage of cells with high green and low red fluorescence observed was the highest for **Pt-ttpy** in a concentration dependent manner, showing a moderate loss of mitochondrial membrane potential (Figure 9B). In contrast, cisplatin and **Pt-tpy** do not show any loss of membrane potential.

Since ROS species can induce and/or result from mitochondrial dysfunction [77], total cell ROS production was quantified using CellROX by flow cytometry. In contrast to cisplatin and **Pt-tpy** treatments, **Pt-ttpy** did not generate any ROS (Figure 9C). This suggests that **Pt-ttpy** has a different mechanism of action from cisplatin, in relation to mitochondria targeting.

We detected a high accumulation of **Pt-ttpy** in mitochondria, indicating that this complex could reach mitochondrial DNA and then could be susceptible to induce mitochondrial DNA damage [76, 78, 79].

Therefore, its potential to induce mitochondrial DNA damage was further evaluated by a real time, quantitative PCR method [80]. Mitochondrial DNA lesions were observed for **Pt-ttpy** as well as cisplatin and **Pt-tpy** in one domain (Figure 9D). Collectively, these data indicates that **Pt-ttpy** efficiently target the mitochondrial compartment inducing a $\Delta\psi_m$ decrease and mitochondrial DNA lesions.

Discussion

Here, we examined the cellular and molecular targets of the G4 ligand tolylterpyridine platinum complex, **Pt-ttpy** [33, 34], that can bind and trap G4s irreversibly by metallic mono-coordination [30, 35]. We used, for comparison, its non-G4-binding ligand derivative, **Pt-tpy**, and another prevalent anti-cancer drug, cisplatin, that mainly binds DNA by bis-coordination between two adjacent guanines. Due to the dual properties of **Pt-ttpy** (G4 ligand and platinum coordinating complex), we analyzed its ability to induce telomere and other DNA damage as well as targeting mitochondria.

In the context of the search for platinum complexes able to overcome cisplatin resistance [81], **Pt-ttpy** and **Pt-tpy** are encouraging complexes from a pharmacological viewpoint, since they do not exhibit any cross-resistance with cisplatin [34]. Indeed, both complexes overcome the reduced influx and enhanced efflux of cisplatin contributing to cisplatin resistance in the A2780cis cell line, in comparison to its sensitive A2780 counterpart (Table 1, Figure 2) [52]. Interestingly, in A2780 cells, while the cellular uptake of both **Pt-ttpy** and **Pt-tpy** is greatly increased (7 to 16-fold) in comparison with cisplatin at iso-effect doses**,** the amount of platinum bound to DNA remains in the same order of magnitude (factor 0.7 to 1.6) for all complexes,. This suggests that their anti-proliferative activity is explained by their DNA binding activity, as previously proposed for many platinum complexes [48, 82]. Conversely, in A2780cis cells, the platinum bound to DNA by cisplatin, **Pt-ttpy** and **Pt-tpy** treatments is not at the same level. This indicates that the DNA binding capacity alone could not entirely explain the drugs anti-cancer activities, especially in A2780-cis cells, that are supposed to have a high tolerance to damaged DNA [45]. This also indicates that circumventing cisplatin resistance involves other molecular and cellular targets that need to be characterized [83]. Indeed, other important cellular targets, such as mitochondria, have been recently suggested as new targets of platinum complexes [39]. Therefore, to further detail of the mechanism of **Pt-ttpy** anti-cancer activities, it was important to decipher whether the effects of **Pt-ttpy** depended on its preferential DNA structure recognition (G4 versus duplex DNA) and/or on its mitochondrial targeting.

Firstly, the ability of **Pt-ttpy** to perturb telomere structure was evidenced. This result is in agreement with previous finding showing that **Pt-ttpy** reaches and binds irreversibly to telomeres [37] and induces chromosome loss in linear human chromosome only when containing telomeres [38]. This can be attributed to its G4-binding property. Indeed, only **Pt-ttpy**, and neither **Pt-tpy** nor cisplatin, induced telomere dysfunctions resulting in a partial release of TRF2 concomitantly with an induction of TIFs**.** This effect has already been reported for other G4 ligands [56-58, 84-86]. Since, the shelterin complex at telomeres is essential to cell viability, in particular its TRF2 and POT1 components which block the activation of DNA damage responses by ATM and ATR respectively at telomeres [12, 87], this telomere dysfunction could participate to cell death. In addition, our results confirm that telomere protection is complex [12] given that telomere dysfunction assessed by TIFs following cell treatment with other G4-binding ligands does not systematically lead to telomere shortening [59, 62, 85, 86], and that partial TRF2 uncapping using cisplatin [63] or sh-RNA against TRF2 [88] is not sufficient to induce telomere damage.

Secondly, at genome-wide level, γ-H2AX chromatin immunoprecipitation followed by Next-Generation-Sequencing (ChIP-seq) showed that the γ-H2AX domains of **Pt-ttpy** treatment did not accumulate in potential G4-forming sequences (PQS) irrespective of the search criterion used (G4L1-12 and G4L1-7) [3, 89] and 2) but followed the same enrichment pattern as cisplatin. This strongly suggests that the preferential genome DNA sequence of **Pt-ttpy-**induced damage response through γ-H2AX is mainly driven by its DNA coordination properties, rather than its G4-binding properties, in contrast to the G4 ligand Pyridostatin for which γ-H2AX domains have been mainly found in oncogene promoters containing PQS [90]. In addition, six prominent consensus DNA damaged sequences were defined to be unique to the **Pt-ttpy** treatment as compared to cisplatin**.** This could be due to a differential ability of the platinum complexes to form various DNA-adducts, as mono adducts for **Pt-ttpy** and intra- and inter-strand crosslinks for cisplatin, that will be processed differently during replication, transcription and/or repair leading consequently to various DNA damage sites [91]. This singular property may be an important feature for the anti-cancer activity of **Pt-ttpy.**

It should be noted that the genome-wide pattern of cisplatin γ-H2AX domains obtained herein, enriched in G- and A-rich sequences, differs significantly from the maps of cisplatin-DNA adduct and cisplatin repair sites recently reported at the single nucleotide base in the human genome [73, 74, 91]. The cisplatin-DNA adduct distribution (using antibodies against cisplatin and high mobility group protein HMGB1 for IP) is dictated primarily by the GG frequency whereas the cisplatin repair sites (using antibodies against TFIIH for IP) are highly heterogeneous and significantly correlated to transcription and chromatin states. To explain this discordance, it was proposed that the chromatin state would limit the accessibility of the Nucleotide Excision Repair (NER machinery), thus impairing its activity [92, 93]. Consequently, the persistence of DBS and of γ-H2AX domains spreading over many kb would depend on the repair efficiency. These arguments could also contribute to explain the γ-H2AX domains patterns reported here. In fact, although the detection of γ-H2AX has been used to identify G4-drug binding sites on DNA [90], our findings indicate that this approach may reflect only partly the DNA-drugs' binding sites, at least in the context where drugs with DNA coordination capacity are used.

The fact that **Pt-ttpy** was found to target mitochondria differently than cisplatin revealed two interesting properties of this complex from a pharmacological point of view. First, at iso-effect doses, it accumulates in mitochondria at a higher level than cisplatin and induces mitochondrial dysfunctions by causing a loss of membrane potential. Given that mitochondria have been causally linked to cisplatin-induced cell death (as cells with low mitochondrial content are more resistant to cisplatin [94]), our work suggests that **Pt-ttpy** could be an effective drug to circumvent cisplatin resistance in cancerous cells with low mitochondrial content, such as in high malignant ovarian cancer cells. Secondly, **Pt-ttpy** treatment does not lead to ROS production in contrast to cisplatin treatment. Since ROS production constitutes a component for cisplatin dose-limiting toxicities [95], the use of **Pt-ttpy** would therefore limit these secondary toxicities. Finally, both platinum complexes induce mt-DNA lesions. However, we suspect that the latter should be different. The real-time-PCR amplification of mitochondrial DNA fragments used to detect mt-DNA lesions is sensitive enough to detect 8 oxo-G induced by ROS [80]. Consequently, the mt-DNA lesions detected for the cisplatin treatment could be

the consequence of ROS production. In contrast, for the **Pt-ttpy** treatment, in the absence of ROS production, we can suggest that mt-DNA lesions could be attributed to direct **Pt-ttpy** adducts. The underlying differential mechanisms of mitochondrial toxicity induced by both complexes need to be further evaluated. Finally, since **Pt-ttpy** does not induce ROS production, a direct crosstalk between telomere dysfunction and mitochondria via ROS production as recently proposed [96, 97] is not conceivable in the case of **Pt-ttpy** treatment.

In conclusion, we showed that **Pt-ttpy** presents unique features for cellular targets compared to cisplatin. **Pt-ttpy** targets telomeres and induces their dysfunction, probably by G4 recognition, while its main genomic DNA damage sequences are not related to its G4 recognition properties. Besides inducing genomic DNA damage, **Pt-ttpy** highly accumulates in the mitochondrial fraction, leading to mitochondrial membrane potential changes associated with the induction of mitochondrial DNA lesions. Since recent studies highlighted that anti-cancer drug sensitivity and the acquisition of drug resistance against cisplatin can be due to reduced drug accumulation in mitochondria, the *in cellulo* activities of **Pt-ttpy** can be exploited in order to circumvent increasing drug resistance in chemotherapy.

Methods

Cell culture.

The ovarian carcinoma cell lines were purchased from ECACC (Salisbury, UK) and were grown in complete RPMI medium supplemented with 10% fetal calf serum, in the presence of penicillin, streptomycin. The resistance of A2780cis cells to cisplatin was maintained by monthly treatment with 1µM cisplatin for 4 days. Cells were treated with various concentrations of **Pt-ttpy**, **Pt-tpy** and **cisplatin** at 37°C under humidity and 5% CO_2 conditions for 96h. Cellular growth was quantified using the particle counter Z2 Coulter®, (Beckman, COULTER®).

Platinum complexes

Cisplatin was provided from Sigma. **Pt-ttpy** and **Pt-tpy** were synthesized following the procedure already described [34]. Aqueous solutions of cisplatin 1 mM, of **Pt-tpy** 1 mM and 6mM DMSO solutions of **Pt-ttpy** were prepared and conserved at -20°C. Diluted solutions of each molecule were freshly prepared.

Platinum uptake measurement

The platinum cellular uptake was quantified by ICP-MS (inductively coupled plasma mass spectrometry) on cellular pellet (5 10^6 cells), DNA extract (using DNeasy kit from Qiagen) as previously described [98] [31] or mitochondria (using the Mitochondrial Isolation Kit from Thermofisher) in A2780 or A2780cis cells treated with various concentrations of **Pt-ttpy**, **Pt-tpy** and **cisplatin** during indicated time treatment. ICP-MS has been used also for monitoring the solubilization of platinum complexes in the aqueous solution. Prior ICP-MS,the sample were digested with concentrated HNO_3 at 95°C.

ChIP assay for detection of TRF2, TRF1, POT1 and H3 binding

ChIP was carried out using a Chromatin IP (ChIP) assay kit according to the manufacturer's instructions (Upstate). Cells were collected after fixation of proteins with formaldehyde, and lysed. DNA of nucleus

was sonicated until fragments of 1 kbp were obtained. 30µl was conserved in order to quantify the number of telomeric sequences before immuno-precipitation (INPUT). Immunoprecipitation was then performed with anti-TRF2 polyclonal antibody (IMG-148A, IMGENEX), anti-TRF1 polyclonal antibody (ab1423, Abcam), anti-POT1 antibody, anti-histone H3 antibody (anti-H3, Abcam), or anti-IgG rabbit antibody (sc-2027, Abcam). 150ng of the immunoprecipitated DNA and from INPUT were blotted onto a Hybond-XL membrane (Ge HealthCare). The telomere sequences were detected using a 800bp telomere repeat (TTAGGG) ^{32}P labelled probe obtained after digestion of the pUC Telo2 plasmid [99] by EcoRI and BamHI and radiolabelled by random priming using dCTP [α^{32}P], TAGGGTTA/TAACCCTA (Eurogentec) as primers and Klenow polymerase (Fermentas). The Alu sequences were detected using a ^{32}P labelled Alu probe that was obtained after the digestion of the pTopo Alu-AII plasmid (obtained after amplification of human genomic DNA with tgaaaccccgtctctactaaaaa and gtctcgctctgtcgccca primers, then cloned in pGEM-T vector (Promega)) by EcoRI and radiolabelled by random priming using dCTP [α^{32}P], the hexanucleotide mix (Roche) as primers and Klenow polymerase (Fermentas). The membranes were first hybridised with the telomere probe, and the amount of radioactivity was quantified using the Phosphorimager and ImageQuant software. The membranes were dehybridised in boiling water containing 1% SDS, and were then hybridised with the Alu probe; the amount of radioactivity was quantified using the Phosphorimager and ImageQuant software. Fold enrichment of the immunoprecipitated fraction compared to INPUT DNA is calculated as the ratio between telomeric DNA signals after precipitation and telomeric DNA signals in the total INPUT DNA for the same amount of blotted DNA (150ng). The values are normalised to the Alu signal in the immunoprecipitated and INPUT fractions for each condition using the (telomere IP/telomere INPUT)/(Alu IP/Alu INPUT) formula. The % of TRF2 bound to telomeres was given as function of TRF2 bound in treated cells/TRF2 bound in untreated cells.

PCR telomere length.

Genomic DNA of A2780 treated cells with cisplatin, **Pt-ttpy** or **Pt-tpy** during four days at doses inducing 75% growth inhibition was extracted using the DNeasy Blood & Tissue Kit (QIAGEN) and the relative telomere length were determined by real-time PCR using the method described by Cawthon [100], adapted for a LightCycler instrument [101].

Southern blot telomere length

Genomic DNA was isolated from cells using the DNAeasy® blood and tissue Kit (Qiagen). Aliquot of 3 µg DNA was digested overnight at 37 °C with restriction enzymes RsaI and HinfI. DNA fragments were separated by agarose gel electrophoresis, and then transferred under denaturing condition to a nylon membrane by Southern blotting. Telomere length was then estimated using the "Telo TAGGG Telomere Length Assay" kit (Roche).

Western Blot

Western blots were performed following Bio-Rad protocol. Briefly, 20 µg proteins were electrophoresed in SDS-PAGE (SDS-Polyacrylamide 10%) under denaturing conditions, then transferred to a PVDF membrane (Polyvinylidin Difluoride) (Amersham Hybond™ P $^{+}$, GE Healthcare), which was hybridized with mouse monoclonal anti-TRF2 antibody (4A794, Upstate) and anti-actin HRP (SC1616-HRP, Santa-Cruz). TRF2 was revealed by the secondary antibody goat anti-mouse IgG-HRP (ab6789, abcam) using the ECL Western Blotting detection reagent. Western-blot membranes were analysed using FluorChem software program.

Immunofluorescence Assays.

A2780 cells plated on coverslips in 6-well plates. After 4 days of treatment cisplatin, **Pt-ttpy** or **Pt-tpy** during 96h at doses inducing 80% growth inhibition, cells were washed with phosphate-buffered saline (PBS), then fixed 10 minutes in 4% formaldehyde. After a wash with PBS, cells were permeabilised 2 min using 0.5% Triton X-100 and washed with PBS. The cells were incubated in blocking buffer (5% bovine serum albumin in PBS) for 30 min before being incubated for 1 h with the primary mouse

monoclonal antibody against TRF2 (clone 4A794). After three washes with PBS, the cells were incubated for an additional 1 h with the Alexa Fluor 488-conjugated secondary antibody (Alexa Fluor 488 goat anti-mouse IgG; Life Technologies). Nuclei were labeled using TO-PRO®-3 (Life Technologies) and the coverslides were mounted with Vectashield™. Acquisitions were performed on a confocal microscope (Zeiss LSM510) in the SCM (Faculté des Sciences Fondamentales et Biomédicales – Université Paris Descartes). ImageJ software

Telo-FISH

A2780 were cultured in their medium supplemented with cisplatin, **Pt-ttpy** or **Pt-tpy** during 96h at doses inducing 80% growth inhibition at 37°C for 96h in a humidified atmosphere containing 5% CO_2. Cells were then incubated with colcemid (0.1 µg/ml, Sigma) at 37°C for 2h. After trypsinisation and centrifugation (1500 r.p.m for 10 min), they were subjected to hypotonic swelling at 37°C for 20 min. Metaphase preparations were then fixed in ethanol:acetic acid (3:1 v/v) overnight at 4°C. The suspension was applied on cold wet slides and the slides were air-dried overnight. Telo-FISH (Telomere-Fluorescence *in situ* hybridization) was carried out using a telomeric Cyanine-3-conjugated $(C_3TA_2)_3$ peptide nucleic acid (PNA) probe (Applied Biosystems) complementary to the G-rich telomeric strand, as described in details in Pennarun (2008). Metaphases were counterstained with DAPI (1µg/ml), mounted in Fluoromount-G (Southern Biotech) and observed under a fluorescence microscope (Olympus AX70).

ChIP sample preparation

The A2780 cells were treated with the IC_{80} doses of **Pt-ttpy** and cisplatin for 96 hours because under these conditions the two complexes induce 40-50% of damage to genomic DNA. At the end of the treatment, the cells were fixed with 4%. After stopping the fixation by glycine (0.125M) the cells are recovered by scraping, centrifuged and lysed with the lysis buffer (5mM PIPES pH8, 85mM KCl, 0.5% NP40, 1X inhibitor cocktail) using piston B (dounce homogenizer) 10 times in ice. The lysed cells are then aliquoted (approximately 2-4 million per tube) the nucleus was then lysed by the buffer (5mM

Tris-HCl pH8, 10mM EDTA, 1% SDS, 1X inhibitor cocktail) and sonicated to obtain fragments of size 200-700bp. The sonicated chromatin was then incubated with ChIP Adembeads protein A / G (Sigma) which have already blocked for 15 minutes with 225 µl of "blocking buffer" and incubated with 1-3 µg of anti γH2AX antibody (anti -babbit ab2893) in IP buffer (0.01% SDS, 1.1% triton X-100, 1.2mM EDTA, 16.7mM Tris-HCl pH8, 16.7mM NaCl) The beads were then washed with several washing buffers which contain increasing concentrations of NaCl, then the magnetic particles are suspended in 300 µl of elution buffer (0.1M NaHCO3, 1% SDS) and proteinase K. DNA was recovered and purified using phenol / chloroform , and its concentration assayed with Nano-drop and qubit. Its quality was assayed by Agilent 2100 expert high sensitivity DNA assay and the library prepared and high-throughput sequencing done on HiSeq2500 (Rapid Flow cell,50 bases Single Read, Illumina TruSeq Read) by the NGS facility of the Institut Curie. The quality of the IP was also validated by contaminating samples with E. coli DNA which is only very weakly immunoprecipitated under these conditions.

ChIP-seq data analysis

Mapping and peak calling. Raw fastq reads were aligned to the human reference genome (version hg19) using the BWA-mem algorithm (v0.7.5) [102]. We removed reads with a mapping quality inferior to ten or marked as positional duplicates. Peaks for ChIP experiments were detected using MACS2 (v.2.1.0) [103], for each replicate independently, with relevant input reads as background, an FDR threshold of 0.05 and default parameters. Peaks were also called for cisplatin and Pt-ttpy γ-H2AX IPs using the untreated condition reads as background. The obtained peaks were further filtered based on the condition fold change > 3. Finally, we created the bed files used in all the analyses by keeping the peaks present at the intersection between replicates. These final bed files were imported into R for MacOSX [104] to generate the plots reported in the manuscript.

Peak annotation and motif search. We used the annotatePeaks.pl Perl script from HOMER software (v4.9) [105] to annotate all the obtained peaks previously described and to calculate enrichments of the identified features. *De novo* and known motif discovery were carried out using the HOMER motif

analysis pipeline. In addition, sequences within peak regions were scanned for for satIII repeats (-$[GGAAT]_n$-), for telomere repeats ($[TTAGGG]_n$), canonical G-quadruplex motifs with up to 7 or 12 nucleotides in the loops ($G_{3-5}N_{1-7}G_{3-5}N_{1-7}G_{3-5}N_{1-7}G_{3-5}$ or $G_{3-5}N_{1-12}G_{3-5}N_{1-12}G_{3-5}N_{1-12}G_{3-5}$ motifs), GG, GA or GNG occurrences by regular expression matching. The log_2 fold-enrichments reported in the figures were calculated by comparing motif counts within peak regions to counts of the same peak regions after random shuffling of the sequences throughout the hg19 reference genome. Shuffling was performed with a Python implementation of the Altschul-Erikson dinucleotide shuffle algorithm.

Mitochondrial membrane potential

The A2780 cells are cultured in a 6 well plate with the IC_{50} and IC_{80} concentration of the drug. After 96 hours of treatment, we use the JC-1 Mitochondrial Membrane Potential Detection Kit (Biotium) to label the cells. We generate a single cell suspension before staining and transfer 0.5 mL cell suspension to a centrifuge tube. Cells are pelleted by centrifugation for 5 minutes at room temperature at 400 xg and resuspended in 0.5 mL 1X JC-1 Reagent working solution. Cells are incubated at 37°C for 15 minutes and centrifuged again. The pellet collected is washed by resuspending in PBS or cell culture medium followed by centrifugation. The step is repeated once more and finally the cell pellet is resuspended in 0.5 mL PBS or cell culture medium.
Mitochondria containing red JC-1 aggregates in healthy cells are detectable in the PE or PI channel (FL2), and green JC-1 monomers in apoptotic cells are detectable in FITC channel (FL1)

ROS detection

The A2780 cells are cultured in a 6 well plate with IC_{80} concentration of the drug for a duration of 96 hours. CellROX Deep Red (Molecular Probes) was added to the cells at the final concentration of 500-1000nM and left to incubate at 37°C for 30-60 minutes protected from light. The cells are washed with PBS once and analyzed using the flow cytometry. The 635nm excitation is used for the detection of CellROX Deep Red. The flow cytometry experiments are analyzed on the BD FACSCalibur from the Curie Platform.

Detection of mt-DNA lesions

Investigating mitochondrial DNA (mt-DNA) damage in the treatment of different metallic complexes was performed as previously described protocol [80]. Generally, total DNA was purified using DNA

Blood and Tissue Kit (Qiagen, Germany) from cells under different drug treatments. DNA quantity and purity was determined by NanoDrop (Themo Fisher). The isolated DNA showed a high purity (A260/ A280>1.8) and was stored at -20°C. The primers used for real time amplification were synthesized and HPLC-purified by Eurogentec. The primers used in this study are: Short amplicon primers Forward: CATGCCCATCGTCCTAGAAT, Short amplicon primers Reverse: ACGGGCCCTATTTCAAAGAT; Long amplicon primers Forward: CATGCCCATCGTCCTAGAAT, Long amplicon primers Reverse: TGTTGTCGTGCAGGTAGAGG. Briefly, the PCR conditions to run long and short fragments by QuantStudio 5 real-time PCR system and the mt-DNA damage calculated as lesion per 10 kb DNA of each mtDNA region were performed in the same manner as previously reported [80].

Author contribution:

Conceptualization, S.B; Conceptualization and Investigation bioinformatics, E.P-L, A.L-V, A.N; methodology, investigation, S.A, D.G, T.J, G.V, L.A, J.P, S.B; writing—original draft preparation, S.B, E.P-L; writing—review and editing, S.B, E.P-L, D.G, T.J, M-P.T-F, A.L-V, A.N; supervision, SB, M-P.T-F, A.L-V, A.N

Acknowledgments:

High-throughput sequencing has been performed by the ICGex NGS platform of the InstitutCurie supported by the grants ANR-10-EQPX-03 (Equipex) and ANR-10-INBS-09-08 (France Génomique Consortium) from the Agence Nationale de la Recherche ("Investissements d'Avenir" program), by the Canceropole Ile-de-France and by the SiRIC-Curie program - SiRIC Grant « INCa-DGOS- 4654 ".

This research was funded by Association pour la Recherche contre le Cancer (ARC grant for DP), the Institut National du Cancer INCA, (2010-1-PLBIO)04-UP5-14835 grant, IC-3i fellowship in Institute Curie under the Marie Sklodowska-Curie Actions (MSCA) Horizon 2020 program by the European union.

References

1. Burge, S., Parkinson, G. N., Hazel, P., Todd, A. K. & Neidle, S. (2006) Quadruplex DNA: sequence, topology and structure, *Nucleic Acids Res.* **34**, 5402-15.
2. Huppert, J. L. & Balasubramanian, S. (2007) G-quadruplexes in promoters throughout the human genome, *Nucleic Acids Res.* **35**, 406-13.
3. Bedrat, A., Lacroix, L. & Mergny, J. L. (2016) Re-evaluation of G-quadruplex propensity with G4Hunter, *Nucleic Acids Res.* **44**, 1746-59.
4. Puig Lombardi, E. & Londoño-Vallejo, A. (2019) A guide to computational methods for G-quadruplex prediction, *Nucleic Acids Res.* **48**, 1-15.
5. Chambers, V. S., Marsico, G., Boutell, J. M., Di Antonio, M., Smith, G. P. & Balasubramanian, S. (2015) High-throughput sequencing of DNA G-quadruplex structures in the human genome, *Nat Biotechnol*.
6. Hansel-Hertsch, R., Beraldi, D., Lensing, S. V., Marsico, G., Zyner, K., Parry, A., Di Antonio, M., Pike, J., Kimura, H., Narita, M., Tannahill, D. & Balasubramanian, S. (2016) G-quadruplex structures mark human regulatory chromatin, *Nat Genet.* **48**, 1267-72.
7. Biffi, G., Tannahill, D., McCafferty, J. & Balasubramanian, S. (2013) Quantitative visualization of DNA G-quadruplex structures in human cells, *Nat Chem.* **5**, 182-6.
8. Granotier, C., Pennarun, G., Riou, L., Hoffschir, F., Gauthier, L. R., De Cian, A., Gomez, D., Mandine, E., Riou, J. F., Mergny, J. L., Mailliet, P., Dutrillaux, B. & Boussin, F. D. (2005) Preferential binding of a G-quadruplex ligand to human chromosome ends, *Nucleic Acids Res.* **33**, 4182-90.
9. Blasco, M. A. (2005) Telomeres and human disease: ageing, cancer and beyond, *Nat Rev Genet.* **6**, 611-22.
10. de Lange, T. (2005) Shelterin: the protein complex that shapes and safeguards human telomeres, *Genes Dev.* **19**, 2100-10.
11. Palm, W. & de Lange, T. (2008) How shelterin protects mammalian telomeres, *Annu Rev Genet.* **42**, 301-34.
12. de Lange, T. (2018) Shelterin-Mediated Telomere Protection, *Annu Rev Genet.* **52**, 223-247.
13. Ivancich, M., Schrank, Z., Wojdyla, L., Leviskas, B., Kuckovic, A., Sanjali, A. & Puri, N. (2017) Treating Cancer by Targeting Telomeres and Telomerase, *Antioxidants.* **6**.
14. Rhodes, D. & Lipps, H. J. (2015) G-quadruplexes and their regulatory roles in biology, *Nucleic Acids Res.* **43**, 8627-37.
15. Maizels, N. (2012) G4 motifs in human genes, *Ann N Y Acad Sci.* **1267**, 53-60.
16. Murat, P. & Balasubramanian, S. (2014) Existence and consequences of G-quadruplex structures in DNA, *Curr Opin Genet Dev.* **25**, 22-29.
17. Gray, L. T., Vallur, A. C., Eddy, J. & Maizels, N. (2014) G quadruplexes are genomewide targets of transcriptional helicases XPB and XPD, *Nat Chem Biol.* **10**, 313-8.
18. Bugaut, A. & Balasubramanian, S. (2012) 5'-UTR RNA G-quadruplexes: translation regulation and targeting, *Nucleic Acids Res.* **40**, 4727-41.
19. Falabella, M., Fernandez, R. J., Johnson, F. B. & Kaufman, B. A. (2019) Potential Roles for G-Quadruplexes in Mitochondria, *Curr Med Chem.* **26**, 2918-2932.
20. Monchaud, D. & Teulade-Fichou, M. P. (2008) A hitchhiker's guide to G-quadruplex ligands, *Org Biomol Chem.* **6**, 627-36.
21. Neidle, S. (2016) Quadruplex Nucleic Acids as Novel Therapeutic Targets, *J Med Chem.* **59**, 5987-6011.
22. Georgiades, S. N., Karim, N. H. A., Kogularamanan Suntharalingam & Vilar, R. (2010) Interaction of Metal Complexes with G-Quadruplex

DNA, *Angew Chem Int Ed.* **49**, 4020-4034.
23. Vilar, R. (2018) Nucleic Acid Quadruplexes and Metallo-Drugs, *Metal ions in life sciences.* **18**, 325-349.

24. Miller, K. M. & Rodriguez, R. (2011) G-quadruplexes: selective DNA targeting for cancer therapeutics?, *Expert Rev Clin Pharmacol.* **4**, 139-42.
25. Müller, S. & Rodriguez, R. (2014) G-quadruplex interacting small molecules and drugs: from bench toward bedside, *Expert Rev Clin Pharmacol.* **7**, 663-79.
26. Falabella, M., Kolesar, J. E., Wallace, C., de Jesus, D., Sun, L., Taguchi, Y. V., Wang, C., Wang, T., Xiang, I. M., Alder, J. K., Maheshan, R., Horne, W., Turek-Herman, J., Pagano, P. J., St Croix, C. M., Sondheimer, N., Yatsunyk, L. A., Johnson, F. B. & Kaufman, B. A. (2019) G-quadruplex dynamics contribute to regulation of mitochondrial gene expression, *Scientific reports.* **9**, 5605.
27. Rao, L. & Bierbach, U. (2007) Kinetically favored platination of adenine in the g-rich human telomeric repeat, *J Am Chem Soc.* **129**, 15764-5.
28. Rao, L., Dworkin, J. D., Nell, W. E. & Bierbach, U. (2011) Interactions of a Platinum-Modified Perylene Derivative with the Human Telomeric G-Quadruplex, *J Phys Chem B.* **115**, 13701-13712.
29. Bertrand H, Bombard S, Monchaud D & Teulade-Fichou, M. P. (2007) A Platinum-Quinacridine Hybrid as G-Quadruplex Ligand, *J Biol Inorg Chem.* **12**, 1003-1014.
30. Bertrand, H., Bombard, S., Monchaud, D., Talbot, E., Guedin, A., Mergny, J. L., Grunert, R., Bednarski, P. J. & Teulade-Fichou, M. P. (2009) Exclusive platination of loop adenines in the human telomeric G-quadruplex, *Org Biomol Chem.* **7**, 2864-71.
31. Betzer, J. F., Nuter, F., Chtchigrovsky, M., Hamon, F., Kellermann, G., Ali, S., M.A., C., Roque, S., Poupon, J., Cresteil, T., Teulade-Fichou, M. P., Marinetti, A. & Bombard, S. (2016) Linking of antitumour trans NHC-Pt(II) complexes to G-quadruplex DNA ligand for telomeric targeting, *Bioconjug Chem.* **27**, 1456.
32. He, L., Meng, Z., Xu, D. & Shao, F. (2018) Dual functional dinuclear platinum complex with selective reactivity towards c-myc G-quadruplex, *Scientific reports.* **8**, 767.
33. Bertrand, H., Monchaud, D., De Cian, A., Guillot, R., Mergny, J. L. & Teulade-Fichou, M. P. (2007) The importance of metal geometry in the recognition of G-quadruplex-DNA by metal-terpyridine complexes, *Org Biomol Chem.* **5**, 2555-9.
34. Morel, E., Beauvineau, C., Naud-Martin, D., Landras-Guetta, C., Verga, D., Ghosh, D., Achelle, S., Mahuteau-Betzer, F., Bombard, S. & Teulade-Fichou, M. P. (2019) Selectivity of Terpyridine Platinum Anticancer Drugs for G-quadruplex DNA, *Molecules.* **24**.
35. Trajkovski, M., Morel, E., Hamon, F., Bombard, S., Teulade-Fichou, M. P. & Plavec, J. (2015) Interactions of Pt-ttpy with G-Quadruplexes Originating from Promoter Region of the c-myc Gene Deciphered by NMR and Gel Electrophoresis Analysis, *Chem Eur J.* **21**, 7798-807.
36. Merle, P., Gueugneau, M., Teulade-Fichou, M. P., Müller-Barthélémy, M., Amiard, S., Chautard, E., Guetta, C., Dedieu, V., Communal, Y., Mergny, J. L., Gallego, M., White, C., Verrelle, P. & Tchirkov, A. (2015) Highly efficient radiosensitization of human glioblastoma and lung cancer cells by a G-quadruplex DNA binding compound, *Sci Rep.* **5**, 16255-16266.
37. Saker, L., Ali, S., Masserot, C., Kellermann, G., Poupon, J., Teulade-Fichou, M. P., Segal-Bendirdjian, E. & Bombard, S. (2018) Platinum Complexes Can Bind to Telomeres by Coordination, *International journal of molecular sciences.* **19**, 1951-1966.
38. Lee, H. S., Carmena, M., Liskovykh, M., Peat, E., Kim, J. H., Oshimura, M., Masumoto, H., Teulade-Fichou, M. P., Pommier, Y., Earnshaw, W. C., Larionov, V. & Kouprina, N. (2018) Systematic Analysis of Compounds Specifically Targeting Telomeres and Telomerase for Clinical Implications in Cancer Therapy, *Cancer Res.* **78**, 6282-6296.
39. Erxleben, A. (2019) Mitochondria-Targeting Anticancer Metal Complexes, *Curr Med Chem.* **26**, 694-728.
40. Groessl, M., Zava, O. & Dyson, P. J. (2011) Cellular uptake and subcellular distribution of ruthenium-based metallodrugs under clinical investigation versus cisplatin, *Metallomics.* **3**, 591-9.
41. Wallace, D. C., Fan, W. & Procaccio, V. (2010) Mitochondrial energetics and therapeutics, *Annual review of pathology.* **5**, 297-348.
42. Andreux, P. A., Houtkooper, R. H. & Auwerx, J. (2013) Pharmacological approaches to restore mitochondrial function, *Nat Rev Drug Discov.* **12**, 465-83.

43. Fulda, S., Galluzzi, L. & Kroemer, G. (2010) Targeting mitochondria for cancer therapy, *Nat Rev Drug Discov.* **9**, 447-64.
44. Wallace, D. C. (2012) Mitochondria and cancer, *Nat Rev Cancer.* **12**, 685-98.
45. Cocetta, V., Ragazzi, E. & Montopoli, M. (2019) Mitochondrial Involvement in Cisplatin Resistance, *International journal of molecular sciences.* **20**.
46. Ourliac Garnier, I. & Bombard, S. (2007) GG sequence of DNA and the human telomeric sequence react with cis-diammine-diaquaplatinum at comparable rates, *J Inorg Biochem.* **101**, 514-24.
47. Jamieson, E. R. & Lippard, S. J. (1999) Structure, Recognition, and processing of Cisplatin-DNA Adducts, *Chem Rev.* **99**, 2467-2498.
48. Jung, Y. & Lippard, S. J. (2007) Direct cellular responses to platinum-induced DNA damage, *Chem Rev.* **107**, 1387-407.
49. Chaney, S. G., Campbell, S. L., Bassett, E. & Wu, Y. (2005) Recognition and processing of cisplatin- and oxaliplatin-DNA adducts, *Crit Rev Oncol Hematol.* **53**, 3-11.
50. Ghezzi, A., Aceto, M., Cassino, C., Gabano, E. & Osella, D. (2004) Uptake of antitumor platinum(II)-complexes by cancer cells, assayed by inductively coupled plasma mass spectrometry (ICP-MS), *J Inorg Biochem.* **98**, 73-8.
51. Corte Rodriguez, M., Alvarez-Fernandez Garcia, R., Blanco, E., Bettmer, J. & Montes-Bayon, M. (2017) Quantitative Evaluation of Cisplatin Uptake in Sensitive and Resistant Individual Cells by Single-Cell ICP-MS (SC-ICP-MS), *Anal Chem.* **89**, 11491-11497.
52. Amable, L. (2016) Cisplatin resistance and opportunities for precision medicine, *Pharmacological research.* **106**, 27-36.
53. Parker, R. J., Eastman, A., Bostick-Bruton, F. & Reed, E. (1991) Acquired cisplatin resistance in human ovarian cancer cells is associated with enhanced repair of cisplatin-DNA lesions and reduced drug accumulation, *J Clin Invest.* **87**, 772-7.
54. Safaei, R., Larson, B. J., Cheng, T. C., Gibson, M. A., Otani, S., Naerdemann, W. & Howell, S. B. (2005) Abnormal lysosomal trafficking and enhanced exosomal export of cisplatin in drug-resistant human ovarian carcinoma cells, *Mol Cancer Ther.* **4**, 1595-604.
55. Lee, R. F. S., Riedel, T., Escrig, S., Maclachlan, C., Knott, G. W., Davey, C. A., Johnsson, K., Meibom, A. & Dyson, P. J. (2017) Differences in cisplatin distribution in sensitive and resistant ovarian cancer cells: a TEM/NanoSIMS study, *Metallomics.* **9**, 1413-1420.
56. Tahara, H., Shin-Ya, K., Seimiya, H., Yamada, H., Tsuruo, T. & Ide, T. (2006) G-Quadruplex stabilization by telomestatin induces TRF2 protein dissociation from telomeres and anaphase bridge formation accompanied by loss of the 3' telomeric overhang in cancer cells, *Oncogene.* **25**, 1955-66.
57. Gomez, D., O'Donohue, M. F., Wenner, T., Douarre, C., Macadre, J., Koebel, P., Giraud-Panis, M. J., Kaplan, H., Kolkes, A., Shin-ya, K. & Riou, J. F. (2006) The G-quadruplex ligand telomestatin inhibits POT1 binding to telomeric sequences in vitro and induces GFP-POT1 dissociation from telomeres in human cells, *Cancer Res.* **66**, 6908-12.
58. Zhou, W. J., Deng, R., Zhang, X. Y., Feng, G. K., Gu, L. Q. & Zhu, X. F. (2009) G-quadruplex ligand SYUIQ-5 induces autophagy by telomere damage and TRF2 delocalization in cancer cells, *Mol Cancer Ther.* **8**, 3203-13.
59. Pagano, B., Amato, J., Iaccarino, N., Cingolani, C., Zizza, P., Biroccio, A., Novellino, E. & Randazzo, A. (2015) Looking for efficient G-quadruplex ligands: evidence for selective stabilizing properties and telomere damage by drug-like molecules, *ChemMedChem.* **10**, 640-9.
60. Rizzo, A., Iachettini, S., Zizza, P., Cingolani, C., Porru, M., Artuso, S., Stevens, M., Hummersone, M., Biroccio, A., Salvati, E. & Leonetti, C. (2014) Identification of novel RHPS4-derivative ligands with improved toxicological profiles and telomere-targeting activities, *Journal of experimental & clinical cancer research : CR.* **33**, 81-89.
61. Qin, H., Zhao, C., Sun, Y., Ren, J. & Qu, X. (2017) Metallo-supramolecular Complexes Enantioselectively Eradicate Cancer Stem Cells in Vivo, *J Am Chem Soc.* **139**, 16201-16209.
62. Salvati, E., Leonetti, C., Rizzo, A., Scarsella, M., Mottolese, M., Galati, R., Sperduti, I., Stevens, M. F., D'Incalci, M., Blasco, M., Chiorino, G., Bauwens, S., Horard, B., Gilson, E., Stoppacciaro, A., Zupi, G.

& Biroccio, A. (2007) Telomere damage induced by the G-quadruplex ligand RHPS4 has an antitumor effect, *J Clin Invest.* **117**, 3236-47.
63. Charif, R., Granotier-Beckers, C., Bertrand, H. C., Poupon, J., Ségal-Bendirdjian, E., Teulade-Fichou, M. P., Boussin, F. D. & Bombard, S. (2017) Association of a platinum complex to a G-quadruplex ligand enhances the telomere disruption, *Chem ResTox.* **38**, 1629-1640.
64. Pennarun, G., Granotier, C., Gauthier, L. R., Gomez, D., Hoffschir, F., Mandine, E., Riou, J. F., Mergny, J. L., Mailliet, P. & Boussin, F. D. (2005) Apoptosis related to telomere instability and cell cycle alterations in human glioma cells treated by new highly selective G-quadruplex ligands, *Oncogene.* **24**, 2917-28.
65. Brassart, B., Gomez, D., De Cian, A., Paterski, R., Montagnac, A., Qui, K. H., Temime-Smaali, N., Trentesaux, C., Mergny, J. L., Gueritte, F. & Riou, J. F. (2007) A new steroid derivative stabilizes g-quadruplexes and induces telomere uncapping in human tumor cells, *Mol Pharmacol.* **72**, 631-40.
66. Simonet, T., Zaragosi, L. E., Philippe, C., Lebrigand, K., Schouteden, C., Augereau, A., Bauwens, S., Ye, J., Santagostino, M., Giulotto, E., Magdinier, F., Horard, B., Barbry, P., Waldmann, R. & Gilson, E. (2011) The human TTAGGG repeat factors 1 and 2 bind to a subset of interstitial telomeric sequences and satellite repeats, *Cell Res.* **21**, 1028-38.
67. Gomez, D., Guedin, A., Mergny, J. L., Salles, B., Riou, J. F., Teulade-Fichou, M. P. & Calsou, P. (2010) A G-quadruplex structure within the 5'-UTR of TRF2 mRNA represses translation in human cells, *Nucleic Acids Res*.
68. Takai, H., Smogorzewska, A. & de Lange, T. (2003) DNA damage foci at dysfunctional telomeres, *Curr Biol.* **13**, 1549-56.
69. Sears, C. R., Cooney, S. A., Chin-Sinex, H., Mendonca, M. S. & Turchi, J. J. (2016) DNA damage response (DDR) pathway engagement in cisplatin radiosensitization of non-small cell lung cancer, *DNA Repair (Amst).* **40**, 35-46.
70. Tsuji, J., Frith, M. C., Tomii, K. & Horton, P. (2012) Mammalian NUMT insertion is non-random, *Nucleic Acids Res.* **40**, 9073-88.
71. Jeong, J. H., Cheol Kang, Y., Piao, Y., Kang, S. & Pak, Y. K. (2017) miR-24-mediated knockdown of H2AX damages mitochondria and the insulin signaling pathway, *Experimental & molecular medicine.* **49**, e313.
72. Choi, Y. S., Jeong, J. H., Min, H. K., Jung, H. J., Hwang, D., Lee , S. W. & Pak, Y. K. (2011) Shot-gun proteomic analysis of mitochondrial D-loop DNA binding proteins: identification of mitochondrial histones, *Molecular BioSystems.* **7**, 1523-1536.
73. Shu, X., Xiong, X., Song, J., He, C. & Yi, C. (2016) Base-Resolution Analysis of Cisplatin-DNA Adducts at the Genome Scale, *Angewandte Chemie.* **55**, 14246-14249.
74. Hu, J., Lieb, J. D., Sancar, A. & Adar, S. (2016) Cisplatin DNA damage and repair maps of the human genome at single-nucleotide resolution, *Proc Natl Acad Sci U S A.* **113**, 11507-11512.
75. Wang, K., Zhu, C., He, Y., Zhang, Z., Zhou, W., Muhammad, N., Guo, Y., Wang, X. & Guo, Z. (2019) Restraining Cancer Cells by Dual Metabolic Inhibition with a Mitochondrion-Targeted Platinum(II) Complex, *Angewandte Chemie.* **58**, 4638-4643.
76. Guo, Y., He, Y., Wu, S., Zhang, S., Song, D., Zhu, Z., Guo, Z. & Wang, X. (2019) Enhancing Cytotoxicity of a Monofunctional Platinum Complex via a Dual-DNA-Damage Approach, *Inorg Chem.* **58**, 13150-13160.
77. Zorov, D. B., Juhaszova, M. & Sollott, S. J. (2006) Mitochondrial ROS-induced ROS release: an update and review, *Biochim Biophys Acta.* **1757**, 509-17.
78. Wisnovsky, S. P., Wilson, J. J., Radford, R. J., Pereira, M. P., Chan, M. R., Laposa, R. R., Lippard, S. J. & Kelley, S. O. (2013) Targeting mitochondrial DNA with a platinum-based anticancer agent, *Chem Biol.* **20**, 1323-8.
79. Zhu, Z., Wang, Z., Zhang, C., Wang, Y., Zhang, H., Gan, Z., Guo, Z. & Wang, X. (2019) Mitochondrion-targeted platinum complexes suppressing lung cancer through multiple pathways involving energy metabolism, *Chem Sci.* **10**, 3089-3095.
80. Rothfuss, O., Gasser, T. & Patenge, N. (2010) Analysis of differential DNA damage in the mitochondrial genome employing a semi-long run real-time PCR approach, *Nucleic Acids Res.* **38**, e24.

81. Galluzzi, L., Senovilla, L., Vitale, I., Michels, J., Martins, I., Kepp, O., Castedo, M. & Kroemer, G. (2012) Molecular mechanisms of cisplatin resistance, *Oncogene.* **31**, 1869-83.
82. Chtchigrovsky, M., Eloy, L., Jullien, H., Saker, L., Segal-Bendirdjian, E., Poupon, J., Bombard, S., Cresteil, T., Retailleau, P. & Marinetti, A. (2013) Antitumor trans-N-heterocyclic carbene-amine-Pt(II) complexes: synthesis of dinuclear species and exploratory investigations of DNA binding and cytotoxicity mechanisms, *J Med Chem.* **56**, 2074-86.
83. Wexeslblatt, E., Yavin, E. & Gibson, D. (2012) Cellular interactions of platinum drugs, *Inorg Chim Acta.* **393**, 75-83.
84. Brassart, B., Gomez, D., De Cian, A., Paterski, R., Montagnac, A., Qui, K. H., Temime-Smaali, N., Trentesaux, C., Mergny, J. L., Gueritte, F. & Riou, J. F. (2007) A new steroid derivative stabilizes G-quadruplexes and induces telomere uncapping in human tumor cells, *Mol Pharmacol*.
85. Muoio, D., Berardinelli, F., Leone, S., Coluzzi, E., di Masi, A., Doria, F., Freccero, M., Sgura, A., Folini, M. & Antoccia, A. (2018) Naphthalene diimide-derivatives G-quadruplex ligands induce cell proliferation inhibition, mild telomeric dysfunction and cell cycle perturbation in U251MG glioma cells, *The FEBS journal.* **285**, 3769-3785.
86. Zheng, X. H., Mu, G., Zhong, Y. F., Zhang, T. P., Cao, Q., Ji, L. N., Zhao, Y. & Mao, Z. W. (2016) Trigeminal star-like platinum complexes induce cancer cell senescence through quadruplex-mediated telomere dysfunction, *Chem Commun (Camb).* **52**, 14101-14104.
87. Arnoult, N. & Karlseder, J. (2015) Complex interactions between the DNA-damage response and mammalian telomeres, *Nat Struct Mol Biol.* **22**, 859-66.
88. Sfeir, A. & de Lange, T. (2012) Removal of shelterin reveals the telomere end-protection problem, *Science.* **336**, 593-7.
89. Huppert, J. L. & Balasubramanian, S. (2005) Prevalence of quadruplexes in the human genome, *Nucleic Acids Res.* **33**, 2908-16.
90. Rodriguez, R., Miller, K. M., Forment, J. V., Bradshaw, C. R., Nikan, M., Britton, S., Oelschlaegel, T., Xhemalce, B., Balasubramanian, S. & Jackson, S. P. (2012) Small-molecule-induced DNA damage identifies alternative DNA structures in human genes, *Nat Chem Biol.* **8**, 301-10.
91. Yimit, A., Adebali, O., Sancar, A. & Jiang, Y. (2019) Differential damage and repair of DNA-adducts induced by anti-cancer drug cisplatin across mouse organs, *Nat Commun.* **10**, 309.
92. Wang, D., Hara, R., Singh, G., Sancar, A. & Lippard, S. J. (2003) Nucleotide excision repair from site-specifically platinum-modified nucleosomes, *Biochemistry.* **42**, 6747-53.
93. Perera, D., Poulos, R. C., Shah, A., Beck, D., Pimanda, J. E. & Wong, J. W. (2016) Differential DNA repair underlies mutation hotspots at active promoters in cancer genomes, *Nature.* **532**, 259-63.
94. Kleih, M., Bopple, K., Dong, M., Gaissler, A., Heine, S., Olayioye, M. A., Aulitzky, W. E. & Essmann, F. (2019) Direct impact of cisplatin on mitochondria induces ROS production that dictates cell fate of ovarian cancer cells, *Cell death & disease.* **10**, 851.
95. Marullo, R., Werner, E., Degtyareva, N., Moore, B., Altavilla, G., Ramalingam, S. S. & Doetsch, P. W. (2013) Cisplatin induces a mitochondrial-ROS response that contributes to cytotoxicity depending on mitochondrial redox status and bioenergetic functions, *PLoS One.* **8**, e81162.
96. Kumar, N., Qian, W. & Van Houten, B. (2020) Sick mitochondria cause telomere damage: implications for disease, *Molecular & cellular oncology.* **7**, 1678362.
97. Qian, W., Kumar, N., Roginskaya, V., Fouquerel, E., Opresko, P. L., Shiva, S., Watkins, S. C., Kolodieznyi, D., Bruchez, M. P. & Van Houten, B. (2019) Chemoptogenetic damage to mitochondria causes rapid telomere dysfunction, *Proc Natl Acad Sci U S A.* **116**, 18435-18444.
98. Betzer, J. F., Nuter, F., Chtchigrovsky, M., Hamon, F., Kellermann, G., Ali, S., Calmejane, M. A., Roque, S., Poupon, J., Cresteil, T., Teulade-Fichou, M. P., Marinetti, A. & Bombard, S. (2016) Linking of Antitumor trans NHC-Pt(II) Complexes to G-Quadruplex DNA Ligand for Telomeric Targeting, *Bioconjug Chem.* **27**, 1456-1470.
99. Amiard, S., Doudeau, M., Pinte, S., Poulet, A., Lenain, C., Faivre-Moskalenko, C., Angelov, D., Hug, N., Vindigni, A., Bouvet, P., Paoletti, J., Gilson, E. & Giraud-Panis, M. J. (2007) A topological mechanism for TRF2-enhanced strand invasion, *Nat Struct Mol Biol.* **14**, 147-54.
100. Cawthon, R. M. (2002) Telomere measurement by quantitative PCR, *Nucleic Acids Res.* **30**, e47.

101. Gil, M. E. & Coetzer, T. L. (2004) Real-time quantitative PCR of telomere length, *Mol Biotechnol.* **27**, 169-72.
102. Li, H. (2013) Aligning sequence reads, clone sequences and assembly contigs with BWA-MEM, *arXivorg* 1303.3997v2.
103. Zhang, Y., Liu, T., Meyer, C. A., Eeckhoute, J., Johnson, D. S., Bernstein, B. E., Nusbaum, C., Myers, R. M., Brown, M., Li, W. & Liu, X. S. (2008) Model-based analysis of ChIP-Seq (MACS), *Genome Biol.* **9**, R137.
104. R Core Team R (2017) R: A language and environment for statistical computing. R Foundation for Statistical Computing,, *Vienna, Austria URL https://wwwR-projectorg*
105. Heinz, S., Benner, C., Spann, N., Bertolino, E., Lin, Y. C., Laslo, P., Cheng, J. X., Murre, C., Singh, H. & Glass, C. K. (2010) Simple combinations of lineage-determining transcription factors prime cis-regulatory elements required for macrophage and B cell identities, *Mol Cell.* **38**, 576-89.

Table

	A2780 cells			A2780cis cells			Resistance factor		
	Cis-Pt	Pt-ttpy	Pt-tpy	Cis-Pt	Pt-ttpy	Pt-tpy	Cis-Pt	Pt-ttpy	Pt-tpy
IC_{50} (µM)	0.33	2.5	3	4	2.5	5	12.1	1	1.7
Uptake	1	16	8	1	2.1	1.6			
DNA	1	1.6	1.2	1	0.4	0.3			
IC_{80} (µM)	0.66	4	5.5	7	4	8	1.6	1	1.5
Uptake	1	9	7.4	1	1.4	1.5			
DNA	1	0.8	0.7	1	0.4	0.3			
Mitochondria	1	12	2.3						

Table 1: IC_{50}, IC_{80} of cisplatin, **Pt-ttpy** and **Pt-tpy** in A2780 and A2780cis cells and their resistance factor (ratio IC A2780cis/IC A2780). Standard error have been evaluated between 5 and 15%. Relative (as compared to cisplatin) cellular uptake of platinum, platinum bound to DNA and platinum mitochondria accumulation in A2780 and A2780cis cells after treatment with cisplatin, **Pt-ttpy** and **Pt-tpy** at their respective IC_{50} and IC_{80}

SCHEME

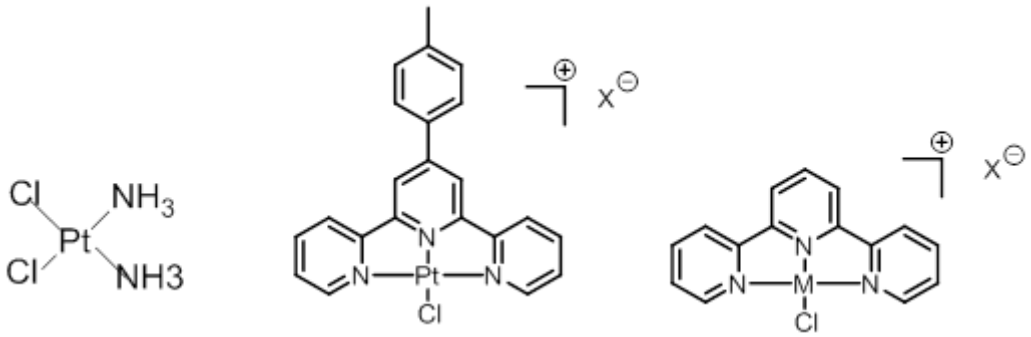

Scheme 1: Chemical structure of cisplatin, **Pt-ttpy** and **Pt-tpy**

Figure legends:

Figure 1: Cell growth inhibition. (A) % cell growth inhibition of A2780 cells by cisplatin, **Pt-ttpy** and **Pt-tpy**. (B) % cell growth inhibition of A2780cis cells by cisplatin, **Pt-ttpy** and **Pt-tpy.** Cell growth was evaluated by cell counting using cell counter (At least 10 experiments).

Figure 2: Cellular uptake and amount of platinum complexes bound to genomic DNA in A2780 and A2780cis cells. The metal content was determined after 96h incubation time at the IC_{50} and IC_{80} doses of cisplatin, **Pt-ttpy** and **Pt-tpy**, respectively**,** in A2780 (grey bars) and A2780cis (black bars) for 5 10^6 cells or rationalized per mg of genomic DNA extracted.

Figure 3: **TRF2 foci quantification detected by immunofluorescence on A2780 and A2780cis cells** treated with cisplatin, **Pt-ttpy** and **Pt-tpy** for 96h at their respective IC_{80} concentration**.** (A) A2780 cells were processed for immunofluorescence using antibodies against TRF2. (B) % of TRF2 foci after A2780 cell treatments with cisplatin, **Pt-ttpy** and **Pt-tpy** (C) % of TRF2 foci after A2780cis cell treatments with cisplatin, **Pt-ttpy** and **Pt-tpy** (mean of at least 3 experiments). ** Indicates a Mann and Withney test P-value <0.01 and * P< 0.05 (GraphPad PRISM software)

Figure 4: **Proteins bound to telomeres quantified from dot-blots.** Dot blots membranes of ChIP of TRF2, TRF1, POT1 and H3 on A2780 cells treated by doses of **Pt-ttpy** (A), **Pt-tpy** (B**) and** cisplatin (C) for 96h at their respective IC_{80} concentration. (D) % of proteins bound to telomeres of A2780 cells. (E) % of proteins bound to telomeres of A2780cis cells. Telomeric sequences were evidenced in a DNA fraction immunoprecipitated by an anti-TRF1, anti-TRF2, anti-H3 antibody using a ^{32}P radiolabelled 800pb telomeric probe and normalized with α ^{32}P radiolabelled Alu sequences in untreated, cisplatin, **Pt-ttpy** and **Pt-tpy** treated cells. 200ng of DNA were blotted for each sample. The % represents the quantitative values of telomeric DNA signals in the samples originating from cells with treatment compared to the cells without any treatment. Quantitative values of telomeric DNA signals are calculated as the ratio between telomeric DNA signal precipitation and telomeric DNA signals in the INPUT for the same amount of blotted DNA. These values have been normalised by the amount of

blotted DNA for each sample quantified by the non-specific Alu probe, following the formula: (telomere IP/telomere INPUT)/(Alu IP/Alu INPUT). (Means of at least 3 experiments)** Indicates a Mann and Withney test P-value <0.01 and * P<0.05 (GraphPad PRISM software)**.** Statistical analysis was made by comparing the amount of protein bound to telomeres for each treatment.

Figure 5: **Western blot of TRF2 and telomere length from A2780 treated cells** with cisplatin, **Pt-ttpy** and **Pt-tpy** for 96h**.** (A) Western blot membranes, (B) TRF2 relative protein level normalized with actin (Mean of 3 experiments), (C) Southern blot or (D) Relative telomere length measured by qPCR. The values were normalized using 36B4u gene (Mean of 3 experiments)

Figure 6: DNA damage activation at telomeres. A2780 cells were treated for 96h with **Pt-ttpy**, **Pt-tpy** and cisplatin at their IC_{80} concentration. Cells were processed for immunofluorescence using antibodies against γ-H2AX and C-rich PNA telomeric probe. (A) Z project of microscopy confocal acquisitions of cells treated with **Pt-ttpy**. (B) Percentages of γ-H2AX positive cells. (C) Percentages of TIFs positive cells in untreated and treated cells. Cells with more than twenty γ-H2AX foci and more than three TIFs were scored as γ-H2AX and TIF positive, respectively. (Mean of at least 3 experiments) * Indicates a Mann and Withney test P-value <0.05 (GraphPad PRISM software)

Figure 7: γ-H2AX domains of cisplatin and Pt-ttpy are enriched in the same chromosomes, notably in mitochondrial DNA. (A) γ-H2AX binding sites (peaks) detected in A2780 cells treated with cisplatin or Pt-ttpy. (B) Circular plot showing the genome-wide peak distribution of cisplatin and **Pt-ttpy** γ-H2AX IPs over the untreated γ-H2AX IP. From the outermost to the innermost circle: orange, GC-content over all chromosomes; red, cisplatin γ-H2AX peaks and; blue, Pt-ttpy γ-H2AX peaks. (C) Relative peak enrichment on each chromosome and mtDNA annotated chrM. Blue, **Pt-ttpy** γ-H2AX peaks; red, cisplatin γ-H2AX peaks.

Figure 8: γ-H2AX domains of cisplatin and Pt-ttpy are enriched in specific G- and A-rich sequences. (A) Annotation of cisplatin and **Pt-ttpy** γ-H2AX IPs over the untreated γ-H2AX IP. Top panel, **Pt-ttpy** treated cells; bottom panel, cisplatin treated cells. (B). Feature enrichments for cisplatin and **Pt-ttpy** γ-

H2AX IPs over the untreated γ-H2AX IP. Six G-rich motifs were assessed: telomeric repeats, [TTAGGG]n>1; canonical G-quadruplex motifs with up to 7 (G4L1-7) or 12 nucleotides (G4L1-12) in the loops, $G_{3-5}N_{1-7}G_{3-5}N_{1-7}G_{3-5}N_{1-7}G_{3-5}$ or $G_{3-5}N_{1-12}G_{3-5}N_{1-12}G_{3-5}N_{1-12}G_{3-5}$; GG, GA or GNG sites; as well as the promoter annotation feature.

Figure 9: Effects of Pt-ttpy on mitochondrial related function as compared to Pt-tpy and cisplatin. (A) Platinum accumulation (ng) in mitochondria of 5 10^6 cells treated at the IC_{80} dose of the respective platinum complex. (B) % Cells with mitochondrial membrane loss (dysfunctional mitochondria) after treatment at the respective IC_{50} and IC_{80} concentrations of the complexes (C) ROS generation after treatment at the IC_{80} concentration of the complexes. (D) Quantification of mitochondrial DNA lesion per 10 kb DNA by SLR rt-PCR amplification of total DNA isolated from A2780 cells treated by **Pt-ttpy, Pt-tpy** and cisplatin in the indicated domain. * Indicates a t-test P-value P< 0.05 (GraphPad PRISM software)

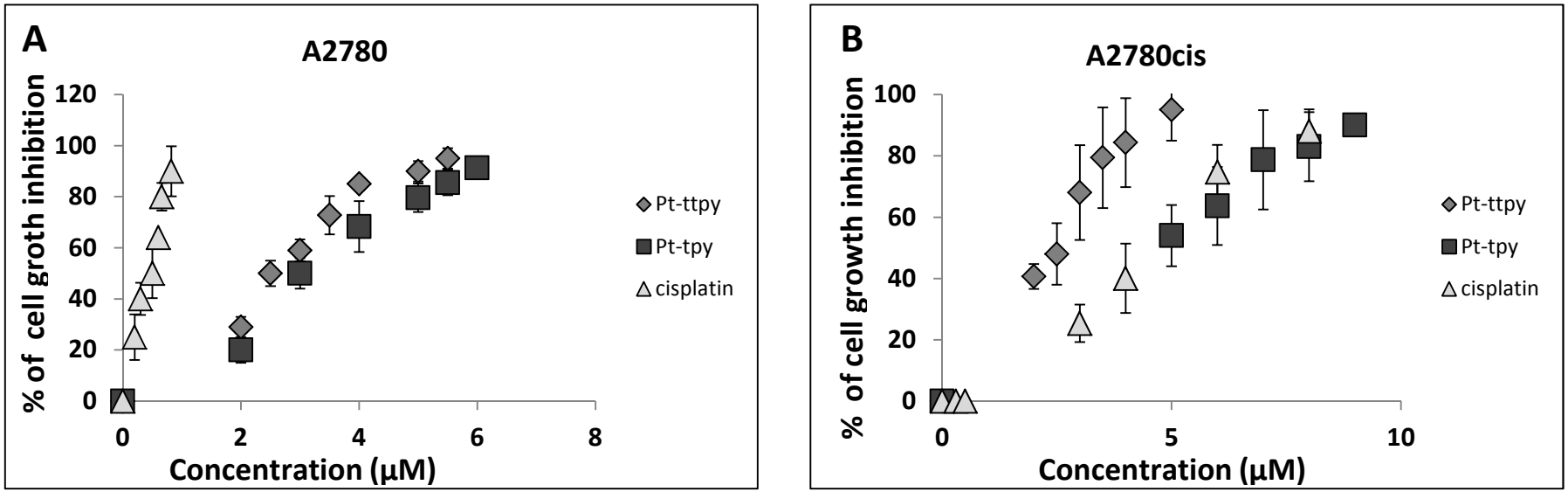
A
A2780
% of cell groth inhibition
120
100
80
60
40
20
0
0
2
4
6
8
Concentration (µM)
Pt-ttpy
Pt-tpy
cisplatin
B
A2780cis
% of cell growth inhibition
100
80
60
40
20
0
0
5
10
Concentration (µM)
Pt-ttpy
Pt-tpy
cisplatin

Figure 1

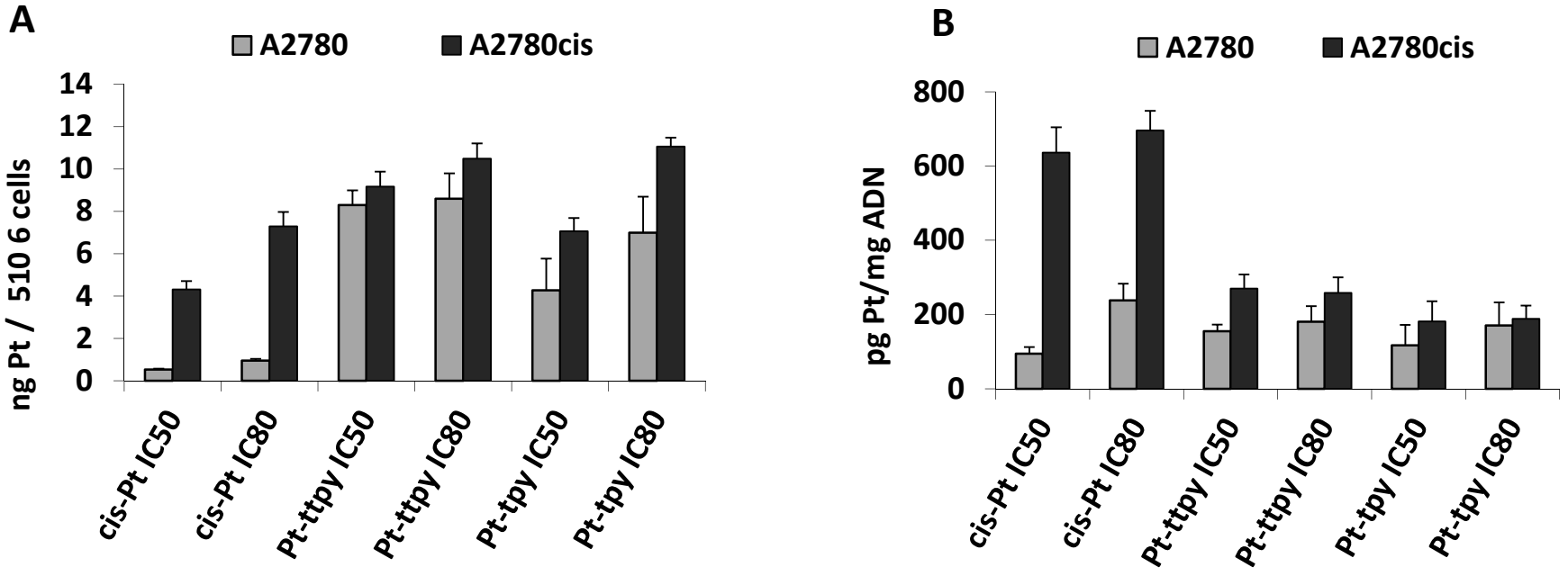
A
A2780
A2780cis
ng Pt / 510 6 cells
14
12
10
8
6
4
2
0
cis-Pt IC50
cis-Pt IC80
Pt-ttpy IC50
Pt-ttpy IC80
Pt-tpy IC50
Pt-tpy IC80
B
A2780
A2780cis
pg Pt/mg ADN
800
600
400
200
0
cis-Pt IC50
cis-Pt IC80
Pt-ttpy IC50
Pt-ttpy IC80
Pt-tpy IC50
Pt-tpy IC80

Figure 2

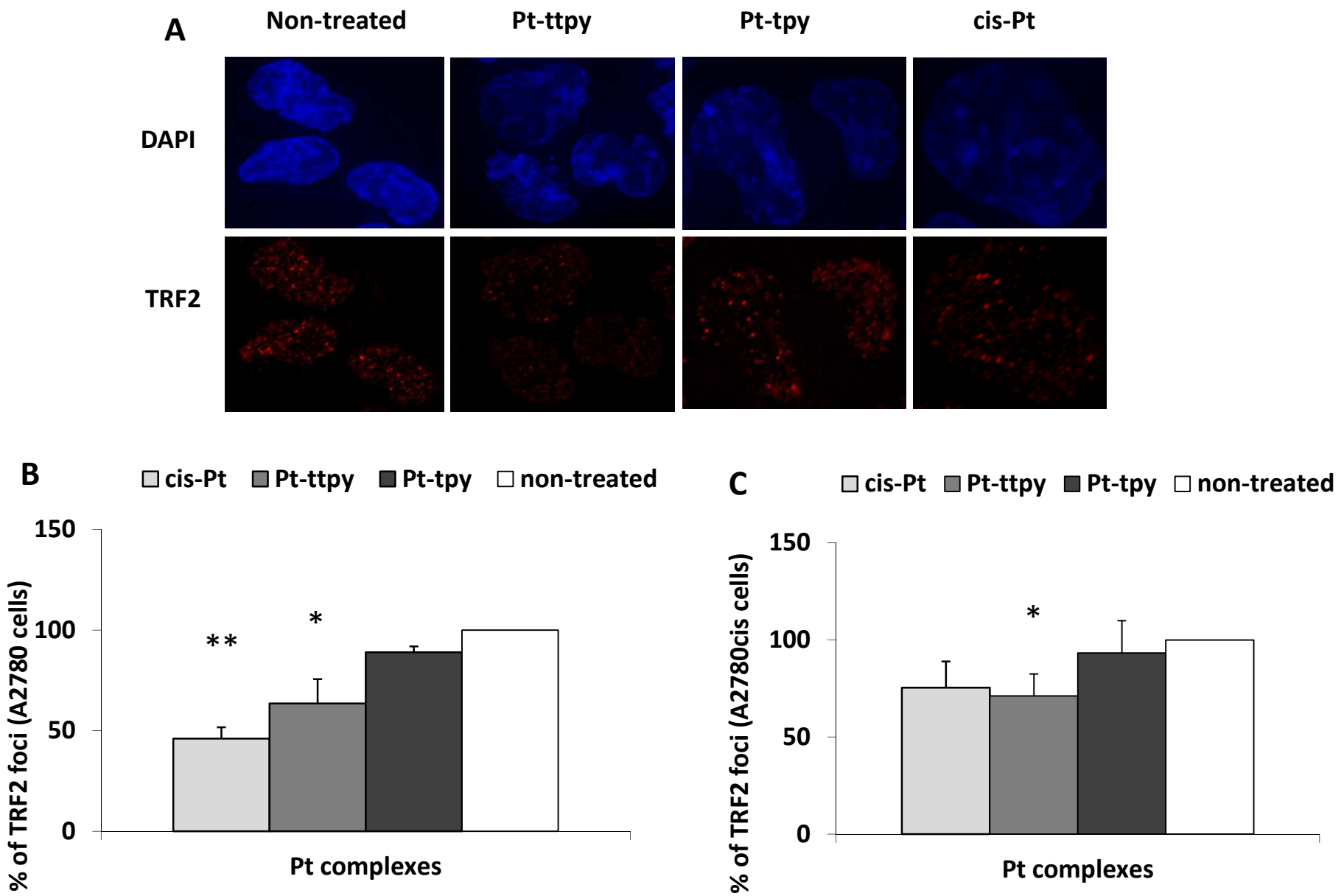
A
Non-treated
Pt-ttpy
Pt-tpy
cis-Pt
DAPI
TRF2
B
cis-Pt
Pt-ttpy
Pt-tpy
non-treated
150
100
50
0
% of TRF2 foci (A2780 cells)
**
*
Pt complexes
C
cis-Pt
Pt-ttpy
Pt-tpy
non-treated
150
100
50
0
% of TRF2 foci (A2780cis cells)
*
Pt complexes

Figure 3

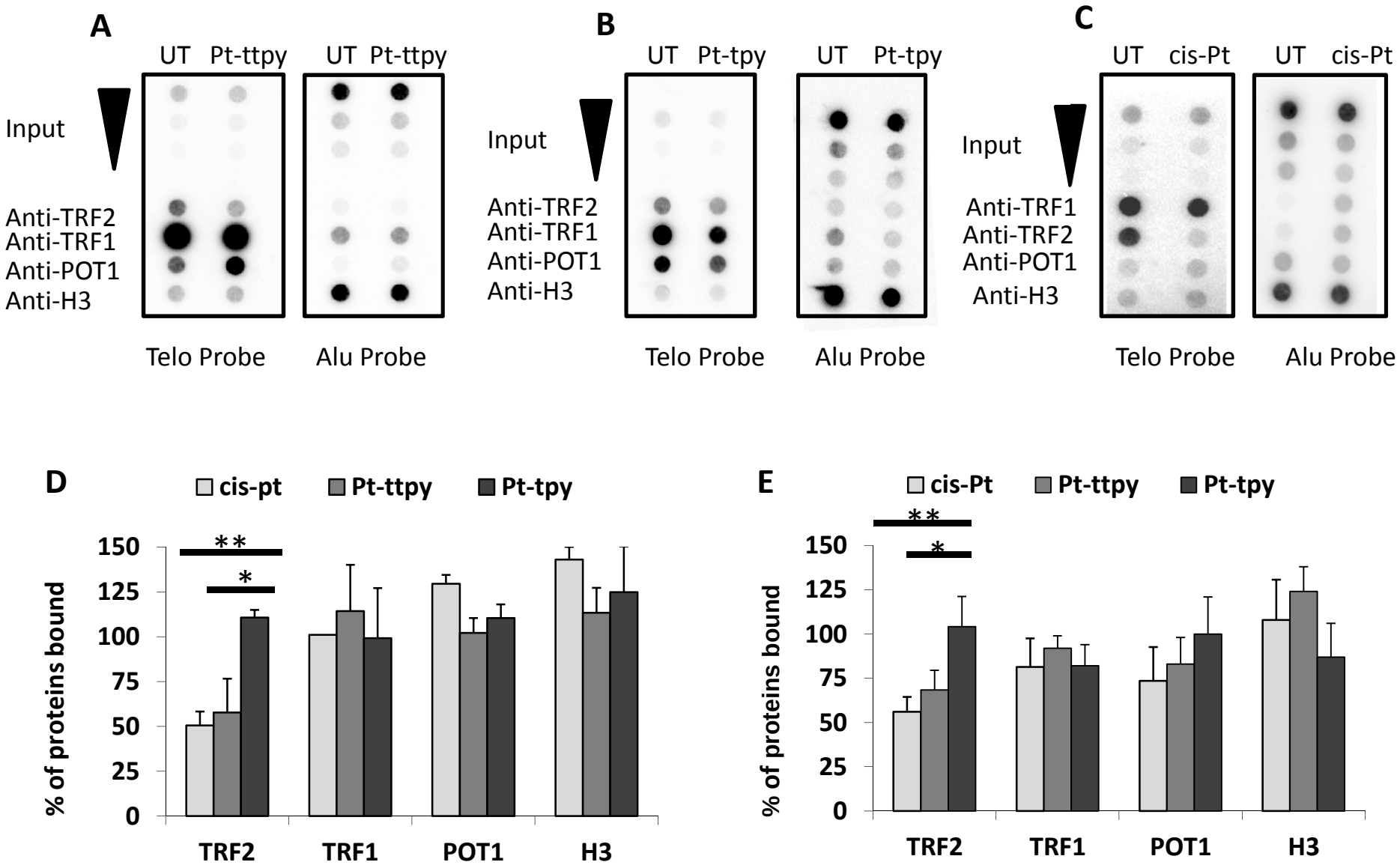
A
UT
Pt-ttpy
UT
Pt-ttpy
Input
Anti-TRF2
Anti-TRF1
Anti-POT1
Anti-H3
Telo Probe
Alu Probe
B
UT
Pt-tpy
UT
Pt-tpy
Input
Anti-TRF2
Anti-TRF1
Anti-POT1
Anti-H3
Telo Probe
Alu Probe
C
UT
cis-Pt
UT
cis-Pt
Input
Anti-TRF1
Anti-TRF2
Anti-POT1
Anti-H3
Telo Probe
Alu Probe
D
cis-pt
Pt-ttpy
Pt-tpy
% of proteins bound
150
125
100
75
50
25
0
**
*
TRF2
TRF1
POT1
H3
E
cis-Pt
Pt-ttpy
Pt-tpy
% of proteins bound
150
125
100
75
50
25
0
**
*
TRF2
TRF1
POT1
H3

Figure 4

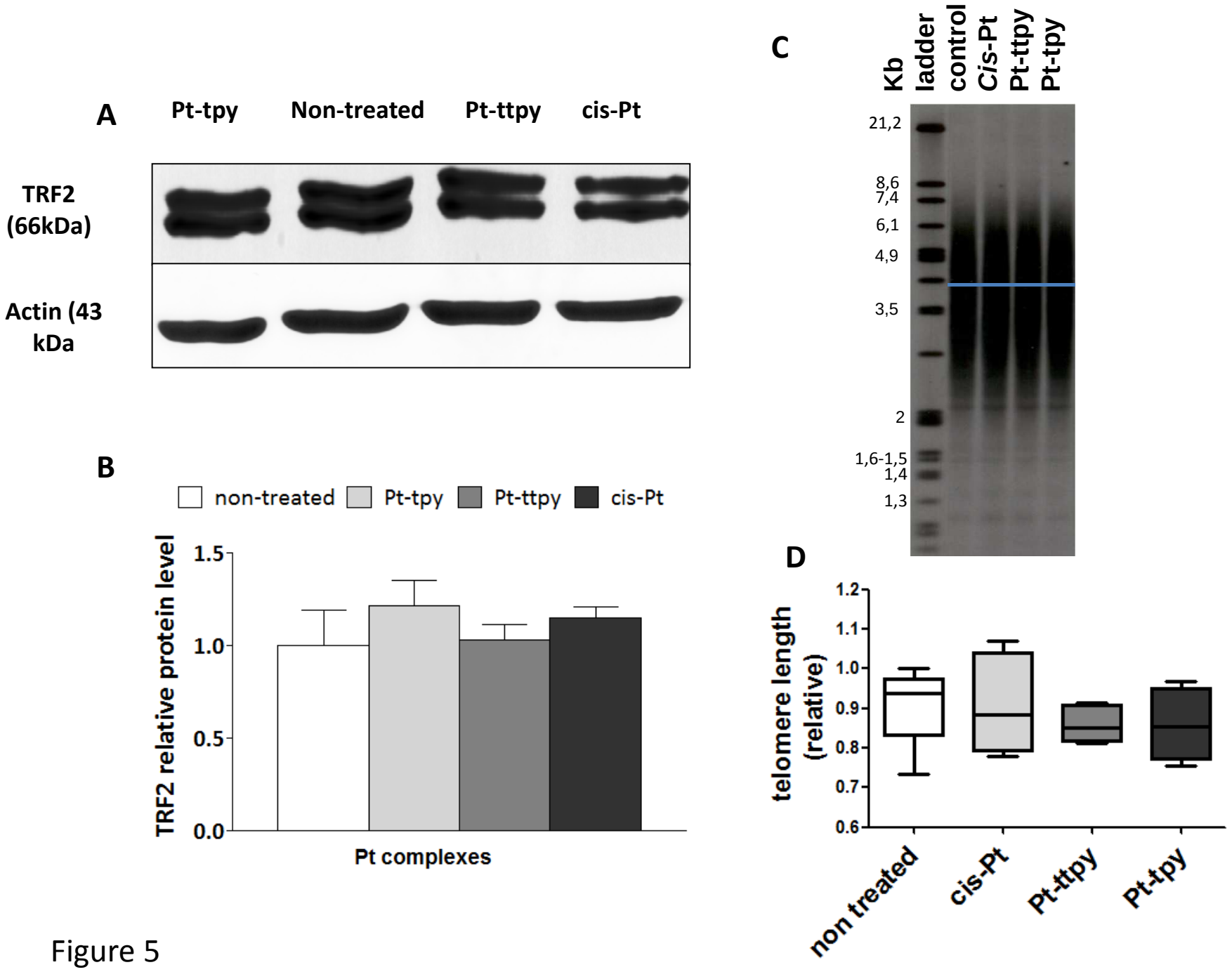
A
Pt-tpy
Non-treated
Pt-ttpy
cis-Pt
TRF2 (66kDa)
Actin (43 kDa
B
non-treated
Pt-tpy
Pt-ttpy
cis-Pt
TRF2 relative protein level
1.5
1.0
0.5
0.0
Pt complexes
C
Kb
ladder
control
Cis-Pt
Pt-ttpy
Pt-tpy
21,2
8,6
7,4
6,1
4,9
3,5
2
1,6-1,5
1,4
1,3
D
telomere length (relative)
1.2
1.1
1.0
0.9
0.8
0.7
0.6
non treated
cis-Pt
Pt-ttpy
Pt-tpy

Figure 5

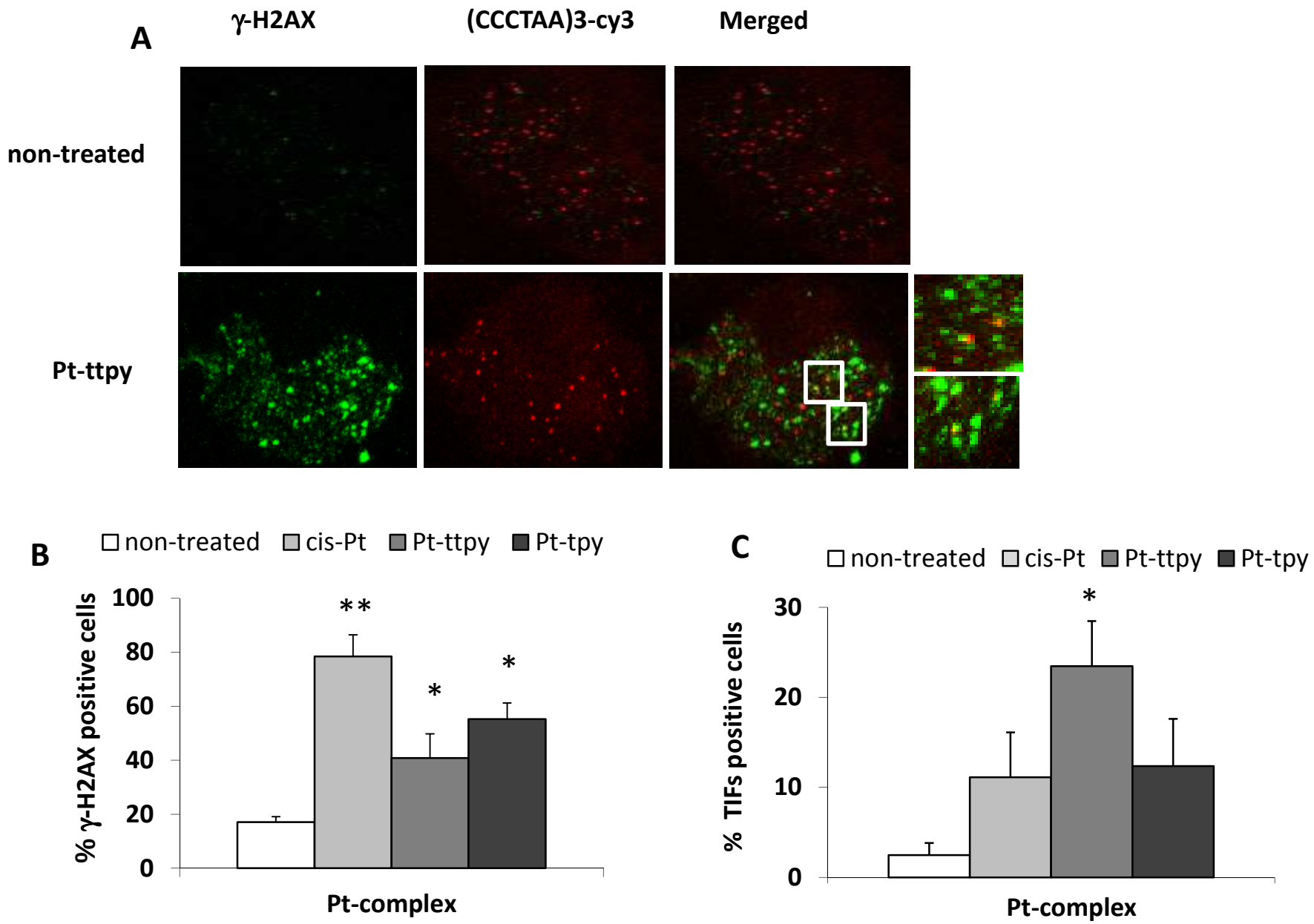
A
γ-H2AX
(CCCTAA)3-cy3
Merged
non-treated
Pt-ttpy
B
non-treated
cis-Pt
Pt-ttpy
Pt-tpy
% γ-H2AX positive cells
100
80
60
40
20
0
**
*
*
Pt-complex
C
non-treated
cis-Pt
Pt-ttpy
Pt-tpy
% TIFs positive cells
30
20
10
0
*
Pt-complex

Figure 6

A

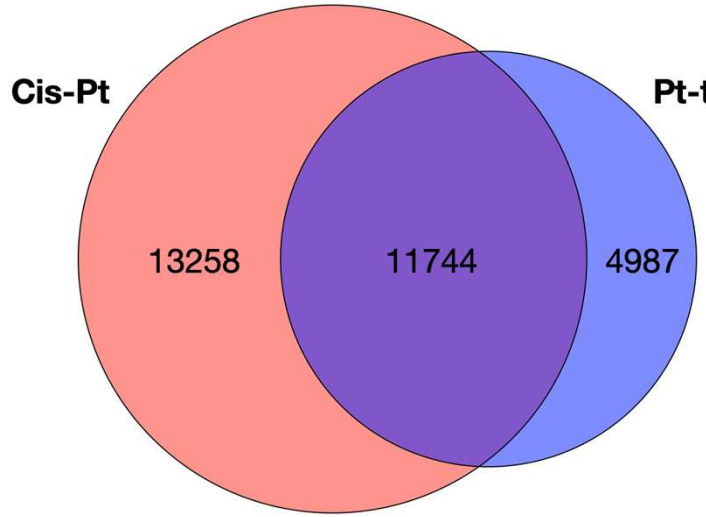

	Cis-Pt IP (over Untreated IP)	Pt-ttpy IP (over Untreated IP)	Untreated IP (over INPUT)
Number of peaks	25788	17682	10050

B

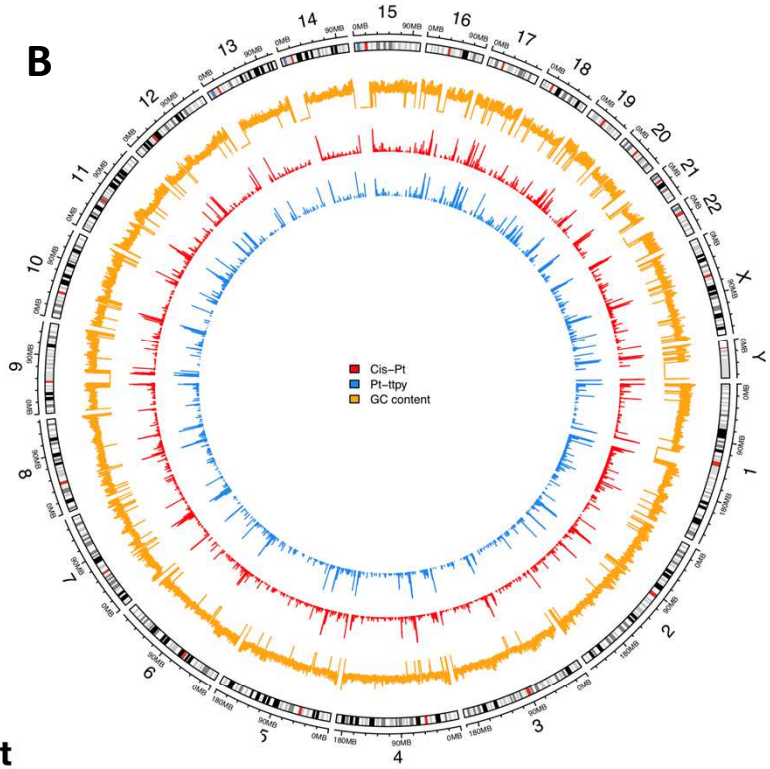

C

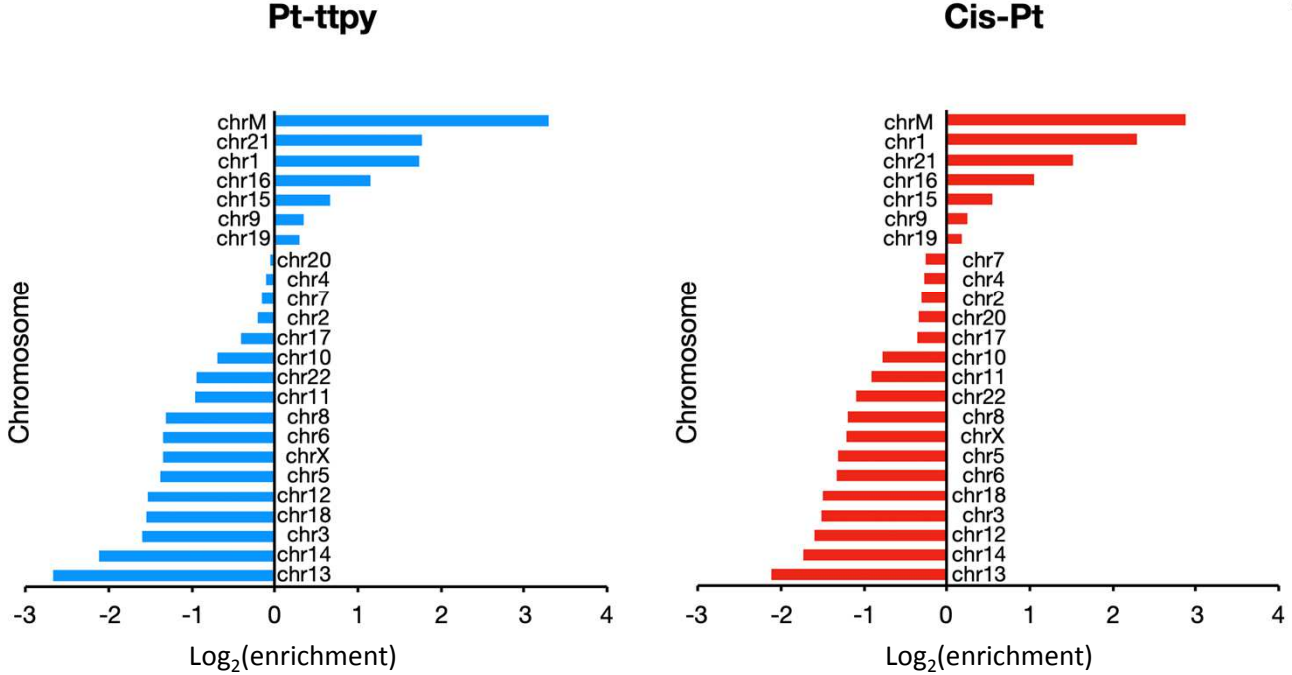

Figure 7

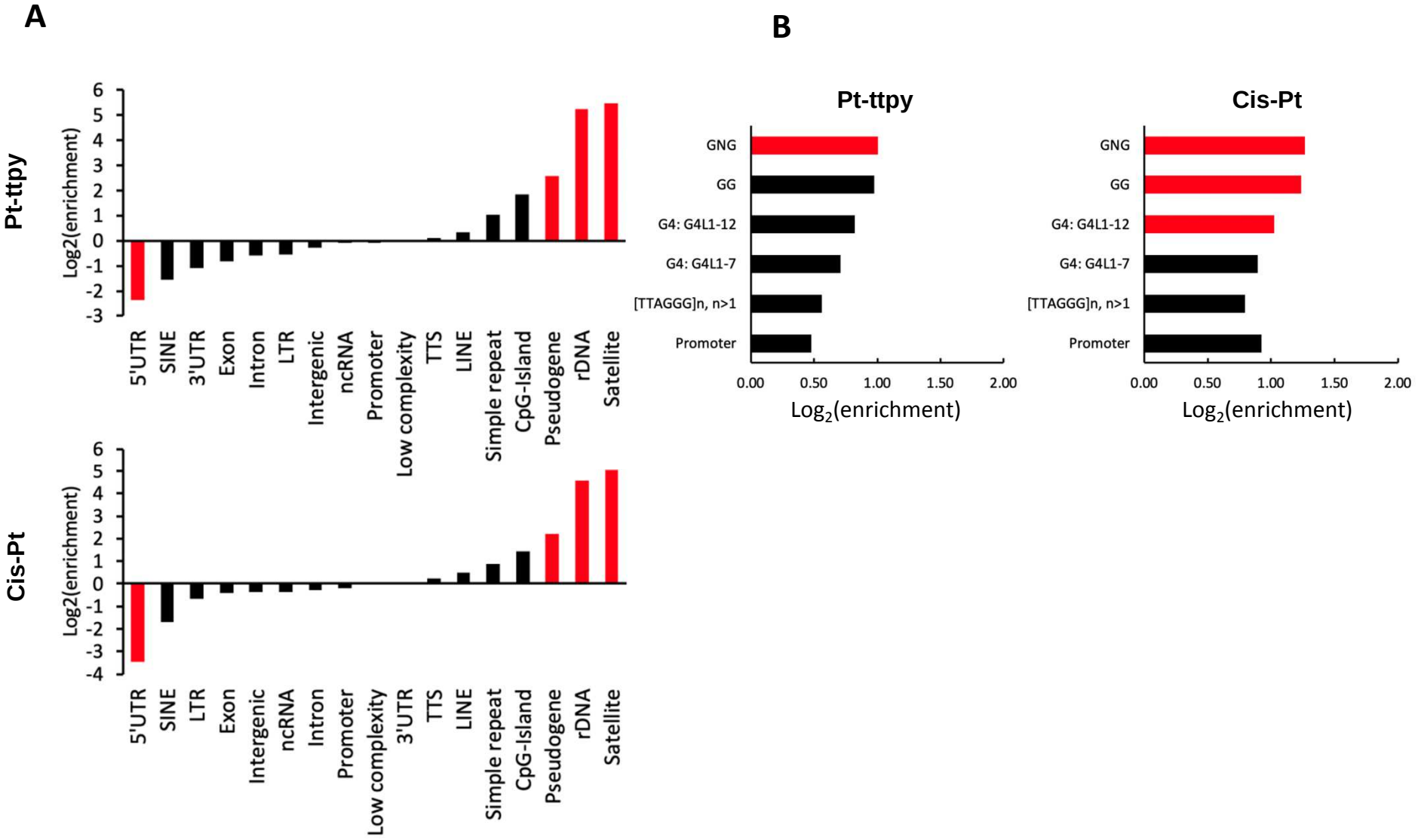
A
Pt-ttpy
Log2(enrichment)
6
5
4
3
2
1
0
-1
-2
-3
5'UTR
SINE
3'UTR
Exon
Intron
LTR
Intergenic
ncRNA
Promoter
Low complexity
TTS
LINE
Simple repeat
CpG-Island
Pseudogene
rDNA
Satellite
Cis-Pt
Log2(enrichment)
6
5
4
3
2
1
0
-1
-2
-3
-4
5'UTR
SINE
LTR
Exon
Intergenic
ncRNA
Intron
Promoter
Low complexity
3'UTR
TTS
LINE
Simple repeat
CpG-Island
Pseudogene
rDNA
Satellite
B
Pt-ttpy
GNG
GG
G4: G4L1-12
G4: G4L1-7
[TTAGGG]n, n>1
Promoter
0.00
0.50
1.00
1.50
2.00
Log2(enrichment)
Cis-Pt
GNG
GG
G4: G4L1-12
G4: G4L1-7
[TTAGGG]n, n>1
Promoter
0.00
0.50
1.00
1.50
2.00
Log2(enrichment)

Figure 8

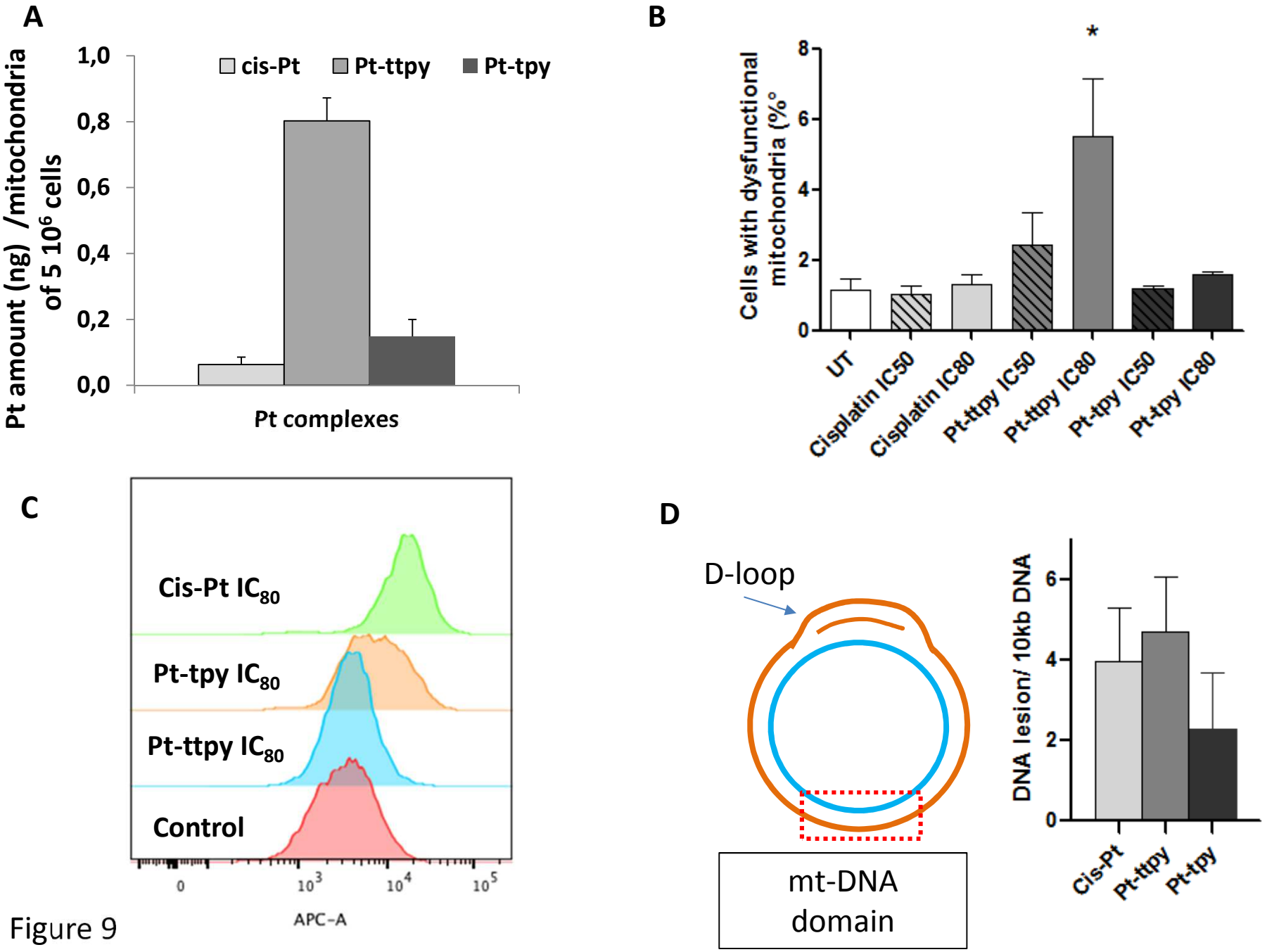
A
Pt amount (ng) /mitochondria of 5 10^6 cells
1,0
0,8
0,6
0,4
0,2
0,0
cis-Pt
Pt-ttpy
Pt-tpy
Pt complexes
B
Cells with dysfunctional mitochondria (%°
8
6
4
2
0
*
UT
Cisplatin IC50
Cisplatin IC80
Pt-ttpy IC50
Pt-ttpy IC80
Pt-tpy IC50
Pt-tpy IC80
C
Cis-Pt IC80
Pt-tpy IC80
Pt-ttpy IC80
Control
0
10^3
10^4
10^5
APC-A
D
D-loop
mt-DNA domain
DNA lesion/ 10kb DNA
6
4
2
0
Cis-Pt
Pt-ttpy
Pt-tpy

Figure 9

RÉSUMÉ

La chimio-radiothérapie est une forme de thérapie courante dans le cancer de nos jours qui implique une radiothérapie couplée à des médicaments. Par conséquent, la recherche de médicaments susceptibles d'induire la sensibilité des cellules cancéreuses à l'irradiation est en augmentation. Dans cette thèse, nous avons criblé différents complexes métalliques qui peuvent reconnaître des structures d'ADN spécifiques appelées G-quadruplexes, pour leur potentiel de radiosensibilisation. Les résultats montrent qu'il n'existe aucune structure-activité pour le potentiel radiosensibilisant des complexes. Une nouvelle famille de complexes Pt a émergé et fait actuellement l'objet d'un brevet. Parmi les ligands de G-quadruplex, Pt-ttpy s'est avéré le complexe le plus prometteur. Il a été montré que Pt-ttpy ralentissait effectivement la réparation des dommages à l'ADN induits lors de l'irradiation. Cette étude ouvre la voie à l'utilisation de nouveaux complexes métalliques en radiothérapie.

MOTS CLÉS

G-Quadruplex, Radiation, Radiosensibilisation, Médicaments à complexe métallique, Télomères

ABSTRACT

Chemo-Radiotherapy is the common form of therapy in cancer nowadays which involves radiation therapy coupled with chemotherapeutic drugs. Hence, the search for drugs that can induce the cells to be more sensitive to irradiation is on the rise. In this thesis we show the screening of different metal complex drugs with some of them recognizing specific DNA structures called G-quadruplexes, for their radiosensitization potential. The results show that there is no structure activity relationship of these drugs with respect to radiosensitization. A new family of Pt-complexes has been highlighted and is now under the process to be patented. Among the G-quadruplex ligands, Pt-ttpy, containing a platinum metal core was found the most radiosensitizer and specific of cancer cells. It was shown to delay the IR-induced DNA damage repair of the cell, possibly by the formation of hard to repair complex DNA damages. This study will open the way for the use of metal complexes in radiotherapy.

KEYWORDS

G-Quadruplex, Radiation, Radiosensitization, Metal complex drugs, Telomeres